Innovation of the Magnetotelluric method and its application to the characterization of the Pyrenean lithosphere

Joan Campanyà i Llovet

Innovation of the Magnetotelluric method and its application to the characterization of the Pyrenean lithosphere

Joan Campanyà i Llovet
Ph.D. Thesis

Supervisor: Juanjo Ledo

Geomodels Research Institute
Departament de Geodinàmica i Geofísica
Facultat de Geologia
Universitat de Barcelona

Geomodels Research Institute
Departament de Geodinàmica i Geofísica
Facultat de Geologia
Universitat de Barcelona

Innovation of the Magnetotelluric method and its application to the characterization of the Pyrenean lithosphere

Aquesta memòria ha estat realitzada per optar al títol de Doctor dins del programa de doctorat de Ciències de la Terra de la Universitat de Barcelona sota la direcció del Dr. Juanjo Ledo Fernández

Joan Campanyà i Llovet

Barcelona, Desembre 2012

Dr. Juanjo Ledo Fernández
Director i Tutor de la tesi

Aquesta Tesi ha estat possible gràcies a la beca predoctoral FI 2010 concedida pel Departament d'Universitats, Investigació i Societat de la Informació de la Generalitat de Catalunya.

Els següents projectes i grups de recerca han col·laborat en el finançament de la Tesi:

MAGBET (CGL2006-101660)

PIERCO2 (CGL2009-07604)

MODES4D (CGL2010-66431-CO2-02/BTE)

INTECTOSAL (CGL2010-21968-CO2-01)

TOPOMED (CGL2008-03474-E/BTE)

Grup de Recerca de Geodinàmica i Anàlisi de Conques (2009SRG1198)

A la Mercè, en Joaquim,

L'Eva, la Neus i la Maria

AGRAÏMENTS

Primerament agrair al meu tutor i director, Juanjo Ledo, per la confiança i el suport que ha dipositat en mi per tirar endavant el projecte d'aquesta tesi, per les hores dedicades a explicar-me MT i a solucionar els múltiples entrebancs que han anat apareixent, pels innombrables consells i especialment pels infinits comentaris sobre els articles presentats.

Seguidament agrair al coautors dels articles, en especial a la Pilar i l'Alex, pels consells i crítiques aportades més enllà dels relacionats amb les publicacions i també per donar-me la confiança, juntament amb el Juanjo, d'entrar a formar part del grup de recerca. Agrair a l'Anton i la Montserrat per ensenyar-me els conceptes bàsics de geologia i geoquímica que m'han sigut de gran ajuda per tirar endavant la interpretació dels models. Thanks to Alan for the comments on the methodological paper, for provide the LMT equipments used in the MT surveys in the Pyrenees and for the days I've been in DIAS learning MT.

Tota aquesta feina tampoc hagués estat possible sense els companys/es i amics i amigues de doctorat, tant del departament com de fora, amb els que après i conviscut un munt d'experiències des de les campanyes de camp, congressos, moltes hores de despatx i les mes agradables birres, dinars, sopars i excursions. Agrair especialment a l'Eloi, na Lena, la Perla, la Xènia, el Fabián, el Manel, l'Oriol, l'Anna i el David amb els que més hores i experiències he conviscut.

Un altre grup que no puc oblidar és tota aquella gent que m'ha acompanyat en les campanyes de camp a Pirineus. M'aventuro a posar noms demanant perdó per si me'n deixo algun ja que han estat quatre anys i un munt de sortides al camp. Començant pels quatre que més ho han viscut, dono les gràcies a en Victor, el Roger, l'Ivan i en Lluís, i segueixo amb els que també han col·laborat a poder tirar endavant aquesta dura tasca: Robert, Clara, Arnau, Gerard, Ari, Savitri, Shankar, Maria, Micke, Maura, Kasturi, Laura, Perla, Dani, Miguel, Lena, Xènia, Oriol, Eloi i David. Moltes gràcies a tots i totes per ajudar-me a muntar estacions, a enterrar els cables i a solucionar els mil contratemps que han anat sortint a les campanyes de camp com les innombrables batalles amb les vaques dels Pirineus de les que no sempre vam sortir vencedors, a treure el cotxe de la neu en camins perduts on no hi havia cobertura o al fet d'haver de muntar una estació amb la no grata companyia, i pitjor olor, d'una ovella que ja havia passat a millor vida.

També agrair als propietaris i els ajuntaments que m'han deixat muntar els aparells de mesura en els seus terrenys així com a l'Office National des Forêts (ONF), Parc National des Pyrénées i als Espais Naturals de Catalunya per facilitar-me la feina en reserves naturals i zones protegides.

I would like also to thank who accompanied me in the international experiences. Firstly, thanks to Collin, Duygu, Shane, Gerardo, Pierpaolo, Yonnas, Ester, Pau, Perla, Roger, Ian, Haula, Matt, Mohamed, Abdel... for the days in the Atlas Mountain in Morocco acquiring MT data. Secondly, many thanks to Graham for give me the opportunity to go to Australia and collaborate with his research group and also to Stephan, Jared, Aixa and the people of KLC for the good times experienced in Adelaide. Finally, many thanks to Martin and Karen for give me the opportunity to participate in the Svalbard cruise and teach me about CSEM. Also thanks people of NOCS and friends from Southampton, especially to Hector, Maxi, Carla, Miguel, Daniela, Neus, Javi and Bedanta, to make me more pleasant the time I had in Southampton, maybe not the most beautiful city but better than the unforgettable "*tuboflo*".

I would like to thank to INTERMAGNET for provide me the data I used in the third paper of thesis and to Koulakov and Amaru for provide me the topographical profiles used to constrain the lithosphere below the Pyrenees.

Sense haver-me ajudat directament en al feina del doctorat però si anímicament a gaudir d'aquests darrers anys vull agrair als companys de la UEC, del *running team* i a tots aquells amb els que hem compartit grans moments i m'heu donant ànims i forces per tirar endavant amb aquest projecte. De forma especial agrair a l'Arnau, el Gerard i al Dani amb els que sempre he pogut contar, aguantant-nos penes i glòries, allà on fóssim repartits pel planeta.

Finalment vull agrair profundament a la meva família els suport incondicional que m'han donat durant tots aquests anys. Perquè tot i no tenir-vos sempre a prop físicament sempre heu estat al meu costat i he pogut contar amb vosaltres pel que ha calgut. Agrair-vos profundament l'educació, les eines i actituds que m'heu donat i que m'han permès tirar endavant i amb èxit projectes com la Tesi i d'altres més complicats. És un plaer tenir-vos al meu costat i és per això que aquesta tesi està dedicada a vosaltres.

Moltes gràcies a tots i totes!

Thank you all!

Joan Campanyà i Llovet

CONTENTS

PROLOGUE

This thesis is a compendium of three papers related to the magnetotelluric (MT) method and its application to the characterization of lithospheric-scale geoelectrical structures. In the first two papers the MT method is applied determining the electrical resistivity distribution under the Pyrenees using broadband magnetotelluric (BBMT) and long period magnetotelluric (LMT) data. In the third article, a new method is proposed for processing MT data of a local site using inter-station tensor relationships between the local site and a neighbouring site. Two of the papers (Campanyà et al., 2011 and Campanyà et al., 2012) are already published and the third one, related to methodological aspects of the MT method, at the day of submission of the thesis, is still under review in a scientific journal indexed in the Journal Citation Reports (ISI).

- **Campanyà, J.;** Ledo, J.; Queralt, P.; Marcuello, A., Jones, A.G., 2013. Processing of Magnetotelluric data using inter-station tensor relationships. *Geophysical Journal International* (Under review).

- **Campanyà, J.;** Ledo, J.; Queralt, P.; Marcuello, A.; Liesa, M.; Muñoz, J.A.; 2012. New geoelectrical characterisation of a continental collision zone in the West-Central Pyrenees: Constraints from long period and broadband magnetotellurics. *Earth and Planetary Science Letters.* **333-334**,112-121. http://dx.doi.org/10.1016/j.epsl.2012.04.018

- **Campanyà, J**.; Ledo, J.; Queralt, P.; Marcuello, A.; Liesa, M.; Muñoz, J.A. 2011. Lithospheric characterisation of the Central Pyrenees based on new magnetotelluric data. *Terra Nova*, **23**, 213 – 219. doi: 10.1111/j.1365-3121.2011.01001.x.

The thesis begins with an Introduction where the motivation and the aims are presented as well as the geological context of the Pyrenees, the previous geophysical studies and the used data set. The Introduction also contains a description of the MT method with basic concepts useful to understand the MT analysis developed in the three papers. Then the three papers are exposed. After the papers, there is a Discussion where the results are commented and compared, extending some of the ideas proposed in the articles and including a new geoelectrical crustal model of the Western Pyrenees. Then there are the Conclusions and proposals of future works related to the MT sites acquired in the Pyrenees and the proposed method for processing MT data. At the end of the thesis there are the references of the cited works and an annex containing a copy of the two published papers and a copy of the submitted manuscript of the third paper.

Focusing on the three papers, which represent the main part of the thesis, the results of the scientific work developed in the last four years are shown and discussed providing new results to better understand the physical processes of the lithosphere and the MT method.

The first published paper, chapter 2 of the thesis, determines the geoelectrical structures below the Central Pyrenees using new BBMT and LMT data acquired close to the ECORS-Pyrenees deep seismic profile. The aim of this study has been to improve the results obtained by Ledo (1996) and Pous et al. (1995a), taking advantage of the progress occurred in the last fifteen years associated with the MT method and the acquisition of MT data. The most important improvements that have been achieved are the better definition of the top of the electrical resistivity structure associated with the Iberian subducted lower crust (IBSLC) and the determination of the lithosphere-asthenosphere boundary (LAB) below the Iberian and the European plates close to the collision zone. In this study we have used sixteen BBMT sites acquired in 1992 and eight new BBMT+LMT sites acquired in spring and summer of 2009. Due to the low solar activity in 2009, the new MT data were recorded over three days, in case of BBMT data, and thirty days, in case of LMT data. The instruments were buried, during the recording days, avoiding problems with animals or other external events.

A geoelectrical model of the subsurface has been determined doing two-dimensional inversion of the apparent resistivity and phase for periods between 0.001 s and 20000 s in a N-S profile across the Central Pyrenees. A non-linear sensitivity test has been done to determine the resolution of the MT model. In the interpretation, the geoelectrical results have been compared with independent geophysical studies. Complementary, an analysis of the geological properties of the lower-crust and the dehydration point of the muscovite and biotite rocks provides more arguments in favour of the hypothesis of partial melting to explain the geophysical observations associated with the IBSLC.

In the second paper, chapter 3 of the thesis, the MT method has been applied to characterize the geoelectrical structures below the West-Central Pyrenees in a new MT profile across the Pyrenean mountain range close to the ECORS-Arzacq deep seismic profile. This new MT profile is 130 km long and is composed by twenty BBMT sites acquired in 2010, seven of them also with LMT data. BBMT data have been recorded for three days and LMT data, thanks to the increase of the solar activity, have been

recorded for fifteen days on average. In this profile the instruments were also buried during the acquisition of the data.

The geoelectrical model of this region has been obtained from the inversion of the MT data in a profile with N16E-S16W direction, due to the geoelectrical structures of the region have a strike 16º clockwise from E-W direction. Consequently, the impedance tensor of each site has been rotated 16º clockwise before the inversion. A non-linear sensitivity test has been carried out to determine the resolution of the constrained geoelectrical structures.

Results have been compared with the ones obtained in the Central Pyrenees characterizing the main geoelectrical variations between the two MT profiles. Independent geophysical studies have also been taken into account to interpret the MT results. An analysis of the thermal re-equilibration of the IBSLC has been developed completing the analysis of the previous paper about the presence or absence of partial melting in the IBSLC. This analysis corroborates partial melting as the best explanation for the low electrical resistivity values of the IBSLC. The LAB below the West-Central Pyrenees has been determined not only below the Iberian and the European plates, as in the Central Pyrenees, but also below the collision zone. Additionally, an unexpected geoelectrical structure completely buried below the Ebro basin has been associated with a Variscan boundary.

In the third paper, chapter 4 of the thesis, a new method is proposed for processing MT data. The proposed method uses the horizontal magnetic fields recorded at a neighbouring site to process the MT data of a local site from inter-station tensor relationships. The motivation for this article comes from the problems experienced in the acquisition of the time series in the MT surveys conducted over the last four years. The proposed method has been tested using the MT data of three LMT sites simultaneously recorded in the Eastern Pyrenees in 2010 and the magnetic data recorded by the Chambon de la Forêt (CLF) and Furstenfeldbruck (FUR) magnetic observatories. Results obtained validate the method. A parameter has been defined in order to determine, in each specific study for each used period, if the proposed

method can be applied. At the end of the paper an example is shown where the proposed method improves the processing of a LMT site when the magnetic fields stop recording after two days in a LMT site where the electric fields have been recorded for twenty days.

As a thesis developed in the Universitat de Barcelona (UB), there is a summary written in Catalan language with the main information of the thesis. References of the works cited in the Catalan extended summary are together with the references cited in the thesis. At the beginning of chapters 2, 3 and 4 there is also a summary of the presented paper in Catalan language.

RESUM EXTENS

CATALAN EXTENDED SUMMARY

R.1 INTRODUCCIÓ I MOTIVACIÓ

La capa més externa de la Terra, la litosfera, està dividida en set grans plaques tectòniques i varies plaques petites o microplaques (p.e. Anderson, 2002 i Gordon, 2000). El moviment relatiu entre elles està dominat pels processos tectònics, responsables de la creació, modificació i destrucció de la litosfera durant milions d'anys. Un dels processos tectònics que juga un paper destacat en el desenvolupament dels continents són les col·lisions continentals, causants de la formació de grans serralades com els Alps i l'Himàlaia. Aquests han estat estudiats a partir de tècniques geofísiques que han permès determinar les propietats físiques del subsòl i han ajudat a entendre millor l'evolució de la litosfera i els processos físics i químics associats (p .e. Cloetingh et al., 2010; Liang et al., 2012 i Unsworth, 2009). Entre les tècniques geofísiques, en aquesta tesi es destaca el paper de la magnetotel·lúrica (MT) que permet determinar les estructures geoelèctriques del subsòl. El gran nombre d'avenços teòrics i tecnològics dels últims anys han permès aplicar el mètode MT a una gran varietat de zones d'estudi, des de les profunditats marines (p.e. Baba et al., 2006; Heinson et al., 2000) fins a les serralades més elevades del planeta (p.e. Kelbert et al., 2012; Le Pape et al, 2012).

En aquesta tesi s'ha utilitzat el mètode magnetotel·lúric (MT) per caracteritzar les estructures geoelèctriques associades amb la zona de col·lisió continental que va

donar lloc als Pirineus. Els resultats s'han obtingut a partir de noves dades MT adquirides als Pirineus i refent els estudis de MT duts a terme per Ledo (1996), Pous et al. (1995a) i Ledo et al. (2000) a partir de dades MT de banda ampla (BBMT). La motivació per tornar a treballar aquestes dades prové de dues millores en el camp de la MT. La primera està relacionada amb el desenvolupament i l'accessibilitat dels codis d'inversió bidimensionals utilitzats per modelitzar la zona d'estudi (Groot-Hedlin and Constable, 1990; Smith and Booker, 1991; Siripunvaraporn and Egbert, 2000 i Rodi and Mackie, 2001). Aquests codis permeten evitar la modelització ajustant les dades de camp per assaig i error solucionant el problema directe. La segona millora va lligada a la capacitat d'enregistrar dades MT de llarg període (LMT), les quals permeten caracteritzar estructures geoelèctriques més profundes que utilitzant dades de BBMT. Les dues millores s'han implementat en els resultats mostrats en aquesta tesi.

A part de l'aplicació del mètode MT per caracteritzar la litosfera geoelèctrica dels Pirineus, també es proposa una innovació metodològica en el processat de dades MT. El mètode proposat permet millorar el processat de dades quan algunes de les components enregistrades s'han truncat. La motivació per desenvolupar aquest nou mètode prové dels problemes experimentats en enregistrar les sèries temporals en les campanyes de camp dutes a terme durant els darrers quatre anys, no només a Pirineus sinó també a la serralada de l'Atlas al Marroc (Ledo et al., 2011) i a la Serralada Bètica (Rosell et al., 2011).

R.1.1 Context geològic dels Pirineus

Els Pirineus es defineixen com un sistema asimètric d'encavalcaments de doble vergència formats com a conseqüència de la col·lisió entre les plaques Ibèrica i Europea entre el Cretaci superior i el Miocè inferior (Muñoz, 2002; Olivet, 1996; Rosenbaum et al., 2002). Aquests s'estenen des de la Mediterrània occidental fins a l'Oceà Atlàntic, pel nord de la península Ibèrica, amb una llargada d'uns 1300 km i una amplada propera als 200 km. Al llarg de la serralada Pirenaica trobem diferències importants a nivell de l'escorça, degut a inversió d'un sistema de rift segmentat en continuïtat amb el Golf de Biscaia (Beaumont et al. 2000; Muñoz, 2002; Roca et al., 2011). Tot i aquestes diferències, l'escorça continental de la placa Ibèrica subdueix

sota l'escorça continental de la placa Europea al llarg de tota la serralada (Muñoz, 2002). Com a resultat de la formació dels Pirineus també es van desenvolupar dues conques d'avantpaís, la conca de l'Ebre i la conca d'Aquitània.

La tesi es centra en els Pirineus que limiten França i Espanya. En aquesta regió hi trobem tres estructures litològiques principals, cadascuna amb el seu propi comportament mecànic. La primera, que constitueix el basament, correspon als materials paleozoics (600-300 Ma). Aquests materials generalment són d'origen sedimentari encara que hi ha algunes intercalacions volcàniques. La segona unitat litològica està constituïda per sediments del Mesozoic (250-50 Ma) també deformats durant la orogènia alpina. Aquesta unitat està desenganxada de l'anterior, pel que les estructures associades no sempre tenen continuïtat en profunditat. Finalment, hi ha els materials sinorogènics del Cenozoic (50-0 Ma). Aquests van ser dipositats al final de la formació dels Pirineus i es poden trobar tant a l'interior de l'orogènia com a les conques de l'Ebre i Aquitània (Figura R.1).

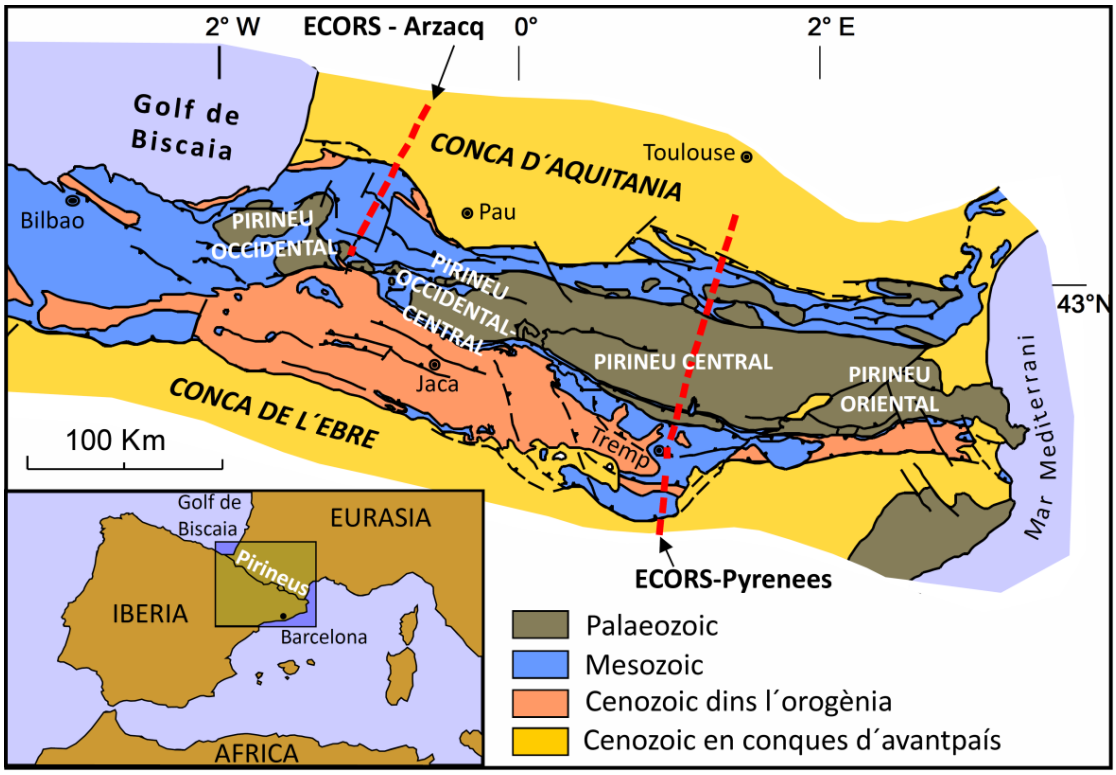

Figura R.1 Mapa geològic dels Pirineus mostrant les principals divisions longitudinals i transversals de la serralada. En vermell els perfils de sísmica profunda fets a Pirineu (Modificat de Teixell (1996)).

Per tal d'entendre les estructures geoelèctriques observades a Pirineus, a part de la col·lisió continental entre les plaques Ibèrica i Europea, que és el procés tectònic principal, ens hem de remuntar a dos processos tectònics anteriors. Per una banda, l'orogènia Herciniana i els esdeveniments tectònics post orogènics que van deformar l'escorça Ibèrica provocant límits entre zones geològiques que ara haurien quedat coberts pels sediments que formen la conca de l'Ebre (Martínez Catalán et al., 2009). Per altra banda, l'obertura del Golf de Biscaia durant el Cretaci Inferior, el qual va produir un aprimament destacat de l'escorça que va donar lloc a l'ascensió de roques de l'escorça inferior i del mantell superior a nivells més superficials (Jammes et al., 2010; Pedreira et al., 2007). Aquests dos fenòmens són d'especial interès per explicar els resultats geoelèctrics obtinguts al Pirineu Occidental-Central.

R.1.2 Estudis geofísics previs

Els estudis geofísics permeten determinar les propietats físiques del subsòl. A partir de les propietats físiques caracteritzades, no només podem conèixer les estructures geològiques en profunditat, sinó també els processos físics i químics que hi tenen lloc. En comparar els resultats obtinguts amb altres tècniques geofísiques independents el nombre d'escenaris possibles que poden explicar els diferents resultats es redueix de forma destacada, facilitant la interpretació d'aquests. A continuació s'exposen els principals resultats geofísics obtinguts als Pirineus.

Primerament tenim dos perfils de sísmica profunda que permeten determinar les estructures geològiques a nivell cortical. Al Pirineu Central es va realitzar el ECORS-Pyrenees, que situa la Moho entre 30 km i 35 km de profunditat sota l'escorça Europea i entre 35 km i 60 km de profunditat sota l'escorça Ibèrica, amb un increment progressiu de sud a nord (ECORS-Pyrenees Team, 1988; Choukroune and ECORS-Pyrenees Team, 1989). Per altra banda al Pirineu Occidental-Central es va realitzar el perfil de sísmica profunda ECORS-Arzacq. En aquesta zona la profunditat de la Moho s'ha caracteritzat entre 30 km i 35 km sota l'escorça Europea i entre 30 km i 50 km sota l'escorça Ibèrica, incrementant la profunditat de la Moho de sud a nord (Muñoz, 2002; Teixell, 1998). La figura R.2 mostra les interpretacions geològiques dutes a terme dels dos perfils per Muñoz (1992,2002).

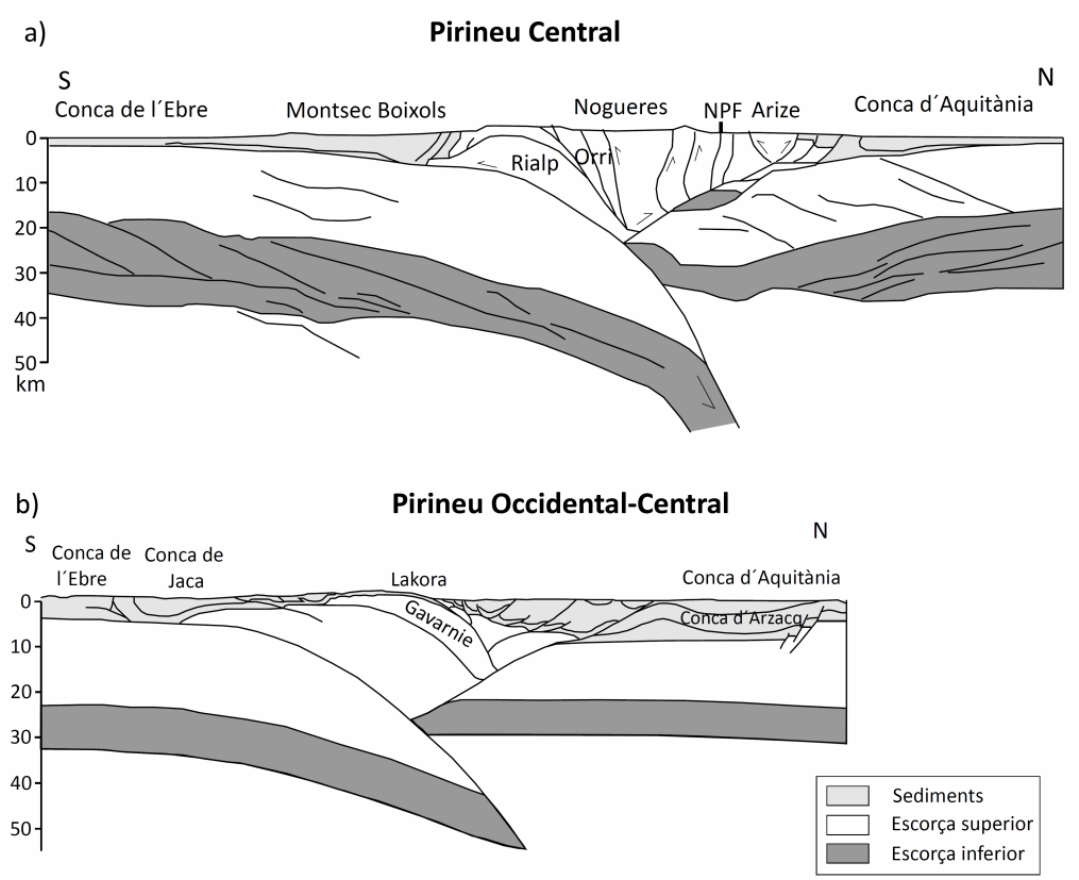

Figura R.2 (a)Model geològics proposat per Muñoz (1992) al Pirineu Central. (b) Model geològic proposat per Muñoz (2002) al Pirineu Occidental-Central

Els estudis de tomografia sísmica realitzats a Pirineus (Amaru et al., 2008; Koulakov et al., 2009; Souriau and Garnet, 1995 i Souriau et al., 2008) mostren, en general, una disminució de velocitats de les ones P i les ones S en la zona associada amb la subducció de l'escorça Ibèrica inferior respecte els valors de l'anomalia de velocitats de les plaques Ibèrica i Europea (Figura R3). Aquest fenomen es dóna tant al Pirineu Central com al Pirineu Occidental-Central. Els models de tomografia sísmica d'ones S proposats per Koulakov et al. (2009) determinen el límit litosfera-astenosfera (LAB) com a límit superior d'una estructura d'anomalia de velocitats negativa situada a la part inferior del model (Figura R3 a,b).

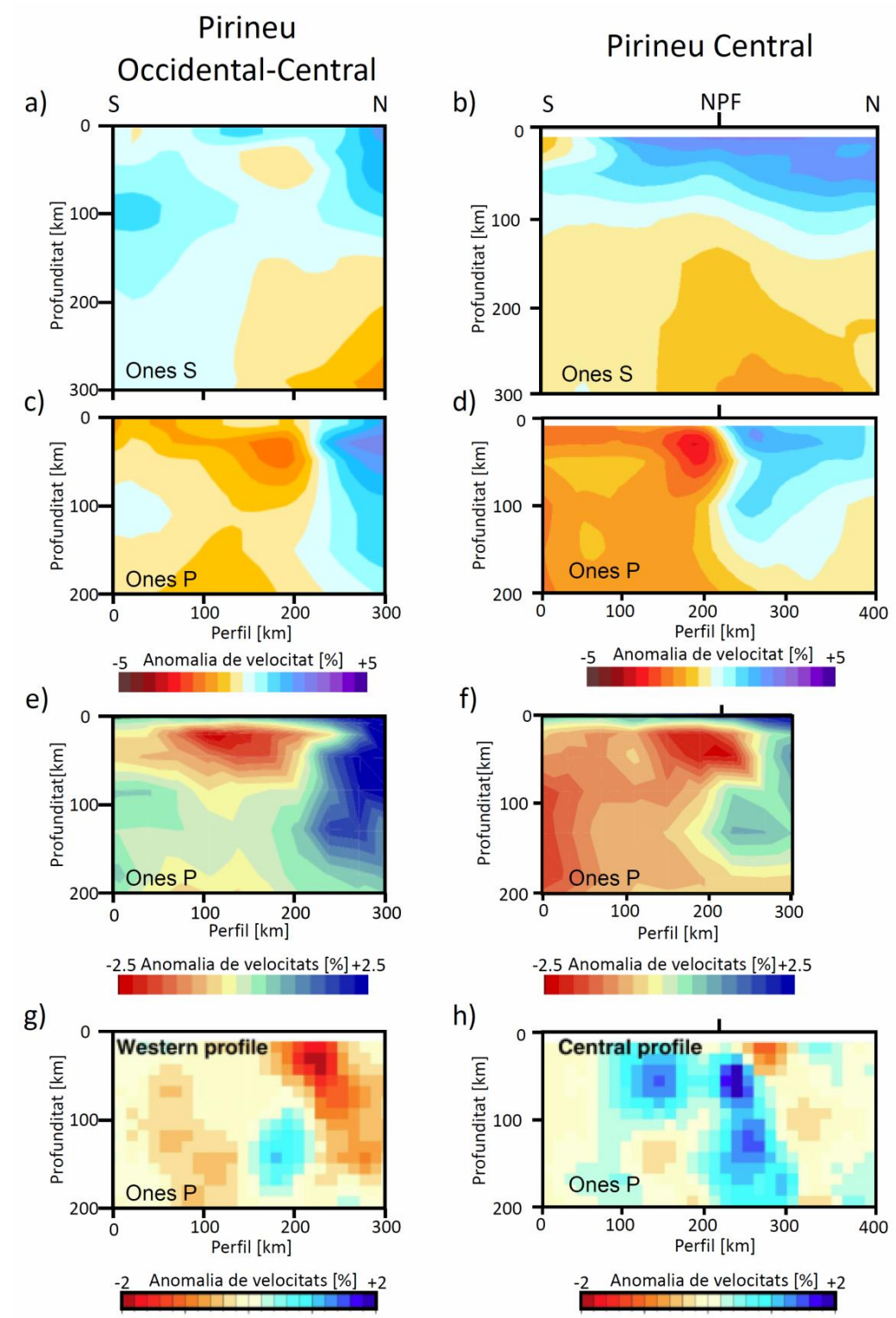

Figura R.3 Models de tomografia sísmica a partir d'ones S proposat per Koulakov et al (2009) al Pirineu Occidental-Central (a) i al Pirineu Central (b). Model de tomografia sísmica d'ones P proposat per Koulakov et al. (2009) al Pirineu Occidental-Central (c) i al Pirineu Central (d). (e) i (f) models de tomografia sísmica d'ones P proposats per Amaru et al. (2008) al Pirineu Occidental-Central i al Pirineu Central, respectivament. (g) i (h) Models de tomografia sísmica d'ones P proposat per Souriau et al. (2008) al Pirineu Occidental-Central i al Pirineu Central, respectivament.

Centrant-nos en els models de resistivitat elèctrica, s'ha realitzat un perfil al Pirineu Central (Ledo, 1996 i Pous et al., 1995a) i un model tridimensional entre el Pirineu Central i els Pirineu Occidental-Central (Ledo et al., 2000). En aquests models trobem dues estructures de baixa resistivitat elèctrica associades amb la subducció de l'escorça Ibèrica inferior (IBSLC) i amb l'astenosfera. (Estructures A i B en la Figura R.4).

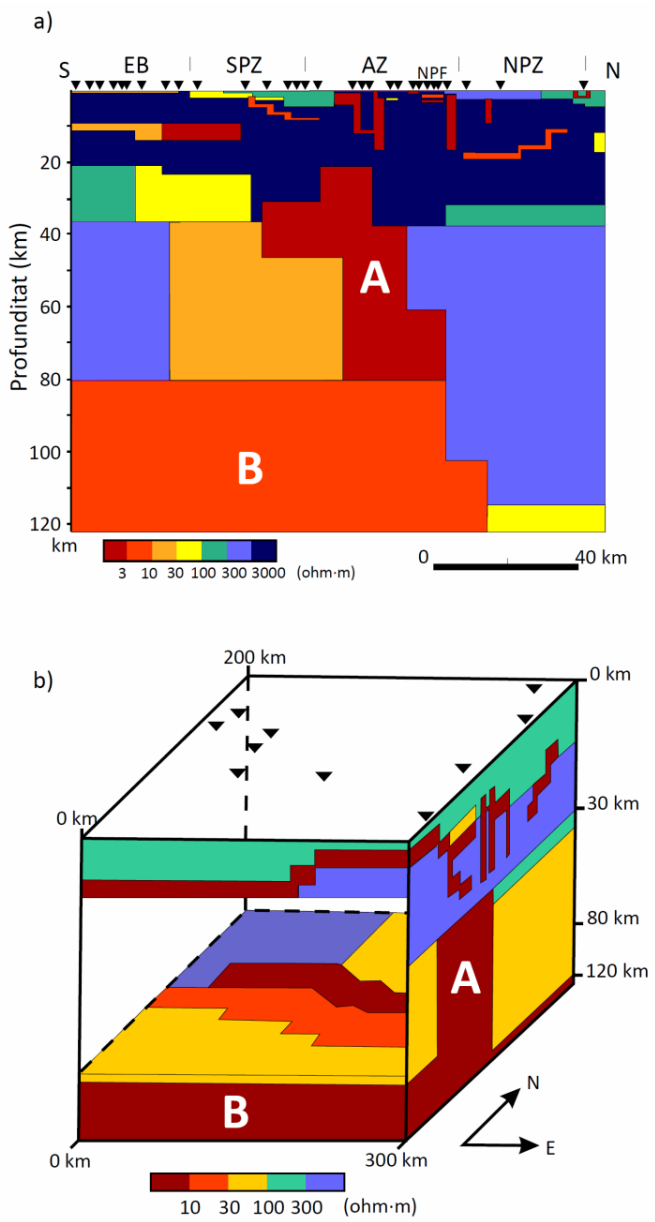

Figura R.4 a) Modificat del model geoelèctric bidimensional del Pirineu Central proposat per Ledo (1996) i Pous et al. (1995a). b) Modificat del model geoelèctric tridimensional de Pirineus proposat per Ledo et al., (2000). En els dos models, A és l'estructura geoelèctrica associada amb la IBSLC i B l'estructura geoelèctrica associada amb l'astenosfera. EB: Ebro basin; SPZ: South Pyrenean zone; AZ:Axial zone; NPZ: North Pyrenean zone; NPF: North Pyrenean Fault.

Els Pirineus també han estat estudiats a partir de dades de gravimetria i d'anomalia del geoide (Casas et al., 1997; Gunnell et al, 2008; Jammes et al., 2010; Ledo et al., 2000; Pedreira et al., 2007; Torné et al., 1989 i Vacher and Souriau, 2001). En tots els casos, els resultats són compatibles amb la subducció de l'escorça Ibèrica inferior. Pel que fa els estudis de flux de calor (Zeyen and Fernández, 1994; Glover et al., 2000 i Tesauro et al., 2009), no s'han trobat anomalies importants de temperatures sota els Pirineus, suggerint que l'equilibri tèrmic després de la subducció de l'escorça Ibèrica inferior ja s'ha produït. Els resultats proposats per Tesauro et al. (2009) suggereixen un LAB tèrmic, definit com la geoterma dels 1200 ^{o}C, situat al voltant dels 120 km de profunditat, entre el Pirineu Central i el Pirineu Occidental-Central.

R.2 OBJECTIUS

Els objectius d'aquesta tesi estan enfocats a caracteritzar la litosfera geoelèctrica dels Pirineus, fent servir dades BBMT i LMT, i a millorar el processat de les dades MT.

Els objectius relacionats amb la caracterització geoelèctrica de la litosfera dels Pirineus a partir de dades MT són:

a) Determinar l'estructura de baixa resistivitat elèctrica associada amb la subducció de l'escorça Ibèrica inferior sota el Pirineu Central amb major precisió que en els estudis previs.
b) Analitzar dades físiques i químiques relacionades amb l'escorça Ibèrica inferior i avaluar la hipòtesi de fusió parcial. Determinar també la quantitat de fusió parcial necessària per explicar els valors de resistivitat elèctrica observats.
c) Caracteritzar les estructures geoelèctriques sota el Pirineu Occidental-Central a partir d'un perfil MT proper al perfil de sísmica profunda ECORS-Arzacq.
d) Determinar l'evolució de les estructures geoelèctriques al llarg de la serralada dels Pirineus entre els perfils del Pirineu Central i del Pirineu Occidental-Central.

e) Ubicar el límit litosfera-astenosfera sota la serralada Pirenaica i caracteritzar els valors de resistivitat elèctrica de l'astenosfera.
f) Interpretar els resultats obtinguts sent consistent amb els resultats d'altres estudis geofísics.

Els objectius associats a la millora metodològica en el processat de dades MT són:

g) Desenvolupar un mètode per millorar el processat de dades MT quan alguna de les components enregistrades al camp ha deixat de registrar abans que les altres.
h) Avaluar les possibilitats i avantatges del mètode proposat.

R.3 ORGANITZACIÓ DE LA TESI

Aquesta tesi s'organitza com a compendi de tres articles, dos dels quals estan publicats i un tercer acceptat a revisió. En tots els casos els articles han estat enviats a revistes científiques internacionals indexades en el Journal Citation Reports de l'ISI. Els dos articles ja publicats són resultat de l'aplicació del mètode MT per caracteritzar la litosfera elèctrica dels Pirineus. Dels resultats obtinguts en destaca la presència de dues estructures de baixa resistivitat elèctrica relacionades amb la subducció de la l'escorça Ibèrica inferior i amb l'astenosfera. Per altra banda hi ha el tercer article, acceptat a revisió, on es proposa una millora metodològica en el processat de dades MT. Aquests tres estudis són els tres capítols dels quals està formada la tesi i constitueixen la part més important d'aquesta.

La tesi comença amb una introducció en la que s'exposen les motivacions del projecte, el context geològic dels Pirineus i els estudis previs realitzats. Tot seguit es presenten els objectius plantejats, les dades adquirides i es fa una descripció del mètode MT. La finalitat d'aquesta introducció és no només introduir la temàtica sinó també fer més entenedora la lectura dels tres capítols principals a aquells lectors no habituats amb el mètode MT i la seva aplicació a la caracterització de la litosfera elèctrica. Tot seguit s'exposen els tres articles en tres capítols per separat. Finalment hi ha una discussió on

es comenten els resultats obtinguts, se'n destaquen les conclusions principals i es proposen noves vies d'investigació.

El primer article presentat s'exposa en el segon capítol de la tesi, mostrant els resultats obtinguts en la caracterització de la litosfera elèctrica del Pirineu Central a partir de dades de BBMT i LMT. En aquest estudi s'han millorat els resultats previs proposats per Ledo (1996) i Pous et al., (1995a). La referència a l'article és:

- **Campanyà, J.**; Ledo, J.; Queralt, P.; Marcuello, A.; Liesa, M.; Muñoz, J.A. 2011. Lithospheric characterization of the Central Pyrenees based on new magnetotelluric data. *Terra Nova*. **23**, 213 - 219. doi: 10.1111/j.1365-3121.2011.01001.x.

El segon article el trobem en el tercer capítol de la tesi, mostrant els resultats obtinguts en l'estudi MT realitzat al Pirineu Occidental-Central. En aquest s'han caracteritzat les estructures geoelèctriques de la zona i s'ha determinat l'evolució de les estructures geoelèctriques al llarg de la serralada. Com a resultat destacat, s'ha observat per primer cop a Pirineus els processos de fusió parcial associats amb la IBSLC desencadenats a partir de tres mecanismes diferents. La referència a aquest article és:

- **Campanyà, J**.; Ledo, J.; Queralt, P.; Marcuello, A.; Liesa, M.; Muñoz, J.A. 2012. New geoelectrical characterization of a continental collision zone in the West-Central Pyrenees: Constraints from long period and broadband magnetotellurics. *Earth and Planetary Science Letters*, **333-334**, 112-121. doi: 10.1016/j.epsl.2012.04.018.

Finalment, el tercer article es mostra en el quart capítol de la tesi i està encarat a la millora de la tècnica geofísica de la MT, proposant un nou mètode per processar dades MT. La referència a l'article associat amb aquesta feina és:

- **Campanyà, J.**; Ledo, J.; Queralt, P.; Marcuello, A., Jones, A.G., 2013. Processing of Magnetotelluric data using inter-station tensor relationships. *Geophysical Journal International* (Under review).

R.4 DADES MT ADQUIRIDES ALS PIRINEUS

Als Pirineus s'han adquirit dos tipus diferents de dades MT. Les dades de banda ampla (BBMT) i les dades de llarg període (LMT). Les dades BBMT cobreixen un rang de períodes entre 0.001 segons i 1000 segons i s'acostumen a fer servir per estudis a escala cortical (p.e. Chandrasekhar et al., 2012; Ledo et al., 2011; Siniscalchi et al., 2012 i Zhao et al., 2012). Les dades LMT cobreixen un rang de períodes entre 20 segons i 20000 segons i s'utilitzen per caracteritzar les estructures geoelèctriques a majors profunditats (p.e. Rosell et al., 2011; Le Pape et al., 2012 i Kelbert et al., 2012). En total als Pirineus s'han enregistrat 82 estacions amb dades de BBMT i 29 amb dades LMT. La majoria de les dades s'han pres al llarg de quatre perfils creuant els Pirineus, cobrint una distància total de més de 500 km. (Figura R.5).

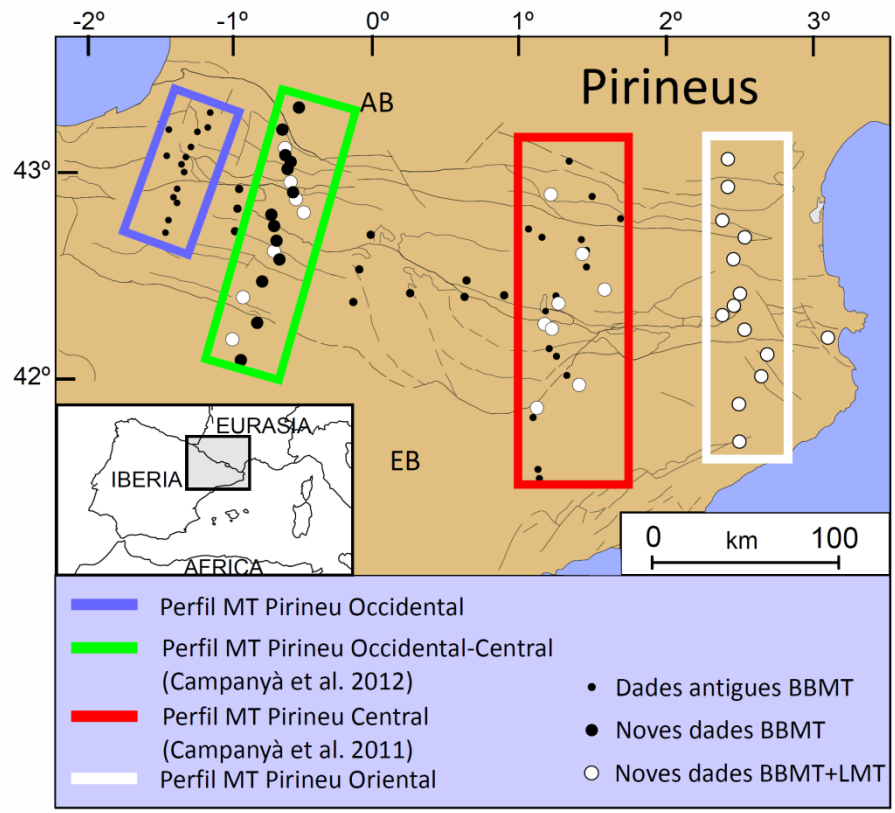

Figura R.5 Ubicació del punts on s'han pres dades MT. EB: Conca de l'Ebre. AB:Conca d'Aquitània.

R.5 MÈTODE MAGNETOTEL·LÚRIC

El mètode MT és una tècnica geofísica utilitzada per caracteritzar la resistivitat elèctrica del subsòl. Aquesta caracterització es du a terme a partir de relacions tensorials, dins el domini de freqüències, entre els camps elèctric i magnètic enregistrats simultàniament a la superfície de la zona d'estudi (Figura R.6). Aquesta relació tensorial també permet determinar la dimensionalitat de les estructures estudiades.

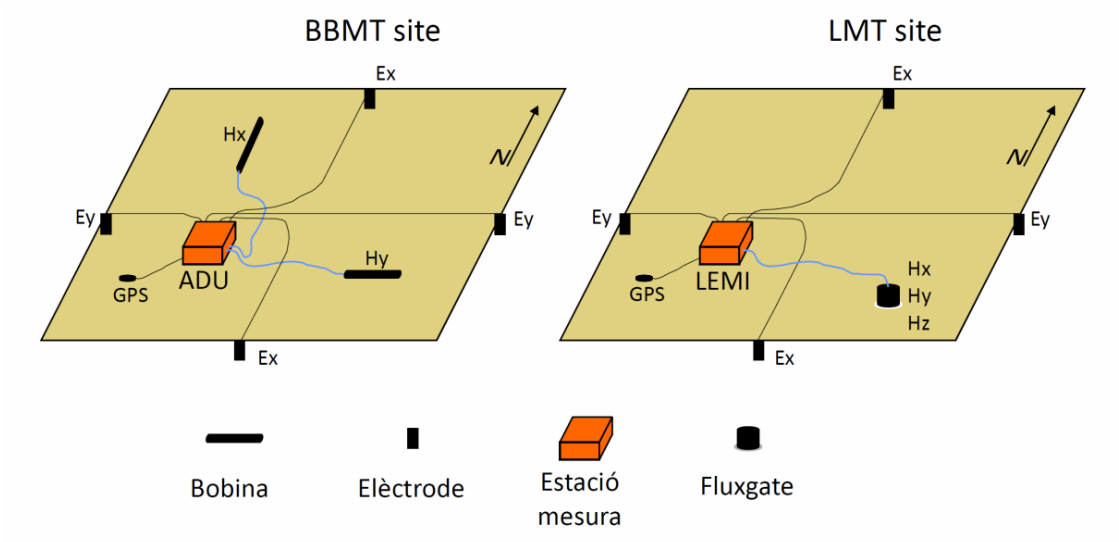

Figura R.6 Disposició dels aparells de mesura per dades BBMT i LMT.

Les variacions de camp elèctric i magnètic enregistrades a la superfície de la zona d'estudi són la superposició d'un camp primari de font natural provinent de la ionosfera i un camp secundari, resultant de la interacció entre el camp primari i les estructures del subsòl. Les relacions que s'estableixen entre els camps són dependents del període analitzat, entre 10^{-4} segons i 10^{5} segons, permetent adaptar el mètode MT a la profunditat d'estudi desitjada. Els períodes més curts s'utilitzen per estudis més superficials, caracteritzant la distribució de resistivitats de les primeres desenes de metres, mentre que els períodes llargs permeten determinar la resistivitat elèctrica d'estructures més profundes de fins a centenars de kilòmetres. Malgrat que en incrementar el període podem assolir majors profunditats, per contrapartida la resolució disminueix.

Els valors de resistivitat elèctrica del subsòl presenten típicament valors entre 10^{-2} ohm·m i 10^{6} ohm·m, mostrant un ampli ventall amb diferències de fins a vuit ordres de magnitud (Figura R7). Aquests valors de resistivitat poden estar relacionats amb diferents factors de manera que a l'hora d'interpretar els models de resistivitat elèctrica no només hem de fixar-nos en les estructures geològiques sinó també en aquells processos físics i químics que hi tenen lloc. És per això que de forma general, abans d'interpretar els valors de resistivitat elèctrica obtinguts, ens referirem a models geoelèctrics i estructures geoelèctriques, independentment de quina sigui la seva causa.

Degut al rang de períodes utilitzats en la MT, així com els valors de resistivitat elèctrica típics del subsòl, la caracterització de les estructures geoelèctriques està dominada per l'equació de difusió. Aquesta característica fa que els models geoelèctrics presentats per explicar les dades de camp siguin una imatge difusa de la resistivitat elèctrica del subsòl.

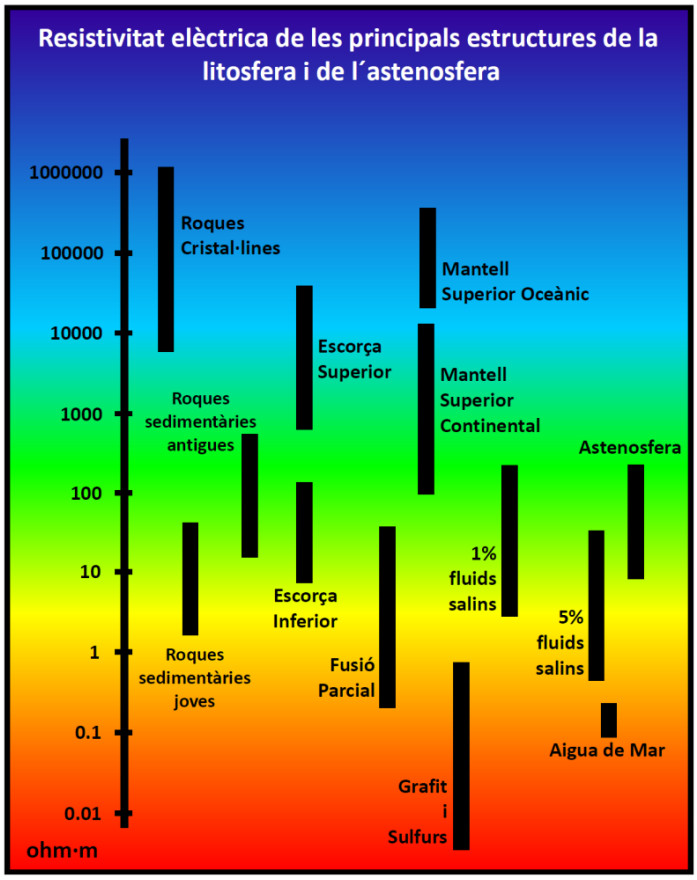

Figura R.7 Resistivitat elèctrica de la litosfera i l'astenosfera. Modificat de Haak and Hutton, 1986.

R.5.1 Funcions de transferència magnetotel·lúriques

Les funcions de transferència MT relacionen les variacions de camp elèctric i magnètic, a una determinada freqüència, aportant informació del subsòl. Aquestes relacions no depenen de les fonts de senyal i són constants al llarg del temps, si les estructures del subsòl no varien. En aquesta tesi es fan servir tres tipus de funcions de transferència. El tensor d'impedàncies MT (Neves, 1957; Cantwell, 1960 i Rokityanski, 1961), el qual permet determinar els valors de resistivitat elèctrica del subsòl. La funció de transferència geomagnètica (Parkinson, 1962 i Weise, 1962), que mostra variacions laterals de resistivitat elèctrica, i el tensor entre magnètics horitzontals (HMT) (Schmucker, 1970; Egbert and Booker, 1989), que relaciona els camps magnètics horitzontals enregistrats simultàniament en dues estacions ubicades en llocs diferents.

R.5.1.1 Tensor d'impedàncies

Es tracta d'un tensor de rang 2 que relaciona les components del camp elèctric horitzontal amb les components del camp magnètic horitzontal, per una certa freqüència, enregistrats simultàniament a la superfície de la zona d'estudi:

$$\begin{pmatrix} E_x(\omega) \\ E_y(\omega) \end{pmatrix} = \begin{pmatrix} Z_{xx}(\omega) & Z_{xy}(\omega) \\ Z_{yx}(\omega) & Z_{yy}(\omega) \end{pmatrix} \begin{pmatrix} B_x(\omega)/\mu \\ B_y(\omega)/\mu \end{pmatrix} \qquad (r.1)$$

on E_i són les components del camp elèctric horitzontal. $B_i = H_i \cdot \mu$, on H_i són les components del camp magnètic horitzontal, μ la permeabilitat magnètica i B_i les components de la inducció magnètica. El subíndex *i=x,y*. Z_{ij} són les components del tensor d'impedàncies MT, on *ij=xx,xy,yx,yy*. ω és la freqüència. A partir del mòdul i la fase de les components complexes del tensor podem determinar dues magnituds escalars i reals: la resistivitat aparent (r.2) i la fase (r.3).

$$\rho_{ij}(\omega) = \frac{1}{\omega\mu}\left|Z_{ij}\right|^2 \qquad (r.2)$$

$$\varphi_{ij}(\omega) = atan\left(\frac{Im\left(Z_{ij}(\omega)\right)}{Re\left(Z_{ij}(\omega)\right)}\right) \qquad (r.3)$$

On ρ_{ij} és la resistivitat aparent, φ_{ij} la fase i *ij=xx,xy,yx,yy*.

R.5.1.2 Funció de transferència geomagnètica

La funció de transferència geomagnètica és un vector complex adimensional i depenent de la freqüència que relaciona la component vertical del camp magnètic amb les components horitzontals del camp magnètic enregistrades simultàniament a la superfície de la zona d'estudi.

$$B_z(\omega) = (W_x(\omega) \quad W_y(\omega)) \begin{pmatrix} B_x(\omega) \\ B_y(\omega) \end{pmatrix} \qquad (r.4)$$

on B_z és la component vertical de la inducció magnètica i W_x i W_y les components de la funció de transferència geomagnètica.

R.5.1.3 Tensor entre magnètics horitzontals (HMT)

L'HMT és un tensor complex i adimensional de rang 2 depenent de la freqüència que relaciona les variacions de camp magnètic horitzontal enregistrades simultàniament en dues estacions 1 i 2.

$$\begin{pmatrix} B_x^1(\omega) \\ B_y^1(\omega) \end{pmatrix} = \begin{pmatrix} M_{xx}(\omega) & M_{xy}(\omega) \\ M_{yx}(\omega) & M_{yy}(\omega) \end{pmatrix} \begin{pmatrix} B_x^2(\omega) \\ B_y^2(\omega) \end{pmatrix} \qquad (r.5)$$

on M_{ij} són les components adimensionals del HMT, tenint $ij = xx, xy, yx, yy$.

R.5.2 Dimensionalitat de les estructures

Com ja s'ha comentat, gràcies a les relacions tensorials podem determinar la dimensionalitat de les estructures geoelèctriques. En aquesta tesi el tensor d'impedàncies i la funció de transferència geomagnètica s'han fet servir per caracteritzar la dimensionalitat de les estructures geoelèctriques dels Pirineus (Figura

R8 i R9). En el cas de la figura R8, la dimensionalitat s'ha determinat a partir del tensor d'impedàncies MT aplicant el mètode proposat per Groom and Bailey (1989) i seguint l'esquema de McNiece and Jones (2001). Les fletxes indiquen la direcció de les estructures i la seva llargada la compatibilitat de les dades amb la direcció proposada. Pel que fa la figura R9, la dimensionalitat s'estudia a partir de la funció geomagnètica representant-la com a vectors d'inducció (Schmucker, 1970) que apunten cap a els estructures de baixa resistivitat elèctrica. En el cas bidimensional les fletxes per diferents períodes han d'apuntar cap a una mateixa direcció, independentment del sentit.

A partir d'aquests resultats s'ha considerat que les estructures geoelèctriques dels tres perfils de més a l'Oest es poden modelitzar a partir de codis d'inversió bidimensionals mentre que en el cas del Pirineu Oriental es necessita fer una modelització tridimensional incloent el mar.

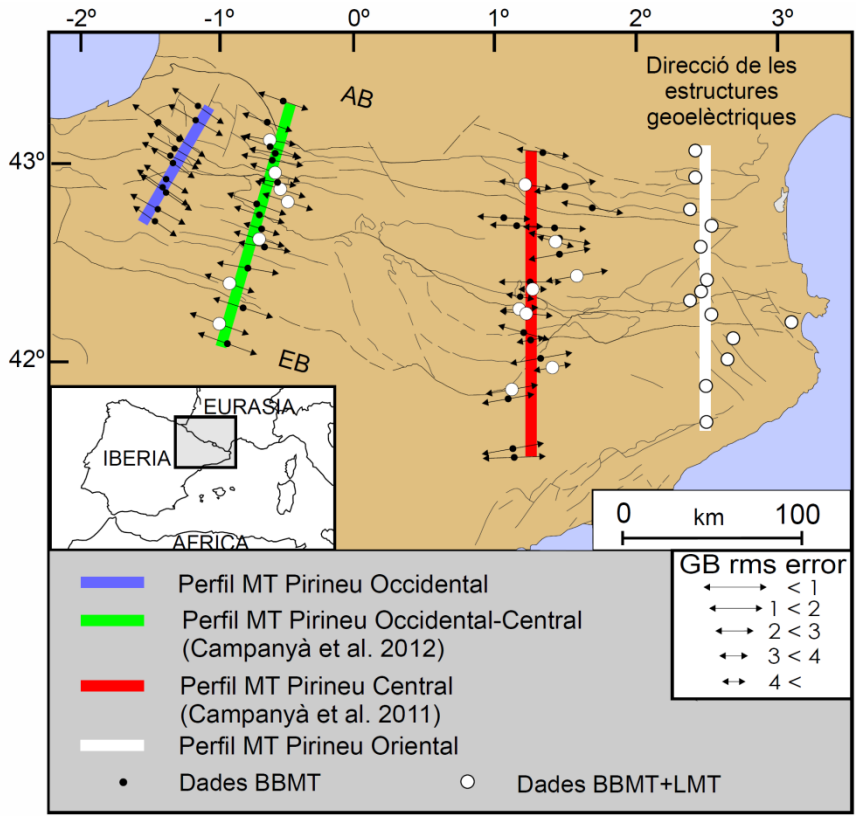

Figura R.8 Ubicació de les estacions MT de Pirineus amb l'anàlisi de la direcció de les estructures. A l'Est no s'han dibuixat ja que la zona és molt tridimensional i s'obtenen valors de RMS molt superiors a 4.EB: Conca de l'Ebre. AB:Conca d'Aquitània.

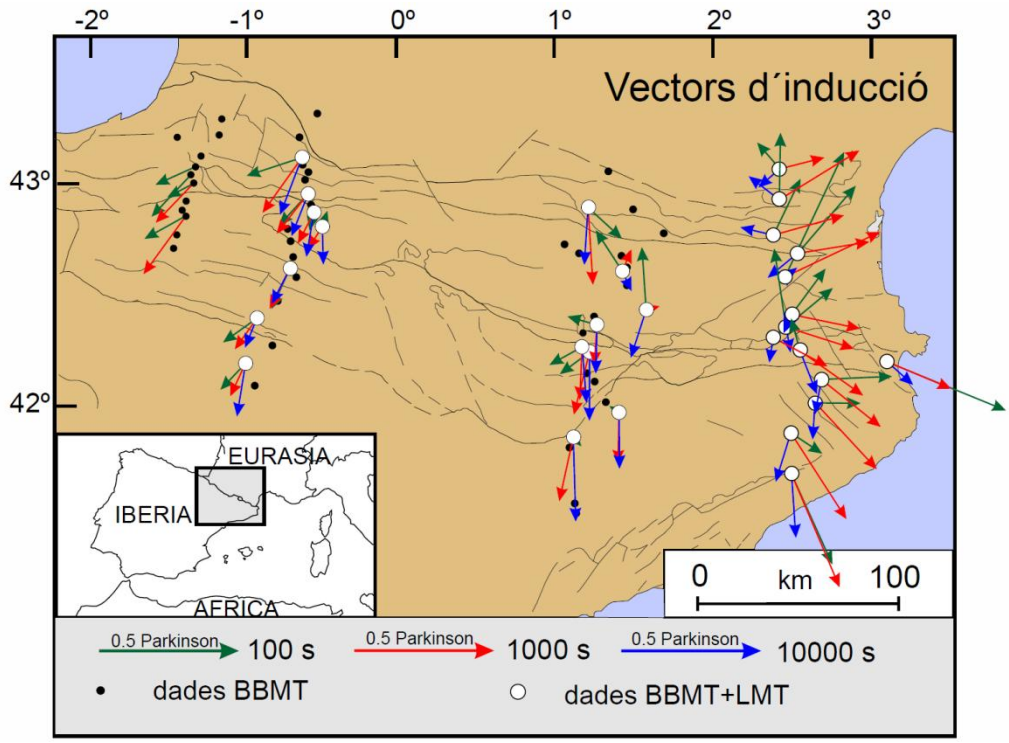

Figura R.9 Ubicació de les estacions MT a Pirineus amb la component real dels vectors d'inducció per tres períodes diferents. Vectors apunten cap a zones de baixa resistivitat elèctrica.

R.6 CARACTERITZACIÓ GEOELÈCTRICA DELS PIRINEUS

La caracterització geoelèctrica dels Pirineus s'ha fet principalment a partir dels resultats publicats al Pirineu Central (Campanyà et al., 2011) i al Pirineu Occidental-Central (Campanyà et al., 2012), capítols 2 i 3 de la tesi. De forma complementària s'han modelitzat també les dades adquirides al Pirineu Occidental ajudant a determinar la continuïtat de les estructures geoelèctriques cap a l'Oest.

R.6.1 Principals estructures geoelèctriques i la seva evolució al llarg de la serralada.

A partir de l'anàlisi de la direcció de les estructures geoelèctriques les dades MT s'han modelitzat solucionant el problema invers fent servir el codi de Rodi and Mackie (2001). Comparant els resultats obtinguts entre el Pirineu Central i el Pirineu Occidental-Central podem determinar les principals estructures geoelèctriques i la seva evolució (Figura R.10). Les dues principals estructures geoelèctriques estan relacionades amb la IBSLC, estructura M en la figura R.10, i amb l'astenosfera, estructura A en la figura R.10. També destaca l'estructura de baixa resistivitat elèctrica associada amb un límit Hercinià sota la conca de l'Ebre, estructura V en la figura R.10, i

el cos de baixa resistivitat elèctrica associat amb la presència de fluids i sediments del Silurià, estructura S en la figura R.10.

L'estructura geoelèctrica associada amb la IBSLC cabussa cap al nord en els dos perfils i té el límit superior voltant dels 30 km de profunditat. Aquesta mostra valors de resistivitat elèctrica, fins a una profunditat de 50 km, d'entre 2 Ω·m i 6 Ω·m. L'anàlisi geoquímic dut a terme per Campanyà et al. (2011) suggereix que les condicions de la IBSLC són les adequades per tenir fusió parcial. Fusió parcial per deshidratació de la moscovita i la biotita s'ha assumit com la hipòtesi que millor explica els resultats geofísics associats amb la IBSLC. Seguint el model proposat per Partzsch et al. (2000), es necessita entre un 4% i un 15% de fusió parcial per explicar els valors de resistivitat elèctrica observats en la IBSLC, fins a una profunditat de 50 km.

A profunditats superiors als 50 km, els dos perfils presenten variacions importants relacionades amb la IBSLC. AL Pirineu Central el cabussament és de 80°, el que fa que les propietats geoelèctriques de major profunditat quedin apantallades i no es puguin caracteritzar. Al Pirineu Occidental-Central, degut a que el cabussament és de 35°, les propietats geoelèctriques de la IBSLC poden ser caracteritzades fins a una profunditat de 70 km. Arribar a aquestes profunditats ha permès observar el procés de fusió parcial per deshidratació de la biotita suggerint una quantitat de fusió parcial entre el 15% i el 25%. Seguint els arguments d'Arzi (1978) aquesta quantitat de fusió parcial és suficient per produir migració de la fosa, el que explicaria la disminució de resistivitat elèctrica observada en el mantell superior de la placa Europea, sobre de la IBSLC.

Si ens fixem en la part inferior dels models geoelèctrics de la figura R.10 observem valors de baixa resistivitat elèctrica, entre 10 Ω·m i 70 Ω·m. Aquesta estructura geoelèctrica han estat associada amb l'astenosfera i el seu límit superior amb el LAB. L'absència de diferències geoelèctriques importants suggereix una astenosfera amb propietats similars sota els dos perfils. A partir de la profunditat del LAB, els models geoelèctrics proposen una placa Europea més gruixuda que la Ibèrica, prop de la zona de col·lisió, ubicant el LAB al voltant de 130 km de profunditat sota la placa Europea i al voltant de 90 km de profunditat sota la placa Ibèrica. Referent a la zona de col·lisió,

aquest s'ha determinat només en el perfil del Pirineu Occidental-Central a una profunditat similar a la obtinguda sota la placa Europea. En el Pirineu Central no s'ha pogut determinar degut a l'efecte d'apantallament generat per l'estructura de baixa resistivitat elèctrica associada amb la IBSLC.

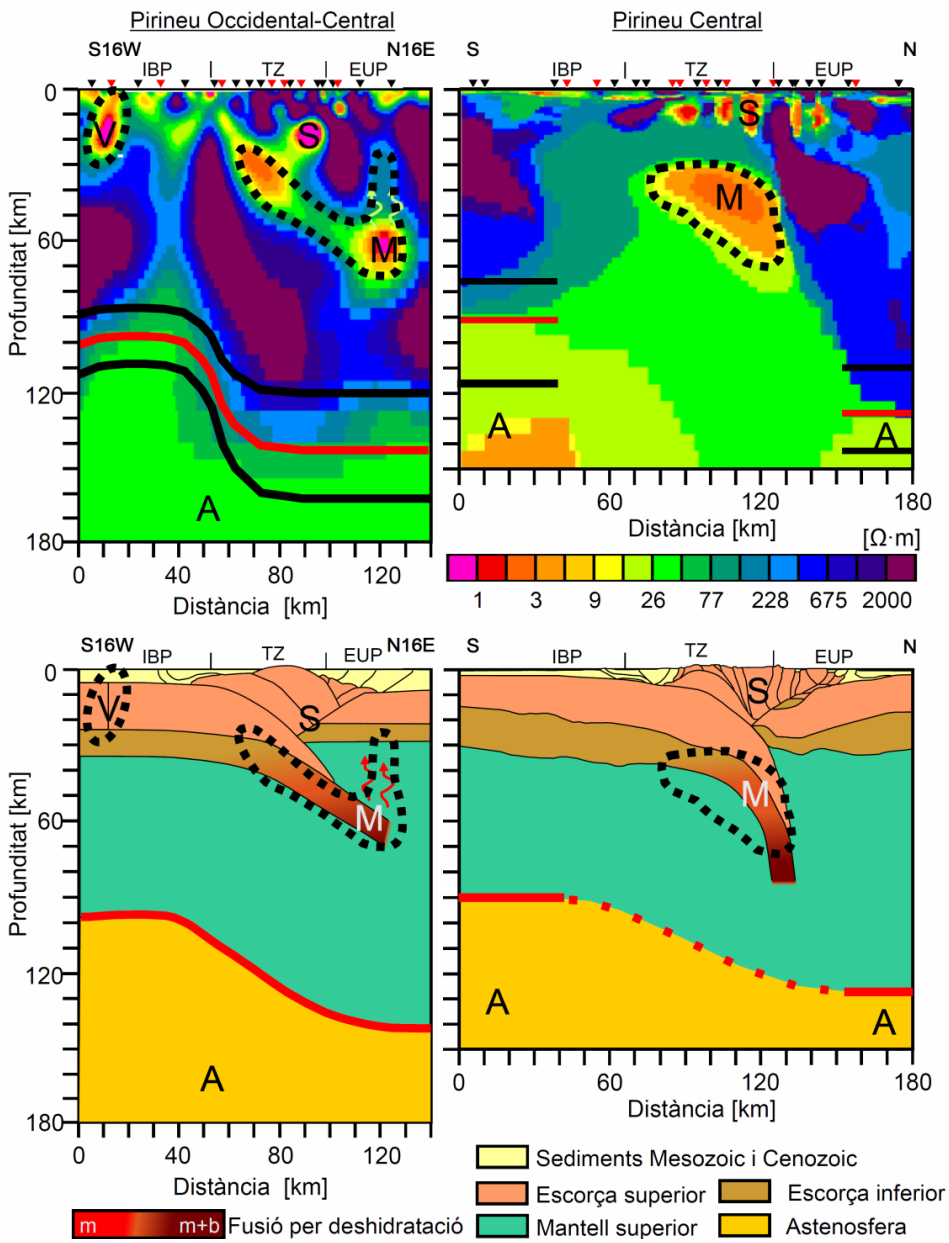

Figura R.10 Models magnetotel·lúrics del Pirineu Occidental-Central (esquerra) i del Pirineu Central (dreta). Línies negre discontinues: contorn de les estructures geoelèctriques. Línia vermella: límit litosfera astenosfera (LAB) determinat a partir de dades MT. Línies negres la resolució en determinar el LAB. A sota, models geològics a partir dels resultats geoelèctrics obtinguts. M, estructura geoelèctrica associada amb la IBSLC. A, estructura geoelèctrica associada amb l'astenosfera. V, estructura geoelèctrica associada amb el límit Hercinià, S, estructura associada amb sediments del Silurià. EUP, placa Europea, TZ, zona de transició; IBP, placa ibèrica. A la llegenda: *m* quan la fusió parcial es produeix per deshidratació de la moscovita. *m+b* quan es produeix per deshidratació de la moscovita i la biotita.

L'anàlisi de les estructures corticals s'ha fet també a partir de les dades adquirides al Pirineu Occidental, les quals s'han modelitzat obtenint per primer cop un model geoelèctric de la regió (Figura R.11a). La figura R.11b compara les dades utilitzades amb les respostes del model proposat. Comparant els resultats geoelèctrics entre els perfils del Pirineu Occidental i del Pirineu Occidenta-Central podem observar la propagació de l'estructura M, associada amb la fusió parcial de la IBSLC, cap a l'Oest (Figura R.12).

A nivells més superficials, en els tres perfils MT, trobem una estructura amb valors baixos de resistivitat elèctrica associada amb fluids i sediments del Silurià (estructura S en les figures R10 i R12). Al Pirineu Central aquesta estructura es troba fins a una profunditat de 10 km, mentre que al Pirineu Occidental-Central i al Pirineu Occidental es troba entre 10 km i 20 km de profunditat. Aquesta diferència es pot explicar a partir del cabussament de les estructures del Pirineu cap a l'Oest, preservant nivells estructurals més alts al Pirineu Occidental-Central que al Pirineu Central, i la corresponent terminació cap a l'Oest de la zona Axial observada al Pirineu Central.

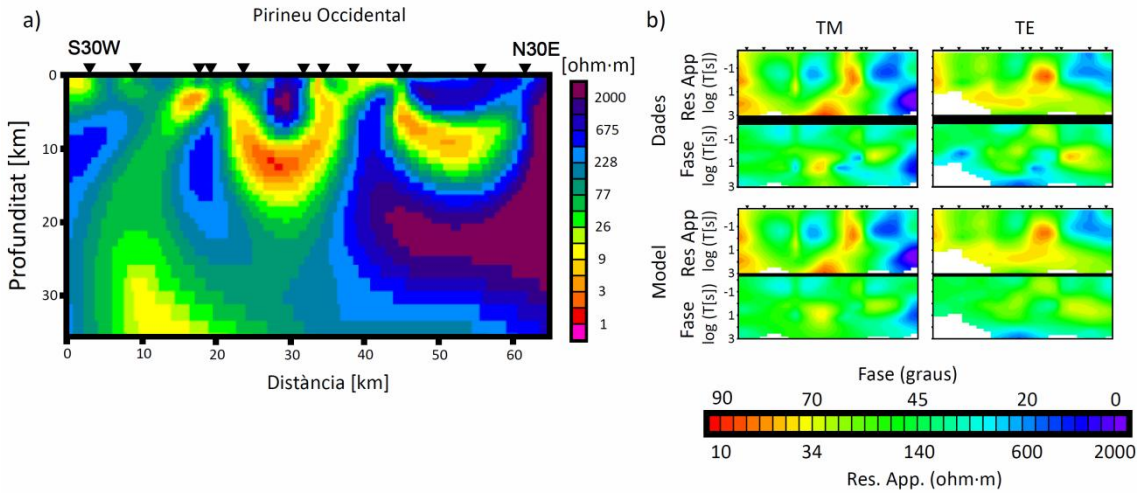

Figura R.11 (a) Model geoelèctric del Pirineu Occidental (b)Comparació entre la resposta del model i les dades fetes servir per la inversió pels modes TE i TM de la resistivitat aparenti la fase. L'ajust entre dades i resposta del model té un error quadràtic mitjà de 1.6.

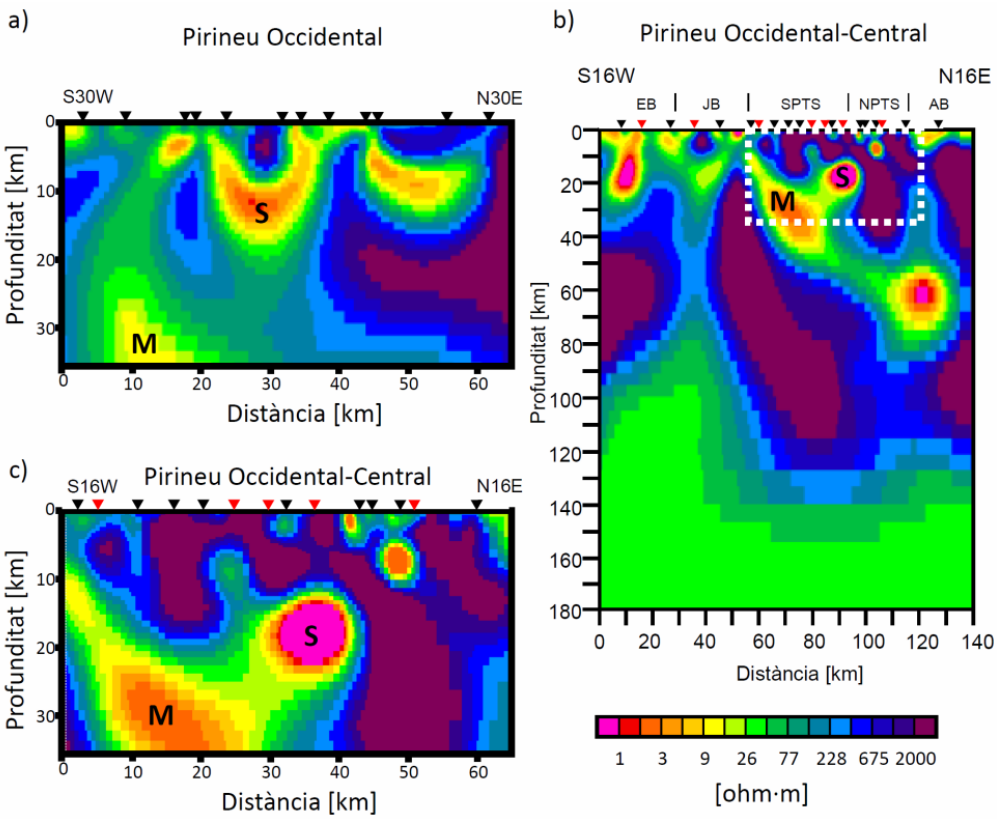

Figura R.12 a) Model geoelèctric del Pirineu Occidental. b) Model geoelèctric del Pirineu Occidental-Central proposat per Campanyà et al. (2012). Línies blanques discontinues marquen la zona equivalent amb el perfil del Pirineu Occidental. c) Ampliació de l'àrea requadrada. S, estructura geoelèctrica associada amb sediments del Silurià. M, estructura geoelèctrica associada amb fusió parcial de la IBSLC. EB: Ebro Basin; SPZ: South Pyrenean zone; AZ: Axial zone; NPZ: North Pyrenean zone; NPF: North Pyrenean fault; AB:Aquitanian Basin;

Finalment trobem l'estructura de baixa resistivitat elèctrica totalment enterrada sota la conca de l'Ebre a profunditats de l'escorça mitja i superior sota el Pirineu Occidental-Central (estructura V en la Figura R.10). Com que no s'observen estructures que afectin la conca de l'Ebre en aquesta zona, l'estructura geoelèctrica V ha estat associada amb processos tectònics de l'orogènia Herciniana. Seguint la divisió feta per Martínez Catalán et al. (2007) aquesta estructura es podria correspondre amb la prolongació del límit entre la zona Asturiana Occidental Lleonesa i la zona Ibèrica Central. Degut a la similitud amb d'altres límits de l'orogènia Herciniana (Da Silva et al. 2007; Muñoz et al., 2008; Pous et al., 2004, 2011) proposem la presència de grafit per explicar els baixos valors de resistivitat elèctrica observats.

R.6.2 Comparació amb models geofísics independents

Comparar els resultants geoelèctrics amb els resultats d'altres tècniques geofísiques ajuda a determinar les propietats físiques i químiques del subsòl així com també les estructures geològiques. A continuació es comparen els resultats geoelèctrics obtinguts a Pirineus amb els d'altres tècniques geofísiques.

R.6.2.1 Comparació amb els perfils de sísmica profunda

Els perfils de sísmica profunda duts a terme al Pirineu Central i al Pirineu Occidental-Central, interpretats per Muñoz (1992) i Muñoz(2002), respectivament, mostren les estructures geològiques a escala cortical. Si les comparem amb els resultats de MT podem associar les anomalies geoelèctriques amb estructures geològiques del subsòl (Figura R.13). Comparant aquestes dades s'ha observat que la IBSLC caracteritzada a partir dels models de sísmica profunda és coincident amb l'estructura de baixa resistivitat elèctrica obtinguda en els models de MT. Aquest tipus de comparació també ha servit per associar l'estructura S amb la presència de fluids i sediments associats amb el contacte de Gavarnie.

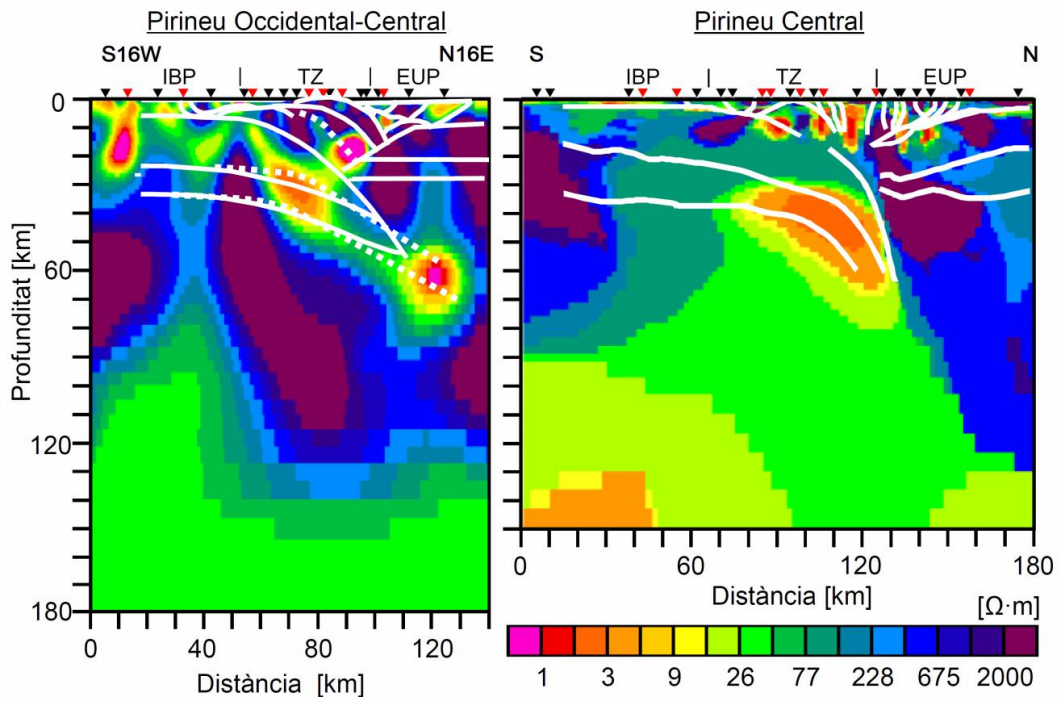

Figura R.13 Model geoelèctric del Pirineu Occidental-Central (Campanyà et al., 2012) i del Pirineu Central (Campanyà et al., 2011). Línies blanques mostren els models geològics proposats per Muñoz (1992) i Muñoz (2002) al Pirineu Central i al Pirineu Occidental-Central, respectivament. Línies blanques discontinues mostren els canvis proposats a partir dels models de MT. EUP: Placa Europea; TZ: Zona de transició; IBP: Placa Ibèrica.

R.6.2.2 Comparació amb models de tomografia sísmica

Sobre els models de tomografia sísmica obtinguts per Amaru et al. (2008) i Koulakov et al. (2009) i Souriau et al. (2008) a la figura R.14 s'han superposat els contorns de les principals estructures geoelèctriques a profunditats del mantell superior (estructures M i A de la figura R.10). Els resultats proposats per Amaru et al. (2008) i Koulakov et al. (2009) són bastant semblants entre ells, però no és el cas del model proposat per Souriau et al. (2008) que difereix de forma considerable dels altres dos models. En l'anàlisi posterior en fixarem en els resultats proposats per Koulakov et al. (2009) i Amaru et al (2008), que al mateix temps són més consistents amb els resultats geoelèctrics.

A partir de la figura R.14 veiem que l'estructura de baixa resistivitat elèctrica associada amb la IBSLC coincideix amb una disminució de la velocitat de les ones P i S. També veiem que, excepte en el model de ones S del Pirineu Central proposat per Koulakov et al. (2009), està associada amb una anomalia negativa de velocitats. A més a més, el límit inferior de la IBSLC caracteritzada al Pirineu Occidental-Central coincideix amb el límit inferior de l'anomalia de velocitats negativa del model d'ones S (Figura R.14a), corroborant una IBSLC fins a 70 km de profunditat. A major profunditat, el models generats a partir d'ones S mostren una anomalia negativa a la part inferior dels models que ha estat associada amb l'astenosfera i el seu límit superior amb el LAB sísmic. Si comparem el LAB elèctric obtingut a partir de models de MT amb el LAB sísmic proposat per Koulakov et al. (2009) veiem que els resultats són similars sota la placa Ibèrica i Europea al Pirineu Central i sota la placa Europea i la zona de col·lisió en el Pirineu Occidental-Central. Sota la Placa Ibèrica al Pirineu Occidental-Central el model de tomografia sísmica presenta variacions molt suavitzades de manera que el LAB sísmic no queda ben determinat.

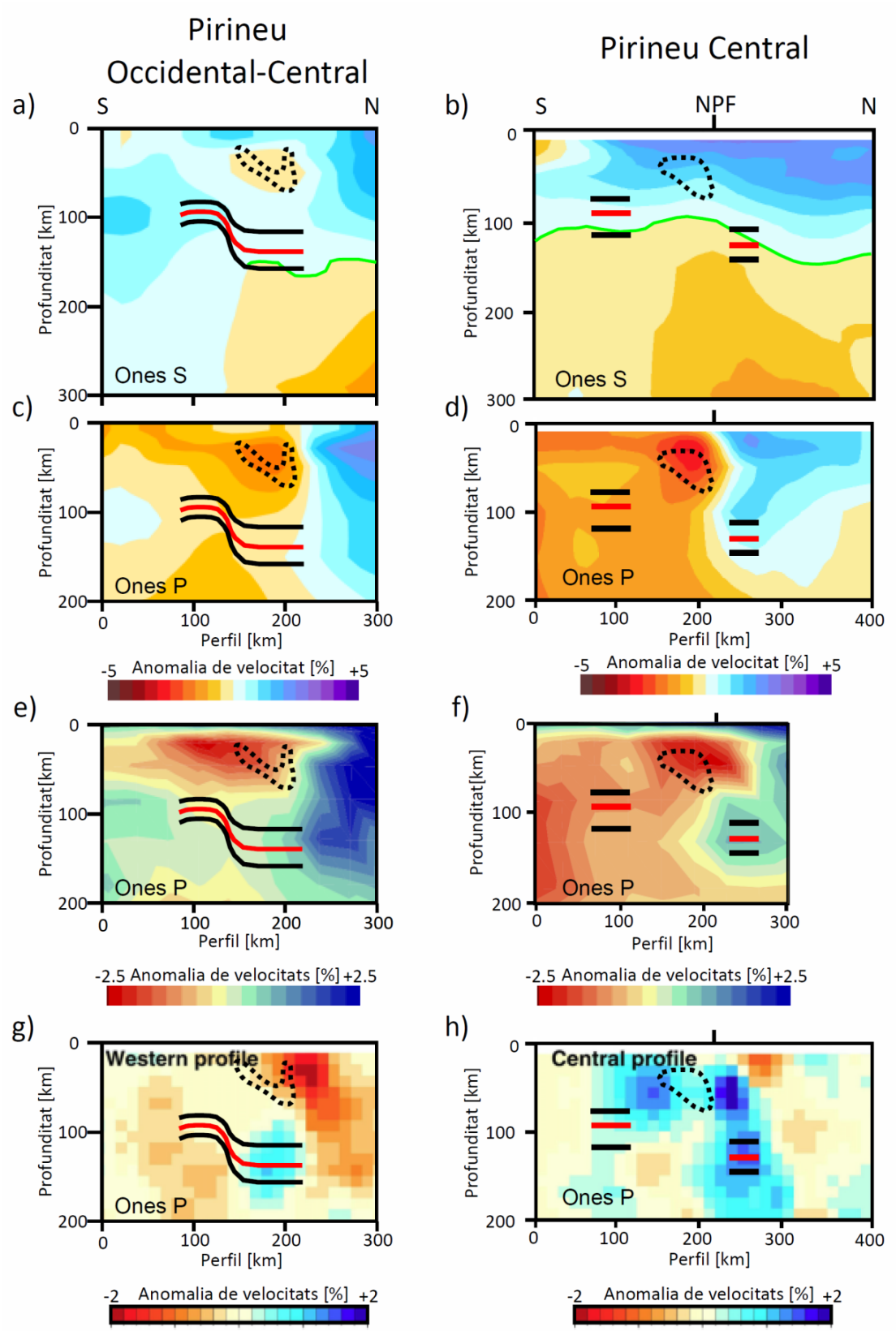

Figura R.14 Models de tomografia sísmica proposats per Koulakov et al. (2009) (*a,b,c* i *d*). Models de tomografia sísmica proposats per Amaru et al. (2008) (*e* i *f*). Models de tomografia sísmica proposats per Souriau et al. (2008) (*g* i *h*). Superposat en els sis models: Contorn de la zona de fusió parcial (línia negre discontinua) i LAB elèctric (línia vermella i les negres).Línia verda: LAB sísmic.

R.6.2.3 Comparació amb estudis basats en dades de flux de calor i gravimetria

Els valors de baixa resistivitat elèctrica associats amb la IBSLC han estat explicats a partir de les geotermes proposades per Glover et al. (2001) i Zeyen i Fernández (1994). S'ha assumit la hipòtesi de fusió parcial per deshidratació de la moscovita i la biotita com a fenomen que millor explica els valors de resistivitat elèctrica observats a la IBSLC sota el Pirineu Central. Els resultats mostrats per Tesauro et al. (2009), els quals mostren que no hi ha grans anomalies tèrmiques entre el Pirineu Central i el Pirineu Occidental-Central, permeten fer servir els mateixos arguments al Pirineu Occidental-Central i al Pirineu Occidental. A major profunditat, el model tèrmic proposat per Tesauro et al. (2009), el qual associa el LAB tèrmic amb la geoterma dels 1200 ^{o}C, suggereix que el LAB es troba al voltant dels 120 km de profunditat, resultat consistent amb els LAB sísmic i elèctric. Pel que fa els models basats en dades gravimètriques, tant al Pirineu Central com al Pirineu Occidental-Central tots els resultats estan d'acord en acceptar la presència de la subducció de l'escorça Ibèrica inferior (p.e. Casas et al., 1997; Jammes et al., 2010; Pedreira et al., 2007 i Vacheur and Souriau, 2001).

R.7 DESENVOLUPAMENT METODOLÒGIC

En aquesta tesi s'ha proposat un nou mètode per processar dades MT d'una estació local a partir de relacions tensorials entre estacions, relacionant les variacions de camp elèctric i magnètic de l'estació local amb les variacions de camp magnètic d'una estació veïna. El mètode proposat permet determinar el tensor d'impedàncies i la funció de transferència geomagnètica de l'estació local *a* [$\boldsymbol{Z}_a(\boldsymbol{e}_a, \boldsymbol{h}_a)$ i $\boldsymbol{W}_a(h_z^a, \boldsymbol{h}_a)$] combinant les relacions tensorials amb una altra estació *b* [$\boldsymbol{Z}_{ab}(\boldsymbol{e}_a, \boldsymbol{h}_b)$, $\boldsymbol{S}_{ab}(h_z^a, \boldsymbol{h}_b)$ i $\boldsymbol{M}_{ba}(\boldsymbol{h}_b, \boldsymbol{h}_a)$] seguint els passos del mètode proposat [$\boldsymbol{Z}_a = \boldsymbol{Z}_{ab}\boldsymbol{M}_{ba}$ i $\boldsymbol{W}_a = \boldsymbol{S}_{ab}\boldsymbol{M}_{ba}$].

$\boldsymbol{e}$ representa les components horitzontals del camp elèctric, $\boldsymbol{h}$ les components horitzontals del camp magnètic, h_z la component vertical del camp magnètic. Els subíndexs *a* i *b* fan referència a l'estació on s'han mesurat els camps. $\boldsymbol{Z}, \boldsymbol{W}, \boldsymbol{S}$ i $\boldsymbol{M}$ són el tensor d'impedàncies MT, la funció de transferència geomagnètica, la funció de

transferència geomagnètica fent servir els camps magnètics de dues estacions diferents i el tensor entre camps magnètics horitzontals, respectivament. Quan només hi ha un subíndex significa que totes les components han estat mesurades al mateix punt i quan tenen dos subíndexs vol dir que es fan servir dades mesurades en dos llocs diferents.

Apart del desenvolupament teòric també s'han fet varies probes amb dades de camp enregistrades al Pirineu Oriental i amb les dades magnètiques proporcionades pels observatoris geomagnètics de Chambon de la Forêt (CLF) i Furstenfeldbruck (FUR) (Figura R.15). Les diferents proves realitzades han permès determinar la validesa i l'aplicabilitat del mètode proposat en determinar el tensor d'impedàncies i la funció de transferència geomagnètica de l'estació local, independentment de les estacions fetes servir com a estacions veïnes. La figura R.16 mostra el resultat obtingut en processar les dades de *a* fent servir els magnètics de *b* o els de *c*, fent referència remota (Gamble et al., 1979ab) amb CLF i FUR, respectivament.

El mètode proposat té l'avantatge que les variacions dels camps elèctric i magnètic de l'estació local no s'han de mesurar simultàniament. Això permet millorar el processat de dades MT quan les series temporals dels camps magnètics s'han truncat al cap de pocs dies de mesura (Figura R.17).

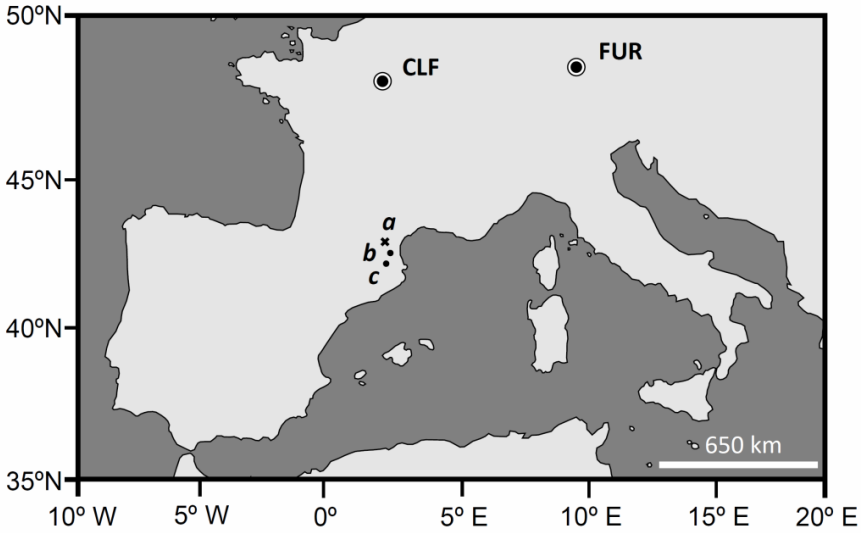

Figura R.15 Mapa amb la ubicació dels punts on s'han pres les dades de MT. *a, b* i *c* són els punts mesurats al Pirineu Oriental. CLF i FUR els observatoris geomagnètics.

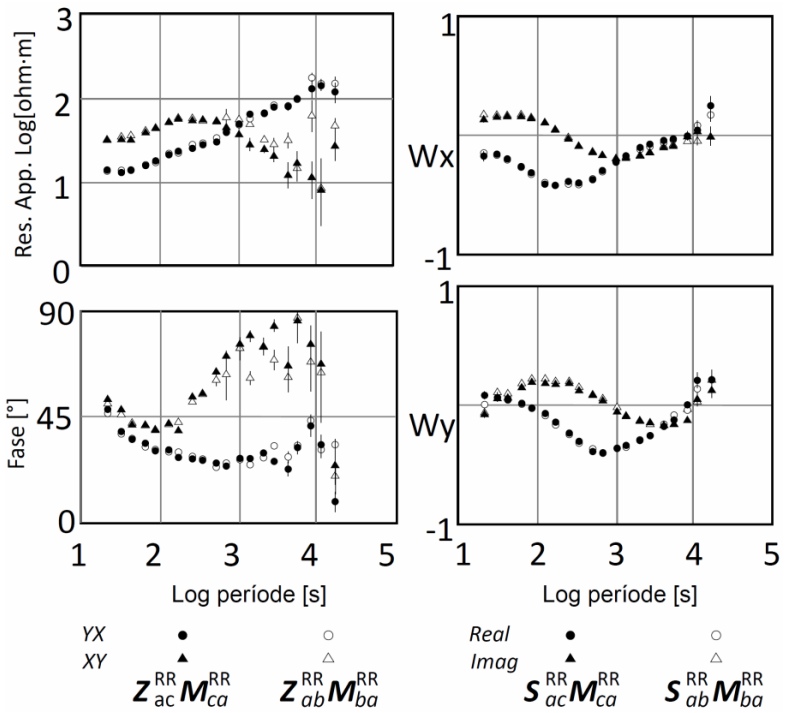

Figura R.16 Resistivitat aparent, fase i funció de transferència geomagnètica de l'estació *a* calculats a partir del mètode proposat fent servir els camps magnètics horitzontals del site *b* fent referència remota amb CLF i fent servir els camps magnètics de l'estació *c* fent referència remota amb FUR.

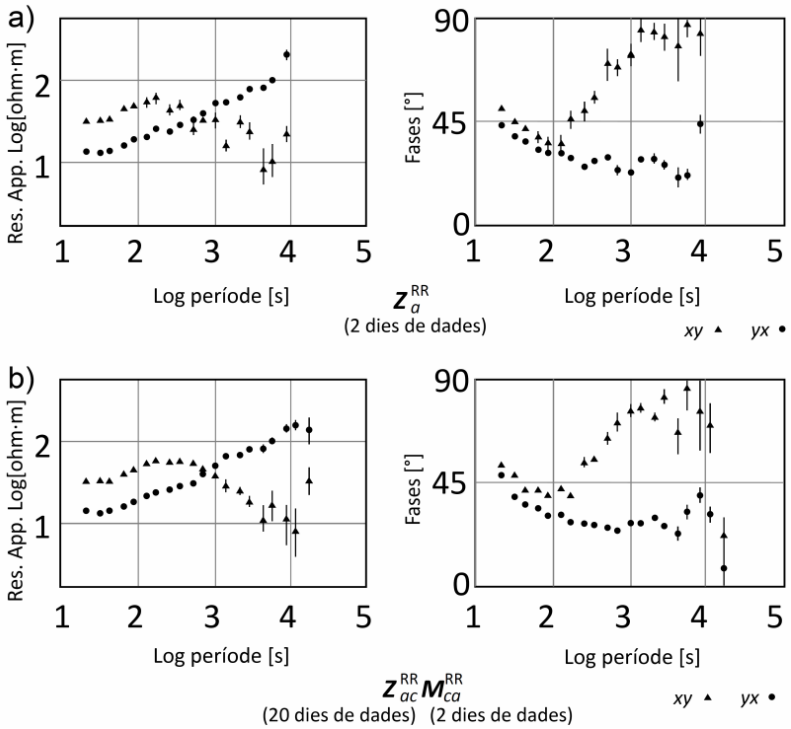

Figura R.17 Resistivitat aparent i fase de l'estació *a* quan els camps elèctrics han estat mesurats durant 20 dies però els magnètics només durant 2 dies. (a) Fent el processat local amb referència remota amb FUR. (b) Processant les dades seguint el mètode proposat utilitzant els magnètics horitzontals de l'estació *c* i fent referència amb l'estació FUR. Amb el processat normal només s'han pogut fer servir dos dies de dades mentre que seguint el mètode proposat s'han pogut aprofitar els 20 dies de dades del camp elèctric.

Com mostra l'exemple de la figura R.17, fent servir el mètode proposat no cal mesurar els camps magnètics durant el mateix nombre de dies que el camp elèctric. Aquesta propietat també permet modificar les campanyes de camp, reduint el nombre de sensors magnètics utilitzats. Permet fer servir un mateix sensor per calcular el camp magnètic a diversos llocs al mateix temps que es mesuren els camps elèctrics de cada un dels llocs.

R.8 CONCLUSIONS

Els objectius de la tesi relacionats amb la caracterització de la litosfera elèctrica dels Pirineus i els desenvolupament metodològic encarat a millorar el processat de dades MT han estat assolits amb els resultats obtinguts a partir dels tres articles dels que consta la tesi. També s'ha mostrat un nou perfil geoelèctric al Pirineu Occidental caracteritzant les estructures geoelèctriques de l'escorça d'aquesta regió.

Una de les principals estructures geoelèctriques observades sota els tres perfils MT és l'associada amb la subducció de l'escorça Ibèrica inferior (IBSLC). La nova caracterització mostra diferències respecte els estudis anteriors (Ledo, 1996; Ledo et al., 2000 i Pous et al, 1995a). Sota del Pirineu Central la diferència més important està relacionada amb el límit superior de l'estructura de baixa resistivitat elèctrica relacionada amb IBSLC, que s'ha determinat 9 km més profund que en els estudis previs. Aquesta modificació encaixa millor amb la hipòtesi de fusió parcial. En el Pirineu Occidental-Central el nou model MT mostra per primer cop als Pirineus tres fases diferents associades amb la fusió parcial de la IBSLC: Fusió parcial per deshidratació de la moscovita, fusió parcial per deshidratació de la moscovita i la biotita i finalment migració de la fosa provinent de la part més profunda de la IBSLC. La coincidència d'aquesta estructura geològica amb la part inferior de l'anomalia de velocitats de les ones S (Koulakov et al., 2009) i la presència d'activitat sísmica en aquesta zona (Koulakov et al., 2009), ha suggerit estendre la IBSLC fins a 70 km de profunditat. En el perfil MT del Pirineu Occidental el límit superior de l'estructura geoelèctrica associada amb la IBSLC es troba també al voltant de 30 km de profunditat,

mostrant valors de resistivitat elèctrica semblants als observats sota el Pirineu Central i el Pirineu Occidental-Central.

Pel que fa a les estructures geoelèctriques corticals, els valors de baixa resistivitat elèctrica observats sota la conca de l'Ebre al Pirineu Occidental-Central s'han associat a la presència de grafit en un límit tectònic Hercinià. A la zona de col·lisió entre plaques, a escala cortical, l'estructura de baixa resistivitat elèctrica associada amb la presència de fluids i sediments del Silurià s'ha observat en els tres perfils de MT, caracteritzant la seva evolució al llarg de la serralada.

Si mirem la base dels models MT del Pirineu Central i del Pirineu Occidental-Central, l'astenosfera s'ha caracteritzat amb valors de resistivitat elèctrica entre 10 Ω·m i 70 Ω·m. El seu límit superior, associat amb el LAB, s'ha determinat al voltant de 130 km de profunditat sota la placa Europea i al voltant de 90 km de profunditat sota la placa Ibèrica, suggerint una placa Europea més gruixuda que la Ibèrica, a prop de la zona de col·lisió.

El fet de comparar els resultats obtinguts amb altres tècniques geofísiques ha permès associar les estructures geoelèctriques amb estructures geològiques a nivell cortical, avaluar la hipòtesis de fusió parcial per explicar els valors de baixa resistivitat elèctrica de la IBSLC, associar amb el grafit l'anomalia elèctrica observada sota la conca de l'Ebre i corroborar la profunditat del LAB elèctric comparant els resultats obtinguts amb els LABs sísmics i tèrmics.

Com a perspectives de futur hi ha dues línies relacionades amb el mètode MT i la seva aplicació als Pirineus que es podrien dur a terme en un futur proper. Primerament, seria interessant modelitzar les dades del Pirineu Oriental a partir d'algoritmes d'inversió tridimensionals que permetessin incloure l'efecte del mar a les dades o directament fer un model tridimensional dels Pirineus des del Mar Mediterrani fins a l'Oceà Atlàntic aprofitant els 82 punts de mesura amb dades MT enregistrades al llarg dels Pirineus. Per altra banda, també seria interessant caracteritzar la propagació

lateral de l'estructura de molt baixa resistivitat elèctrica descoberta sota la conca de l'Ebre.

Pel que fa a la millora metodològica, s'ha proposat un nou mètode per processar dades MT d'una estació local fent servir relacions tensorials amb una estació veïna, sense haver d'enregistrar les variacions dels camps elèctrics i magnètics de l'estació local simultàniament. Els diferents tests duts a terme amb dades de camp han corroborat la validesa i fiabilitat del mètode. S'han mostrat dos avantatges importants relacionats amb el fet de no haver d'enregistrar simultàniament les variacions de camp elèctric i magnètic de l'estació local. La millora el processat de dades MT quan les series temporals dels camps magnètics s'han truncat i la possibilitat de modificar les campanyes de camp traient més profit dels equips de mesura.

1. INTRODUCTION

1.1 MOTIVATION AND OVERVIEW

The outermost layer of the Earth, the lithosphere, is divided in seven major tectonic plates and several micro-tectonic plates (i.e. Anderson, 2002 and Gordon, 2000). These plates are non-stables and the relative motion between them is dominated by the tectonic processes, which have been creating, shaping and destroying the lithosphere over millions of years. A main tectonic process that plays a primary role in the development of the continents, responsible for the formation of large mountain ranges like the Himalaya and Alps, is continental collision. Geophysical techniques determine the physical properties of the subsurface and help to understand the evolution of the lithosphere and the physical and chemical processes associated with this tectonic scenario (i.e. Cloetingh et al., 2010; Liang et al., 2012 and Unsworth, 2009). This thesis shows the role of the magnetotelluric (MT) geophysical technique constraining the geoelectrical structures of the subsurface at lithospheric scale. In the last thirty years, large amount of theoretical and technological improvements have allowed the use of the MT method in many regions with different aims, adapting the MT method to the specific requirements of each study. Thanks to this developments, MT studies have been undertaken from the deep sea (i.e. Baba et al., 2006; Heinson et al., 2000) to the highest mountain ranges on Earth (i.e. Le Pape et al., 2012; Kelbert et al., 2012) constraining the electrical resistivity of the subsurface in a large variety of regions for academic and commercials proposes.

In this thesis the MT technique has been used to characterize the geoelectrical structures, at lithospheric-scale, associated with the continental-collision zone that resulted in the Pyrenees. New MT data acquired in the Pyrenees, as well as old data (Ledo, 1996; Ledo et al., 2000 and Pous et al., 1995a) reworked in this work, has been

used. The motivation to reconsider the previous MT data comes from two main improvements in the MT method that have not been applied in the previous studies. The first improvement is the development of two-dimensional inversion codes (deGroot-Hedlin and Constable, 1990; Rodi and Mackie, 2001; Siripunvaraporn and Egbert, 2000 and Smith and Booker, 1991), avoiding to have to obtain the geoelectrical models of the Pyrenees by trial-and-error fitting of the data. The second improvement is the possibility of acquire long period magnetotelluric (LMT) data, which better determine the geoelectrical structures of the upper-mantle. Both advances have been applied to obtain the geoelectrical models of the Pyrenees.

The thesis also contains a methodological innovation to process MT data of a local site using inter-station tensor relationships with a neighbouring site. The processing of the MT data consist in calculate the tensor relationships between the electric and magnetic time-varying fields simultaneously recorded on the surface of the study area. This process implies that if one of the recorded components became useless the tensor relationship of the local site cannot be constrained. The proposed method improves the results obtained when some of the components recorded at the local site have been truncated. The motivation of this methodological innovation comes from the problems experienced in the acquisition of the electric and magnetic fields time series in the MT surveys carried out in the last four years, not only in the Pyrenees, but also in the Atlas mountains in Morocco (Ledo et al., 2011) and in the Betic Cordillera (Rosell et al., 2011).

1.1.1 Geological context of the Pyrenees

The Pyrenees are a doubly-vergent collisional orogen resulted from the continental collision between Iberian and European plates from Late Cretaceous to Early Miocene. This convergence resulted in the subduction of the Iberian continental crust below the continental crust of the European plate along the range. (Muñoz, 1992; Olivet, 1996 and Rosenbaum et al., 2002). The Pyrenean range extends for some 1300 km from the Eastern Alps, along the Mediterranean coast to the Atlantic Ocean northwest of the Iberian Peninsula (Muñoz, 2002). In this thesis we are focused on the Pyrenees that

borders France and Spain, which are flanked by the Aquitaine basin and the Ebro basin to the north and to the south, respectively.

This part of the Pyrenees has some differences along the strike at crustal depths, which led to divide it in three main regions: the Eastern Pyrenees, the Central Pyrenees and the West-Central Pyrenees (Figure 1.1). In the Central Pyrenees the crustal structural geometry consists of an asymmetric double-wedge orogenic system with the Southern Pyrenees being wider and involving more than 100 km of the shortening of the total estimated shortening of 165 km across the entire orogeny (Beaumont et al., 2000). In the West-Central Pyrenees the structural style changes with respect the Central Pyrenees and the basement thrust sheets of the interior part of the chain are imbricate instead of being piled on the top of each other to form antiformal stack (Muñoz, 2002; Teixell, 1998). In the Eastern Pyrenees, the South Pyrenean Trust sheets are narrower in a N-S direction than in Central Pyrenees and provided that the amount of shortening is similar in both regions a change in the structural geometry must occur. In fact, the Eastern Pyrenees thrust sheets are mainly piled one on top of each other instead of imbricate as observed in Central Pyrenees (Vergés et al., 1995).

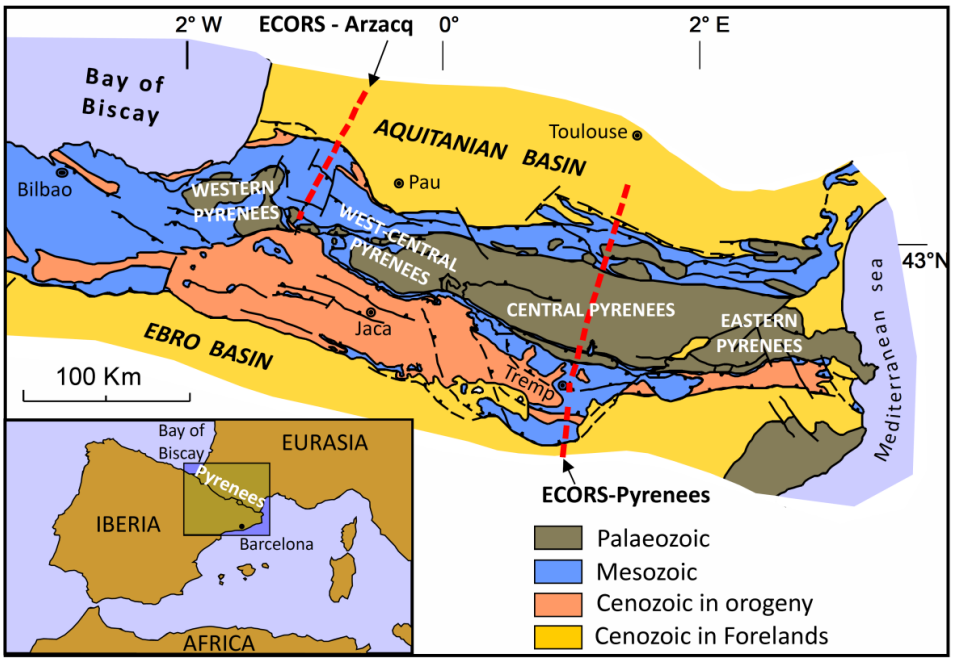

Figure 1.1 Geologic sketch map of the Pyrenees showing the main longitudinal and transverse divisions of the chain. Red lines are deep seismic profiles (Modified from Teixell (1996)).

In the study area, the Pyrenees can be divided in three main lithological units, each one with their own mechanical behaviour. The first one, which constitutes the basement rocks, corresponds to Palaeozoic materials (600-300 Ma). These materials generally are from sedimentary origin although there are some volcanic intercalations. The second lithological unit consists of Mesozoic sediments (250-50 Ma) also deformed during the Alpine orogeny. This unit uses to be detached from the basement, which means that the associated structures have no continuation in depth. Finally there are the sinorogènic materials from Cenozoic (50-0 Ma), deposited at the end of the formation of the Pyrenees. These sediments can be found in the orogeny or in the Ebro and Aquitaine basins (Figure 1.1).

The formation and the evolution of the Pyrenees is influenced by the position of the Iberian plate between the European and the African plates during two major geological events of divergence and convergence (Srivastava et al., 1990 and Rosenbaum et al., 2002). Figure 1.2 shows the evolution of the Iberian plate respect the European and the African plate in the last 160 Ma.

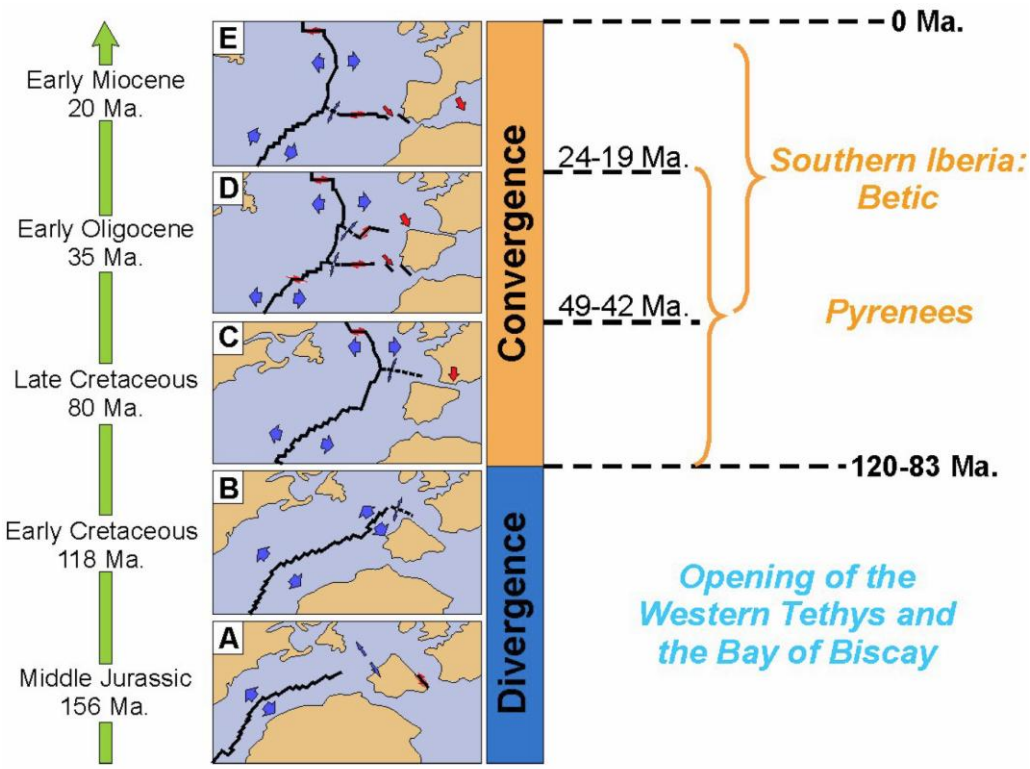

Figure 1.2 Paleokinematic reconstruction of the South and Central North Atlantic with the evolution of the different plate boundaries (Ferrer, 2012 modified from Srivastava et al., 1990).

The first episode corresponds to the displacement of the Iberian plate towards the south with respect to the European plate (Figure 1.2A). This tectonic episode is related to the breakup of Pangea with the consequent opening of the Central Atlantic Ocean during Jurassic times, propagating northwards during cretaceous with the opening of the Bay of Biscay (Figure 1.2B) (Savostin et al., 1986; Srivastava et al., 1990 and Tucholke et al., 2007). Then a counter-clockwise rotation of the Iberian plate respect to the European plate an ESE trending rift system, known as Pyrenean Rift, developed along the future boundary between the Iberian and European plates. (Garcia-Mondejar, 1989 and Vergés and Garcia-Senz, 2001). The faster opening of the South Atlantic Ocean from the middle Santonian (Late Cretaceous) changed this overall framework with the northwards drift of Africa producing the convergence between the Iberia and European plates (Figure 1.2C) (Rosenbaum et al., 2002). This event marked the end of the extensional opening process of the North-Iberian margin and started the build-up of the Pyrenean orogen along the boundary between Iberian and European plates (Muñoz, 1992; Vergés et al., 2002). Whereas the extensional basins from the Pyrenean Rift were inverted and incorporated to the Pyrenean orogen in the Eastern and Central Pyrenees, more to the west the exhumed mantle and the oceanic crust of the Bay of Biscay were subducted below the North-Iberian passive margin. This orogen developed until middle Miocene times when Iberia and Eurasia welded and the contractional deformation concentrated in the southern boundary of Iberia (Figure 1.2E) (Rosenbaum et al., 2002).

1.1.2 Previous geophysical studies

Geophysical studies determine the physical properties of the subsurface. From the constrained physical properties, not only the geological structures of the subsurface are characterized, but also physical and chemical processes. Comparing the results obtained with independent geophysical techniques, the number of possible scenarios able to explain the data is reduced, facilitating the interpretation of thereof. Previous geophysical studies carried out in the Pyrenees, used to interpret the MT results obtained, are presented below.

1.1.2.1 Deep seismic profiles

Two deep seismic profiles were undertaken in the Pyrenees: the ECORS-Pyrenees deep seismic profile crossing the Central Pyrenees and the ECORS-Arzacq deep seismic profile north of the West-Central Pyrenees (Choukroune et al., 1989 and Daignières et al., 1994). In these profiles the depth of the reflecting surface between mediums with different seismic velocity are constrained, providing information about the geological structures of the subsurface.

The ECORS-Arzacq deep seismic profile was interpreted by Muñoz (2002) and Teixell (1998) with a similar interpretation for the upper and middle crust. In both cases the depth of the Moho have been constrained between 30 km and 35 km depth below the European crust and between 30 km and 50 km depth below the Iberian crust, progressively deepening from south to north. In the ECORS-Pyrenees deep seismic profile the depth of the European Moho varies between 30 km and 35 km, while the Iberian Moho increases progressively from south to north from 35 km to 60 km depth (ECORS-Pyrenees Team, 1988 and Choukroune and ECORS-Pyrenees team, 1989). In both profiles these differences in the Moho depth below the Iberian and the European crust are related with the limited subduction of the Iberian lower crust below the European crust and the stacking of basement thrust sheets in the Southern Pyrenees (Muñoz, 1992 and Muñoz, 2002). Geological models proposed by Muñoz (1992) in the Central Pyrenees and by Muñoz (2002) in the West-Central Pyrenees are shown in figure 1.3.

1.1.2.2 Tomographic models

Various seismic tomographic models determine the velocity anomalies of the Pyrenean range from P- and S- waves (Amarou, et al., 2008; Koulakov et al., 2009 and Souriau et al., 2008). These anomalies have been constrained in relation with an initial model of the subsurface, which consist of parallel layers with homogeneous conditions, analyzing the propagation of the P- and S- waves resulted from the earthquakes. In determine the velocity anomalies models at a lithospheric scale the non differentiation between the crustal and the upper mantle structures can strongly influence the results obtained (i.e. Waldhauser et al., 2002). The employment of a crustal model in a global

tomography determines a more reliable velocity distribution in the upper-mantle (Ekström and Dziewonski, 1998).

Results obtained by Amaru et al. (2008), Koulakov et al. (2009) and Souriau et al. (2008) across the Central Pyrenees and the West-Central Pyrenees, all of them including crustal corrections, are shown in figure 1.4. A decrease of the P- and S- wave velocity anomaly has been observed for all cases within the collision zone, except in Souriau et al. (2008) in the West-Central Pyrenees where results are not consistent with the obtained by Amaru et al. (2008) and Koulakov et al. (2009).

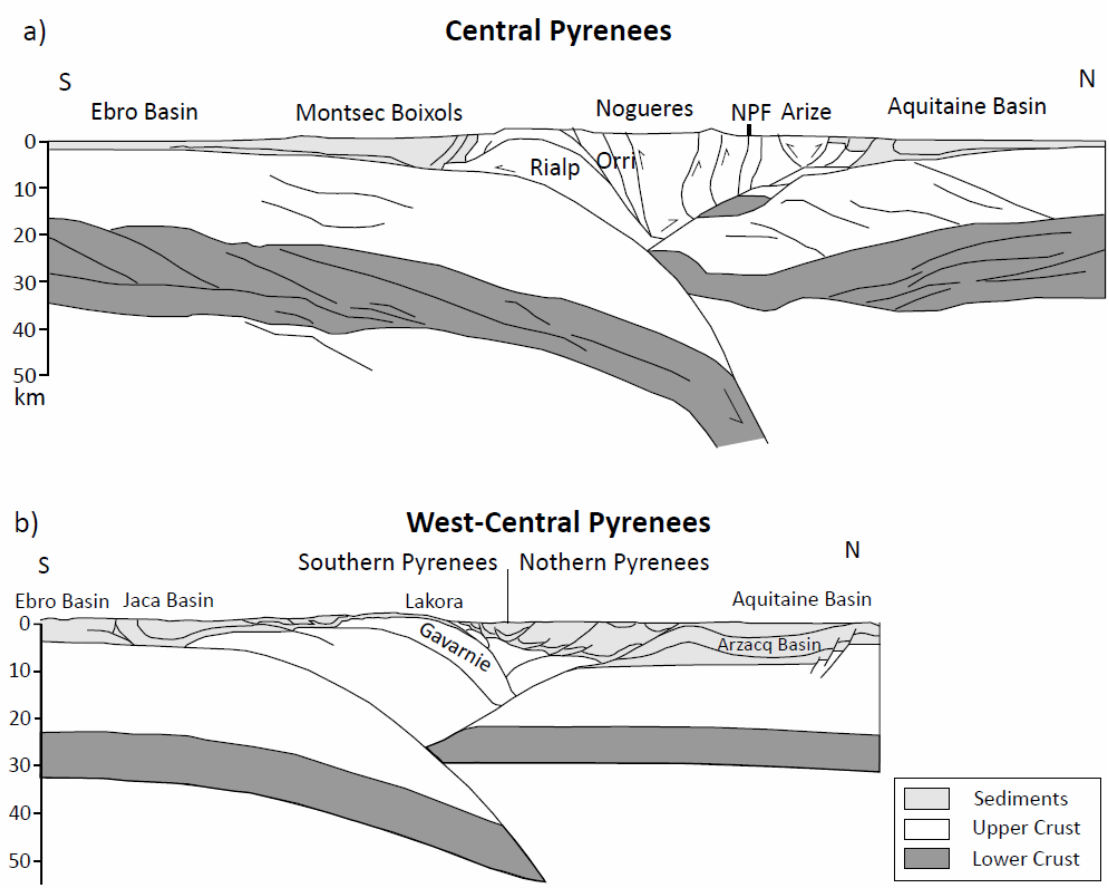

Figure 1.3 Geological models suggested by Muñoz (1992) in the Central Pyrenees (a) and by Muñoz (2002) in the West-Central Pyrenees (b).

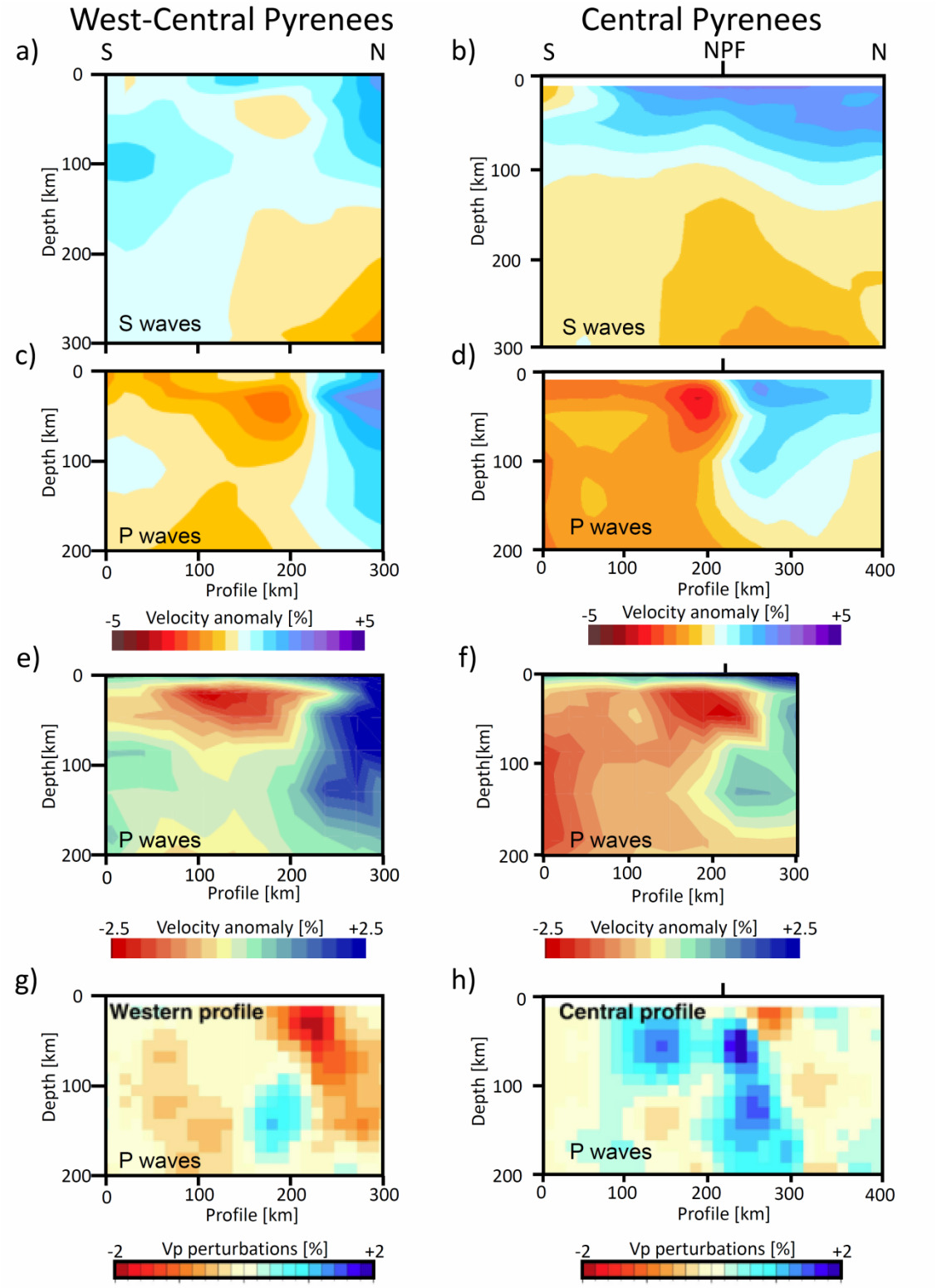

Figure 1.4 Seismic tomography models from S-waves obtained by Koulakov et al. (2009) in the West-Central Pyrenees and the Central Pyrenees a) and b) respectively. Seismic tomography models from P-waves obtained by Koulakov et al. (2009) in the West-Central Pyrenees and the Central Pyrenees c) and d), respectively. e) and f) Seismic tomography model from P-waves obtained by Amaru et al. 2008 in the West-Central Pyrenees and the Central Pyrenees, respectively. g) and h) Seismic tomography model from P-waves obtained by Souriau et al. 2008 in the West-Central and in the Central Pyrenees, respectively.

1.1.2.3 Geoelectrical models

Applying the MT method, the electrical resistivity values below the study area can be determined from the acquired electric and magnetic fields. The previous MT studies of the Pyrenees are focused on a MT profile crossing the Central Pyrenees (Ledo, 1996 and Pous et al., 1995a) and a three-dimensional model covering the area between the Central and West-Central Pyrenees constraining lateral variations along the strike (Ledo et al., 2000). In all cases, the geoelectrical structures of the subsurface were constrained using BBMT data and the MT models were obtained by trial-and-error fitting of the data.

These results show a low electrical resistivity structure below the collision zone related to the Iberian subducted lower crust (IBSLC) and a low electrical resistivity structure at the bottom of the MT models that has been associated with the asthenosphere and its top with the LAB. Figure 1.5 shows the geoelectrical models obtained by Ledo (1996), Ledo et al. (2000) and Pous et al. (1995a). The geoelectrical structures A and B are related to the IBSLC and the asthenosphere, respectively.

Various authors (Pous et al., 1995a; Pous et al., 1995b; Ledo, 1996; Glover et al., 2000 and Ledo et al., 2000) associate the electrical resistivity values of the IBSLC with partial melting. However, other hypothesis is proposed (Vacheur and Souriau, 2001 and Souriau et al., 2008) creating an open debate between the presence or absence of partial melting.

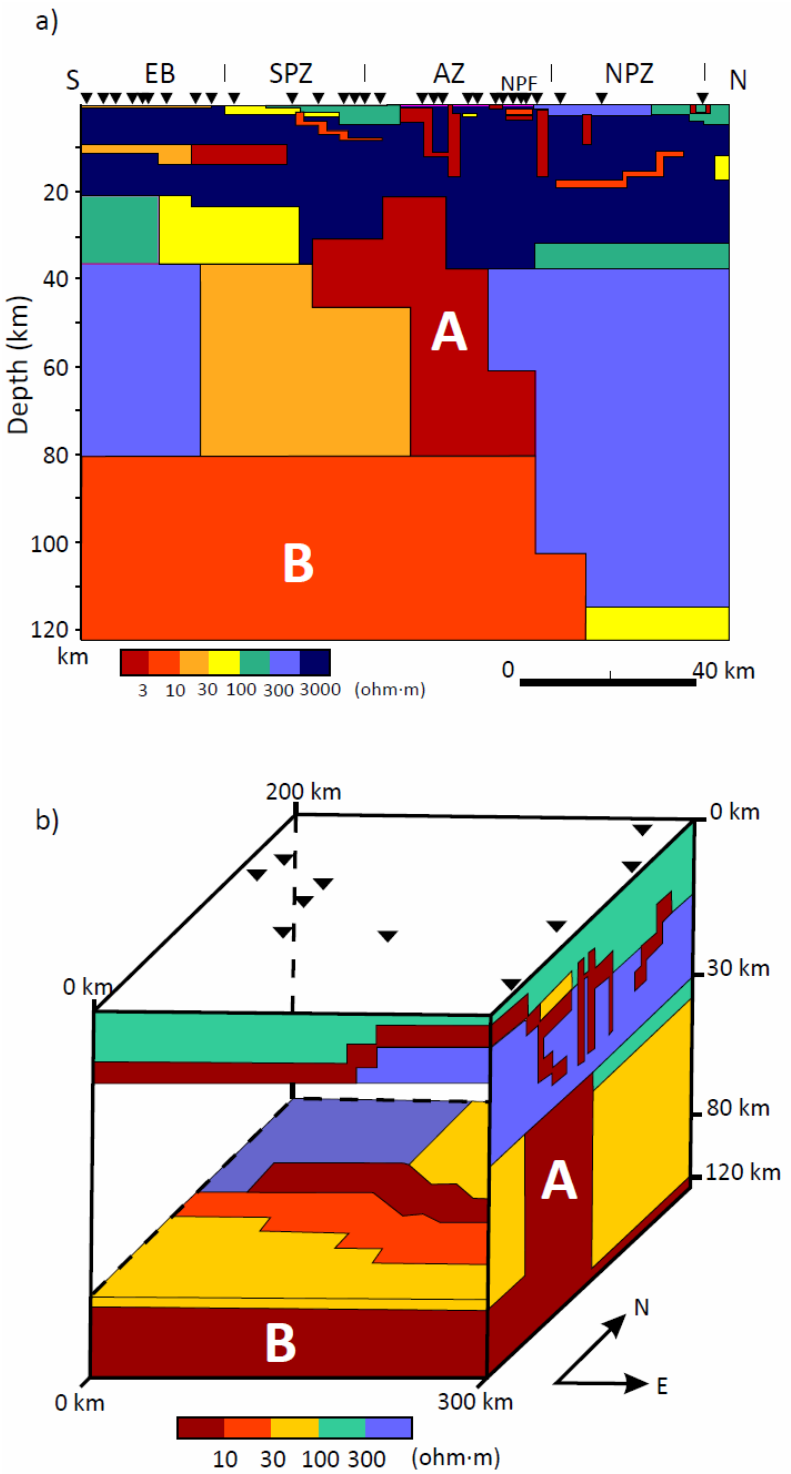

Figure 1.5 a) Modified from the two dimensional geoelectrical model of the Central Pyrenees suggested by Ledo (1996) and Pous et al. (1995a). b) Modified from the three dimensional geoelectrical model of the Pyrenees proposed by Ledo et al., (2000). In both models, A is the geoelectrical structure associated with the IBSLC and B the geoelectrical structure associated with the asthenosphere.

1.1.2.4 Gravity data

Several studies based on gravity data have been carried out in the Pyrenees (i.e. Casas et al., 1997; Jammes et al., 2010; Ledo et al., 2000; Gunnell et al., 2008; Pedreira et al., 2007; Torné et al., 1989 and Vacheur and Souriau, 2001). Gravity data characterise the density distribution of the subsurface determining the main density anomalies. Figures 1.6 and 1.7 shows some of the gravity models proposed for the Central and West-Central Pyrenees, respectively. Models have been modified showing the same colour for each one of the following layers: sediments, upper-crust, lower-crust, upper-mantle and asthenosphere. In all cases gravity profiles agree with the subduction of the IBSLC.

Vacheur and Souriau (2001) suggested the presence of free water to explain the geophysical observations of the IBSLC. This result, based on gravity data, disagree with the hypothesis of partial melting.

1.1.2.5 Thermal studies

Thermal studies determine the temperature distribution below the study area from the heat flow coming from the subsurface. Zeyen and Fernández (1994) and Glover et al. (2000) determine the temperature of the lithosphere below the Central Pyrenees suggesting no major anomalies related with the IBSLC. These results implies that the thermal re-equilibration is already occurred. Tesauro et al. (2009), in a general thermal model of Europe, show no main differences between the Central and West-Central Pyrenees at upper-mantle depths and determines the thermal LAB at around 120 km depth. Figure 1.8 shows the thermal models proposed by Tesauro et al. (2009) at 60 km depth (Figure I8a) and the depth of the thermal LAB (Figure 1.8b). The temperature distribution below the Central Pyrenees proposed by Glover et al. (2000) and Zeyen and Fernández (1994) is shown in (Figure 1.8c) and (Figure 1.8d), respectively.

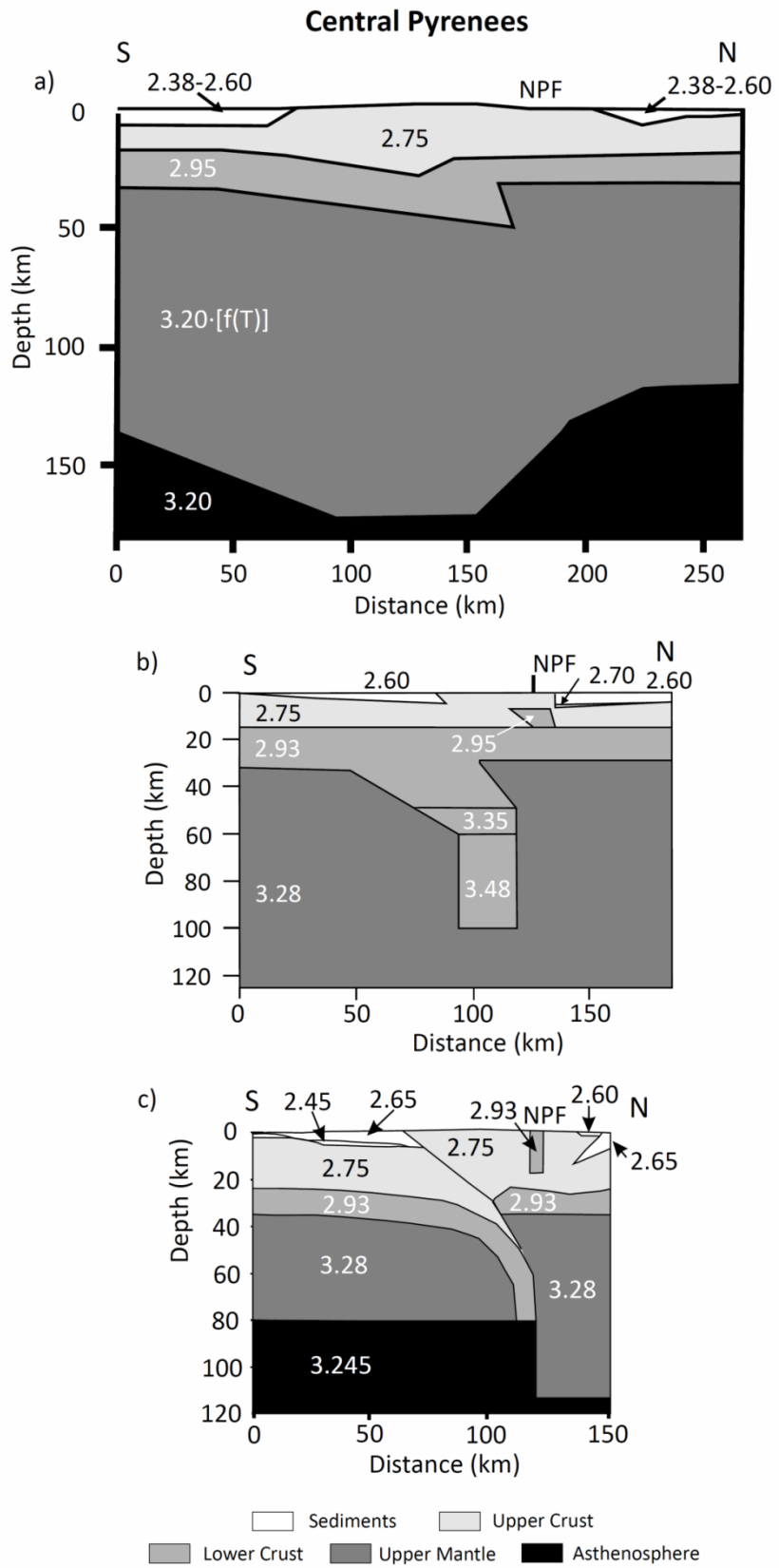

Figure 1.6 Density models proposed by Gunnell et al. (2008) (a), Vacheur and Souriau (2001) (b) and Ledo et al. (2000) (c). Density values are in (Mg/m^3 Density values are in (Mg/m^3). Colours and proportions have been modified to unify criteria and facilitate the comparison between models. $f(T)$ in (a) is a function dependent of the temperature: $f(T) = 1 + 3.5 \cdot 10^{-5} \cdot (1300 - T)$.

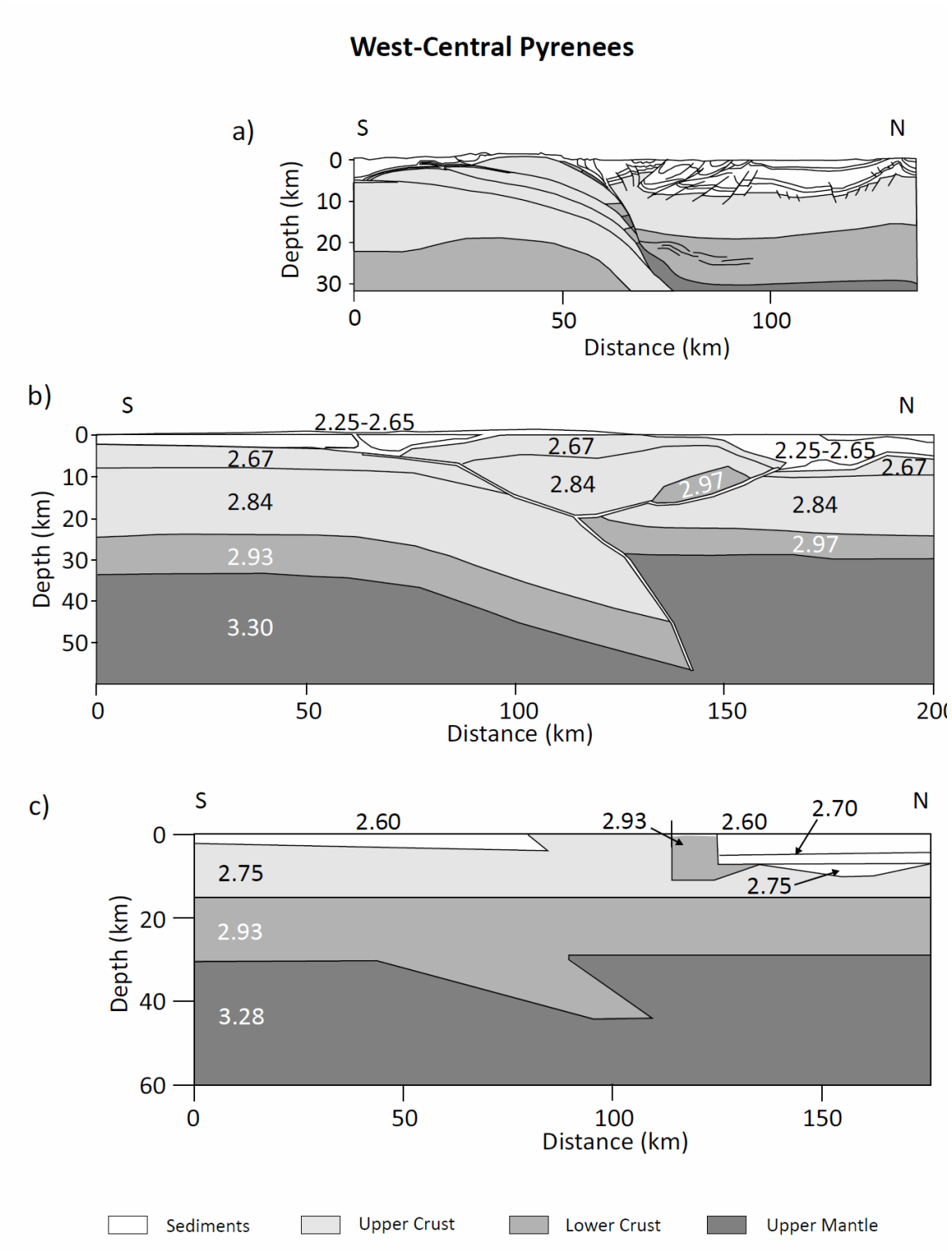

Figure 1.7 (a) Modified from geological model suggested by Jammes et al. (2010) based on gravity data. (b) Modified from density model proposed by Pedreira et al. (2007). (c) Modified from density model proposed by Vacheur and Souriau (2001). Density values are in (Mg/m^3). Colours and proportions have been modified to unify criteria and facilitate the comparison between models.

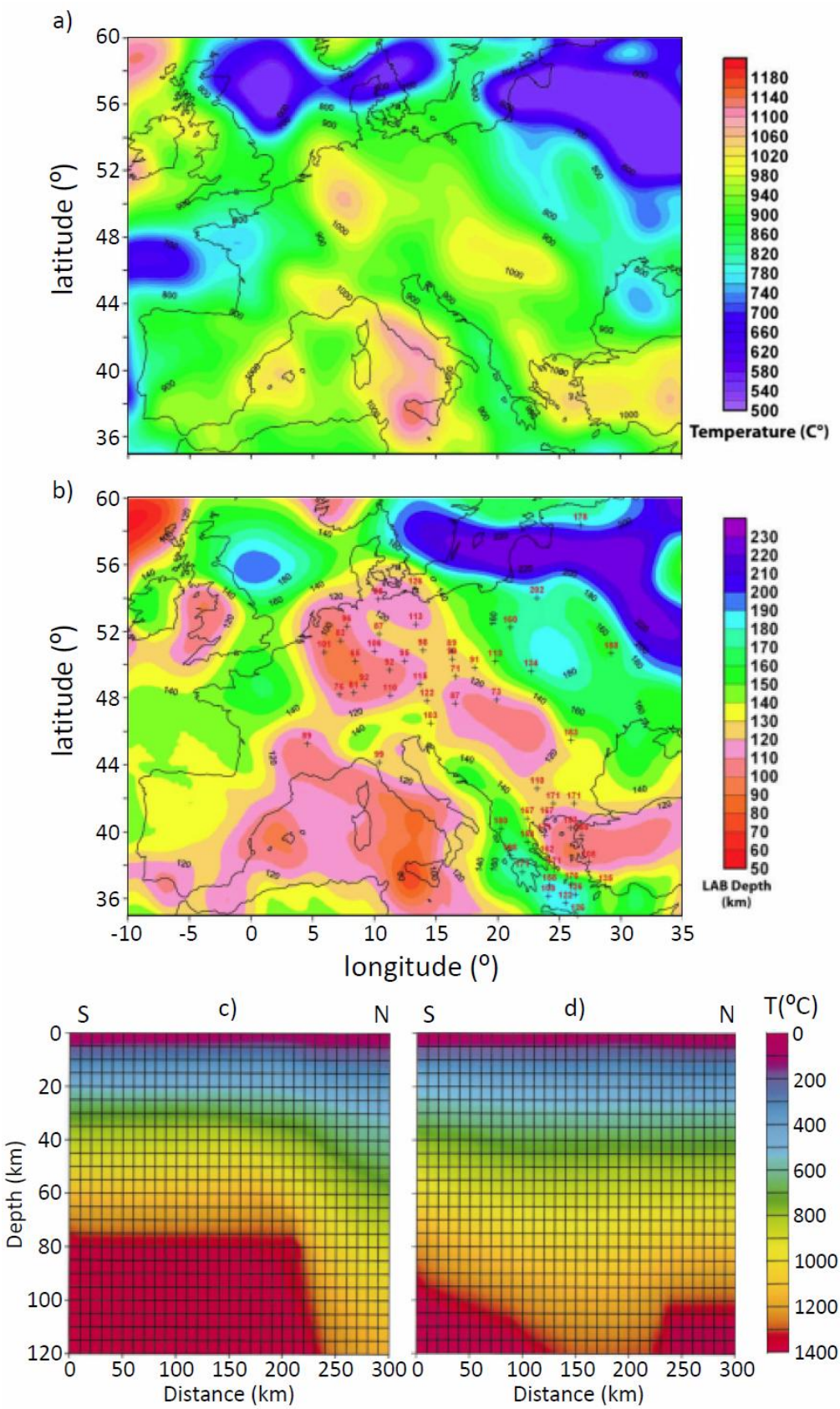

Figure 1.8. a) Temperature (ºC) at a depth of 60 km (Tesauro et al. 2009). b) Depth of the isotherm of 1200 ºC marking the lithosphere-asthenosphere boundary (Tesauro et al. (2009). c) Temperature profile of the Central Pyrenees suggested by Glover et al. 2000. d) Temperature profile of the Central Pyrenees suggested by Zeyen and Fernández (1994).

1.2 AIMS

The aims of the thesis are associated with the characterization of the geoelectrical structures below the Pyrenees using BBMT and LMT data and with the improvement of the processing of the MT data.

The aims associated with the geoelectrical characterization of the Pyrenean lithosphere are:

a) Constrain the low electrical resistivity structure associated with the IBSLC below the Central Pyrenees with major resolution than the previous MT studies.

b) Analyze physical and chemical data related to the IBSLC and evaluate the hypothesis of partial melting. Calculate the amount of partial melting necessary to explain the electrical resistivity values of the IBSLC.

c) Constrain the geoelectrical structures below the West-Central Pyrenees from a new MT profile close the ECORS-Arzacq deep seismic profile.

d) Determine the evolution of the electrical resistivity values between the Central Pyrenees and the West-Central Pyrenees.

e) Characterize the LAB below the Pyrenees and the electrical resistivity values of the asthenosphere.

f) Interpret the MT results being consistent with previous geophysical studies.

The aims associated with the improvement of the processing of the MT data are:

g) Develop a new method that improves the processing of MT data when some of the components of a MT site stop recording before the others.

h) Evaluate the possibilities and advantages of the proposed method.

1.3 MAGNETOTELLURIC DATA SET IN THE PYRENEES

In the Pyrenees we have acquired two different types of MT data. The broadband magnetotelluric (BBMT) data, which cover a period range between 0.001 s and 1000 s, and the long period magnetotelluric (LMT) data, which cover a period range between 20 s and 20000 s. The BBMT data is frequently used for crustal studies (i.e. Chandrasekhar et al., 2012; Ledo et al., 2011; Siniscalchi et al., 2012 and Zhao et al., 2012) and LMT data for studies at lithospheric scale (i.e. Rosell et al., 2011; Le Pape et al., 2012 and Kelbert et al., 2012).

A total of 82 BBMT sites, 29 of them also with LMT data, have been acquired between the Mediterranean Sea to the Atlantic Ocean, most of them distributed in four profiles across the Pyrenees (Figure 1.9). In total, adding the distance of the four MT profiles, 500 km have been covered across the Pyrenean range. Table 1.1 shows the location of the MT sites acquired in the Pyrenees for each profile differencing between sites with BBMT and sites with BBMT+LMT data.

Forty of the BBMT sites were recorded before the beginning of this thesis. Sixteen of them were acquired in 1992 in a MT survey across the Central Pyrenees, following the ECORS-Pyrenees deep seismic profile (Ledo, 1996 and Pous et al., 1995a). Other fourteen were acquired in 1999 in a MT profile across the Western Pyrenees. The time series recorded in this profile have been processed in this thesis to obtain the impedance tensor for each site. Moreover these data have been inverted and the

model is presented in the Discussion. Finally, ten BBMT sites were acquired between the two profiles.

In this work 42 new BBMT sites have been acquired, 29 of them also with LMT data. In 2009 the MT profile of the Central Pyrenees has been completed with eight new BBMT+LMT sites (Campanyà et al., 2011). In summer of 2010, a new MT profile composed of thirteen BBMT sites and seven BBMT+LMT sites has been carried out across the West-Central Pyrenees from Ejea de los Caballeros (Spain) to a bit north of Oloron-Sainte-Marie (France), close to the ECORS-Arzacq deep seismic profile (Campanyà et al., 2012). In autumn of 2010 a new profile with thirteen BBMT+LMT sites has been done in the Eastern Pyrenees from the Montseny (Spain) to Limoux (France). Also a BBMT+LMT site has been recorded close to the Mediterranean Sea helping constrain the effect of the seawater on the MT data acquired in the Eastern Pyrenees.

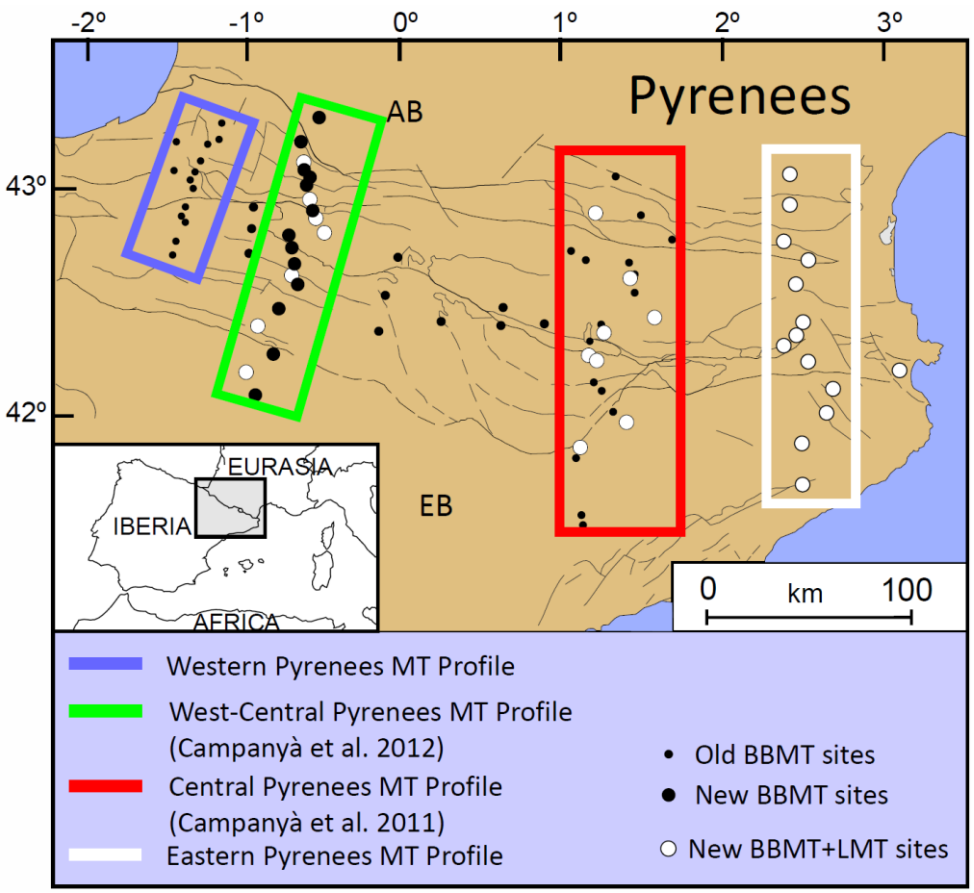

Figure 1.9 Location of the MT sites in a structural sketch of the study area. AB: Aquitanian basin; EB: Ebro Basin.

Western PYR		West-Central PYR		Central PYR		Eastern PYR	
Lat (º)	**Long (º)**	**Lat (º)**	**Long (º)**	**Lat (º)**	**Long (º)**	**Lat (º)**	**Long (º)**
43.2402	-1.1858	43.2718	-0.6298	43.0706	1.2817	**43.0127**	**2.3502**
43.1836	-1.1977	43.1699	-0.7049	**42.9066**	**1.2052**	**42.8838**	**2.3691**
43.1736	-1.4388	**43.0814**	**-0.6875**	42.8807	1.3512	**42.7275**	**2.3297**
43.1600	-1.2638	43.0641	-0.6913	42.7800	1.4835	**42.6800**	**2.4691**
43.1013	-1.2969	43.0183	-0.6641	42.7360	1.1191	**42.5794**	**2.4063**
43.0625	-1.4530	43.0037	-0.6750	42.6818	1.1761	**42.4444**	**2.4422**
43.0594	-1.3288	**42.9398**	**-0.6672**	42.6732	1.3077	**42.3894**	**2.4144**
43.0269	-1.3494	42.8941	-0.6482	42.6013	1.3216	**42.3288**	**2.3375**
42.9947	-1.3391	**42.8716**	**-0.6436**	**42.5386**	**1.3438**	**42.2711**	**2.5011**
42.9283	-1.3808	**42.8122**	**-0.5858**	42.4258	1.4263	**42.2369**	**3.0638**
42.8902	-1.3988	42.8076	-0.7737	**42.3958**	**1.2315**	**42.1786**	**2.6008**
42.8675	-1.3805	42.7635	-0.7642	42.3488	1.2688	**42.0697**	**2.5641**
42.7988	-1.4291	42.7098	-0.7478	**42.3179**	**1.1923**	**41.9413**	**2.4369**
42.7441	-1.4494	**42.6589**	**-0.7642**	42.2480	1.1916	**41.7786**	**2.4591**
		42.6252	-0.7358	**42.2227**	**1.2152**		
		42.5342	-0.8375	**42.1261**	**1.1899**		
		42.4652	**-0.9463**	42.0898	1.2134		
		42.3642	-0.8675	42.0081	1.2723		
		42.2917	**-1.0088**	41.9492	1.3085		
		42.2092	-0.9677	**41.9433**	**1.3336**		
				41.8258	**1.1763**		
				41.7845	1.1234		
				41.5228	1.1548		
				41.4781	1.1421		

Table 1.1 Coordinates, in WGS 1984, of the MT sites acquired in the Pyrenees for each profile. Ordered from north (top) to south (bottom). Coordinates of the sites with LMT data are in bold type. In green the LMT sites used to test the method proposed for processing MT data in chapter 4.

1.4 THE MAGNETOTELLURIC METHOD

A comprehensive explanation of the MT method fundamentals and applications can be found in Berdichevsky and Dmitriev (2008), Chave and Jones (2012) and Simpson and Bahr (2005), among others. In the following paragraphs the basics of the MT method related to the objectives of this thesis are presented.

The MT method characterizes the electrical resistivity of the subsurface using tensor relationships, in the frequency domain, between the electric and magnetic time-varying fields simultaneously recorded on the surface of the study area (Figure 1.10). As tensor relationships, also the dimensionality of the electrical resistivity structures of the subsurface can be constrained.

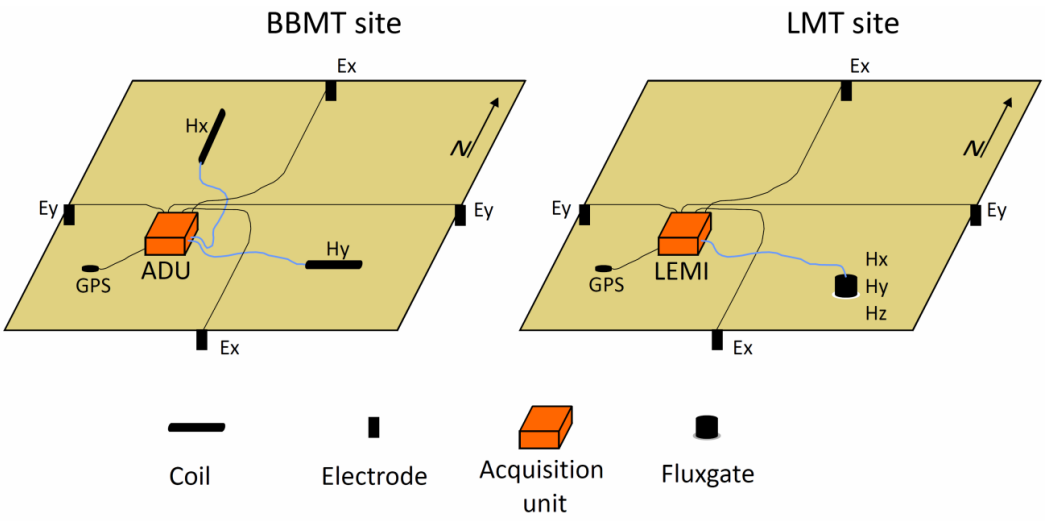

Figure 1.10 Layout of the BBMT and LMT sites acquired in the Pyrenees. All sensors are buried, except GPS. Ex, Ey are the recorded electric fields and Hx, Hy and Hz the acquired magnetic fields. *x* for north-south direction, *y* for East-West direction and *z* for vertical component.

The electric and magnetic time-varying fields recorded on the surface of the study area are the superposition of a primary field, natural source coming from the ionosphere, and a secondary field, resulted from the interaction of the primary field with the electrical resistivity structures of the subsurface. If analyse the shorter periods, from 10^{-4} seconds, they will be affected by the shallower structures, allowing constrain the subsurface from the first tens of meters. If analyse the longer periods, until 10^{5} seconds, they will be mostly affected by deeper structures, determining the electrical

resistivity until hundreds of kilometres depth. Although the use of longer periods increases the depth of study, in counterpart the resolution decreases.

The typical electrical resistivity values of the subsurface varies between 10^{-2} ohm·m and 10^{6} ohm·m, having a wide range of electrical resistivity values of up to eight orders of magnitude (Figure 1.11). These values are not only associated with geological structures and in many cases are related with the presence of physical and chemical processes. This is why, in general, we will refer to geoelectrical structures, regardless of whether the causes of these values are geological structures or the physical and chemical process associated.

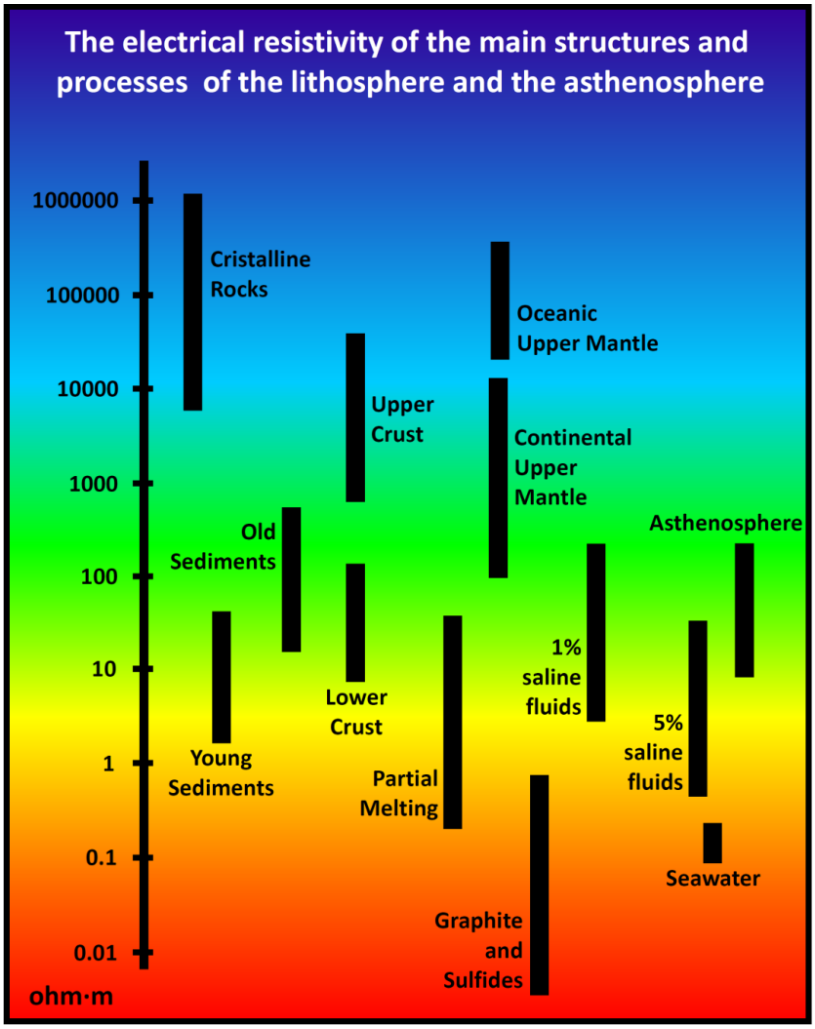

Figure 1.11 The electrical resistivity of the lithosphere and the asthenosphere. Modified from Haak and Hutton, 1986.

Due to the range of periods used in the MT method and the typical electrical resistivity values of the subsurface, the characterization of the geoelectrical structures is dominated by the diffusion equation. This means that the geoelectrical models created to interpret the MT data are a fuzzy image of the subsurface electrical resistivity (Figure 1.12).

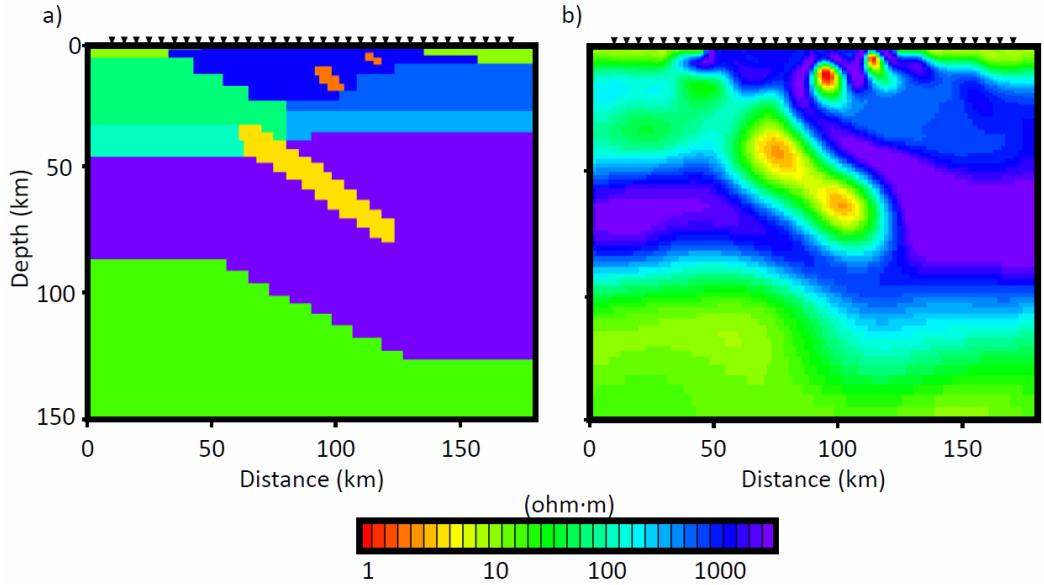

Figure 1.12 a) A two-dimensional synthetic geoelectrical model of the lithosphere. b) Two-dimensional geoelectrical model obtained from the inversion of the forward responses of the model a). Inverted triangles are sites with BBMT and LMT data (0.001 s to 10000 s). Models have been obtained using the algorithm of Rodi and Mackie (2001).

1.4.1 Brief history of the beginnings of the MT method

Below we expose the main historical events associated with the beginnings of the MT method and the definition of the tensor relationships used in the thesis. The following paragraphs are mainly based on Chave and Jones (2012). The bases of the MT method begin after numerous studies made in the late XIX century and the early of the XX century, where several works characterize the behaviour of electromagnetic waves and their interaction with the environment. However, we can consider the beginnings of the MT method with the results presented by Hirayama (1934) and later by Rikitake (1948). These studies suggest that, in a homogeneous medium, the result of E/B, being E the electric field and B the magnetic field, has amplitude proportional to the root of the period and a constant phase of 45°. Additionally, Hatakeyama and Hirayama (1934) reported simultaneous measurements showing variations of the phase with periods,

having phase smaller than 45° for long periods. It was not until Kato and Kikuchi (1950 a,b) and Rikitake (1951) that the observed changes of amplitude and phase with period were rigorously explained, suggesting are related with differences in the electrical resistivity values of the subsurface.

The theory of MT method was introduced by Tikhonov (1950) and Cagniard (1953), where a scalar relationship between the electric and magnetic fields recorded simultaneously on surface were used determining the geoelectrical structures of the subsurface. This theory was limited and only useful for studies in one-dimensional geoelectrical regions where the results were not dependent on the orientation of the axes of measurement. It was not until Neves (1957), Cantwell (1960) and Rokityanski (1961) that the tensor relationship between horizontal electric and magnetic fields was defined as the MT impedance tensor. The components of the MT impedance tensor are complex values that allow calculate the apparent resistivity and phase parameters, which constrain the geoelectrical structures of the subsurface. These studies establish the bases for a more general theory of the MT, applicable in regions with lateral variations of the electrical resistivity.

Another currently used tensor relationship, which is particularly sensitive to the lateral variations of the electrical resistivity, has been described by Parkinson (1962) and Weise (1962) as the geomagnetic transfer function. This function relates the vertical component of the magnetic field with the horizontal components of the magnetic field. Schmucker (1970) represents the geomagnetic transfer function as vectors allowing to laterally locating the low electrical resistivity structures. Later, Berdichevsky (1968) and Schmucker (1970) defined the horizontal magnetic tensor (HMT). This tensor relationship relates the time-varying horizontal magnetic fields simultaneously recorded at two different sites. Due to be simultaneously affected by the geoelectrical structures located below the two sites this tensor relationship does not directly provides the electrical resistivity distribution below the analysed site.

In the last thirty years, theoretical and technological developments have allowed to apply the MT method in many regions with different aims, characterizing the geology

and the physical and chemical processes of the subsurface from the constrained geoelectrical structures.

1.4.2 Natural electromagnetic sources

The natural sources time-varying EM waves observable on the surface of the Earth are generated by distant lighting activity at high frequencies and by the interaction of the Earth magnetosphere-ionosphere with particles ejected by the Sun at low frequencies. The MT death band is associated with the transition between these two sources, and is characterized by a period range with poor quality data between those two types of fluctuations (Schmucker, 1985; Vozoff, 1991) (Figure 1.13). In the MT studies of the Earth electrical resistivity, the source is assumed as a plane wave vertically incident to the subsurface. This assumption is valid in the Pyrenees and in the most parts of the world except in areas affected by the auroral and equatorial electrojets, where source distortions effects may distort the acquired MT data (i.e. Carrasquilla and Rijo, 1998; Osipova et al., 1989; Padilha et al., 1997 and Varentsov et al., 2003).See McPherron (2005) for a complete review of MT sources.

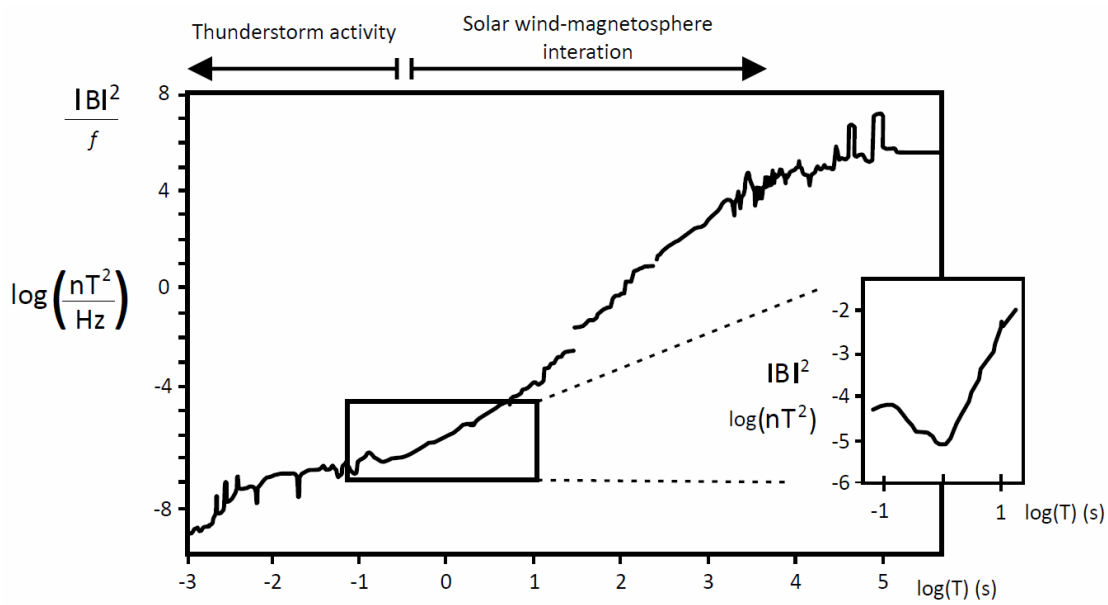

Figure 1.13 Power spectrum of natural magnetic fields variations. The inset depicts the minimized signal power spectra in the dead band. (Modified from Junge, 1996).

In lithospheric-scale MT studies the mostly important source is the signal coming from the solar activity, due to is associated with longest periods. This dependence implies

that the intensity of the signal used for MT studies at a lithospheric-scale depends on the solar activity. As observed years ago by Schwabe (1844) and Wolf (1877) the number of sunspots, which are related with the geomagnetic solar activity, has a periodicity of at around 11 years (Figure 1.14).

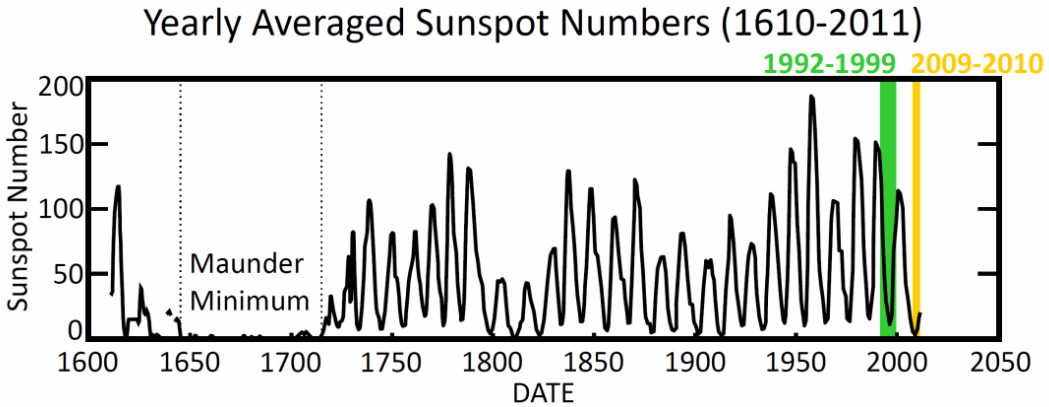

Figure 1.14 Sunspot cycle from 1610-2011. Yellow line (acquisition of the new MT data). Green line (acquisition of the old MT data). Modified from (NASA, http://solarscience.msfc.nasa.gov/SunspotCycle.shtml)

Although the geomagnetic activity increases with the number of sunspots, the relation is not proportional. Figure 1.15 shows the number of geomagnetic storms coming from the Sun superposed to the sunspot cycle. Although are good correlated, in some cases the geomagnetic activity lags behind the solar cycle.

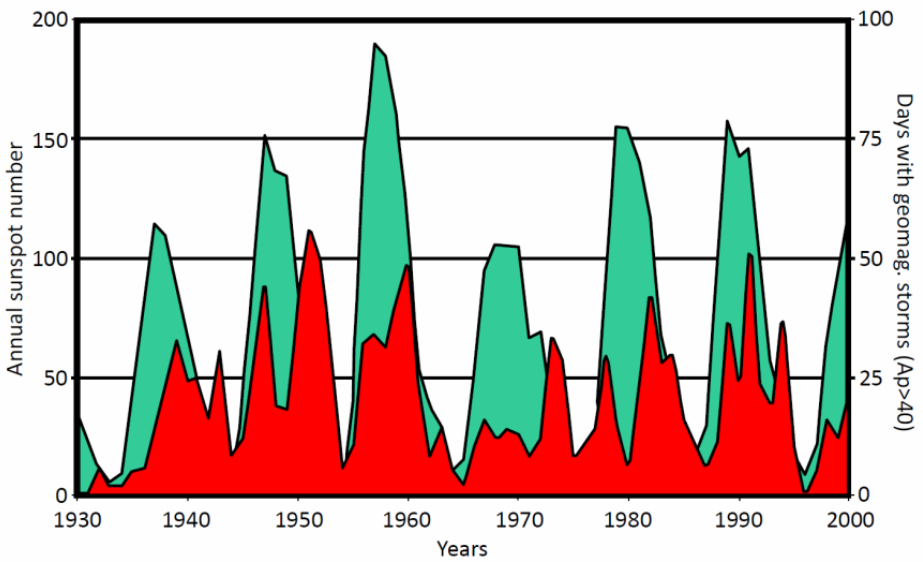

Figure 1.15. A plot of the number of sunspots (green) and the number of days with geomagnetic storms with enough intensity, Ap>45, to provoke auroras (red). Modified from (Woods Hole Oceanographic Institution (http://www.whoi.edu/oceanus/viewImage.do?id=11151&aid=5280)).

When there is low geomagnetic signal the quality of the MT data decrease, making difficult the characterization of the MT transfer functions. In this situation, the problem can be solved, or at least reduced, increasing the number of days recording MT data. This problem was strongly present in 2009, where LMT data in the Central Pyrenees had to be recorded over more than 30 days. In 2010 the solar activity increased enough to reduce by half the number of days recording the LMT data.

1.4.3 Fundamentals of the MT method

In the MT method, the horizontal components of the electric field, E_x and E_y, and the three components of the magnetic field, the horizontal components H_x and H_y and the vertical component H_z, are recorded to determine the geoelectrical structures of the subsurface. Its propagation through the environment and its interaction with the geoelectrical structures is governed by the Maxwell equations.

Using the constitutive relations of the medium, where bold letters are vectors:

$$\boldsymbol{J} = \sigma \boldsymbol{E} \qquad (1.1)$$

$$\boldsymbol{B} = \mu \boldsymbol{H} \qquad (1.2)$$

$$\boldsymbol{D} = \varepsilon \boldsymbol{E} \qquad (1.3)$$

Where σ is the electric conductivity (S/m), inverse of the electric resistivity ρ (ohm·m), μ is the magnetic permeability (Vs/Am) and ε is the electric permittivity (As/Vm). ***J*** is the current electric density (A/m^2), ***E*** is the intensity of the electric field (V/m), ***B*** is the magnetic induction (T), ***H*** is the magnetic field (A/m) and ***D*** is the electric displacement (C/m^2). In presume that σ, μ and ε are scalars parameters we assume an isotropic media. In this thesis we assume that properties of the materials are isotropic. From the typical values of the Earth the electrical permittivity and the magnetic permeability can be assumed as the values of the electrical permittivity and magnetic permeability in the vacuum, having $\varepsilon \approx \varepsilon_0 = 8.85 \cdot 10^{-12}$ (As/Vm) and $\mu = \mu_0 = 4\pi \cdot 10^{-7}$ (Vs/Am).

The Maxwell equations can be written as follow:

$$\nabla \cdot \boldsymbol{E} = \frac{q_{free}}{\varepsilon} \qquad (1.4)$$

$$\nabla \cdot \mathbf{B} = 0 \qquad (1.5)$$

$$\nabla \times \mathbf{E} = -\frac{\partial \mathbf{B}}{\partial \mathrm{t}} \qquad (1.6)$$

$$\nabla \times \frac{\mathbf{B}}{\mu} = \frac{\mathbf{E}}{\rho} + \varepsilon \frac{\partial \mathbf{E}}{\partial \mathrm{t}} \qquad (1.7)$$

Equation (1.4) is the Gauss law, referred to the electrostatics for an isolated charge, q_{free}. Equation (1.5) is the Gauss law for magnetism and implies there are no magnetic monopoles. Equation (1.6) is the Faraday's law, which relates the inducted electric field with variations of the magnetic field with time. Finally, equation (1.7) is the Ampare's law with Maxwell's addition, which relates the inducted magnetic field due the presence of current density, first term, and the variation with time of the electric field, second term.

Across a discontinuity between two materials, named 1 and 2, the boundary conditions to be applied to the electromagnetic fields and currents described by Maxwell's equations are:

$$\hat{n} \times (\boldsymbol{E}_1 - \boldsymbol{E}_2) = 0 \qquad (1.8)$$

$$\hat{n} \times (\boldsymbol{H}_1 - \boldsymbol{H}_2) = \boldsymbol{j}_s \qquad (1.9)$$

$$\hat{n} \times (\boldsymbol{D}_1 - \boldsymbol{D}_2) = \rho_s \qquad (1.10)$$

$$\hat{n} \cdot (\boldsymbol{B}_1 - \boldsymbol{B}_2) = 0 \qquad (1.11)$$

$$\hat{n} \cdot (j_1 - j_2) = 0 \qquad (1.12)$$

where $\hat{n}$ is the unit vector normal to the discontinuity boundary, j_s (A/m^2) is the current density along the boundary surface and ρ_s (C/m^2) is the surface charge density.

From the Maxwell equations the electric and magnetic fields can be separated obtaining the following equations:

$$\nabla^2\mathbf{E} - \frac{\mu}{\rho}\frac{\partial\mathbf{E}}{\partial t} - \mu\varepsilon\frac{\partial^2\mathbf{E}}{\partial t^2} = 0 \qquad (1.13)$$

$$\nabla^2\mathbf{B} - \frac{\mu}{\rho}\frac{\partial\mathbf{B}}{\partial t} - \mu\varepsilon\frac{\partial^2\mathbf{B}}{\partial t^2} = 0 \qquad (1.14)$$

The second term of equations (1.13) and (1.14) is related with the conduction term and the third one with the displacement.

In the MT method, the primary field is assumed as a plane wave that propagates vertically towards the Earth surface, the plane wave hypothesis (Vozoff, 1972). Assuming that temporal dependence of the electric and magnetic field is harmonic $\left(\propto e^{i\omega t}\right)$, for a single frequency, equations (1.13) and (1.14) can be written as:

$$\nabla^2\mathbf{E} - \left(\frac{i\mu\omega}{\rho} + \mu\varepsilon\omega^2\right)\mathbf{E} = 0 \qquad (1.15)$$

$$\nabla^2\mathbf{B} - \left(\frac{i\mu\omega}{\rho} + \mu\varepsilon\omega^2\right)\mathbf{B} = 0 \qquad (1.16)$$

where ω is the frequency (Hz). From the range of frequencies used in MT and the range of electrical resistivity values of the Earth, focusing on the terms inside the parenthesis in equations (1.15) and (1.16), the first term is dominant respect the second one, allowing to remove the second term from the equations. In that case we are assuming the quasi-stationary approximation. The same approximation can be used in controlled source electromagnetic (CSEM) data, due to it works with similar frequencies than MT. This is not the case of ground penetrating radar (GPR), light or radio waves, where the used frequencies are much higher than MT and consequently the dominant term would be the second one.

From the quasi-stationary approximation and assuming a homogeneous half-space medium with electrical conductivity σ, we can calculate the solution of the electric and magnetic equations obtaining:

$$\boldsymbol{E} = E_0 e^{i\omega t - \gamma z} \qquad (1.17)$$

$$\boldsymbol{B} = B_0 e^{i\omega t - \gamma z} \qquad (1.18)$$

where *z* the depth penetration in meters and γ is:

$$\gamma = \sqrt{i\omega\mu\sigma} = \sqrt{\frac{\omega\mu\sigma}{2}} + i\sqrt{\frac{\omega\mu\sigma}{2}} \qquad (1.19)$$

From these results we can calculate the skin depth δ_s as the value of *z* for which the real part of the term $e^{-\gamma z}$ decays $1/e$.

$$e^{-z\sqrt{\frac{\omega\mu\sigma}{2}}} = \frac{1}{e} \rightarrow \delta_s = \sqrt{\frac{2}{\omega\mu\sigma}} \approx 500\sqrt{\rho T} \qquad (1.20)$$

where *T* is the period (s). Using these results, the equations of the electric and magnetic fields can be written as:

$$\boldsymbol{E} = E_0 e^{i\left(\omega t - \frac{z}{\delta_s}\right) - \frac{z}{\delta_s}} \qquad (1.21)$$

$$\boldsymbol{B} = B_0 e^{i\left(\omega t - \frac{z}{\delta_s}\right) - \frac{z}{\delta_s}} \qquad (1.22)$$

having a phase associated with the time and the depth penetration and an attenuation term depending on the penetration in the environment.

1.4.4 The electrical resistivity of a half-space homogeneous medium

The following example shows a way to obtain the electrical resistivity of a homogeneous half-space medium from the electric and magnetic fields recorded on surface.

From Faraday's law (1.6), in the frequency domain, the relationships between **E** and **B** fields are governed by the following equations:

$$\frac{\partial E_z}{\partial y} - \frac{\partial E_y}{\partial z} = -i\omega B_x \qquad (1.23)$$

$$\frac{\partial E_x}{\partial z} - \frac{\partial E_z}{\partial x} = -i\omega B_y \qquad (1.24)$$

$$\frac{\partial E_y}{\partial x} - \frac{\partial E_x}{\partial y} = -i\omega B_z \qquad (1.25)$$

For a uniform plane wave propagating in *z* direction, equation (1.23) and (1.24), in a homogeneous half-space environment the derivatives of E_z are zero. Also both derivatives in equation (1.25) are zero having B_z component equal to zero. Due we are in a homogeneous half-space the constrained values do not depend with the orientation of the axis of measurement, having the same results if relate E_x with B_y or E_y with B_x. Thit is why we will do the following steps only for one of the two cases.

Adding equation (1.17) and (1.18) in (1.23), same results if (1.17) and (1.18) in (1.24), we define the Z scalar impedance of the medium as:

$$Z = \mu \frac{E_y}{B_x} = -\frac{i\omega\mu}{\sqrt{i\omega\mu\sigma}} = \frac{\omega\mu}{2\sqrt{\frac{\omega\mu\sigma}{2}}} + i\frac{\omega\mu}{2\sqrt{\frac{\omega\mu\sigma}{2}}} = \sqrt{\frac{\omega\mu}{\sigma}} \cdot e^{i\varphi} \qquad (1.26)$$

where the phase, φ, is defined as:

$$\varphi = arctan\left(\frac{Im(Z)}{Re(Z)}\right) \quad (1.27)$$

In a homogeneous half-space the phase, φ, is 45° , because real and imaginary components of *Z* are the same.

From the modulus of Z, we can define the apparent resistivity ρ_a, which is coincident with the electrical resistivity of the medium in the homogeneous half-space situation:

$$\rho_a = \frac{\mu}{\omega}\left|\frac{E_x}{B_y}\right|^2 \qquad (1.28)$$

From equations (1.27) and (1.28) the electrical resistivity of a homogeneous half-space medium is constrained and is demonstrated that the phase is 45°.

In practice, rarely the study areas are a homogeneous half-space having more complex situations where the tensor relationship between electric and magnetic fields is required. How to obtain the parameters of the MT impedance tensor in more complex situations is described, with references to the original works, in Chave and Jones (2012).

1.4.5 MT transfer functions

The MT transfer functions relate the registered time-varying electromagnetic fields components at given frequencies providing information of the geoelectrical structures of the subsurface. These functions do not depend on the electromagnetic source and are constant on time, if the subsurface geoelectrical structures do not change.

In this thesis we used three different types of transfer functions. The MT impedance tensor, which constrains the electrical resistivity values of the subsurface, the geomagnetic transfer function, which determine lateral variations of the electrical

resistivity, and the horizontal magnetic tensor (HMT), which relates the horizontal magnetic fields simultaneously recorded by two sites at a different locations. In the following equations the notation have been modified respect the previous analysis to be consistent with the paper published in chapter 4.

1.4.5.1 The MT impedance tensor

The MT Impedance tensor is a second rank tensor (2x2) relating the horizontal components of the electric field with the horizontal components of the magnetic field at a given frequency recorded simultaneously on the surface of the study area.

$$\begin{pmatrix} e_x(\omega) \\ e_y(\omega) \end{pmatrix} = \begin{pmatrix} Z_{xx}(\omega) & Z_{xy}(\omega) \\ Z_{yx}(\omega) & Z_{yy}(\omega) \end{pmatrix} \begin{pmatrix} h_x(\omega) \\ h_y(\omega) \end{pmatrix} \qquad (1.29)$$

where e_i is the *i* component of the electric field, h_i is the *i* component of the magnetic field, having $i = x, y$. Z_{ij} are the complex components of the MT tensor and can be expressed in a Cartesian form $Z_{ij} = Re(Z_{ij}) + i \cdot Im(Z_{ij})$, or a polar form $Z_{ij} = |Z_{ij}| e^{i\varphi_{ij}}$, where *ij=xx,xy,yx,yy*.

From the modulus and phase of the polar expression two scalar real magnitudes, apparent resistivity and phase, are constrained.

$$\rho_{ij}(\omega) = \frac{1}{\omega\mu} |Z_{ij}(\omega)|^2 \qquad (1.30)$$

$$\varphi_{ij}(\omega) = atan\left(\frac{Im\left(Z_{ij}(\omega)\right)}{Re\left(Z_{ij}(\omega)\right)}\right) \qquad (1.31)$$

The apparent resistivity and phase values vary in function of the period and the geoelectrical structures located below (Figure 1.16).

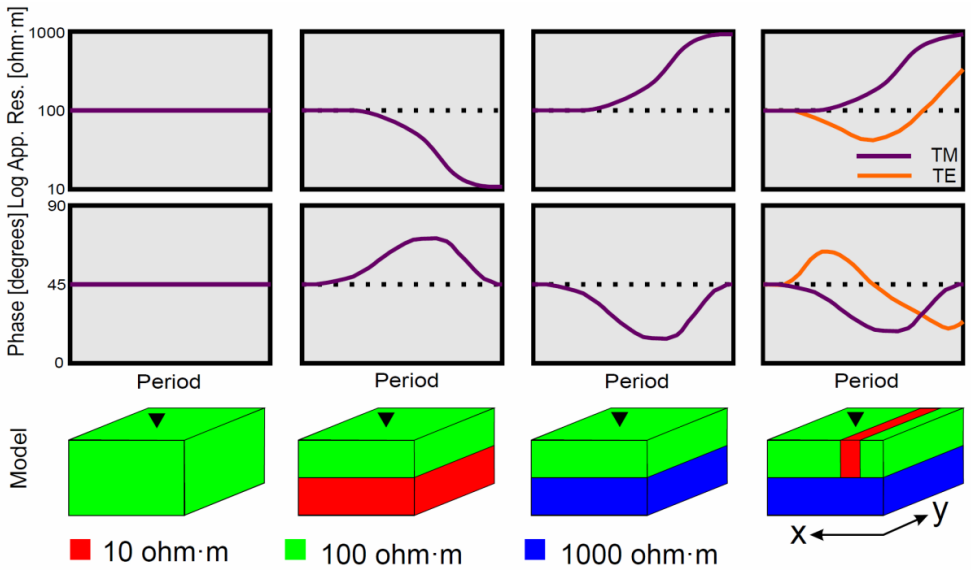

Figure 1.16 Apparent resistivity and phase for four different geoelectrical models. Periods increase from left to right. TE mode when E field parallel to strike and magnetic field perpendicular to the strike. TM mode when E field perpendicular to the strike and H field parallel to the strike.

In a two-dimensional situation, having the recorded axis parallel and perpendicular to the strike direction, there are two modes commonly used to characterize the geoelectrical structures of the subsurface, the TE and TM modes. The TE mode is obtained from the relation between the electric component parallel to the strike direction and the magnetic component perpendicular to the strike direction. The TM mode is obtained from the relation between the electric component perpendicular to the strike direction and the magnetic component parallel to the strike direction. In the two-dimensional situation of figure 1.16, model to the right, the TE mode is associated with the Z_{yx} component and the TM mode is associated with the Z_{xy} component.

1.4.5.2 The geomagnetic transfer function

The geomagnetic transfer function is a dimensionless complex vector magnitude defined as the relation between the vertical component of the magnetic field and the two horizontal components of magnetic field, at a given frequency, simultaneously recorded on the surface of the study area.

$$h_z(\omega) = \begin{pmatrix} W_x(\omega) & W_y(\omega) \end{pmatrix} \begin{pmatrix} h_x(\omega) \\ h_y(\omega) \end{pmatrix} \qquad (1.32)$$

where h_z is the vertical component of the magnetic field and W_i is the *i* component of the geomagnetic transfer function, having $i = x, y$. This transfer function do not directly provide the electrical resistivity values of the subsurface but helps to determine lateral variations of the electrical resistivity and the dimensionality of the geoelectrical structures. A useful way of displaying the geomagnetic transfer function is using the induction arrows (Schmucker, 1970). Figure 1.17 shows the behaviour of the induction arrows for three synthetic geoelectrical models.

1.4.5.3 The horizontal magnetic tensor (HMT)

The HMT is a dimensionless complex tensor magnitude defined as the relation between the time-varying horizontal magnetic fields simultaneously recorded at sites 1 and 2.

$$\begin{pmatrix} h_x^1(\omega) \\ h_y^1(\omega) \end{pmatrix} = \begin{pmatrix} M_{xx}(\omega) & M_{xy}(\omega) \\ M_{yx}(\omega) & M_{yy}(\omega) \end{pmatrix} \begin{pmatrix} h_x^2(\omega) \\ h_y^2(\omega) \end{pmatrix} \qquad (1.33)$$

where M_{ij} are the dimensionless *ij* components of the HMT, having $ij = xx, xy, yx, yy$.

This tensor relationship can be also used to determine the geoelectrical structures of the subsurface. However, as is affected by the electrical resistivity structures below the two sites the HMT do not directly determines the geoelectrical structures below the analyzed site. If the base site, site 2, is located at a horizontally homogeneous zone the HMT will be only affected by the geoelectrical structures situated below site 1. Assuming two-dimensional structures below site 1, an homogeneous half space below site 2 and that the x-axis runs along the strike direction; figure 1.18 shows the modulus of M_{yy}, for different sites and periods, associated with four synthetic geoelectrical models. Other components are not shown due to have constant values: null for M_{yx} and M_{xy} components and one for M_{xx} component (Berdichevsky and Dmitriev, 2008).

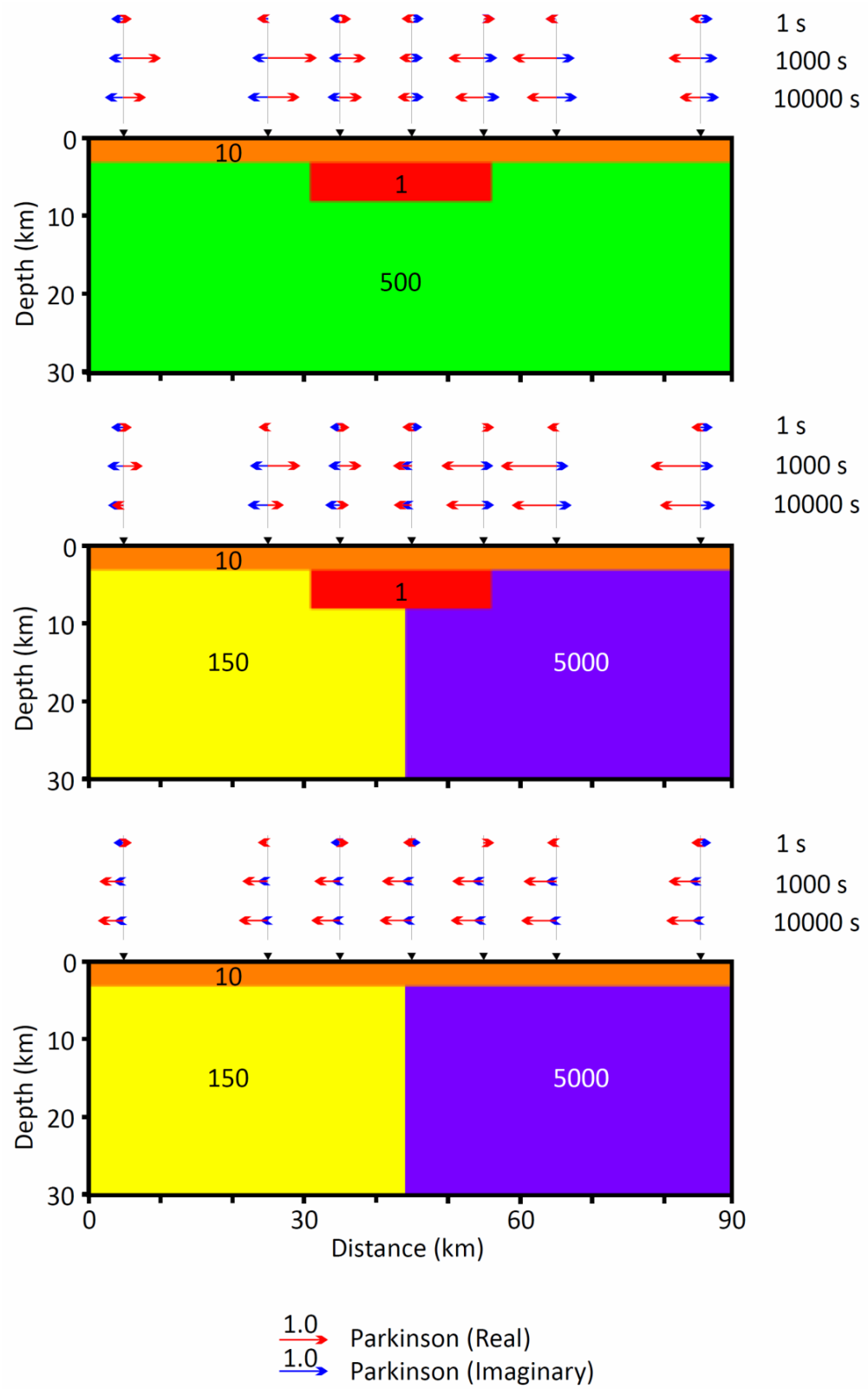

Figure 1.17 Induction arrows for three different two-dimensional geoelectrical models at three different periods (1 s, 1000 s and 10000 s). Units of the electrical resistivity values are in ohm·m. Sites are represented by the inverted triangles.

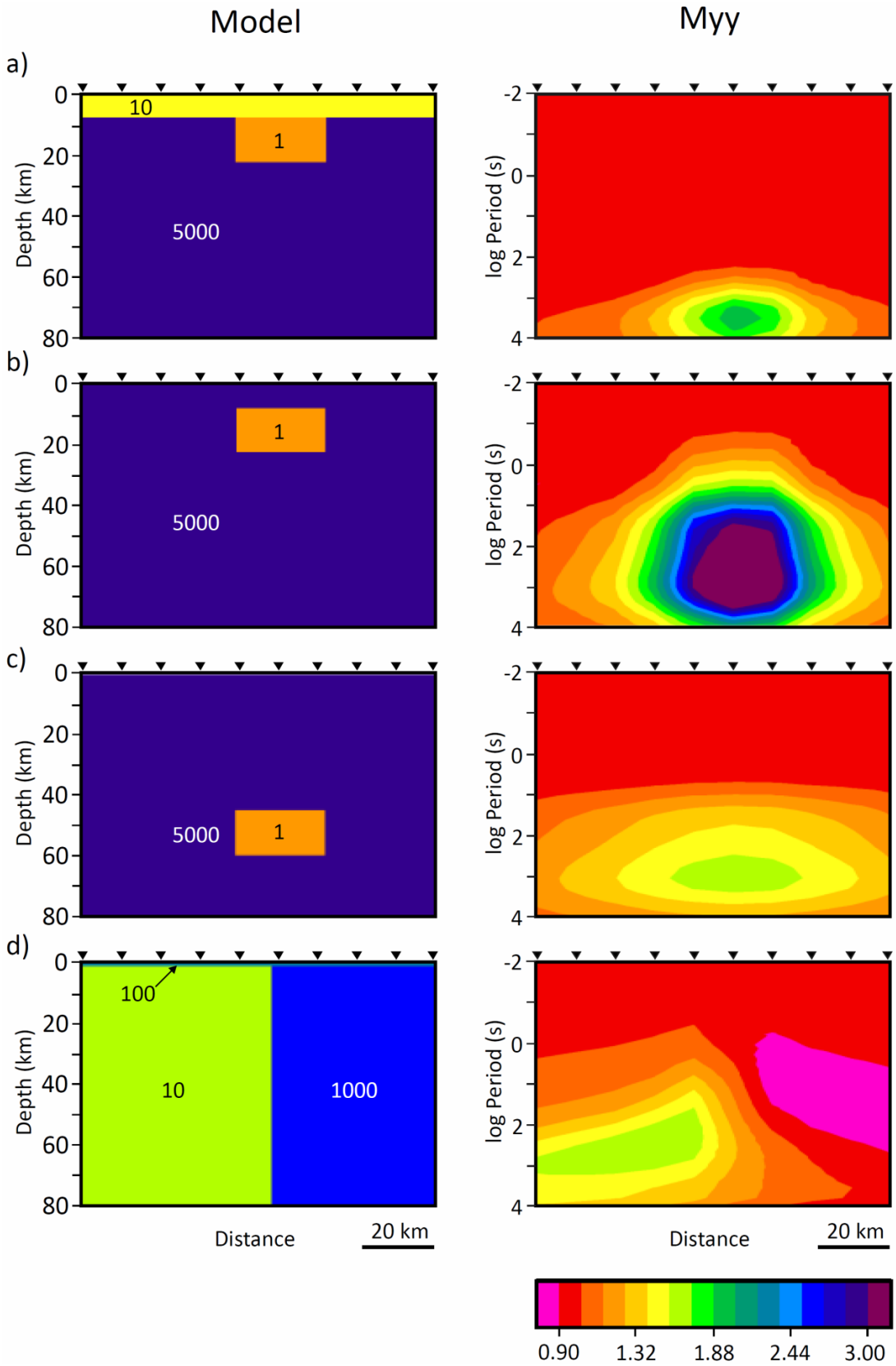

Figure 1.18 Left, two-dimensional electrical resistivity models. Units of the electrical resistivity values are in ohm·m. Right, pseudosection of the modulus of M_{yy} component, which is adimensional, for all the sites and analysed periods. Sites are represented by the inverted triangles.

1.4.5.4 Processing of the MT data

The processing of the MT data consist in determine the MT tensor relationships from the recorded time series solving a statistical problem from multiple calculations of the target transfer function. To determine the target transfer function the recorded time series are divided in several segments and, having converted the time series of each segment from time domain to frequency domain, all these segments are used to determine the transfer function of the study area. Below there is the mathematical development used to determine the MT tensor relationships from the electric and magnetic time-varying fields recorded at the surface of the study area.

Assuming we are in the frequency domain. The transfer functions of equations ((1.29), (1.32) and (1.33)) can be written as

$$\boldsymbol{e} = \boldsymbol{Z}\boldsymbol{h} \qquad (1.34)$$

$$h_z = \boldsymbol{W}\boldsymbol{h} \qquad (1.35)$$

$$\boldsymbol{h}_1 = \boldsymbol{M}\boldsymbol{h}_2 \qquad (1.36)$$

where $\boldsymbol{h}$ is a vector of length two comprising the two horizontal magnetic components $[h_x, h_y]$. $\boldsymbol{e}$ is a vector of length two comprising the horizontal electric components $[e_x, e_y]$ and h_z is the vertical component of the magnetic field. The sub-index 1 and 2 differentiate the MT data recorded at two different sites. $\boldsymbol{Z}$ and $\boldsymbol{M}$ are 2x2 complex matrix relating the two correspondent vectors and $\boldsymbol{W}$ is a 1x2 complex vector relating h_z and $\boldsymbol{h}$.

For each segment on of the time series the transfer functions are calculated from the following equations:

$$\boldsymbol{Z} = [\boldsymbol{e}\boldsymbol{k}][\boldsymbol{h}\boldsymbol{k}]^{-1} \qquad (1.37)$$

$$\boldsymbol{W} = [h_z\boldsymbol{k}][\boldsymbol{h}\boldsymbol{k}]^{-1} \qquad (1.38)$$

$$\boldsymbol{M} = [\boldsymbol{h}_1\boldsymbol{k}][\boldsymbol{h}_2\boldsymbol{k}]^{-1} \qquad (1.39)$$

where $\boldsymbol{k}$ is the vector used as a complex conjugate (Vozoff, 1972). In case of remote reference (Gamble et al., 1979a) $\boldsymbol{k} = \boldsymbol{h_r}$, where $\boldsymbol{h_r}$ is vector of length two comprising the horizontal magnetic fields recorded at a remote site. The value $[\boldsymbol{pq}]$ is the spectral density matrix for the fields $\boldsymbol{p}$ and $\boldsymbol{q}$, defined by Gamble et al. (1979b), viz.

$$[\boldsymbol{pq}] = \begin{bmatrix} \langle p_x q_x^* \rangle & \langle p_x q_y^* \rangle \\ \langle p_y q_x^* \rangle & \langle p_y q_y^* \rangle \end{bmatrix} \qquad (1.40)$$

The asterisk denotes the complex conjugate and $\langle \quad \rangle$ denotes ensemble averaging either by summation over neighbouring frequencies or by averaging different estimates at the same frequency, or both.

In case of $[h_z \boldsymbol{h}_r]$

$$[\boldsymbol{pq}] = [\langle p_x q_x^* \rangle \quad \langle p_x q_y^* \rangle] \quad (1.41)$$

Gamble et al. (1979b) also provide the inverse of the matrix $[\boldsymbol{pq}]$

$$[\boldsymbol{pq}]^{-1} = \frac{\begin{bmatrix} \langle p_y q_y^* \rangle & -\langle p_x q_y^* \rangle \\ -\langle p_y q_x^* \rangle & \langle p_x q_x^* \rangle \end{bmatrix}}{\langle p_x q_x^* \rangle \langle p_y q_y^* \rangle - \langle p_y q_x^* \rangle \langle p_x q_y^* \rangle} \qquad (1.42)$$

Knowing how to determine the values of the transfer functions for each segment and each frequency, the processing of the MT data consist in determine the transfer functions that reduce the differences between predictions and observations.

The residual of the observation *i* with the obtained transfer function is calculated from:

$$r_{x,i}^2 = \left(a_{x,j} - a_{p,x,i}\right)^2 \quad (1.43)$$

where $a_{x,j}$ would be the recorded electric field when determine the MT transfer function, the recorded vertical component of the magnetic field when characterize the geomagnetic transfer function or the recorded horizontal magnetic fields of a neighbouring site when constrain the HMT. $a_{p,x,i}$ would be the same component of $a_{x,j}$ obtained from the following equation:

$$a_{p,x,i} = G_{xx}\, h_{x,i} + G_{xy}\, h_{y,i} \qquad (1.44)$$

where G_{xx} and G_{xy} are the associated transfer functions depending on the analysed variable and $h_{x,i}$ and $h_{y,i}$ are the horizontal magnetic fields recorded on the study area. Equivalent steps are followed for the electric and magnetic fields recorded on the *y* direction when obtain the MT impedance tensor and the HMT.

In case of processing doing robust processing (Chave et al., 1987; Egbert and Booker, 1986 and Junge, 1992), the function to minimise is:

$$\sum_i \rho_i \left(\frac{a_{x,j} - a_{p,x,i}}{\sigma_i}\right) \qquad (1.45)$$

where σ_i is the standard deviation and ρ_i is a function used to reduce the presence of erratic points. An example of the ρ_i function can be found in Egbert and Booker (1986) where

$$\rho = \begin{cases} \dfrac{r^2}{2} & |r| < r_0 \\ \dfrac{r_0}{|r|} - \dfrac{r_0}{2} & |r| \geq r_0 \end{cases} \qquad (1.46)$$

Authors suggest a value of 1.5 for r_0.

Two different robust programs have been used to process the MT data acquired in the Pyrenees. The BBMT data have been processed using Metronix software (Friedrich, 2003) and the LMT data using Birrp.5 academic program (Chave and Thompson, 2004).

1.4.6 Dimensionality analysis

As suggested, the tensor relationship between electromagnetic fields determines the dimensionality of the geoelectrical structures of the subsurface. Below, each tensor is used to obtain the dimensionality of different geoelectrical models.

1.4.6.1 The MT impedance tensor

The MT impedance tensor varies depending of the dimensionality of the geoelectrical structures. In a one-dimensional case, where $\rho = \rho(z)$, the diagonal components of the impedance tensor are null, $Z_{xx} = Z_{yy} = 0$. Due to no lateral variations of the electrical resistivity the components of the anti-diagonal are the same, with different signal, $Z_{xy} = -Z_{yx}$.

In a two-dimensional case, where $\rho = \rho(y, z)$, assuming *x* strike direction, also the diagonal components are null, $Z_{xx} = Z_{yy} = 0$, but in this case, due to the lateral variations of the electrical resistivity, the anti-diagonal components are different $Z_{xy} \neq Z_{yx}$. This is only valid when the orientation of the recording axis (*x,y*) are parallel and perpendicular to the strike direction of the geoelectrical structures. Otherwise, all the components of the impedance tensor are not null and can be different between them. In case to do not record the electric and magnetic fields with the axis oriented following the strike direction, these can be reoriented following the equation (1.47).

$$\begin{pmatrix} 0 & Z_{\parallel} \\ Z_{\perp} & 0 \end{pmatrix} = \begin{pmatrix} \cos\alpha & \sin\alpha \\ -\sin\alpha & \cos\alpha \end{pmatrix} \begin{pmatrix} Z_{xx} & Z_{xy} \\ Z_{yx} & Z_{yy} \end{pmatrix} \begin{pmatrix} \cos\alpha & -\sin\alpha \\ \sin\alpha & \cos\alpha \end{pmatrix} \quad (1.47)$$

where $Z_{\perp}$ and $Z_{\parallel}$ are the perpendicular and parallel components of the impedance tensor when axis are oriented perpendicular and parallel with the strike direction, and α is the angle between the orientation of the measured axis and the strike direction.

In a three-dimensional case, where $\rho = \rho(x, y, z)$, all the components of the impedance tensor are different and not null, having no rotation angle for which the diagonal components of the MT impedance tensor are nulls. Figure 1.19 shows the impedance tensor depending on the dimensionality of the geoelectrical structures of the subsurface.

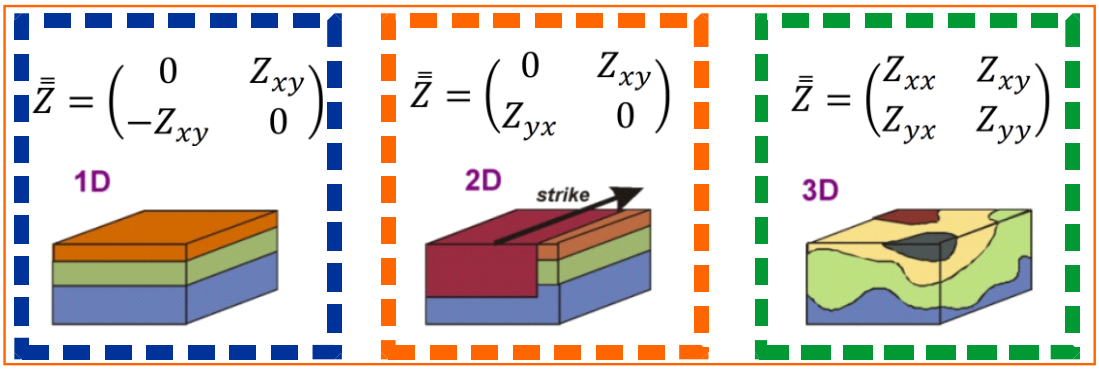

Figure 1.19 MT impedance tensor depending on the dimensionality of the geoelectrical structures. Modified from Martí (2006).

1.4.6.1.1 Galvanic distortion

The values of the MT impedance tensor can be affected by three-dimensional surface distortions or heterogeneities, which are smaller than the targets of interest and the skin depths analyzed. These bodies can cause charge distributions and inducted currents that modify the MT responses at the studied or regional scale (Kaufman, 1988; Chave and Smith, 1994). This kind of distortions can be inductive or galvanic. Inductive distortion, generated by current distributions, has a small magnitude and decays with the periods and in the MT conditions, $\sigma \gg \omega\varepsilon$ (quasi-stationary approximation), can be ignored (Berdichevsky and Dmitriev, 1976). The galvanic distortion, frequency-independent, is caused by charge distribution accumulated on the surface of shallow bodies producing anomalous fields with the same order of magnitude than the recorded signal (Bahr, 1988; Jiracek, 1990). From these results, the

galvanic distortion is treated as the existence of an anomalous electric field having no appreciable influence on the magnetic fields.

The effect of this distortion can be represented by a 2x2 real, frequency independent and dimensionless, matrix *C* (Berdichevsky and Dmitriev, 1976).

$$C = \begin{pmatrix} C_1 & C_2 \\ C_3 & C_4 \end{pmatrix} \qquad (1.48)$$

The MT tensor affected by galvanic distortion can be defined by

$$Z^m(\omega) = C \cdot Z^R(\omega) \qquad (1.49)$$

where $Z^m(\omega)$ is the tensor affected by galvanic distortion, the measured tensor, and $Z^R(\omega)$ is the regional tensor, with no presence of galvanic distortion.

In one- and two-dimensional environments affected by galvanic distortion, the diagonal components of the impedance tensor became different than zero also when the axis are parallel and perpendicular to the strike direction.

$$Z^m(\omega) = \begin{pmatrix} C_1 & C_2 \\ C_3 & C_4 \end{pmatrix} \begin{pmatrix} 0 & Z_{\parallel}(\omega) \\ Z_{\perp}(\omega) & 0 \end{pmatrix} = \begin{pmatrix} C_2 \cdot Z_{\perp}(\omega) & C_1 \cdot Z_{\parallel}(\omega) \\ C_4 \cdot Z_{\perp}(\omega) & C_3 \cdot Z_{\parallel}(\omega) \end{pmatrix} \qquad (1.50)$$

Different methodologies have been proposed to remove the effect of the galvanic distortion over one-dimensional and two-dimensional structures (i.e. Zhang et al., 1987; Bahr, 1988; Groom and Bailey, 1989 and Smith, 1995).

In this thesis we used the Groom and Bailey (1989) method, where the distortion matrix *C* is determined for all the frequencies at the same time. Following this methodology the MT impedance tensor affected by galvanic distortion can be decomposed as:

$$Z^m(\omega) = gRTSAZ^R(\omega)R^T \qquad (1.51)$$

where the matrix distortion *C* has been decomposed by:

$$C = TSgA = \begin{pmatrix} 1 & -t \\ t & 1 \end{pmatrix} \begin{pmatrix} 1 & e \\ e & 1 \end{pmatrix} g \begin{pmatrix} 1+s & 0 \\ 0 & 1-s \end{pmatrix} \quad (1.52)$$

where *R* is the rotational tensor and R^T is the transpose. *T* is the twist tensor, *S* is the shear tensor, *A* the anisotropy tensor and *g* is a gain parameter.

If multiply the regional impedance tensor, Z^R, by the anisotropy tensor, *A*, and the gain parameter, *g*, the resulted tensor still having zeros on the diagonal components. The effect of *A* and *g* is to apply the same gain for all the frequencies, vertically displacing the apparent resistivity curves, without affect the phases.

This new tensor, as a result of multiplying the regional tensor with the anisotropy tensor and the gain parameter, can be defined as:

$$Z^{R*}(\omega) = gAZ^R(\omega) \qquad (1.53)$$

being able to write the measured impedance tensor as:

$$Z^m(\omega) = RTSZ^{R*}(\omega)R^T \qquad (1.54)$$

From equation (1.54) we have a system of equations with eight equations and seven unknown parameters. Solving these equations the strike direction of a two-dimensional subsurface, where the diagonals components of the impedance tensor are zero, can be constrained.

In this thesis we followed the method proposed by McNeice and Jones (2001) to constrain the distortion parameters, from the Groom and Bailey (1989) decomposition,

and determine the strike direction of the geoelectrical structures below the Pyrenean range. Results obtained can be found in figure 1.20.

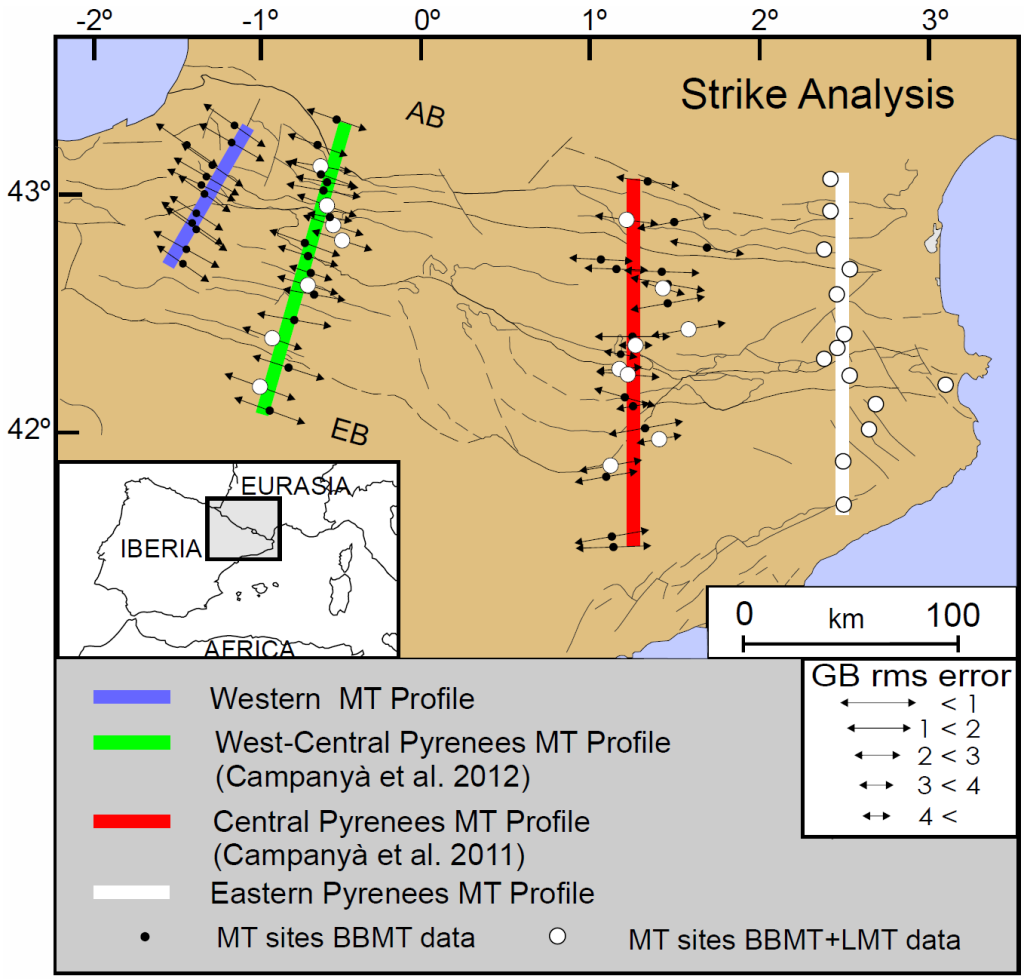

Figure 1.20 Location of the MT sites in the Pyrenees with the associated strike direction for all available data. In the Eastern Pyrenees arrows are not plotted due to data is very three-dimensional, obtaining RMS values much higher than 4. AB: Aquitanian basin; EB: Ebro Basin.

In a three dimensional case the effect of the galvanic distortion on the MT impedance tensor is more complex and frequency depends, which modify the curves of apparent resistivity and phase due to the interaction between different components of the regional MT impedance tensor, $Z^R(\omega)$.

$$Z^m(\omega) = C \cdot Z^R(\omega) = \begin{pmatrix} C_1 & C_2 \\ C_3 & C_4 \end{pmatrix} \begin{pmatrix} Z_{xx}(\omega) & Z_{xy}(\omega) \\ Z_{yx}(\omega) & Z_{yy}(\omega) \end{pmatrix}$$

$$= \begin{pmatrix} C_1 \cdot Z_{xx}(\omega) + C_2 \cdot Z_{yx}(\omega) & C_1 \cdot Z_{xy}(\omega) + C_2 \cdot Z_{yy}(\omega) \\ C_3 \cdot Z_{xx}(\omega) + C_4 \cdot Z_{yx}(\omega) & C_3 \cdot Z_{xy}(\omega) + C_4 \cdot Z_{yy}(\omega) \end{pmatrix} \qquad (1.55)$$

In this case, the effect of the galvanic distortion has to be well determined to avoid future misinterpretations. Ledo et al. (1998), Garcia and Jones (1999, 2002) and Utada and Munekane (2000) have suggested some methodologies to correct the galvanic distortion in three dimensional situations.

Alternative methods like Bahr invariant (Bahr, 1988) and the phase tensor (Caldwell et al., 2004) can be used to obtain the dimensionality of the geoelectrical structures characterizing or avoiding the effect of the galvanic distortion. In this thesis the WALDIM program proposed by Martí et al. (2009b) based on the Bahr invariants has been used to corroborate the results obtained.

1.4.6.2 The geomagnetic transfer function

The geomagnetic transfer function can be represented using the induction arrows (Schmucker, 1970), which are composed of a real part and an imaginary part. From equation (1.32) the real and the imaginary component of the induction arrows can be written as:

$$V_{Re} = ReT_x \cdot \hat{n}_x + ReT_y \cdot \hat{n}_y \qquad (1.56)$$

$$V_{Im} = ImT_x \cdot \hat{n}_x + ImT_y \cdot \hat{n}_y \qquad (1.57)$$

where $\hat{n}_x$ and $\hat{n}_y$ are unitary vectors in the respective directions. Depending on the used convention, the induction arrows point to the concentration of currents (Parkinson convention) or the opposite way (Schmucker or Weise conventions).

In a one-dimensional Earth, the induction arrows are zero. In a two-dimensional Earth, the real and imaginary vectors point to the same direction for all the periods, perpendicular to the strike direction. In a three-dimensional Earth, the direction of the induction arrows varies with frequency, and real and imaginary vectors are not parallel (Figure 1.21).

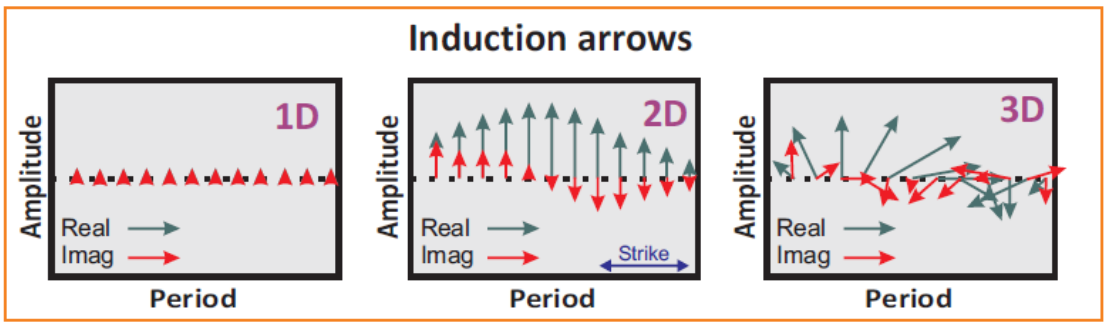

Figure 1.21 Induction arrows depending of the dimensionality of the geoelectrical structures. Periods increase from left to right.

The real component of the induction arrows, at different frequencies, constrained in the Pyrenees are shown in figure 1.22, corroborating the results shown in figure 1.20.

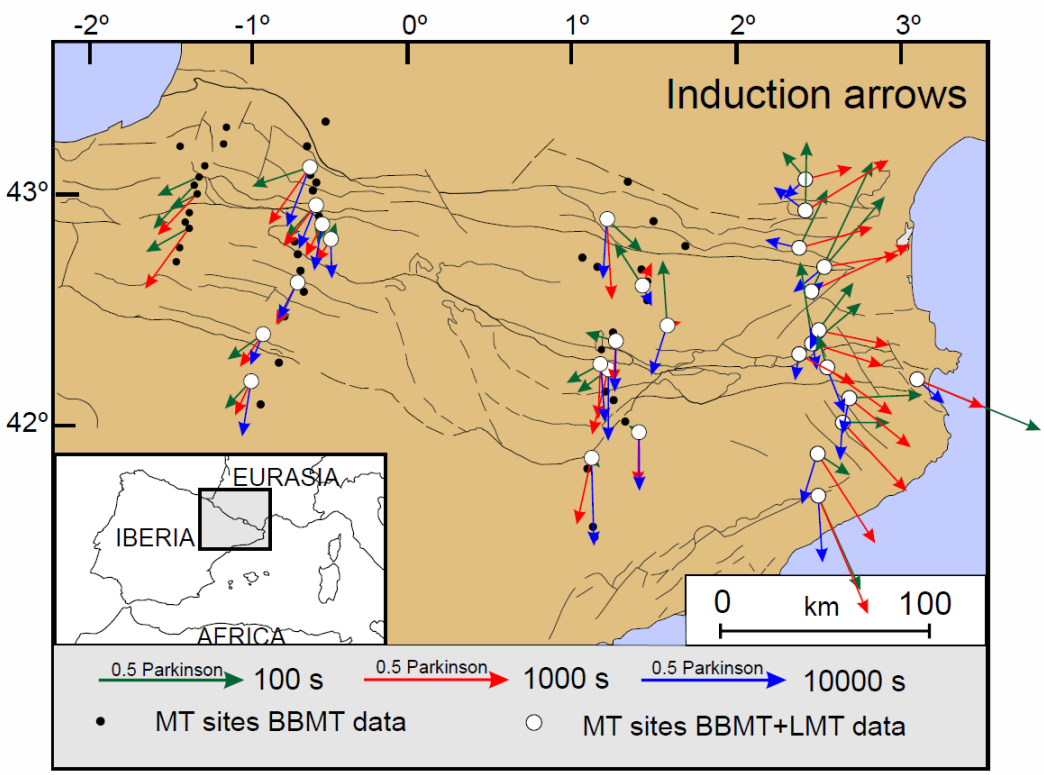

Figure 1.22 Location of the MT sites in the Pyrenees with the associated real components of the induction arrows for three different periods.

1.4.6.3 The horizontal magnetic tensor

Kusi (1997) suggest a method to determine the strike direction from the HMT. From the results obtained in equation (1.33) relating the horizontal magnetic fields of two different sites the proposed method provides a θ' angle, which is the angle that the

measured axis have to be clockwise rotated to fit with the strike direction of the geoelectrical structures. Two different ways can be followed to obtain the θ' angle.

$$\theta' = \frac{1}{2}\left[atan\left[\left(M_{xx} - M_{yy}\right)/\left(M_{xy} + M_{yx}\right)\right] - atan\left[\left(M_{yy} + M_{xx}\right)/\left(M_{xy} - M_{yx}\right)\right]\right] \quad (1.58)$$

$$\theta' = \frac{1}{2}\left[atan\left[\left(M_{xx} - M_{yy}\right)/\left(M_{xy} + M_{yx}\right)\right] + atan\left[\left(M_{yy} + M_{xx}\right)/\left(M_{xy} - M_{yx}\right)\right]\right] \quad (1.59)$$

Given that the results should be the same, differences between (1.58) and (1.59) will give an idea of the resolution obtained in determine the strike direction, in case of a two-dimensional medium. In case of one-dimensional medium the angle will be zero. In case of two-dimensional medium the obtained angle will be the angle needed to rotate to the strike direction and in case of three-dimensional medium the two obtained angles will differ.

1.4.7 Static shift

In a one- and two-dimensional geoelectrical region affected by galvanic distortion, following the steps shown in "1.4.6.1.1 Galvanic distortion", we can recover the regional phases and the strike direction but not the real values of the apparent resistivity, which are distorted by the anisotropic tensor, *A*, and the gain value, *g*. This distortion produces a vertically displacement of the apparent resistivity curve, do not representing the geoelectrical structures of the subsurface. This effect is known as *static shift*. Additional information use to be required to remove the effect of the *static shift*. In this thesis we used the method suggested by Jones (1988) where a geological parameter, associated with a change in resistivity, has to be known. We use the depth of the basement, associated with an increase of the electrical resistivity, obtained from Lanaja and Querol (1987).

There are other methodologies to remove the effect of the *static shift*. We can use the electrical resistivity values of the subsurface recorded in a resistivity-log carried out in the study area or constrain the electrical resistivity of the first meters using controlled source electromagnetic methods. In case of having large amount of sites in a similar

geological region, the average apparent resistivity values associated with the shorter periods can be used as a representative value of the first meters. An alternative method is suggested by Ledo et al. (2002), solving the effect of the *static shift* using the geomagnetic transfer function.

1.4.8 Modelling MT data

Having constrain the MT transfer functions and correct the distortion parameters, one of the most commonly ways to interpret the results is determine a geoelectrical model able to explain the MT data acquired on the study area. Different programs have been created for modelling depending on the dimensionality of the geoelectrical structures (i.e. One-dimensional: OCCAM1D (Constable et al., 1987). Two-dimensional: RLM2DI (Rodi and Mackie (2001), OCCAM2D (deGroot-Hedlin and Constable, 1990) and REBOCC (Siripunvaraporn and Egbert, 2000). Three-dimensional: WSINV3DMT (Siripunvaraporn et al., 2005) modEM (Egbert and Kelbert, 2012), the 3D inversion of Winglink® (Mackie and Madden, 1993) and x3D-INV (Avdeeva, 2008). In the inversion process, the error floor associated with each type of data has strong influence on the final results. Gabàs and Marcuello (2003) determine the error ratio between different components to give the same weight for all of them.

From the analysis of the transfer functions determined in the Central and the West-Central Pyrenees the dimensionality of the geoelectrical structures below the subsurface have been assumed as two-dimensional. Before the inversion, the MT transfer functions have been rotated fitting with the strike direction. The algorithm proposed by Rodi and Mackie (2001) has been applied to determine the geoelectrical models used to explain the acquired MT data in the Central and the West-Central Pyrenees. This algorithm is a finite-difference code that employs a nonlinear conjugate gradient scheme to minimize an objective function associated with the 2D isotropic inverse problem that penalizes data residuals and second spatial derivatives of resistivity.

CHAPTER 2

Terra Nova

doi: 10.1111/j.1365-3121.2011.01001.x

Lithospheric characterization of the Central Pyrenees based on new magnetotelluric data

Joan Campanyà,[1] Juanjo Ledo,[1] Pilar Queralt,[1] Alex Marcuello,[1] Montserrat Liesa[2] and Josep A. Muñoz[1]

[1]*Institut Geomodels, Departament de Geodinàmica i Geofísica, Universitat de Barcelona, C/Martí Franquès s/n Barcelona, 08028, Spain;*
[2]*Departament de Geoquímica, Petrologia i Prospecció Geològica, Universitat de Barcelona, C/Martí Franquès s/n Barcelona, 08028, Spain*

RESUM

Els Pirineus són els resultat de la col·lisió continent-continent entre la placa Ibèrica i la placa Europea durant l'orogènia Alpina. Tot i que la subducció de la l'escorça Ibèrica inferior és acceptada, els processos físics que tenen lloc en el límit entre plaques és encara avui en dia tema de discussió, com es mostra en el debat obert sobre la presència o absència de fusió parcial a l'escorça Ibèrica inferior subduida. Les dades de llarg període enregistrades per primer cop al Pirineu Central han permès determinar els valors de resistivitat elèctrica de l'escorça Ibèrica inferior subduida millor que en estudis previs, caracteritzant el límit superior d'aquesta 9 km més profund. A més a més, les dades magnetotel·lúriques de llarg període han permès determinar el límit litosfera astenosfera a 90 km i 130 km de profunditat sota les plaques Ibèrica i Europea, respectivament. També s'han caracteritzat els valors de resistivitat elèctrica de l'astenosfera, entre 10 Ω·m i 18 Ω·m.

SUMMARY

The Pyrenees resulted from the continent–continent collision between the Iberian and European plates during the Alpine orogeny. Although the subduction of the Iberian lower crust is currently accepted, the physical processes that occur at the boundary between the plates are still a topic of open discussion today, as illustrated by the debate about the presence or absence of partial melting in the Iberian Subducted Lower Crust. Long Period Magnetotelluric data acquired for the first time in the Central Pyrenees constrain the low electrical resistivity structure in the Iberian Subducted Lower Crust better than previous studies, plotting their upper limit 9 km deeper. This new upper limit reinforces the hypothesis of partial melting. Additionally, Long Period Magnetotelluric data constrain the lithosphere–asthenosphere boundary at 90 and 130 km deep below the Iberian and European plates, respectively, and are compatible with electrical resistivity values between 10 and 18 Ω·m for the asthenosphere.

2.1 INTRODUCTION

Continent-continent collision is a fundamental tectonic process that plays a primary role in the development of continents. The electromagnetic signature of continent-continent collision zones depends on the age of the collision and usually presents a major low electrical resistivity structure at crustal or upper-mantle depths associated with water, melt, sulphides or graphite (i.e. Wei et al., 2001; Türkoğlu et al., 2008; Martí et al., 2009a; and Selway et al., 2009). In active collisions the low electrical resistivity structure appears, usually, in the middle crust. In contrast, when it becomes more stable they appear at lower-crustal and upper-mantle depths (see Unsworth, 2009 for a review). Within the Alpine-Himalayan mountain belt, the collision between the Iberian and the European plates from the Late Cretaceous to the Early Miocene resulted in the formation of the Pyrenees (Muñoz, 1992). This mountain range offers a unique opportunity to study orogenic processes due to the well constrained geological evolution and the significant amount of geophysical data available (see Muñoz, 2002 for a review).

We present a joint interpretation of the available geophysical and geological data together with the first Long Period Magnetotelluric (LMT) data collected in the Pyrenees. These new data confirm the hypothesis of partial melting in the Iberian Subducted Lower Crust (IBSLC) and constrain the lithosphere-asthenosphere boundary (LAB) and the electrical resistivity of the asthenosphere. The geoelectrical characterization of the Pyrenean lithosphere will help us to gain insight into the evolution of the lithosphere in continental-collision zones.

2.2 GEOLOGICAL SETTING AND PREVIOUS STUDIES

The Central Pyrenees is a double-wedge orogenic system bounded by two foreland basins: the Ebro Basin (EB) southwards, and the Aquitaine Basin (AB) northwards (Figure 2.1). The south Pyrenean wedge consists of south directed thrust sheets involving Mesozoic and Paleogene sedimentary successions (SPTS). Northwards, the basement rocks initially located underneath the cover successions of the South

Pyrenean Thrust Sheets were synchronously underthrusted and piled into an antiformal stack. These south Pyrenean basement thrust sheets only involve upper crustal rocks which crop out along the central part of the Pyrenees and have been historically referred as the Axial Zone (AZ). The North Pyrenean Thrust Sheets (NPTS) involve a complete crustal section of cover and basement rocks. Restoration of the Pyrenean thrust sheets gives a minimum shortening of 150-160 km across the Central Pyrenees (Muñoz, 1992; and Beaumont et al., 2000).

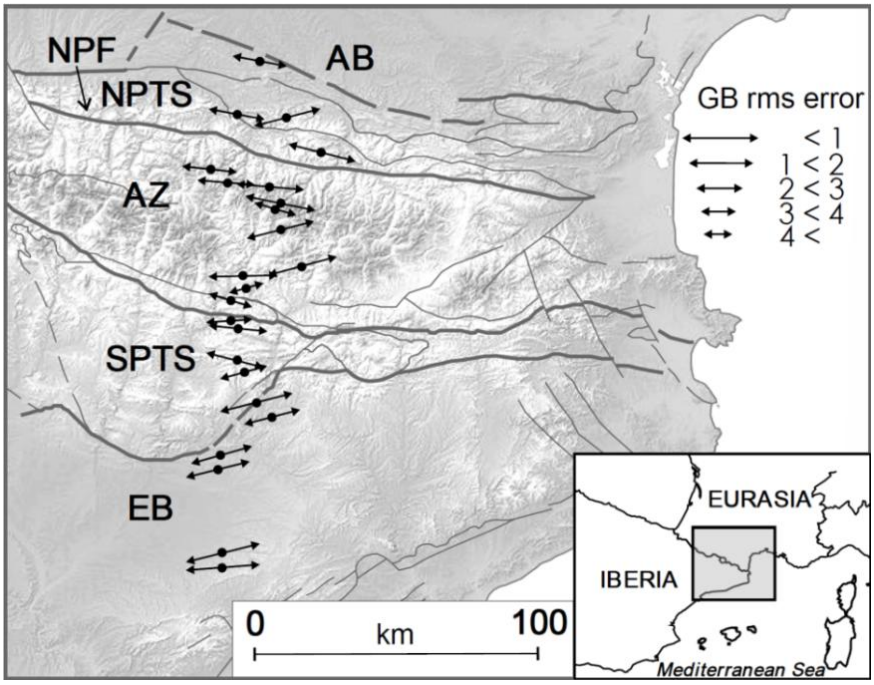

Figure 2.1 Location of the MT stations (Black spots) in a structural sketch of the study area on a topographic map of the Pyrenees. The arrows indicate the strike direction of each site and their lengths are associated with the compatibility of the data to assume 2-D data in the suggested strike direction. EB (Ebro Basin), SPTS (South Pyrenean Thrust Sheets), AZ (Axial Zone), NPTS (North Pyrenean Thrust Sheets), AB (Aquitaine Basin), NPF (North Pyrenean Fault).Thick lines divide the main geological units and thin lines are the internal divisions.

Several refraction and deep reflection seismic profiles constrain the crustal thickness in the Pyrenean domain (Muñoz, 2002).The depth of the European Moho varies between 30 km and 35 km. The depth of the Iberian one increases progressively from south to north from 35 km to 60 km (ECORS-Pyrenees team, 1988; and Choukroune and ECORS Team, 1989). These differences are related to the limited subduction of the Iberian lower crust below the European one and the stacking of basement thrust sheets in the southern Pyrenees (Muñoz, 1992).

A tomographic model from teleseismic P-waves travel times (Souriau and Granet, 1995) showed a negative V_p anomaly below the Central Pyrenees which pointed to the subduction of the Iberian lower crust down to 80-100 km depth. A recent tomographic model from teleseismic P and PKP-waves travel times (Souriau et al., 2008) include crustal corrections before inversion and the negative V_p anomaly disappear, suggesting that it was an artefact. Authors alleged that the data are not at odds with the subduction hypothesis, although did not confirm it. Nevertheless, a new tomographic model (Koulakov et al., 2009), also including crustal corrections, has obtained a negative V_p anomaly beneath the Central Pyrenees. Koulakov et al. (2009) also show an S-waves model without a major V_s anomaly associated with the IBSLC.

Ledo (1996) and Ledo et al. (2000) obtained a three-dimensional electrical resistivity model for the Central and Western Pyrenees using Broad Band Magnetotelluric (BBMT) data. The three-dimensional model validated a previous two-dimensional model of the Central Pyrenees (Pous et al., 1995a) and corroborated the validity of considering the behavior of Central Pyrenees resistivity structure as two-dimensional (Pous et al., 1995a). All these models, obtained by trial-and-error fitting of the data, show a low electrical resistivity anomaly in the Iberian lower crust associated with the subduction of the Iberian plate and attributed to a small portion of partial melting (Pous et al., 1995b, Ledo et al., 2000; and Glover et al., 2000).

Gravity and geoid anomaly models are compatible with the subduction of the Iberian lower crust (Ledo et al., 2000; Vacher and Souriau, 2001) and so does a recent work integrating heat flow, gravity, geoid anomaly and topography data (Gunnell et al., 2008). Heat flow related studies (Zeyen and Fernández, 1994; Glover et al., 2000; Tesauro et al., 2009) constrain the geotherms below the Pyrenees at lithospheric scale, without observing any anomaly associated to the subduction of the Iberian lower crust, suggesting that thermal reequilibration has already ended.

Subduction of the Iberian lower crust below the European one is currently accepted but the physical processes that occur in the boundary between the plates are still an

open discussion, as illustrated by the debate about the existence of partial melting in the subducted slab (Pous et al., 1995b; Vacher and Souriau, 2001; Souriau et al., 2008).

2.3 MAGNETOTELLURIC DATA

The previous magnetotelluric (MT) data were acquired along a 180 km North-South profile, parallel to ECORS-Pyrenees seismic profile, and were composed of 16 BBMT sites (Pous et al. 1995a; and Ledo, 1996) collected between 1992 and 1993. In 2009, new BBMT and LMT data were acquired in eight new sites along the ECORS profile. BBMT data were recorded using a Metronix ADU06 system and were processed using Metronix software (Friedrichs, 2003). LMT data were recorded using a LEMI system designed by the Lviv Centre of Institute of Space Research and processed using Birrp.5 (Chave and Thompson, 2004). The combination of BBMT and LMT data allows us to cover a period range between 0.001 s and 20000 s.

In order to determine the dimensionality of the regional structures and to obtain the regional impedance tensor we applied the Groom and Bailey (1989) method following the scheme of McNeice and Jones (2001). Geoelectric strike directions of individual sites were estimated from the MT impedance tensors at each site for all the periods with an error floor of 5% on the impedance tensor components (Figure 2.1). Two-dimensional data dimensionality is assumed with a dominant East-West strike direction. These results were confirmed by the rotational invariants (Weaver et al., 2000) using the WALDIM code (Martí et al., 2009b). The static shift was corrected using seismic and well data (Lanaja and Querol, 1987) to fix the contact between the Mesozoic and the Palaeozoic basement following the method of Jones (1988).

2.4 TWO-DIMENSIONAL INVERSION

Two-dimensional inversion of the data was done using the algorithm of Rodi and Mackie (2001) using the TE- and the TM-mode of the apparent resistivity and phases. We fitted the logarithm of the apparent resistivity data to within 10% and the phases to within 2.86^{o}. The model obtained is shown in figure 2.2. The residuals between the

observed data and the model responses are random and no strong feature in the data is unexplained (Figure 2.3).

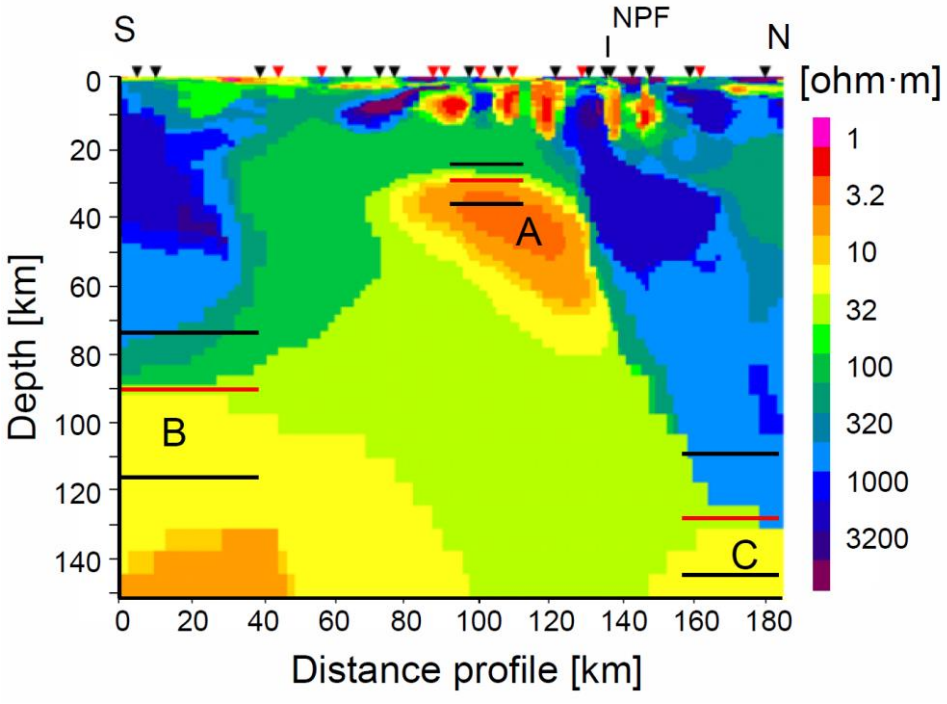

Figure 2.2 Two-dimensional electrical resistivity model obtained from the joint inversion of TE and TM mode for apparent resistivity and phases. Red lines show the position of the upper limit of **A**, **B** and **C** structures suggested in this work. Black lines show the possible variations of the upper-limits, resulted from the sensitivity test, for structures **A**, **B** and **C**. Sites are represented by inverted triangles (red sites have BBMT and LMT data and black sites have BBMT data).NPF (North Pyrenean Fault).

The most striking features of the electrical resistivity model (Figure 2.2) have been labelled **A** (associated to the IBSLC), **B** and **C** (associated to the asthenosphere below the Iberian and European plates, respectively). Nonlinear sensitivity tests (Ledo and Jones, 2005) were carried out to determine their upper and lower electrical resistivity bounds and the bounds on their top depths. Thus, the electrical resistivity for structure **A** should range between 3.2 ohm·m and 5.6 ohm·m and its upper-limit between 25 km and 38 km depth. The electrical resistivity for structures **B** and **C,** assuming structures with homogeneous electrical resistivity, should range between 10 ohm·m and 18 ohm·m. The upper-limit of structure **B** should be between 75 km and 115 km depth and between 110 km and 145 km depth for **C** (Figure 2.2). The low electrical resistivity values of structure **A** screen the structures below it but the non linear sensitivity test gave a minimum value of 30 ohm·m for the region below.

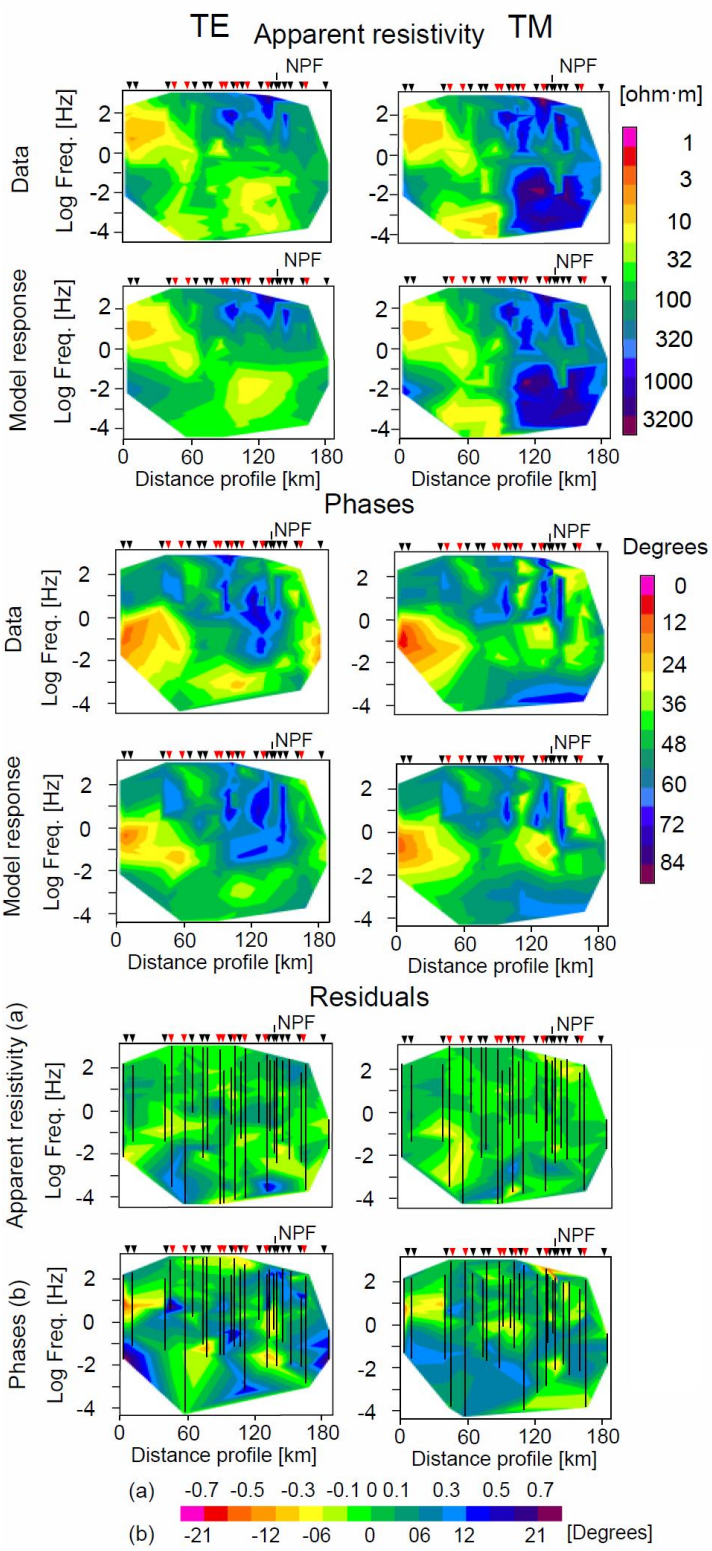

Figure 2.3 Comparison between the observed data and the model responses. At the top the pseudosection of the apparent resistivity. At the middle the pseudosecion of the phases. At the bottom the pseudosecion of the residuals for the apparent resistivity (Model responses minus raw data divided by raw data) and the phases (Model responses minus raw data).In both cases for TE and TM mode (left and right respectively). Sites are represented by inverted triangles (red sites have BBMT and LMT data and black sites have BBMT data). Black lines in the residual pseudosection show the range of periods used for each site for the inversion. The misfit between the data and the model responses has an RMS value of 3.1”

2.5 DISCUSSION AND CONCLUSIONS

2.5.1 Subduction of the Iberian lower crust

Some authors have proposed the presence of partial melting in the IBSLC (Pous et al., 1995b; Ledo et al., 2000; Glover et al., 2000; and Partzsch et al., 2000). Conversely, Vacher and Souriau (2001) suggest the presence of free water released from metamorphic reactions in the amphibolite to eclogite facies transition. This facies change could also account for the density increase of the subducted slab. Gravimetric and geoid anomaly data accept both homogeneous and increasing density gradient of the subducted slab (Ledo et al., 2000; and Vacher and Souriau, 2001).

Our results suggest that the top of structure **A** is located at 30 km depth, 9 km deeper than the previous MT models (Pous et al., 1995a; and Ledo 1996). This limit coincides with the lower–upper crust limit suggested by Muñoz (1992) (Figure 2.4). At this depth, the geotherms calculated by Vacher and Souriau (2001) and Glover et al. (2000) intersect the granite wet solidus curve at approximately 630°C (Figure 2.5). Figure 2.5 also shows that the rocks of structure **A** would be in amphibolite facies and at temperatures high enough to melt if the rock composition is favourable and provided an aqueous fluid phase is present (Thompson and Connolly, 1995).The new characterization of structure **A** solves the problem associated with the hypothesis of partial melting present in the previous MT model (Figure 2.5).

Geologic data suggest that in high-grade metamorphic events, fluid-undersaturated conditions prevail (Clemens, 2006) as free water expelled by metamorphic reactions escapes (Bailey, 1990). When temperature conditions are high enough to cause partial melting, dehydration-melting reactions of hydrous minerals such as muscovite and biotite are the main reactions producing melts. Muscovite dehydration-melting takes place at temperatures near the granite wet solidus. This reaction releases a small amount of melt which does not migrate as the critical melt percentage is not achieved. Extensive melting only occurs at temperatures over 800°C, generally associated with dehydration-melting reactions of biotite. The deeper levels outcropping in the North Pyrenean and Axial Zone suggest that the Pyrenean middle and lower crust is formed

by pelites and greywackes metamorphosed during Variscan orogeny to amphibolite and granulite facies (Vielzeuf, 1984). Thus, the rocks contain a limited amount of water in their structures stored in the hydrous phases, mainly in muscovite and biotite at lower temperatures (amphibolite facies) and biotite at higher temperatures (granulite facies). If temperature is high enough to produce partial melting, as shown in figure 2.5, an undersaturated melt will be stable and the fluid will migrate to the melt as soon as it is formed. Using the Modified Brick Layer Model (MBLM) suggested by Partzsch et al. (2000), the amount of partial melting necessary to explain the low electrical resistivity of structure **A** is between 2.5 vol% and 9 vol%. This volume is far below the critical melt percentage (20 vol%) necessary to migrate and rise to the surface.

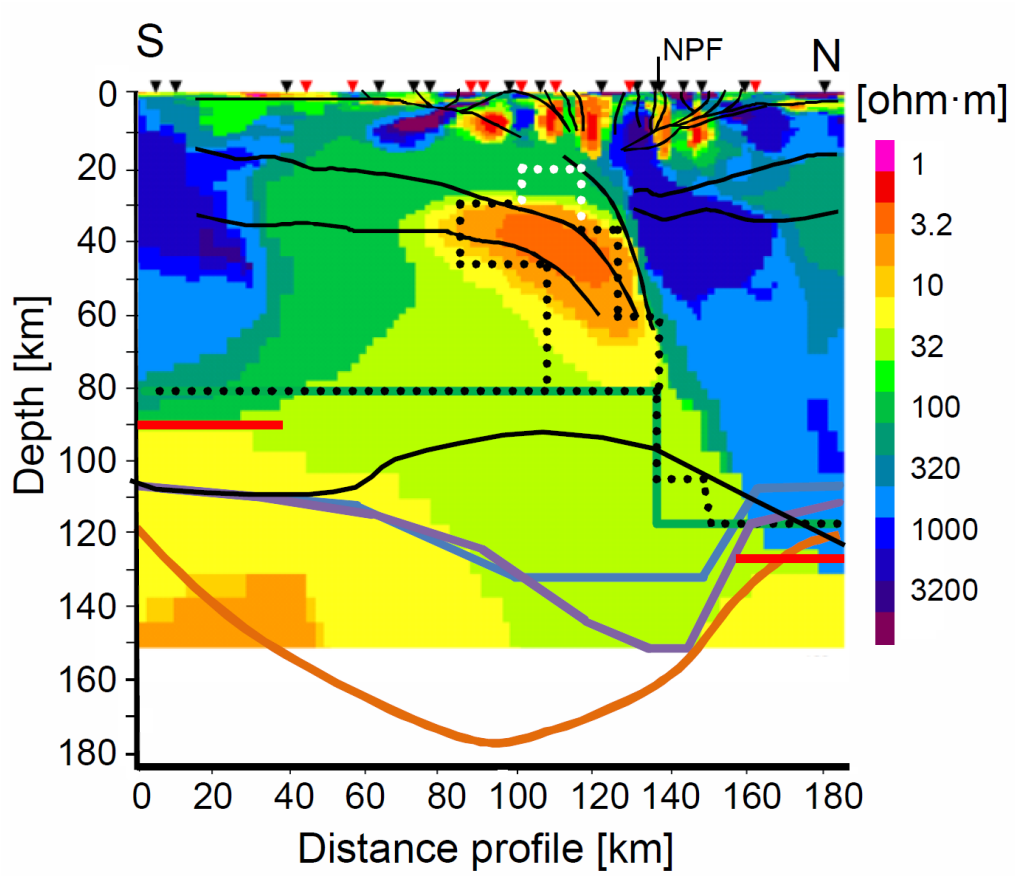

Figure 2.4 Cross-section showing the main structural lithospheric features superimposed on the electrical resistivity model of figure 2.2. In the upper part we have superimposed a simplification of the geological interpretation realized by Muñoz (1992). In the lower part we have included the LAB suggested by different geophysical studies: Ledo *et al.*, (2000) (green), Gunnell *et al.*, (2008) (orange), Zeyen and Fernández, (1994) (blue), Frison *et al.* (2004) (purple). Black line is the LAB obtained from the S-waves model provided by Koulakov *et al.* (2009). Red lines are the LAB suggested in this work from BBMT and LMT data. Black points represent the equivalent of the structure **A** and the LAB obtained by Pous *et al.* (1995a) and Ledo (1996). White dashed line shows the difference of the upper-limit of structure **A** between the previous and the new MT model.

Despite the disagreement between the two most recent studies from seismic tomography (Souriau et al., 2008; and Koulakov et al.,2009) it should be noted that in both cases there is a local minimum of the V_p anomaly corresponding to structure **A** (Figure 2.6), a structure associated with the IBSLC and the presence of partial melting. The absence of a major V_s anomaly in the S-waves model (Koulakov et al., 2009) associated with structure **A** (Figure 2.6) could be related to the small amount of partial melting and to the absence of a thermal anomaly in this region.

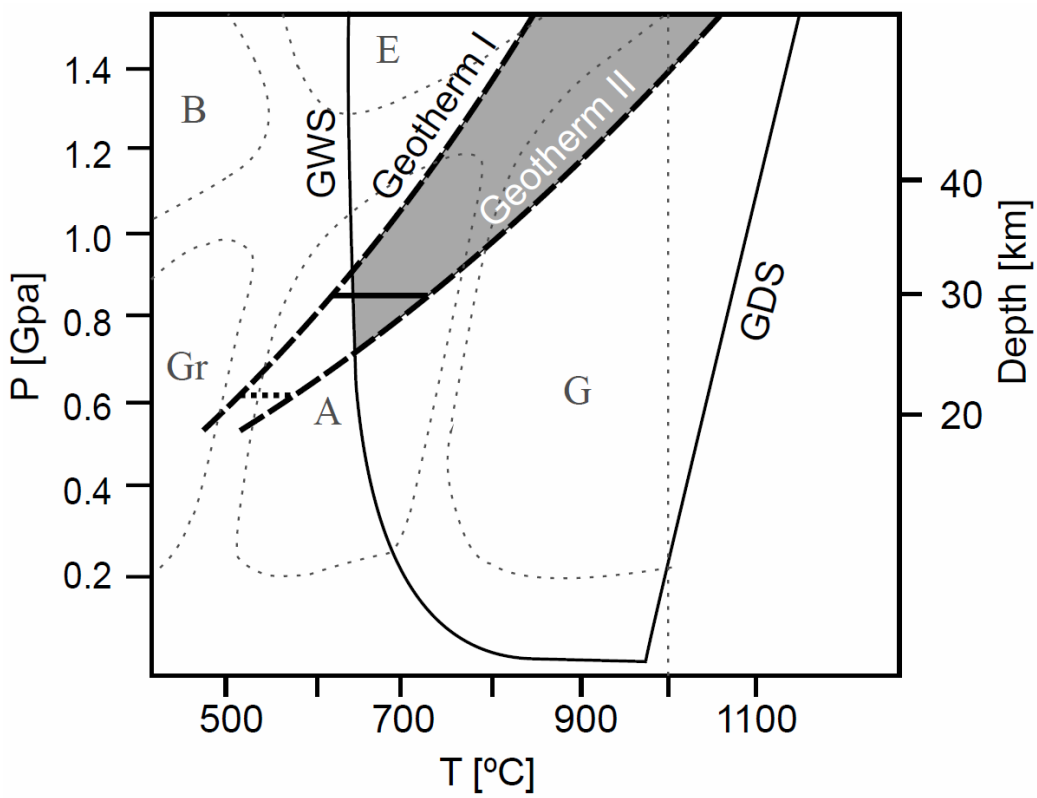

Figure 2.5 Influence of the water on the melt temperature of the granite (common crustal rock). Geotherm I: Geotherm suggested by Vacher and Souriau (2001) based on the data and calculations of Zeyen and Fernández (1994). Geotherm II: Geotherm suggested by Glover *et al.* (2000). The gray zone gives the range of pressure and temperature where we have the appropriate conditions to obtain partial melting of a granite rock in the presence of free water. The dotted thick line and continuous thick line indicate the depth at which the previous MT model (Pous *et al.*, 1995a; and Ledo, 1996) and the model obtained in this work respectively have the upper limit of the low electrical resistivity structure associated with the partial melting zone. Smooth dashed lines represent the main metamorphic facies of mafic crustal rocks (Modifies of Bucher and Frey, 1994). (GWS: Granite wet solidus, GDS: Granite dry solidus, A: Amphibolite, B: Blueschist, E: Eclogite, G: Granulite and Gr: Greenschist). Modified from Thompson (1992).

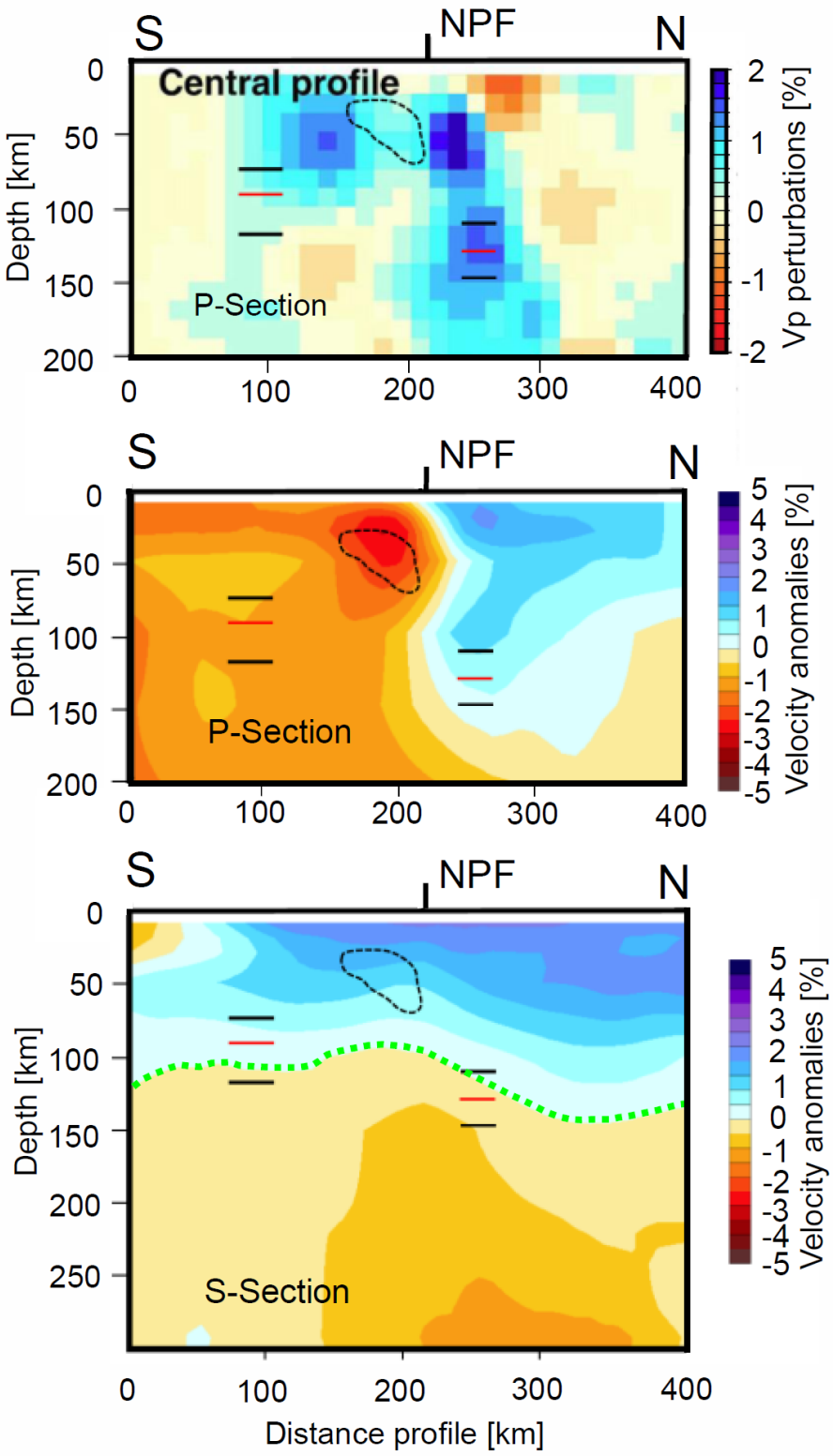

Figure 2.6 Seismic tomography models from P-waves obtained by Souriau *et al.* (2008) (top) and Koulakov et al. (2009) (middle) and the S-wave model obtained by Koulakov et al. (2009) (bottom). Superimposed on the three models the contour of the structure **A**, the low electrical resistivity structure associated with the IBSLC (black dashed line), and the LAB beneath Iberian and European plates (black and red lines) obtained in this work. In the S-waves model the upper limit of the negative V_s anomaly associated with the LAB (green dashed line).

2.5.2 Lithosphere-Asthenosphere Boundary below the Iberian and the European plates

The electrical resistivity and the upper limit of structures **B** and **C**, associated with the asthenosphere, are consistent with the results obtained in other areas (Heinson, 1999; Korja, 2007; and Jones et al., 2010). The LAB below the IBSLC cannot be accurately determined due to the screening effect of the low electrical resistivity associated with partial melting.

Different geophysical studies have been done to constrain the LAB beneath Central Pyrenees, among them: topography, Bouguer anomaly and heat flow data (Zeyen and Fernández, 1994), BBMT data (Pous et al., 1995a;and Ledo, 1996), BBMT, geoid anomaly and Bouguer anomaly data (Ledo et al., 2000) and topography, geoid anomaly, gravity and heat flow data (Gunnell et al., 2008). Figure 2.4 shows the LAB suggested by these studies, jointly with the LAB suggested by Frizon de Lamotte et al. (2004) and by Koulakov et al. (2009) and they are all superposed on the MT model obtained in this work. The thermal and rheological model suggested by Tesauro et al. (2009) gives values in the order of 120 km for the LAB in the area. It is worth nothing that MT models show a European plate thicker than the Iberian one in agreement with the LAB observed in Koulakov et al. (2009) (Figures 2.4 and 2.6).The proposed depths for the LAB below the Iberian and European plates are similar in all the models. However, they significantly differ below the IBSLC up to 100 km, emphasising the poor characterization of the LAB at the plate boundary.

In summary, the better characterization of the upper limit of the low electrical resistivity structure beneath the Central Pyrenees, structure **A**, jointly with the available geophysical and geological data of the region, allow us to reinforce the presence of partial melting in the IBSLC. In addition, structures **B** and **C** show an European plate thicker than the Iberian one and an asthenosphere with an electrical resistivity between 10 ohm·m and 18 ohm·m.

CHAPTER 3

Contents lists available at SciVerse ScienceDirect

Earth and Planetary Science Letters

journal homepage: www.elsevier.com/locate/epsl

New geoelectrical characterisation of a continental collision zone in the West-Central Pyrenees: Constraints from long period and broadband magnetotellurics

Joan Campanyà [a,*], Juanjo Ledo [a], Pilar Queralt [a], Alex Marcuello [a], Montserrat Liesa [b], Josep A. Muñoz [a]

[a] Institut Geomodels, Departament de Geodinàmica i Geofísica, Universitat de Barcelona, C/Martí Franquès s/n, Barcelona 08028, Spain
[b] Departament de Geoquímica, Petrologia i Prospecció Geològica, Universitat de Barcelona, C/Martí Franquès s/n, Barcelona 08028, Spain

RESUM

Les col·lisions continentals dominen el desenvolupament d'un gran nombre de serralades del planeta. Tot i que l'evolució geològica d'aquestes està altament estudiada, els processos físics que tenen lloc, a escala litosfèrica, estan menys determinats i les seves interpretacions acostumen a diferir. Un nou perfil magnetotel·lúric creuant el Pirineu Occidental-Central amb dades de banda ampla i de llarg període determina les estructures geoelèctriques d'aquesta col·lisió continental caracteritzant la geologia i els processos físics que hi tenen lloc. Per primer cop als Pirineus s'han observat tres estructures geoelèctriques associades amb la presència de fusió parcial i la seva migració, suggerint una subducció de l'escorça Ibèrica inferior de fins a 70 km de profunditat. Aquests resultats, recolzats per un estudi de l'evolució tèrmica de l'escorça Ibèrica inferior subduida, reforça a la hipòtesis de fusió parcial. A partir de les dades de llarg període, s'ha associat l'astenosfera a una estructura geoelèctrica amb valors de resistivitat entre 20 Ω·m i 70 Ω·m. El límit litosfera astenosfera prop de la zona de col·lisió s'ha determinat entre 90 km i 110 km de profunditat sota la placa Ibèrica i entre 120 km i 160 km de profunditat sota la zona de col·lisió i la placa Europea, estant d'acord amb altres resultats geofísics. A més a més s'han observat altres anomalies geoelèctriques associades amb un límit Hercinià completament enterrat sota la conca de l'Ebre del qual no se'n tenia coneixement previ, amb la presència de sediments Silurians i fluids lliures en el contacte de Gavarnie, i amb un gruix important de sediments del Juràssic i el Cretàcic Inferior situats sota el nivell de desenganxament nord Pirenaic.

SUMMARY

Continental collision dominates the development of a large number of mountain ranges on Earth. Although the geological evolution of these regions is highly studied, lithospheric-scale physical processes are less well characterised and their interpretations frequently differ. A new magnetotelluric profile crossing the West-Central Pyrenees with broadband and long period magnetotelluric data constrains the geoelectrical features of this continental collision zone confining the geological and physical processes that take place at a lithospheric scale. Three geoelectrical structures associated with partial melting and its melt migration are imaged for the first time in the West-Central Pyrenees suggesting an Iberian subducted lower crust reaching the depth of 70 km. This result, supported by an analysis of the thermal evolution of the Iberian subducted lower crust, reinforces the hypothesis of partial melting in this region. From the long period magnetotelluric data, the asthenosphere has been imaged as a geoelectrical structure with electrical resistivity values between 20 Ω·m and 70 Ω·m. The lithosphere–asthenosphere boundary close to the collision zone has been constrained between 90 km and 110 km depth below the Iberian plate and between 120 km and 160 km depth below the transition zone between plates and the European plate, in agreement with the previous geophysical data. Additionally, other geoelectrical anomalies imaged have been associated with an unexpected major Variscan boundary located below the Ebro basin, Silurian sediments and free fluids in the Gavarnie thrust, and with a thick sequence of Jurassic and Early Cretaceous sediments situated below the North Pyrenean Thrust Sheet.

3.1 INTRODUCTION

Tectonic processes dominate the development of the outermost layer of the Earth creating, shaping and destroying the lithosphere over millions of years. Continent-continent collision systems, responsible for the formation of large mountains ranges like the Himalaya and Alps, play a primary role in the development of the continents. To comprehend the physical and geological properties associated, several magnetotelluric (MT) studies have been made constraining their electrical resistivity (see Korja, 2007; Unsworth, 2009 for reviews). The use of broadband magnetotelluric (BBMT) and long period magnetotelluric (LMT) data allows characterising the geoelectrical structures at a lithospheric scale (i.e. Campanyà et al., 2011; Muller et al., 2009; Rosell et al., 2011).

A particular case of continental collision resulted in the Pyrenees during the Alpine orogeny. The significant amount of available geophysical data and the highly studied geological evolution make this mountain chain an ideal area to study continental collision systems (see Muñoz, 2002 for a review). However, two main questions concerning the lithospheric structure and its physical stage are still open: i) the presence of partial melting in the Iberian Subducted Lower Crust (IBSLC) (Campanyà et al., 2011; Glover et al., 2000; Ledo 1996; Pous et al., 1995a; Vacheur and Souriau, 2001); ii) the cause of the positive gravimetric anomaly observed below the North Pyrenean Thrust Sheets (NPTS) in the West-Central Pyrenees (Casas et al., 1997; Jammes et al., 2010; Pedreira et al., 2007; Vacheur and Souriau, 2001). In addition, the lithosphere-asthenosphere boundary (LAB) in this region has been not accurately determined.

The geoelectrical information obtained from MT data is independent of other physical properties typically analysed in lithospheric studies like density, velocity anomaly and temperature (i.e. Gunnell et al., 2008; Koulakov et al., 2009; Tesauro et al., 2009). Comparison of the MT data with independent available geological and geophysical data better determines the geological and physical processes of the study area (i.e. Jegen et al., 2009; Jones et al., 2010; Pinto et al., 2010).

The new BBMT and LMT data collected in the West-Central Pyrenees, jointly with the latest results obtained in the Central Pyrenees by Campanyà et al. (2011) and the available geological and geophysical data, are used to constrain the geological and geophysical processes of the West-Central Pyrenees and the lateral variations along the strike in the Pyrenees. More specifically, this study has the aim to characterise the physical properties and the depth of the partial melting region associated with the IBSLC, the LAB and the electrical resistivity of the asthenosphere. At crustal depths, we constrain the geoelectrical structures related with the presence of fluids, sediments and graphite, associating them with the respective geological processes. The results obtained in the West-Central Pyrenees help us to deepen our understanding about the continental collisions and the related physical properties.

3.2 GEOLOGICAL SETTING

The Pyrenees resulted from the convergence between the Iberian and European plates from Late Cretaceous to Middle Eocene times (Olivet, 1996; Rosenbaum et al., 2002). The Pyrenean orogen extends from the western Mediterranean to the Atlantic Ocean along northern Iberia. Its shows significant along-strike differences in the structural style at a crustal scale, which resulted from the inversion of a previous segmented rift system in continuation with the Bay of Biscay (Beaumont et al., 2000; Muñoz, 2002; Roca et al., 2011). In spite of such differences, the Iberian continental crust subducted below the European crust, even in the Cantabrian region where the Pyrenean orogenic system is adjacent to oceanic crust of the Bay of Biscay. Crustal structure has been imaged by the numerous deep reflection and wide angle seismic profiles acquired all along the orogen since the 80's (Choukroune et al., 1989; Fernández-Viejo et al., 2000; Ferrer et al., 2008; Pulgar, et al., 1996; Roca et al., 2011). Among them, the best known crustal section is the ECORS profile across the Central Pyrenees (Choukroune et al., 1989; Muñoz, 1992). In that section, the crustal structural geometry consists of an asymmetric double-wedge orogenic system with the southern Pyrenees being wider and involving more than 100 km of the shortening of the total estimated shortening of 165 km across the entire orogen (Beaumont et al., 2000). In the West-Central Pyrenees, the structural style changes with respect the ECORS section. Here, the

basement thrust sheets of the interior part of the chain are imbricated instead of being piled on the top of each other to form an antiformal stack, as observed in the ECORS section (Muñoz, 2002; Teixell, 1998). Crustal structure is not so well constrained, as the only existing deep reflection seismic profile (ECORS-Arzacq) only registered the northern part of the orogen (Teixell, 1998). Southwards, the south directed imbricated basement thrust sheets forming the middle and higher part of the orogen, the southern Pyrenees are characterized by a wide sinclynorium. This sinclynorium supports the Paleogene piggy-back basin filled by an up to 8 km thick succession from the Middle Eocene turbidites to the Upper Oligocene continental conglomerates (Hogan and Burbank, 1996; Teixell, 1996). These sediments, together with a prekinematic succession of the Upper Cretaceous-Middle Eocene limestones, were detached into the Triassic evaporites and transported southwards on top of the Palogene to lower Miocene sediments of the Ebro foreland basin (Millan, 1996). The West-Central Pyrenees MT profile, herein presented, traverses the western part of the Paleozoic basement-involved Gavarnie thrust sheet, which is the upper unit of the basement stack of thrust sheets (also referred as the Axial Zone). Northwards, south-directed thrusts inverted Early Cretaceous extensional basins which were floored by an exhumed continental mantle (Jammes et al., 2009, 2010). North-directed thrust structures are restricted, along the MT profile, to the north-Pyrenean thrust front which transported northwards the Mauleon basin on top of the Arzacq basin, part of the Aquitanian foreland (Teixell, 1998).

To comprehend the geological and geophysical features observed in the West-Central Pyrenees, two main tectonic processes prior to the continental collision between the Iberian and European plates should be taken into account. Firstly, the opening of the Bay of Biscay during the Early Cretaceous rifting, which caused extreme crustal thinning and the rise of lower crustal and/or upper mantle rocks to upper and middle crustal depths. (Jammes et al., 2010; Pedreira et al., 2007). Secondly, the Variscan orogenic and post-orogenic events that yielded a structural grain to the Iberian crust before the Cretaceous extensional event (Martinez Catalán et al., 2009).

3.3 PREVIOUS GEOPHYSICAL STUDIES

Several geophysical studies have been taken into account to interpret the geoelectrical structures observed in the West-Central Pyrenees MT profile.

3.3.1 ECORS Arzacq deep seismic profile

ECORS Arzacq deep seismic profile was undertaken close to the northern part of the West-Central Pyrenees MT profile (Figure 3.1). The geological interpretations of this profile (Muñoz, 2002; Teixell, 1998) are similar between them for the upper and middle crust and suggest a similar depth for the Moho. The Moho depth is 30 km to 35 km below the European crust and 30 km to 50 km below the Iberian crust, deepening progressively from south to north. These differences are related with the IBSLC and the stacking of the basement thrust sheets in the Southern Pyrenees (Muñoz, 2002). The main discrepancies between the two geological interpretations (Muñoz, 2002; Teixell, 1998) are in constraining the geological structures located in the transition zone between plates, and the depth of the IBSLC.

3.3.2 Tomographic models and seismic activity

A recent tomographic model from teleseismic P-waves travel times (Amaru et al., 2008), including crustal corrections before the inversion, suggests the presence of a negative V_p anomaly associated with the transition zone between the Iberian and European plates as well as below the Iberian plate. The tomographic model of Souriau et al. (2008) which includes crustal corrections, also suggests the presence of a low V_p anomaly associated with the transition between the Iberian and European plates below the West-Central Pyrenees MT profile. Similarly, a new tomographic model (Koulakov et al., 2009), including crustal corrections, has obtained a negative V_p anomaly beneath the West-Central Pyrenees. Koulakov et al. (2009) also shows an S-waves model of the region with a negative V_s anomaly in the transition zone between the Iberian and European plates and a negative V_s anomaly at the deeper parts which could be related with the asthenosphere.

The seismic activity in the West-Central Pyrenees is basically located at upper and middle crustal depths, down to 20 km depth, below the northern Pyrenees although

seismic activity is occasionally registered at greater depths (Koulakov et al., 2009; Rigo et al., 2005; Ruiz et al., 2006).

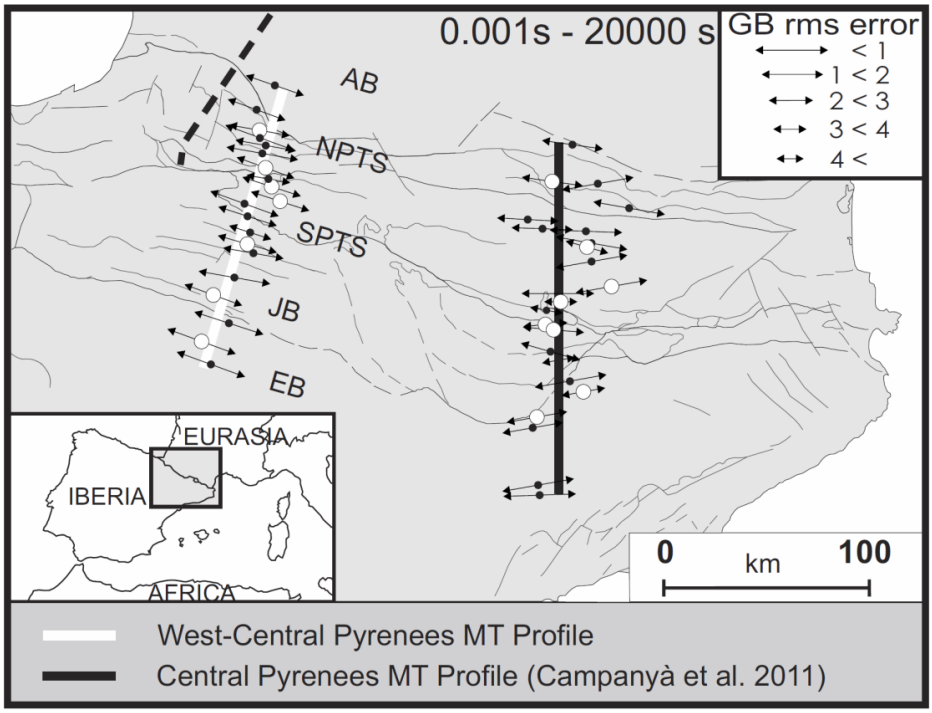

Figure 3.1 Location of the MT stations in a structural sketch of West-Central and Central Pyrenees. Black spots correspond to stations with BBMT data and white spots stations with BBMT and LMT data. The arrows indicate the strike direction of each site. The lengths of the arrows indicate the compatibility of the data to the assumed two-dimensional strike direction. Strikes for Central Pyrenees from Campanyà et al. (2011). Black dashed line corresponds to the ECORS Arzacq deep seismic profile. EB, Ebro Basin; JB, Jaca Basin; SPTS, South Pyrenean Thrust Sheets; NPTS North Pyrenean Thrust Sheets; AB, Aquitaine Basin. Thin lines divide the main geological units of the region.

3.3.3 Geoelectrical models

Using BBMT data, Ledo (1996) and Pous et al. (1995a) showed a two-dimensional geoelectrical model of the Central Pyrenees and Ledo et al. (2000) obtained a three-dimensional electrical resistivity model of the Central and West-Central Pyrenees. The three models were obtained by trial-and-error fitting of the data. Although there were numerous BBMT sites located in the Central Pyrenees there were only three in the West-Central Pyrenees. Recently, Campanyà et al. (2011), constrain the geoelectrical structures of the Central Pyrenees, from BBMT and LMT data, using a two dimensional inversion code. All the MT models show a low electrical resistivity structure associated with the IBSLC and various studies (Campanyà et al., 2011; Glover et al., 2000; Ledo,

1996; Pous et al. 1995a) support the hypothesis of partial melting to explain the low electrical resistivity values associated with the IBSLC. At the deepest part of the models, a low electrical resistivity structure is related with the asthenosphere and therefore maps the lithosphere-asthenosphere boundary (LAB) below the Iberian and European plates, suggesting a thicker European plate close the collision zone.

3.3.4 Gravity data

Several gravity studies have been made in the West-Central Pyrenees (Casas et al., 1997; Jammes et al., 2010; Pedreira et al., 2007; Vacheur and Souriau, 2001). In all cases, the presence of high density bodies located at upper and middle crustal depths below the NPTS is constrained but whether these bodies represent lower crustal or upper mantle rocks is still a matter of debate. Gravity models are compatible with the IBSLC, but the studies do not agree with the physical processes associated, in particular with the presence or absence of partial melting.

3.3.5 Thermal studies

There are no specific thermal studies done in the West-Central Pyrenees. In a large scale, Tesauro et al. (2009) obtained the geotherms of the European lithosphere from 60 km to greater depths. They show no significant thermal differences between the Central and West-Central Pyrenees. Zeyen and Fernández (1994) suggest that the thermal equilibration below the Central Pyrenees has already ended. Due to the proximity of the MT profiles, it is assumed that the geotherms used by Campanyà et al. (2011) in the Central Pyrenees are approximately valid for the West-Central Pyrenees.

For the deepest parts of the lithosphere, Tesauro et al. (2009) show a slight increase in the temperature at the southern part of the West-Central Pyrenees which could be interpreted as the thinning of the lithosphere.

Taking into account the previous geophysical information two main debates are open in the West-Central Pyrenees. Firstly, the IBSLC below the West-Central Pyrenees is currently accepted by the geological and geophysical communities but the depth of the

crustal root and the associated physical processes are still in debate. Secondly, the source of the high density body at upper/middle crustal depths observed below the NPTS. About the LAB, prior MT and thermal studies not accurately constrain it below the West-Central Pyrenees suggesting an European plate thicker than the Iberian plate, close to the collision zone.

3.4 NEW MAGNETOTELLURIC DATA

New MT data were acquired in the summer 2010 at 20 sites along a 140 km profile crossing the West-Central Pyrenees. The BBMT data were recorded in all the sites and LMT data at seven of the BBMT sites. On average, the distance between the sites with BBMT data and between the sites with BBMT+LMT data is 6.5 km and 15 km, respectively. Recording times were at least three days for sites with BBMT data and fifteen days for sites with LMT data.

The BBMT data were recorded using a Metronix ADU06 and ADU07 systems and processed using Metronix software (Friedrichs, 2003). The LMT data were recorded using a LEMI system designed by the Lviv Center of the Institute of Space Research and processed using Birrp.5 (Chave and Thompson, 2004). Remote reference has been used between sites located in the northern half of the profile and sites located in the southern half of this in order to avoid the effect of a possible local noise. The combination of BBMT and LMT data allows us to cover a period range between 0.001 s and 20000 s. The LEMI stations allow us to also constrain the induction arrows for the LMT data, covering a period range between 50 s and 20000 s. Anomalous phases, > 90°, have been observed in the TE mode for periods longer than 10 s (see sites 15, 17, 18, 19 in Figure S1) in the sites located at the NPTS. To explain these anomalous data we use the arguments suggested by Lezaeta and Haak (2003). They demonstrate that in a 2D/3D geoelectrical model the presence of current channelling affects the magnetotelluric data on the TE mode causing phases greater than 90° as happen in the anomalous data observed in the West-Central Pyrenees. Current channelling in this region can be explained by low electrical resistivity structures associated with the

shear zones presents in the NPTS. These data were not considered during the inversion procedure.

Geoelectric strike direction was computed from the MT impedance tensors at each site for all the periods applying the Groom and Bailey (1989) method, following the scheme of McNeice and Jones (2001). A 5% error floor on the impedance tensor components is applied. The rotational invariants (Weaver et al., 2000) using the WALDIM code (Martí et al., 2009b) have been used to corroborate the results. Two-dimensional data is constrained with a 106°, clockwise from North, strike direction. Figure 3.1 shows the fit of the data in assume a geoelectrical strike direction close to 106° for each site for all period bands and compare with the strike obtained in the Central Pyrenees by Campanyà et al. (2011). Figure S2 show the geoelectrical strike direction split in two period bands (BBMT: 0.001-100 s and LMT: 10-20000 s). In both cases two dimensional geoelectrical structures with a 106° strike direction is constrained. In addition, the induction arrows obtained from the LMT data corroborate this strike (Figure 3.2). The static shift was corrected using the depth of the contact between the Mesozoic and Palaeozoic basement obtained from (Lanaja and Querol, 1987) which is observed as an important increase of the electrical resistivity in the TM mode. In 80% of the cases the static shift values are less than half decade and in no case exceed a decade and a half.

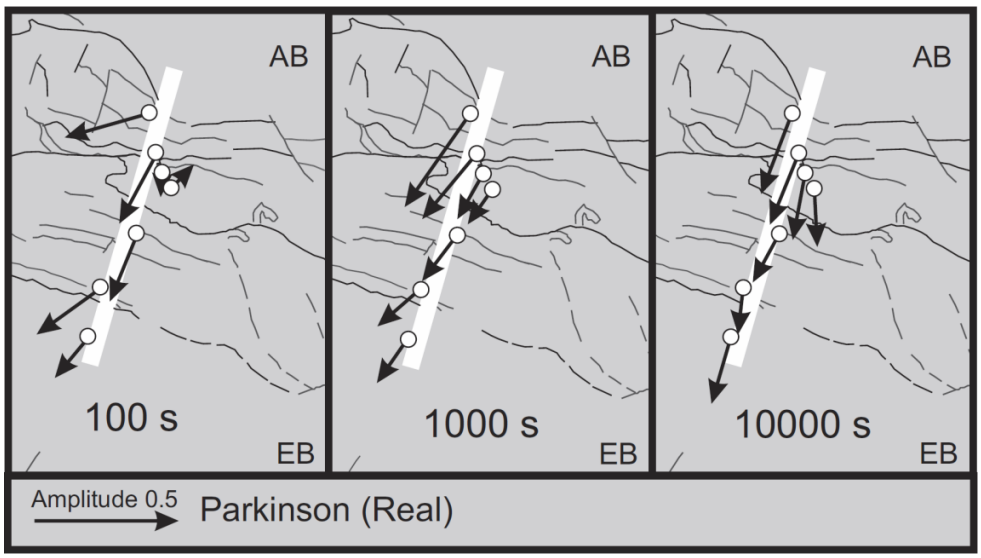

Figure 3.2 Structural sketch of the West-Central Pyrenees profile showing the transfer functions for the sites with LMT data for periods of 100 s, 1000 s and 10000 s. Parkinson (real) arrow point to the low electrical resistivity structure observed from the site.

3.5 TWO-DIMENSIONAL INVERSION

Two-dimensional inversion of the TE and TM mode apparent resistivity and phase data was made using the algorithm of Rodi and Mackie (2001). An error of 10% for the apparent resistivity and 2.86^{o} for the phases has been used for the inversion process giving equal weight to all data type (Gabàs and Marcuello, 2003). The MT model was obtained using smooth curves with 10% D+ values (Beamish and Travassos, 1992).This type of smoothing force the curves to have coherence between apparent resistivity and phases. Figure S3 show the obtained smooth curves superimposed on the raw data. The smooth curves have been used in the two-dimensional inversion process with the aim to avoid unnecessary structures as much as possible and fill the gap in sites where some periods have no data (Figure S1). These periods without data are usually related with low natural signal.

The two-dimensional inversion process using BBMT and LMT data does not clearly obtain geoelectrical structures at the bottom of the model, below the white dashed line in Figure 3.3. To better constrain this region we fixed the obtained electrical resistivity values until 110 km depth and inverted using only LMT data (between 1000 s and 20000 s). The MT model of the West-Central Pyrenees profile, obtained from the two inversion process, is shown in Figure 3.3.

To compare data and model responses, in all the cases we use the responses of the final model shown in Figure 3.3. Figure 3.4 compares the smooth data used for the inversion and model responses in pseudosection format for the apparent resistivity and phases and shows the misfit between them. Figure S1 shows the curves of the raw data and the model responses. The misfit between the data and the model responses has an RMS value of 1.6 for the smooth curves and 2.3 for raw data. The RMS of the second inversion process, using only periods between 1000 s and 20000 s, decrease from 4.1, MT model obtained from the first inversion process, to 2.7, definitive MT model.

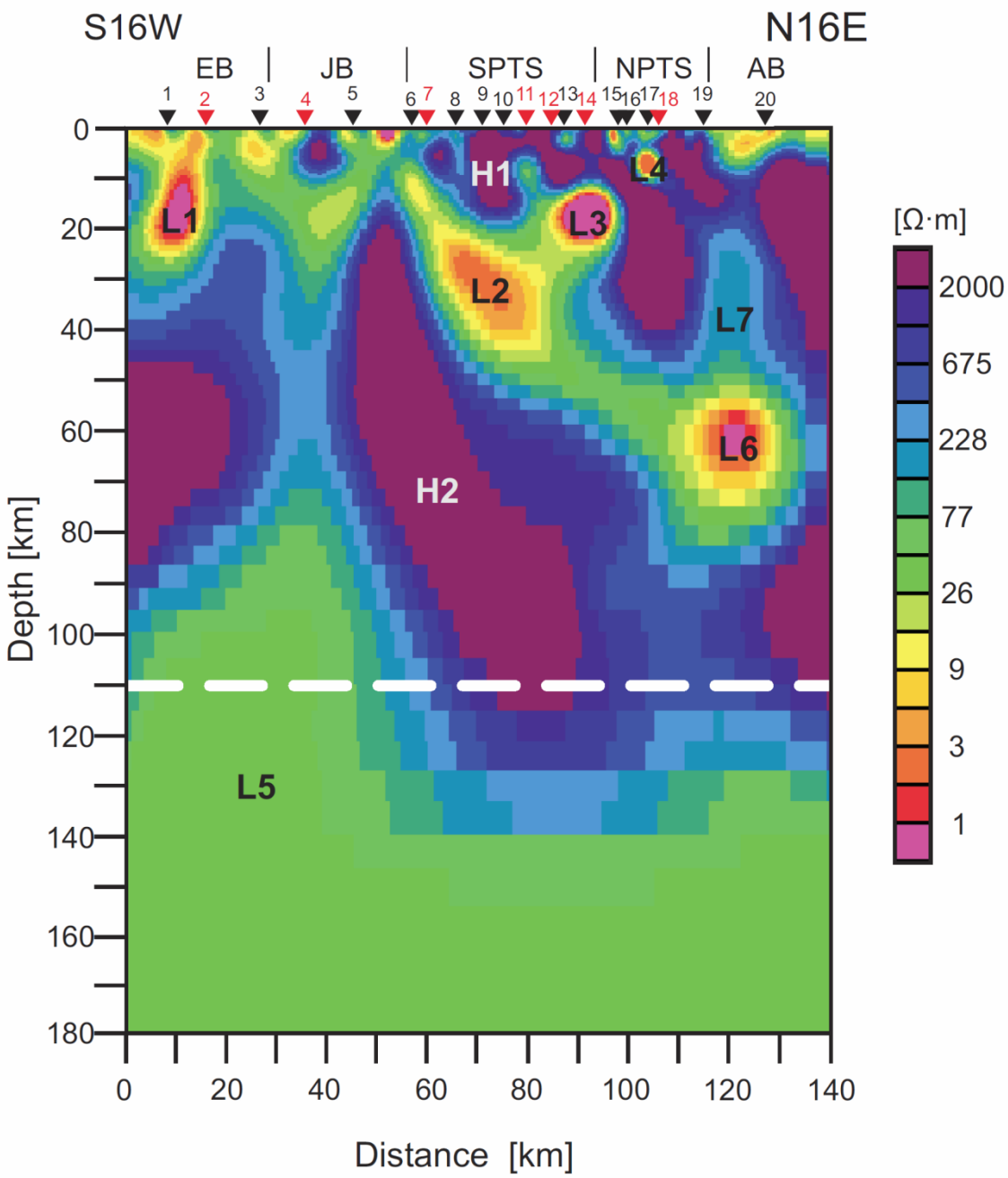

Figure 3.3 Two-dimensional electrical resistivity model obtained from the joint inversion of the TE and TM modes for apparent resistivities and phases. Sites are represented by inverted triangles (in red sites with BBMT and LMT data and in black sites with BBMT data). The white dashed line delineates the region of the MT model obtained using only long period data and fixing the electrical resistivity of modelabove. EB, Ebro Basin; JB, Jaca Basin; SPTS, South Pyrenean Thrust Sheets; NPTS, North Pyrenean Thrust Sheets; AB, Aquitaine Basin. Labels L1-L7 and H1, H2 denote model features discussed and interpreted in text.

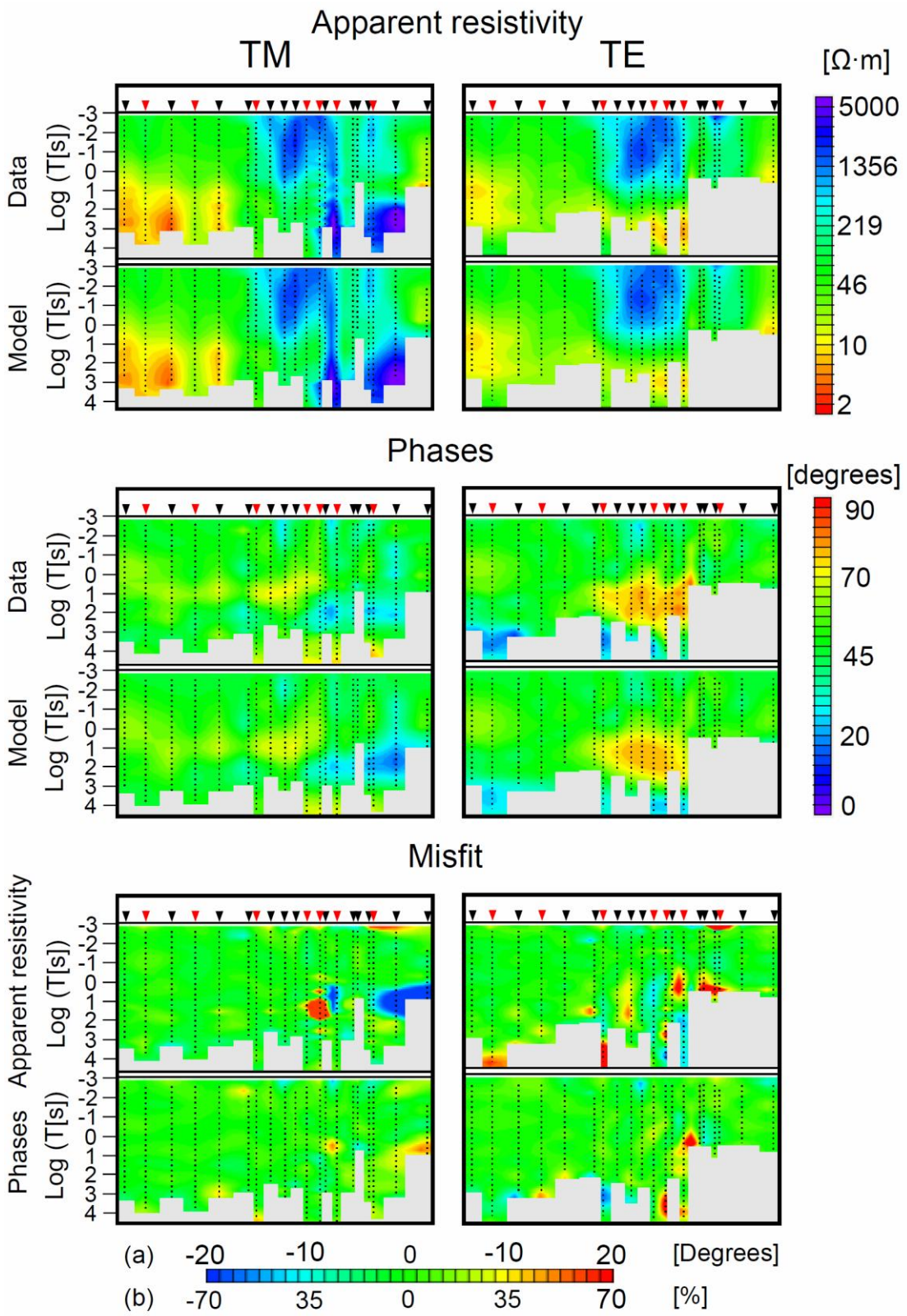

Figure 3.4 Comparison between the smoothed data and the model responses in pseudosection format for the apparent resistivity (top) and phases (middle). The misfit between smoothed data and model responses is shown in pseudosection format to the bottom. In both cases for TM and TE mode (left and right respectively). Sites are represented by inverted triangles (in red sites with BBMT and LMT data and in black sites with BBMT data). Tiny black dots are smooth data points used for the inversion.

3.5.1 Electrical resistivity structures

The main geoelectrical features have been labelled "L" for low electrical resistivity structures and "H" for high electrical resistivity structures (Figure 3.3). The model contains seven main low electrical resistivity structures. Features L1, L3 and L4 are associated with upper and mid crustal structures while features L2, L6 and L7 are located at lower crustal and upper mantle depths. L5 structure is related with the asthenosphere. Two main high electrical resistivity structures are observed in the model, H1 located at crustal depth and H2 located on the transition zone between the Iberian and European plates. The areas with high electrical resistivity values at the edges of the MT model are associated to the Iberian (south) and European (north) lithospheres.

3.5.2 Non-linear sensitivity test

A non-linear sensitivity test was carried out to justify the presence of the geoelectrical structures and appraise the resolution of the MT model. The test consists on comparing the differences between the final MT model (Figure 3.3) and a modified model, where some properties of the studied feature have been changed such as the geometry of the structures or their electrical resistivities. If the difference between the MT model responses is greater than 10% on the apparent resistivity or 2.86^{o} on the phase the modification is excluded. Conversely, if the differences are lower than the values exposed we assume that the data have no resolution to constrain between the final MT model and the modified model and the change is accepted due we have no resolution to differentiate between the two models.

Firstly, the requirement of all the main geoelectrical structures obtained by the inversion procedure has been examined. The main geoelectrical structures have been removed changing their electrical resistivity values by the neighbour's electrical resistivity values. Differences in model responses are in all the cases greater than 10% on the apparent resistivity and/or great than 2.86^{o} on the phases and we observe a significant increase of the RMS in some sites suggesting that all the structures here analysed are necessary to explain the data (Figure S4). Figure S4 also shows which sites and periods are sensitive to the main geoelectrical structures.

Secondly, once we know which structures are necessary to explain the data, we use the sensitivity test to constrain the resolution we have on these structures. The sensitivity test constrains that the electrical resistivity values of L1 should range between 0.6 Ω·m and 0.8 Ω·m, their upper boundary between 9 km and 11 km depth and the lower boundary between 19 km and 24 km depth. This test also suggests that structure L1 has no lateral continuity. The electrical resistivity of L2 should range between 2 Ω·m and 6 Ω·m and their upper boundary between 21 km and 28 km depth. Assuming a homogeneous electrical resistivity of 2 Ω·m for L2 structure the sensitivity test constrain that the lower boundary of L2 could reach 65 km depth, connecting with L6. L3 electrical resistivity should range between 0.1 Ω·m and 0.2 Ω·m and its upper boundary between 13 km and 15 km depth. The electrical resistivity values of L4 should range between 2 Ω·m and 6 Ω·m. The electrical resistivity values of L5 should range between 20 Ω·m and 70 Ω·m and its upper boundary should be located between 90 km and 110 km depth below the Iberian plate and between 120 km and 160 km depth below the transition zone between plates and the European plate. The electrical resistivity values of L6 should range between 1 Ω·m and 20 Ω·m. L7 structure has electrical resistivity values between 90 Ω·m and 250 Ω·m and its upper boundary should range between 22 km and 28 km depth. This large range of electrical resistivity values for structures L6 and L7 is associated with the lack of long periods for the TE data on the stations located above them.

For the high electrical resistivity features the non linear sensitivity test suggests values of the electrical resistivity between 5000 Ω·m and 15000 Ω·m for H1 and between 6000 Ω·m and 20000 Ω·m for H2. It also indicates that the upper boundary of H2 should be between 15 km and 17 km depth.

3.6 DISCUSSION

3.6.1 Interpretation of the main geoelectrical structures

3.6.1.1 Low electrical resistivity structure below Ebro Basin (L1)

The L1 feature is a sub-vertical low electrical resistivity structure completely buried below the Ebro Basin at upper and middle crustal depths. As there is not any structure affecting the sedimentary infilling of the Ebro Basin above this electrical resistivity structure, it could be associated with the previous Variscan tectonic events. According to the subdivision of the Variscan belt (see Martínez Catalán et al. 2007 for further information) it could correspond to the prolongation of the limit between the Western Asturian Leonese and Central Iberian zones below the Ebro Basin. In the southwester part of the Iberian plate, the Variscan boundaries between the different geological units (the Ossa Morena Zone (OMZ) and the South Portugese Zone, (SPZ) and between the Ossa Morena and the Central Iberian Zones (CIZ)) have been imaged by MT data (Da Silva et al., 2007; Muñoz et al., 2008; Pous et al., 2004; Pous et al., 2011). These boundaries appear as sub-vertical low electrical resistivity structures located in the upper and middle crust, similar to the L1 structure, and are associated with graphite. In the Cantabrian mountains, Pous et al. (2001) also associate a low electrical resistivity structure located at lower crustal depths with graphite as a signature of the Variscan convergence. Due to the geoelectrical similarities within the Variscan boundaries constrained in the Iberian plate and the geoelectrical similarities with L1, we suggest the presence of graphite along a major Variscan tectonic boundary to explain the low electrical resistivity values of the structure L1. Nevertheless, more geophysical studies should be done to better constrain this buried structure which has not been previously observed below the Ebro Basin.

3.6.1.2 Iberian subducted lower crust (L2, L6 and L7).

From the non-linear sensitivity test, L2 and L6 structures can be connected suggesting that they can be associated with the same geological processes. Comparison of the MT model with the geological models of Muñoz (2002) and Teixell (1998) suggests that L2 and L6 structures are related with the IBSLC (Figure 3.5). The top of the L2 structure coincides with the top of the low electrical resistivity structure constrained by Ledo et al. (2000).

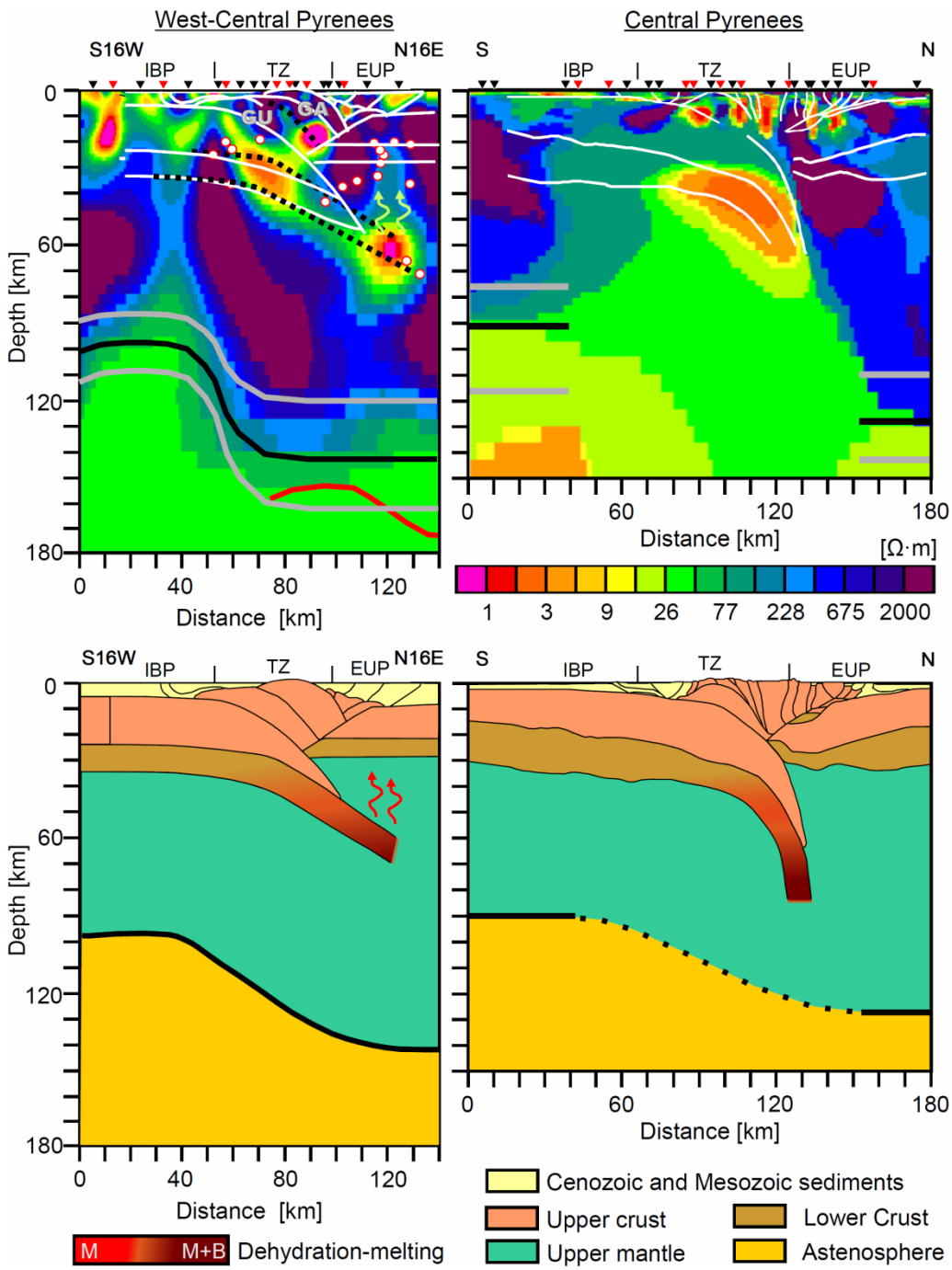

Figure 3.5 (TOP) West-Central Pyrenees MT model (left) compared with Central Pyrenees MT model (right) obtained by Campanyà et al. (2011). White lines correspond to the geological model suggested by Muñoz et al. (2002) in West-Central Pyrenees and by Muñoz (1992) in Central Pyrenees. Black dashed lines are modifications on the geological models suggested by MT results. White-red spots are the earthquakes recorded below 20 km depth from Koulakov et al. (2009). Green arrows indicate melt migration. Black line: lithosphere-asthenosphere boundary suggested by MT results. Grey lines: resolution constraining the lithosphere asthenosphere boundary from the sensitivity test. Red line: lithosphere-asthenosphere boundary from Koulakov et al. (2009) in West-Central Pyrenees. GA, Gavarnie thrust; GU, Guarga thrust. (BOTTOM) Cartoon geological sections of the West-Central and the Central Pyrenees with our interpretation of the partial-melting region and the LAB. In the dehydration melting process: M when Muscovite produce dehydration melting and M+B when Muscovite and Biotite produce dehydration melting. White dashed interpolated LAB below Central Pyrenees due no resolution in this region."

As suggested by Campanyà et al. (2011), Glover et al. (2000), Ledo et al. (2000) and Pous et al. (1995a), partial melting could be the cause of the low electrical resistivity values observed in the IBSLC. Following the analysis of Campanyà et al. (2011), a percentage of partial melting between 4% and 15% melt from dehydration-melting of muscovite, which take place at temperatures of 650°C or higher, can explain the low electrical resistivity values observed in L2 (Partzsch et al., 2000). At the position of L6, Tesauro et al. (2009) suggest a temperature around 900°C. This temperature is sufficiently high to produce dehydration-melting of muscovite and also of biotite, which produce extensive melting (Patiño Douce and Harris, 1998; Vielzeuf and Holloway, 1988). From the Modified Brick Layer Model of Partzsch et al. (2000), the amount of partial melting necessary to explain the electrical resistivity range of L6 obtained from the non-linear sensitivity test is between 3 % and 27 %, being between 15 % and 25 % to explain the electrical resistivity values which better fit the data, between 1.3 Ω·m and 2 Ω·m. From Arzi (1987), melt percentage of 20% or higher can be associated with melt migration, suggesting 20% melting as the critical melt percentage to have melt migration. The melt values obtained in L6 can exceed the 20%, suggesting that melt migration is possible as the critical melt percentage can be exceeded. A small amount of melt could have migrated upwards from the IBSLC explaining the decrease of the electrical resistivity values in the European upper mantle associated with L7 structure.

As we know that convergence of the Pyrenees stopped 20 million years ago, we have calculated the thermal evolution of the IBSLC (Fowler, 2005, p. 283) in order to estimate the time needed to heat the structure L6 at a temperature over 850°C. According to Figure 3.5, the Iberian subducted lower crust is represented by a 10 km thick layer (Pedreira et at., 2003) at an initial temperature of 500°C (Zeyen and Fernandez, 1994). In the deeper parts, the IBSLC is located in the European upper mantle between 60km and 70 km depth. The European upper mantle temperatures at these depths are 900°C and 1000°C, respectively (Tesauro et al., 2009).

From these parameters, temperatures above 850°C for the structure L6 would be achieved between 3 Ma and 16 Ma after the end of the orogeny. This means that, at present there could be melt mostly produced by dehydration melting of biotite, which

occurs at a temperature higher than 850°C (Vielzeuf and Holloway, 1988). This result agrees with the idea of assuming magmatic activity in order to explain the decrease of electrical resistivity observed in L7. The presence of earthquakes located around structure L7 is consistent with this hypothesis (Figure 3.5).

The low electrical resistivity structures L2, L6 and L7 coincide with the negative velocity anomaly of P and S waves observed in the different tomographic models (Amaru et al., 2008; Koulakov et al., 2009; Souriau et al., 2008) (Figure 3.6). The decrease of the P and S velocity anomalies is consistent with the presence of partial melting in the IBSLC. The location of the geoelectrical structure L6 also agrees with the deep seismic activity, suggesting that the IBSLC was subducted down until the depth of 70 km (Figure 3.5). These results are consistent with the lower boundary of the negative S-wave velocity anomaly suggested by Koulakov et al. (2009) (Figure 3.6).

3.6.1.3 Intersection between major faults (L3)

L3 structure is located at the transition zone between the Iberian and European plates, close to the intersection between the Gavarnie thrust and the North Pyrenean sole thrust as suggested by the geological models (Figure 3.5). Observing the low electrical resistivity area dipping north above structure L3 we suggest to modify the geometry of the Gavarnie thrust at depth with respect to the previous geological models increasing its dip and associating L3 with the branching between the Gavarnie and the sole thrusts (Figure 3.5). The presence of the Silurian sediments, previously deformed by the Variscan orogeny, together with the presence of fluids explains the low electrical resistivity values observed in L3.

3.6.1.4 Jurassic and Early Cretaceous sediments (L4)

The low electrical resistivity values of L4 are explained by the presence of a great amount of Jurassic and Early Cretaceous sediments preserved in the Lower Cretaceous extensional basins that resulted from the opening of the Bay of Biscay, and were subsequently inverted during the continental collision. The anomalous phases observed for the sites located in this area (sites 15, 17, 18 and 19), see Figure S1, delineate a region which is coincident with the positive gravimetric anomaly observed

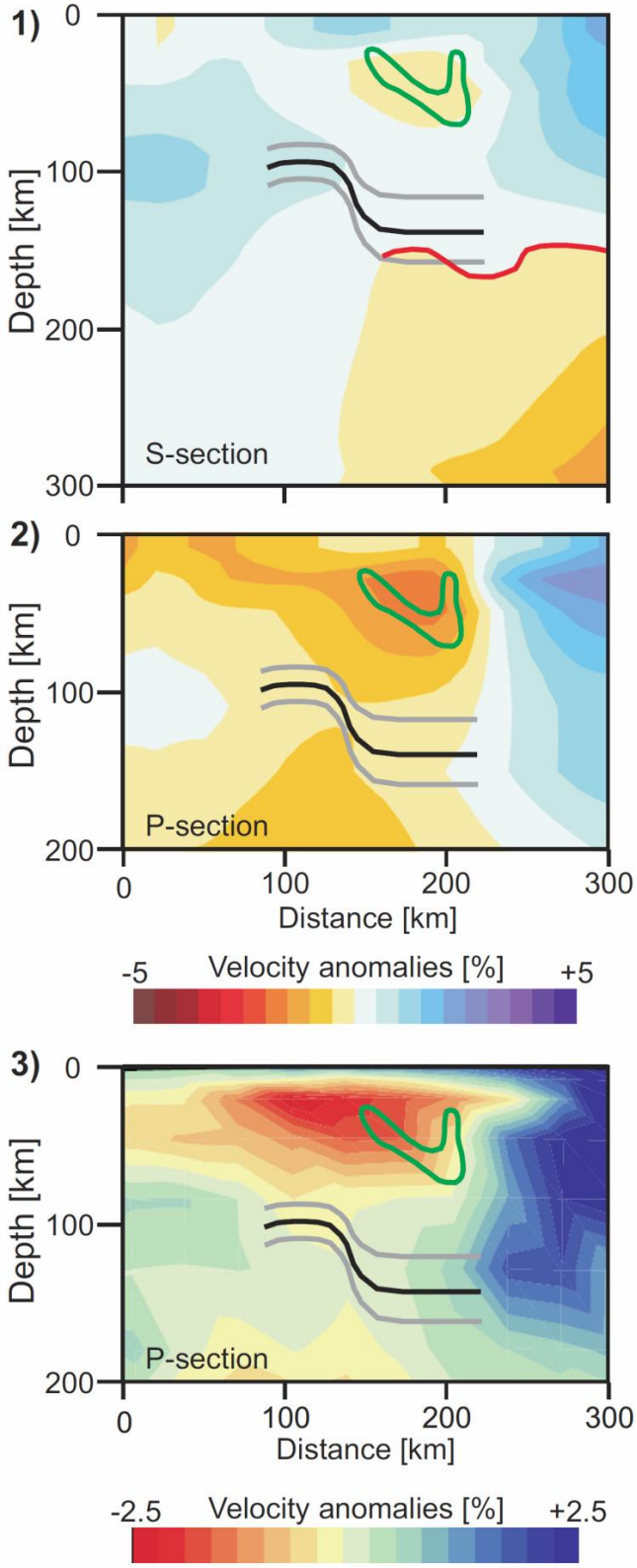

Figure 3.6 Seismic tomography model from S-waves obtained by Koulakov et al. (2009) (1). Seismic tomography models from P-waves obtained by Koulakov et al. (2009) (2) and Amaru et al. (2008) (3). Superimposed on the three models: contour of the partial melting region (green line) and geoelectrical lithosphere-asthenosphere boundary (black and grey lines) obtained in this work. In panel (1), the upper boundary of the negative Vs anomaly is associated with the seismic lithosphere-asthenosphere boundary (red line).

in the West-Central Pyrenees (Casas et al., 1997; Jammes et al., 2010; Pedreira et al., 2007; Vacheur and Souriau, 2001), but no evidences directly relate both anomalies with the same cause.

3.6.1.5 Lithosphere-asthenosphere boundary, LAB (L5)

The MT model obtained suggests a LAB between 90 km and 110 km depth below the Iberian plate and between 120 km and 160 km depth below the transition zone between plates and the European plate close to the collision zone. The electrical resistivity values of the asthenosphere have been constrained between 20 Ω·m and 70 Ω·m. These values are consistent with the results obtained in other areas (Heinson, 1999; Jones et al., 2010; Korja, 2007). The S-wave model of Koulakov et al. (2009) suggests a deep negative V_s anomaly that can be associated with the asthenosphere. The V_s seismic LAB below the transition zone between plates and below the European plate agrees with the geoelectrical LAB observed in the MT model. Below the Iberian plate, the variations of the V_s anomalies are smooth and the V_s seismic LAB is not well constrained (Figure 3.6). In Tesauro et al. (2009), the thermal LAB below the West-Central Pyrenees associated with the geotherm of 1200°C is approximately at the depth of 130 km, a bit shallower below the Iberian plate, being also consistent with the geoelectrical LAB obtained in this study.

3.6.1.6 High electrical resistivity structures H1 and H2

The H1 high electrical resistivity structure is located at the shallower depths of the transition zone between plates and is associated with the basement-involved Guarga and Gavarnie thrust sheets. These thrust sheets are separated by a low electrical resistivity region dipping north associated with the Gavarnie thrust. The H2 high electrical resistivity structure is located below L3 structure showing that in West-Central Pyrenees our MT model has enough resolution to constrain the bottom of the partial melting area. The H2 structure is related with rocks from the Iberian lower crust and upper mantle without the presence of partial melting.

3.6.2 Comparison between the West-Central and Central Pyrenees

Comparison between the two models will be carried out following the main five regions in which the sections have been divided: the Iberian subducted lower crust, the Iberian plate, the European plate, the structures located at the transition zone between plates at upper and middle crustal depths and the lithosphere-asthenosphere boundary. The West-Central and the Central Pyrenees MT models with the same electrical resistivity colour scale are shown in Figure 3.5.

3.6.2.1 Iberian subducted lower crust

In this region, the main difference between the two models is the dip of the low electrical resistivity structure associated with the partial melting of the IBSLC. In Central Pyrenees, the maximum dip of the IBSLC is 80°, while in West-Central Pyrenees 35°. This difference is associated with a greater amount of subduction in the Central Pyrenees and the gravity effect associated, which increased the dip of the subducted plate. The upper boundary and the electrical resistivity values of the area which resulted from partial melting by muscovite dehydration-melting are similar in both models. Conversely, the geoelectrical properties associated with partial melting by dehydration-melting of biotite and melt migration in the Central Pyrenees are screened due to the verticality of the IBSLC and cannot be compared.

3.6.2.2 Iberian plate

In the West-Central Pyrenees, the Iberian plate shows electrical resistivity values around 50 Ω·m at upper and middle crustal depths. These values are lower than those observed for the lower crust which are around 200 Ω·m. On the other hand, at the Central Pyrenees the electrical resistivity values for the Iberian upper, middle and lower crusts are similar and around 100 Ω·m. In West-Central Pyrenees the electrical resistivity is increasing below the Moho, associated with the upper-mantle, but not in Central Pyrenees. Another important difference is the presence of the L1 structure below the Ebro basin in the West-Central Pyrenees profile and the absence of such structure in the Central Pyrenees profile. This difference and the lack of geoelectrical structures with electrical resistivity values as those from L1 in the Central Pyrenees suggest that the possible major Variscan tectonic boundary inferred in the West-

Central Pyrenees profile would be located southwards from the southern edge of the Central Pyrenees MT profile, as suggested by structural interpretations (Martínez Catalán 2007 and references therein).

3.6.2.3 European plate

The European plate displays high electrical resistivity values at crustal an upper mantle depths in both models, but a significant difference is observed. The region with low electrical resistivity values associated with L7 structure at the upper mantle depths in the West-Central Pyrenees, which has been interpreted as melt migration, is not observed in the Central Pyrenees where the vertical dip of the partial melting region in the IBSLC could be interpreted as the overlap between in situ partial melting and migrated melt.

3.6.2.4 Transition zone between plates at upper and middle crustal depths

In the Central Pyrenees, the transition zone between plates is dominated by low electrical resistivity structures containing fluids and Silurian sediments in the sub-vertical faults of the Axial Zone whereas in the West-Central Pyrenees. The transition zone between plates is dominated by high electrical resistivity values associated with the Guara and Gavarnie basement-involved thrust sheets, at shallow depths, and by a very low electrical resistivity structure (L3), between 10 km and 20 km depth. The L3 structure is associated with the Gavarnie thrust and it is branching with the North Pyrenean sole thrust. The dip of the structures to the west, preserving higher structural levels in the West-Central Pyrenees than in the Central Pyrenees and the related westward termination of the Axial Zone antiformal stack of the Central Pyrenees would explain these differences. The sub-vertical low electrical resistivity structures in the northern limb of the Axial Zone antiformal stack in the Central Pyrenees are equivalent to the L3 structure in the West-Central Pyrenees.

3.6.2.5 Lithosphere-asthenosphere boundary (LAB)

The geoelectrical LAB observed in both models suggests an European plate thicker than the Iberian plate close to the collision zone. No major changes are observed in the

depth of the LAB along the strike, which suggest similar form and depth of the LAB between these regions going from 90 km depth below the Iberian Plate to 130 km depth below the European plate. The similar electrical resistivity values obtained for the asthenosphere below the two profiles suggest no big differences on the asthenosphere properties below the Pyrenees.

3.7 CONCLUSIONS

The new geoelectrical characterisation of the West-Central Pyrenees constrains the electrical resistivity values at lithospheric scale. The main structure is the partial melting zone associated with the IBSLC which shows, for the first time in the Pyrenees, the geoelectrical responses associated with partial melting by dehydration of muscovite (L2 structure), dehydration-melting of muscovite and biotite (L6 structure) and melt migration (L7 structure). The coincidence of the bottom of structure L6 with the bottom of the negative V_s anomaly and the presence of seismic activity in this region suggest extending the IBSLC to the depth of 70 km. The coherence between the results gives new arguments in favour of the partial melting of the IBSLC.

The unexpected sub-vertical low electrical resistivity feature L1, constrained at upper-middle crustal depths and completely buried below the Ebro Basin, has been associated with graphite in a major Variscan tectonic boundary zone. In the transition zone between plates, at crustal depths, a low electrical resistivity structure associated with the presence of Silurian sediments and fluids suggests that there is an increase of the dip of the Gavarnie thrust at depth. The electrical resistivity values observed in the NPTS (L4) has been associated with the presence of Jurassic and Early Cretaceous sediments and we associate the anomalous phases observed in this region with the presence of current channelling in a 2D/3D region in the two-dimensional MT profile. The geoelectrical LAB constrained below the West-Central Pyrenees suggest an European plate thicker than the Iberian plate, close to the collision zone.

Comparison between the West-Central and Central Pyrenees MT profiles shows major differences related with the transition zone between the European plate and the Iberian plate. The steeper dip of the IBSLC indicates greater shortening in the Central Pyrenees. For the Iberian plate, the values of electrical resistivity in the Central Pyrenees are more homogeneous than those in the West-Central Pyrenees where geoelectrical differences between the upper-middle crust and lower crust depth and between crustal and upper mantle depths are observed. In the transition zone between plates, at crustal depths, differences in the location of the Silurian sediments preferentially located along major faults are explained by the west plunge of the basement-involved thrusts observed in the core of the Pyrenees. In the European plate, the low electrical resistivity values observed at upper mantle depths, which have been attributed to magma batches, are not observed in the Central Pyrenees due the vertical dip of the IBSLC. The geoelectrical LAB constrained below the two MT profiles suggest an European plate thicker than the Iberian plate, close to the collision zone, and an asthenosphere with electrical resistivity values between 10 Ω·m and 70 Ω·m.

3.8 SUPPLEMENTARY MATERIAL

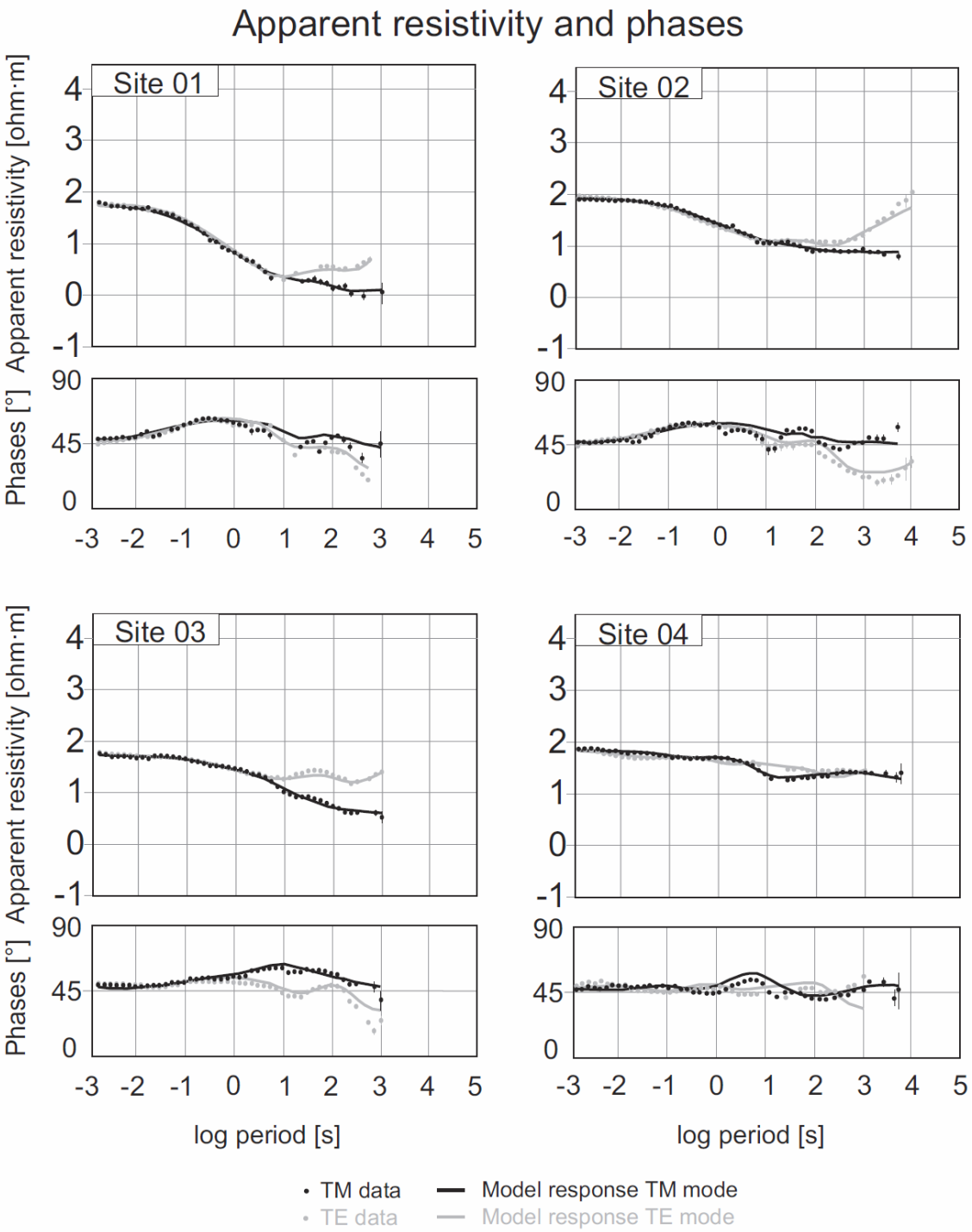

Figure 3.S1 Comparison of the apparent resistivity and phases between raw data and model responses for TE and TM modes.

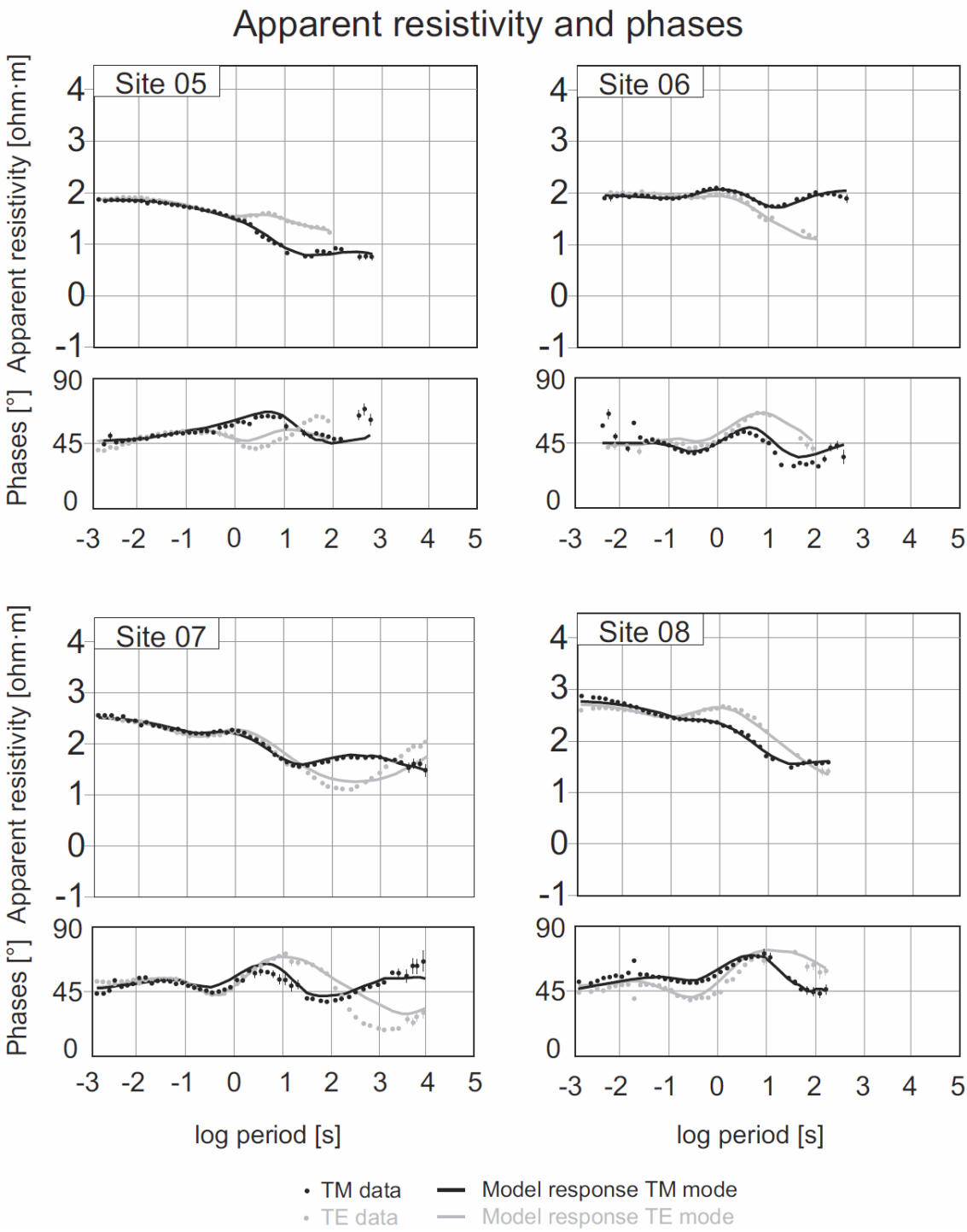

Figure 3.S1 Comparison of the apparent resistivity and phases between raw data and model responses for TE and TM modes.

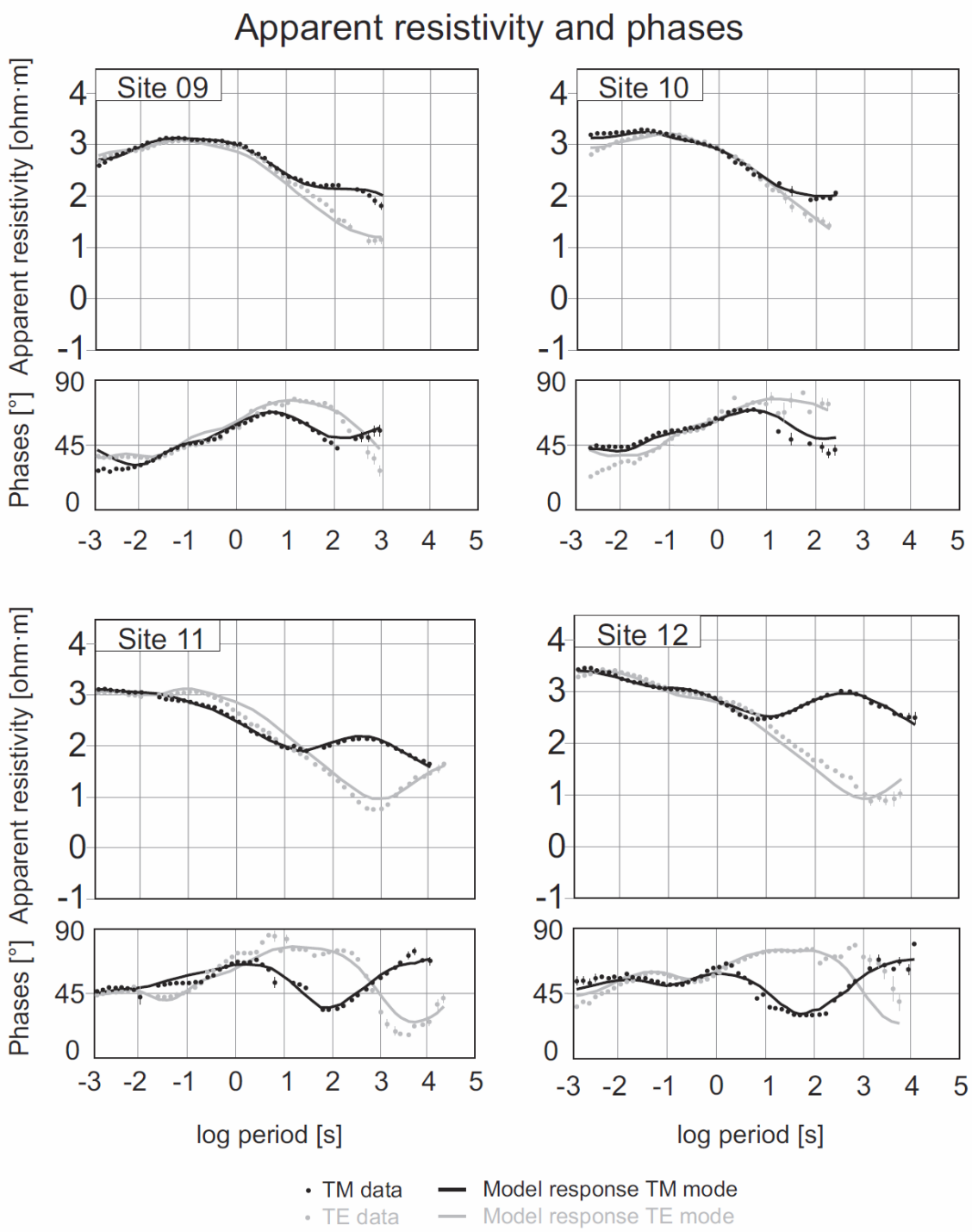

Figure 3.S1 Comparison of the apparent resistivity and phases between raw data and model responses for TE and TM modes.

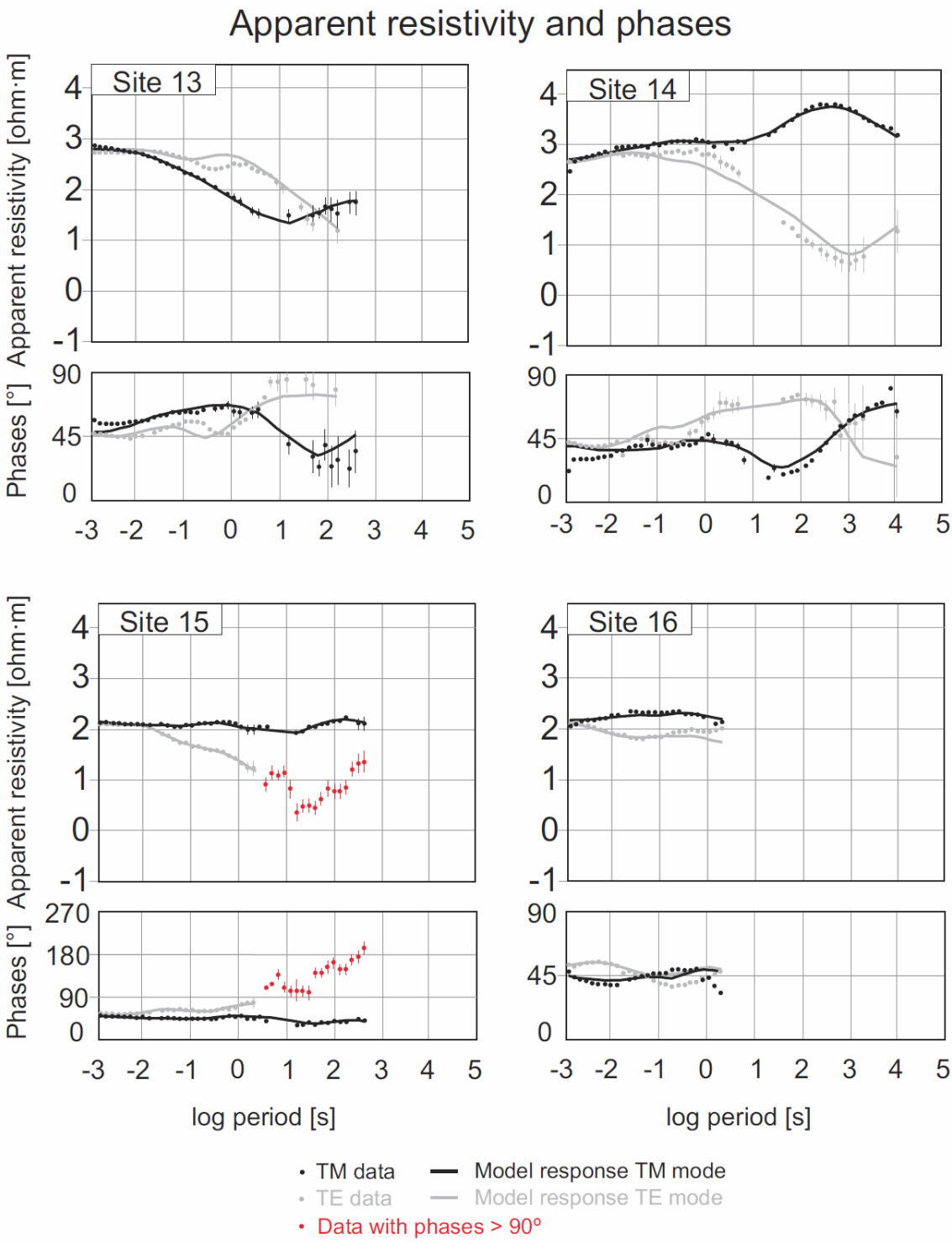

Figure 3.S1 Comparison of the apparent resistivity and phases between raw data and model responses for TE and TM modes.

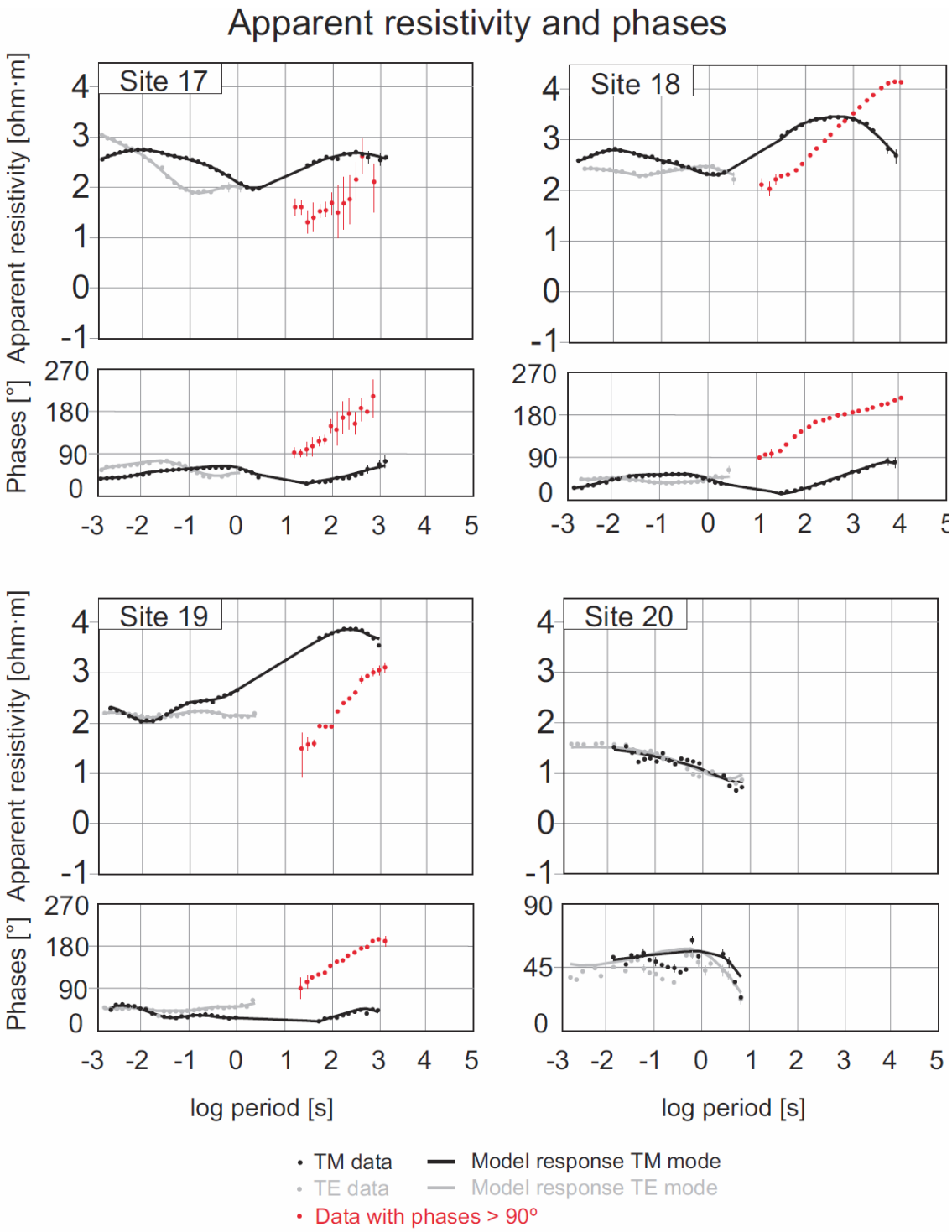

Figure 3.S1 Comparison of the apparent resistivity and phases between raw data and model responses for TE and TM modes.

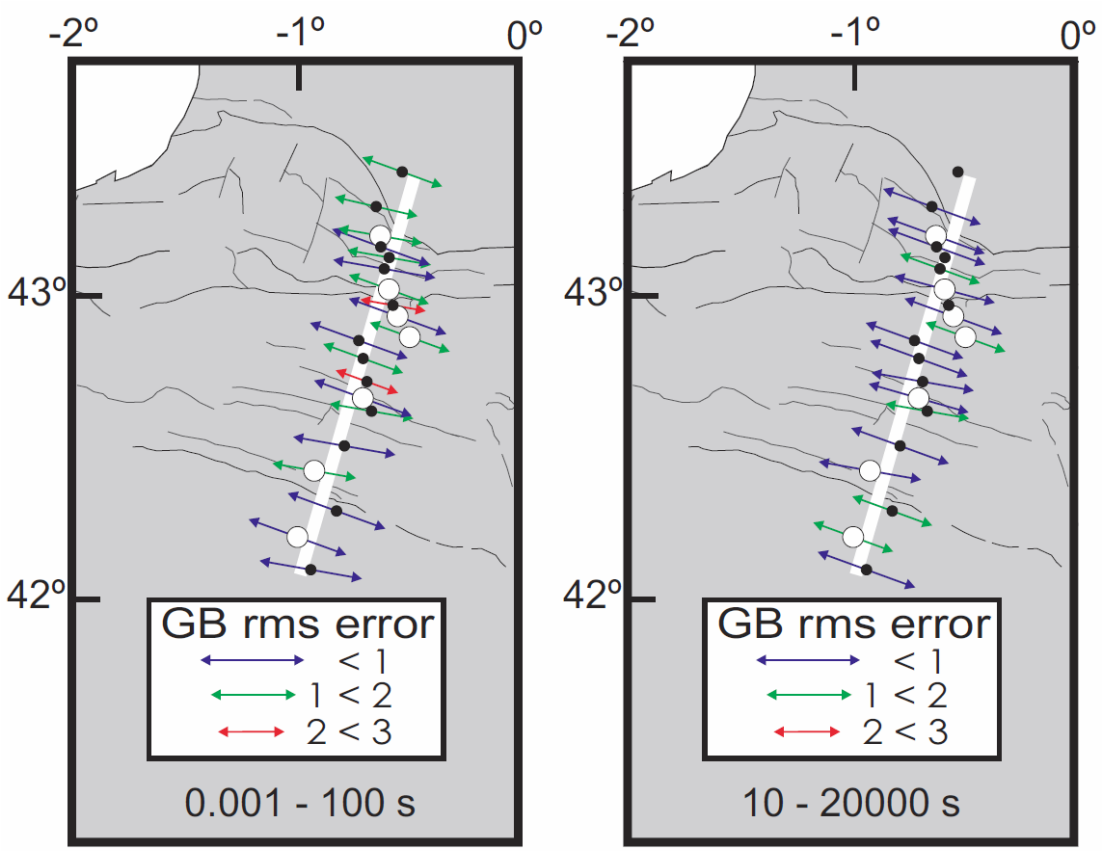

Figure 3.S2 Location of the MT stations in a structural sketch of West-Central Pyrenees. Black spots correspond to stations with BBMT data and white spots stations with BBMT and LMT data (Left strike analysis using BBMT data, right the strike analysis using LMT data). The arrows indicate the strike direction of each site, for the corresponding periods (BBMT: 0.001-100 s left and LMT: 10-20000 s right). The lengths of the arrows and colours indicate the compatibility of the data to the assumed two-dimensional strike direction (GB rms error). Thin lines divide the main geological units of the region.

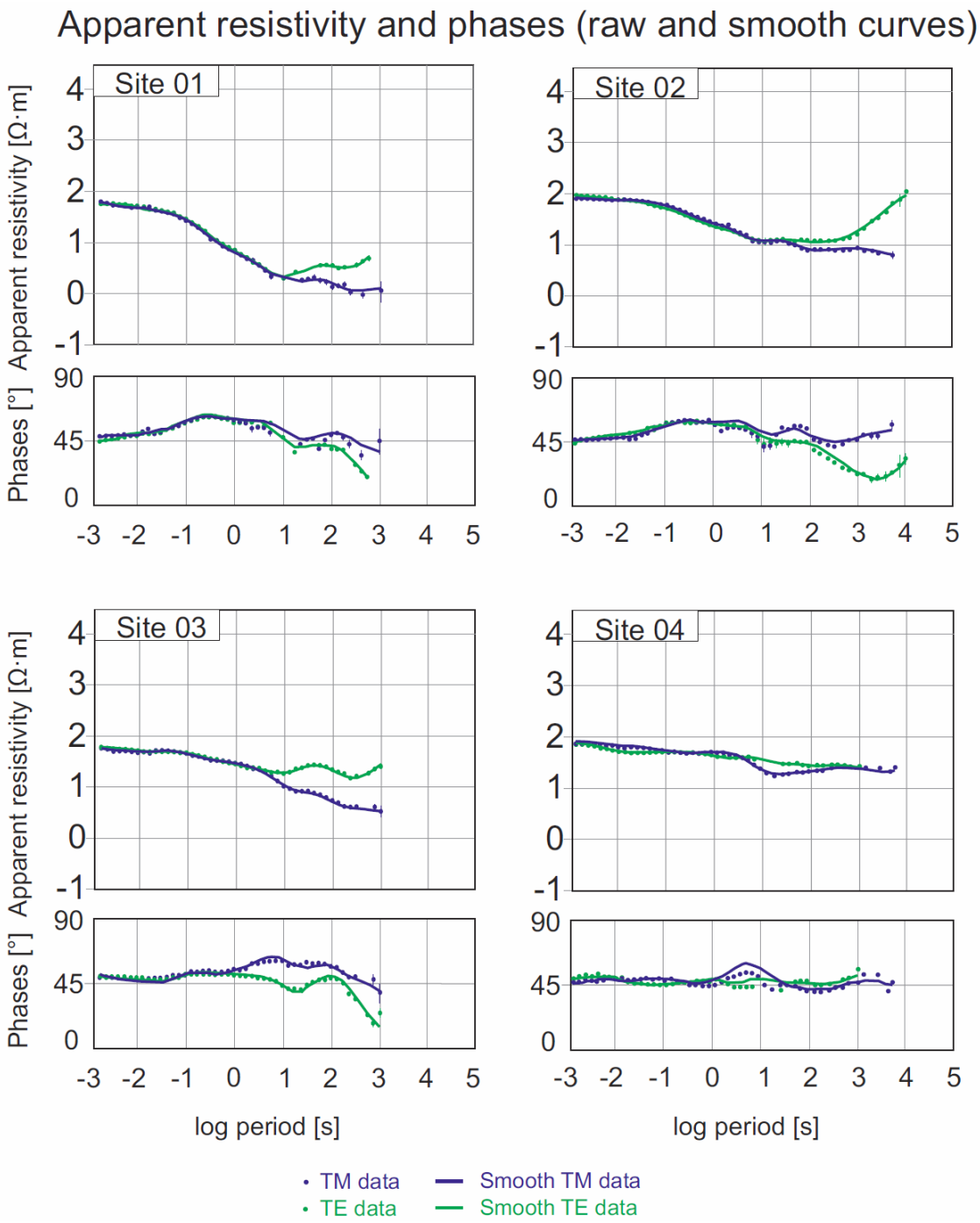

Figure 3.S3 Comparison of the apparent resistivity and phases for TE and TM modes between the raw data and the smooth data used for the inversion process.

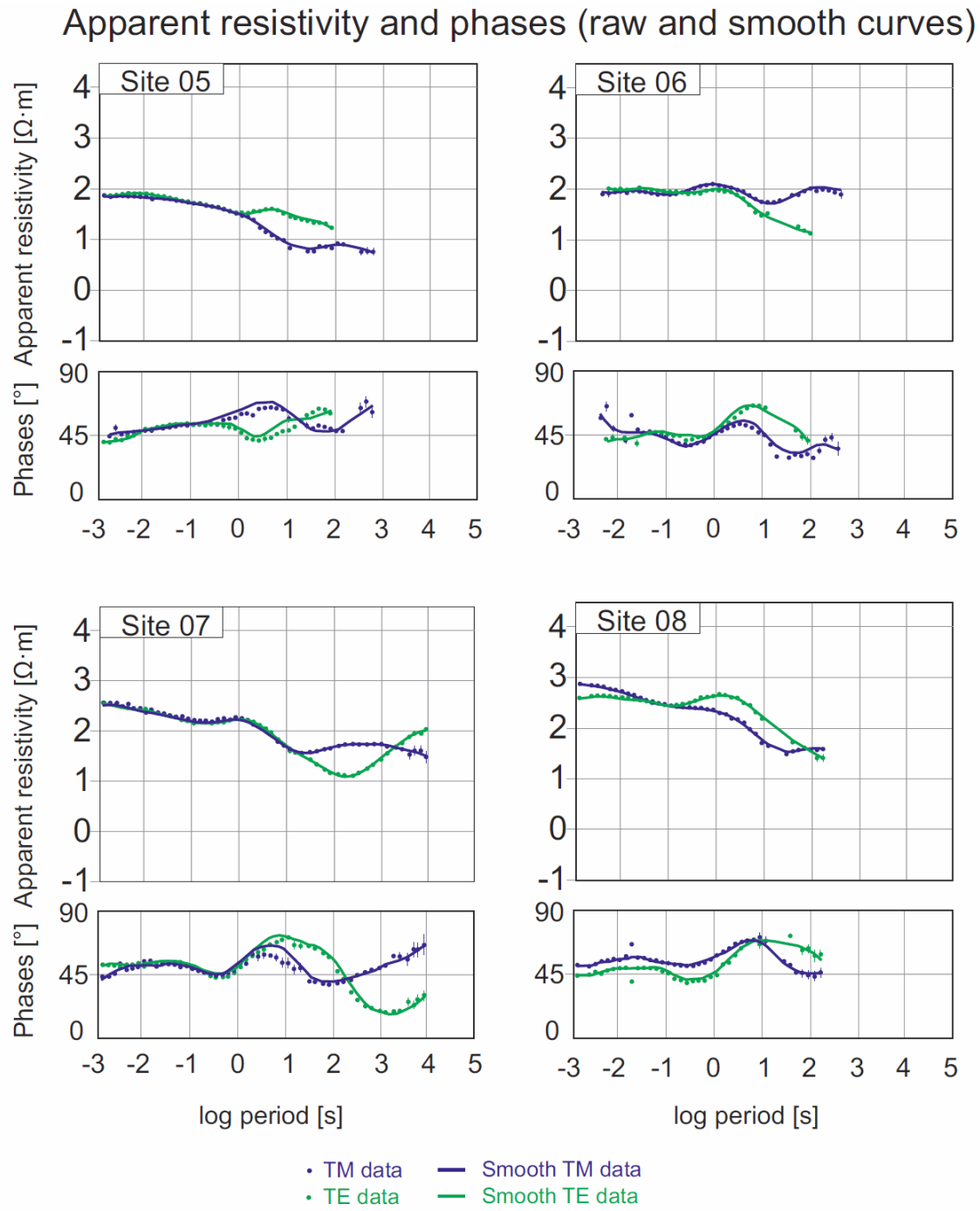

Figure 3.S3 Comparison of the apparent resistivity and phases for TE and TM modes between the raw data and the smooth data used for the inversion process.

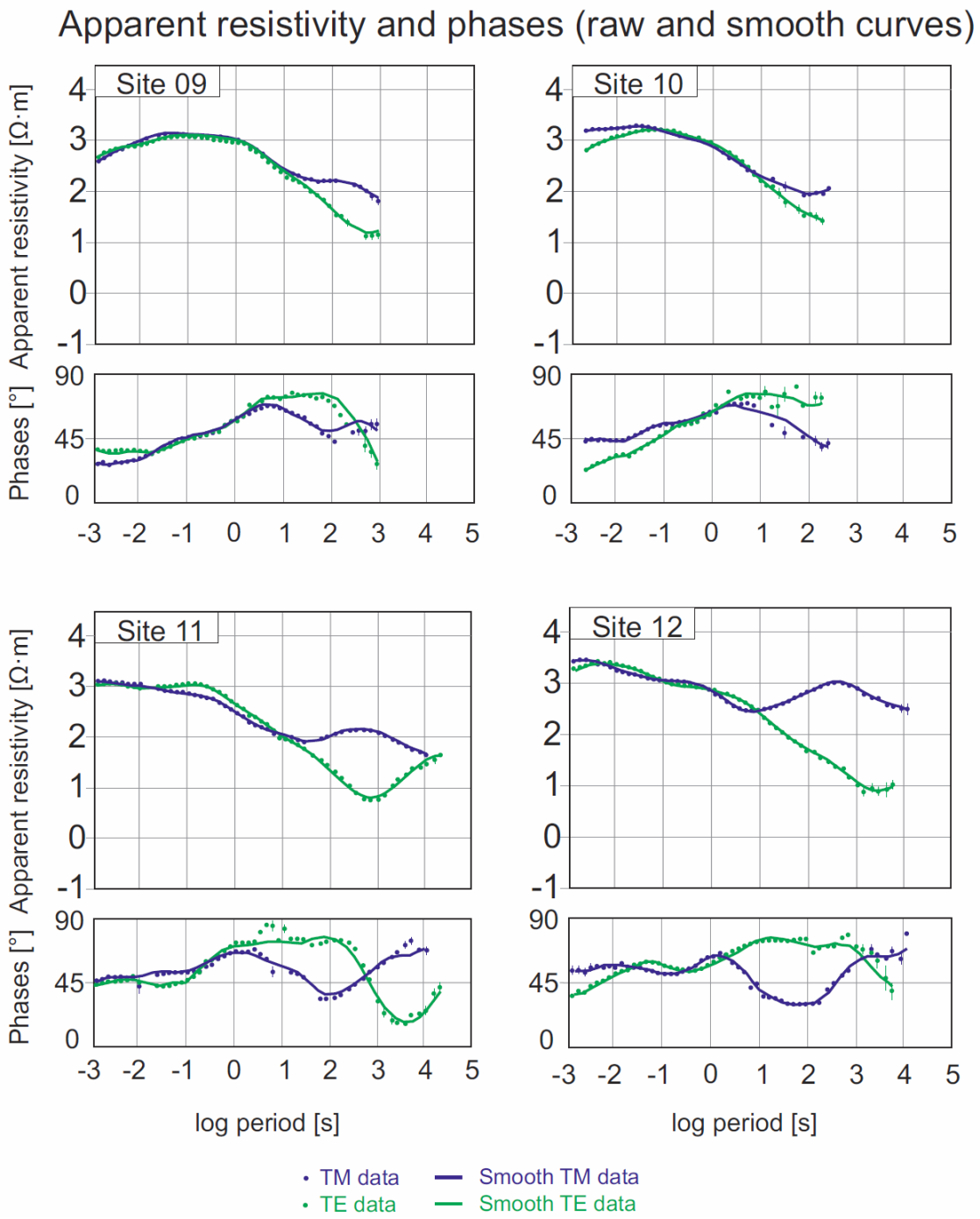

Figure 3.S3 Comparison of the apparent resistivity and phases for TE and TM modes between the raw data and the smooth data used for the inversion process.

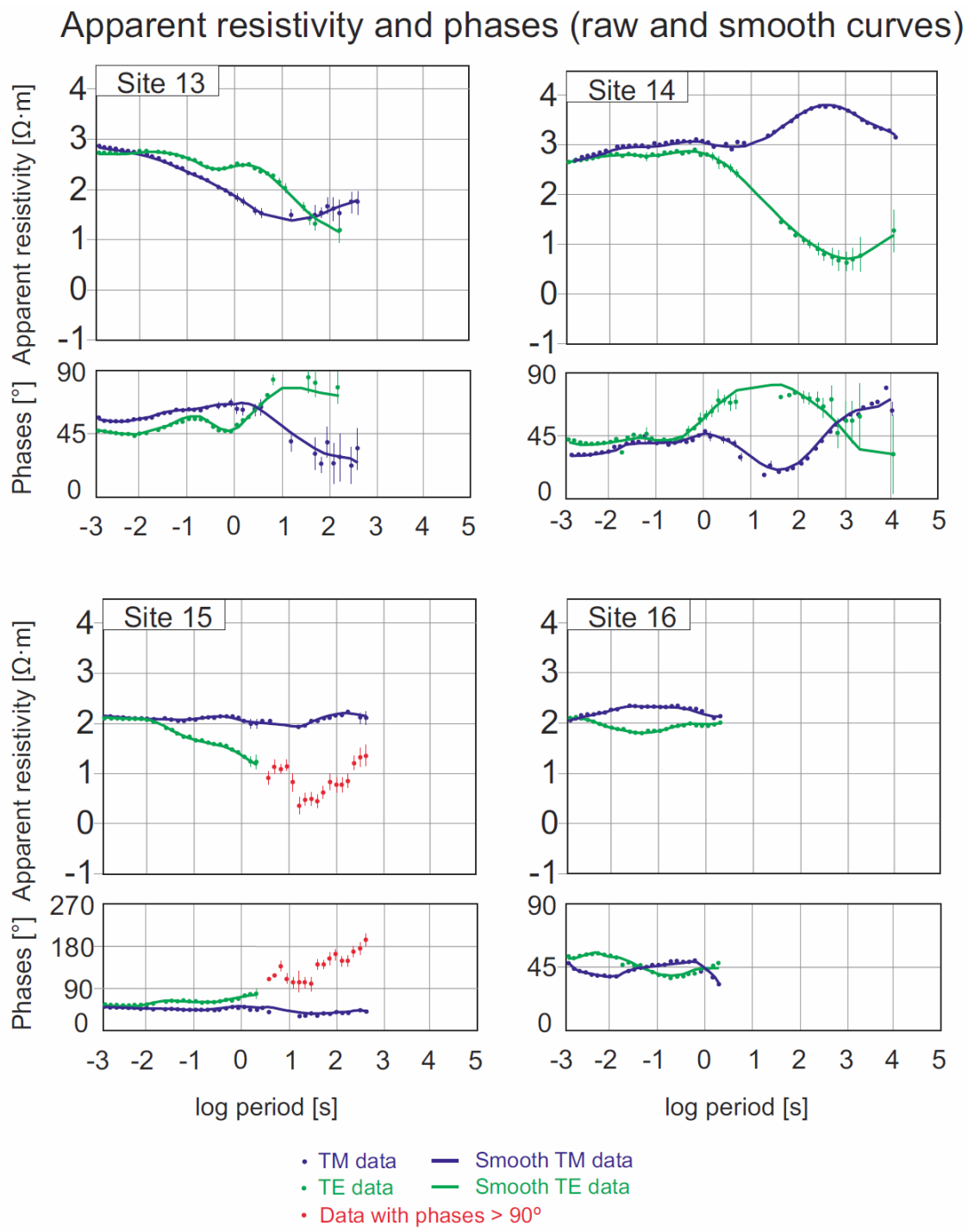

Figure 3.S3 Comparison of the apparent resistivity and phases for TE and TM modes between the raw data and the smooth data used for the inversion process.

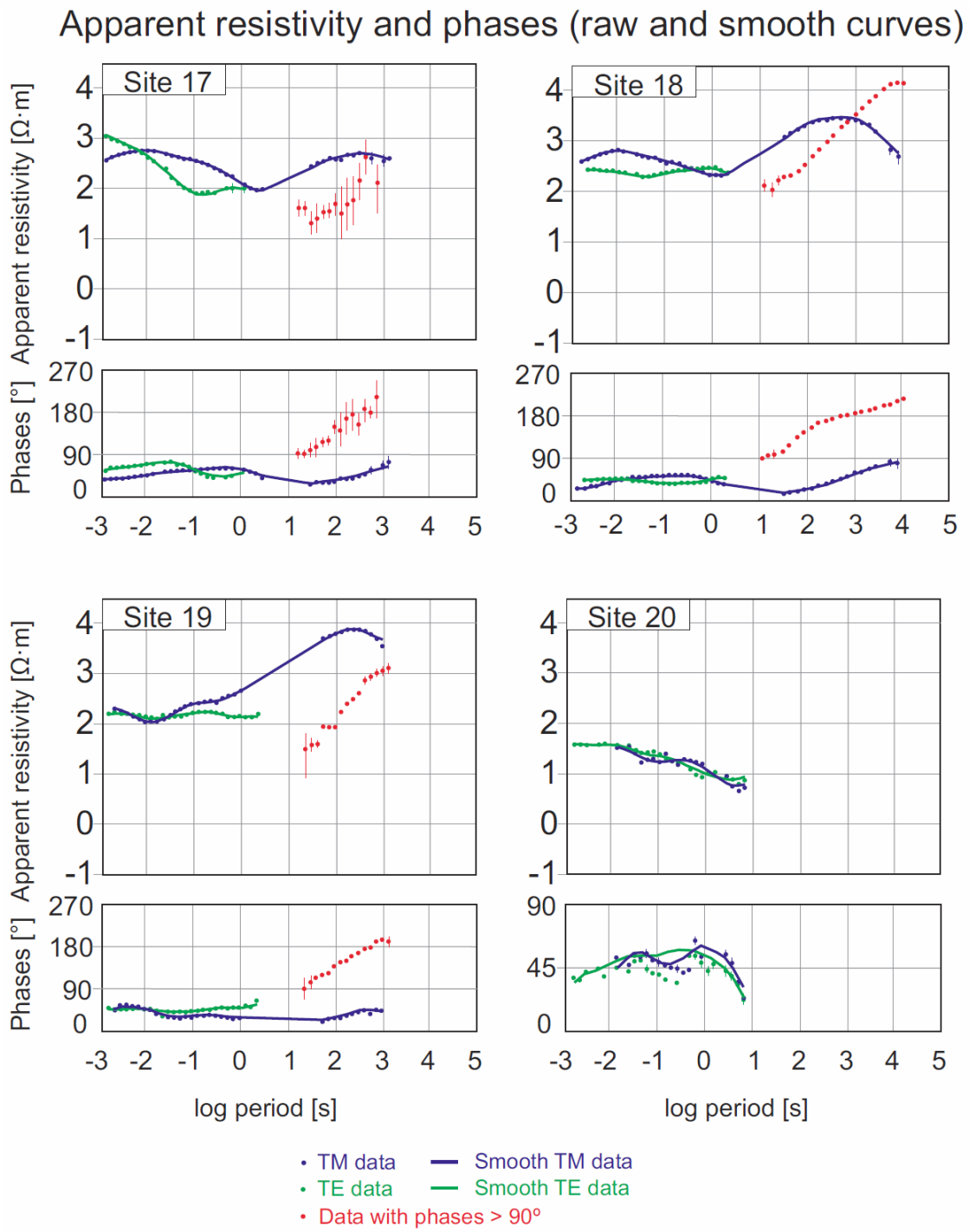

Figure 3.S3 Comparison of the apparent resistivity and phases for TE and TM modes between the raw data and the smooth data used for the inversion process.

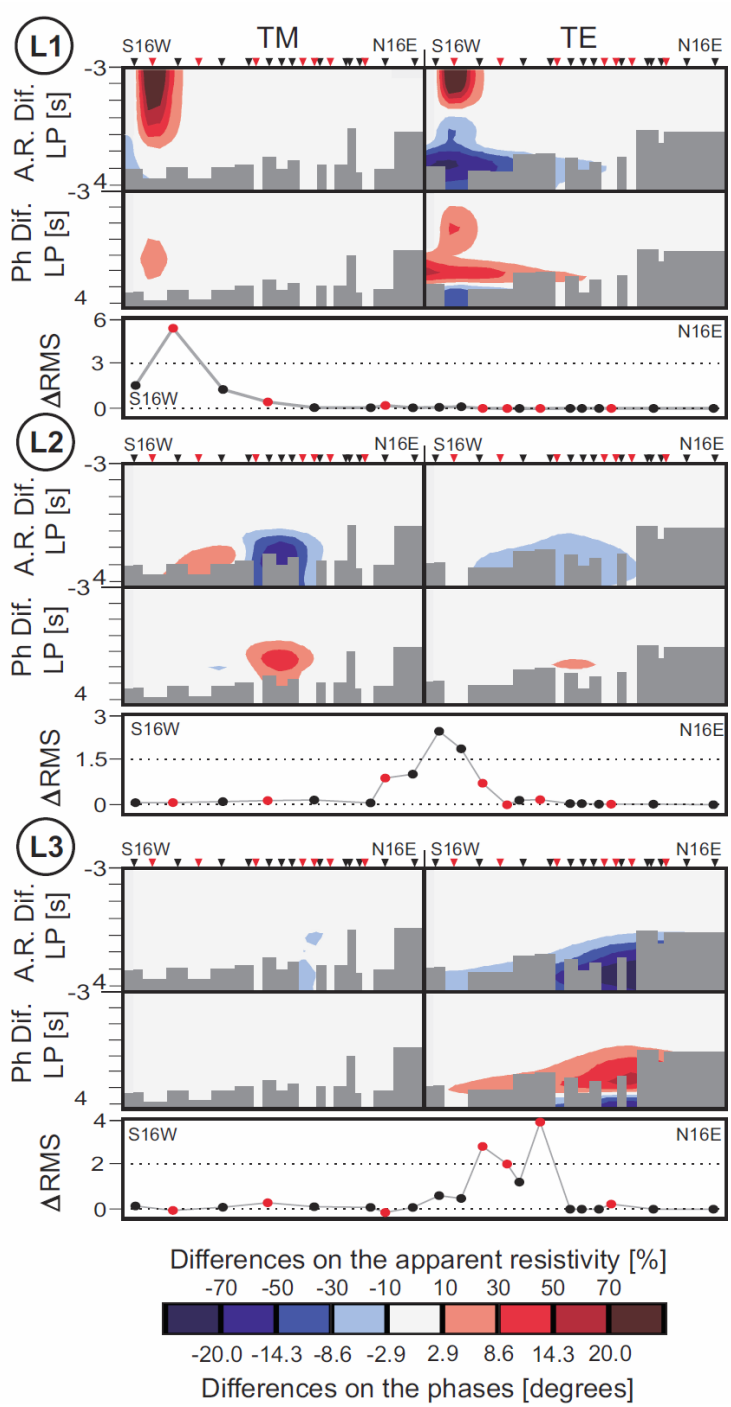

Figure 3.S4 Differences in model responses between the MT model shown in figure 3 and a modified one where geoelectrical structures (L1, L2, L3, L4, L5, L6, L7, H1 or H2) have been removed, one at a time. For each geoelectrical structure: On top, pseudosections with the observed differences in the apparent resistivity and phases for TE and TM modes (responses of the MT model shown in Fig. 3 minus responses of the modified MT model). At the bottom, variation of the rms (rms of the sites in the modified MT model minus rms of the sites in the MT model shown in Fig. 3). The electrical resistivity values used to remove the geoelectrical structures are 25 Ω·m for L1, 100 Ω·m for L2, 100 Ω·m for L3, 500 Ω·m for L4, 4000 Ω·m for L5, 3000 Ω·m for L6, 2500 Ω·m for L7, 30 Ω·m for H1 and 150 Ω·m for H2. Sites are represented by inverted triangles in the pseudosections and by circles in the rms section (in red sites with BBMT and LMT data and in black sites with BBMT data). Gray rectangles in pseudosections correspond to region without data. A.R. Dif.: Differences in apparent resistivity; Ph Dif.: Differences in phases; LP: Lg (period).

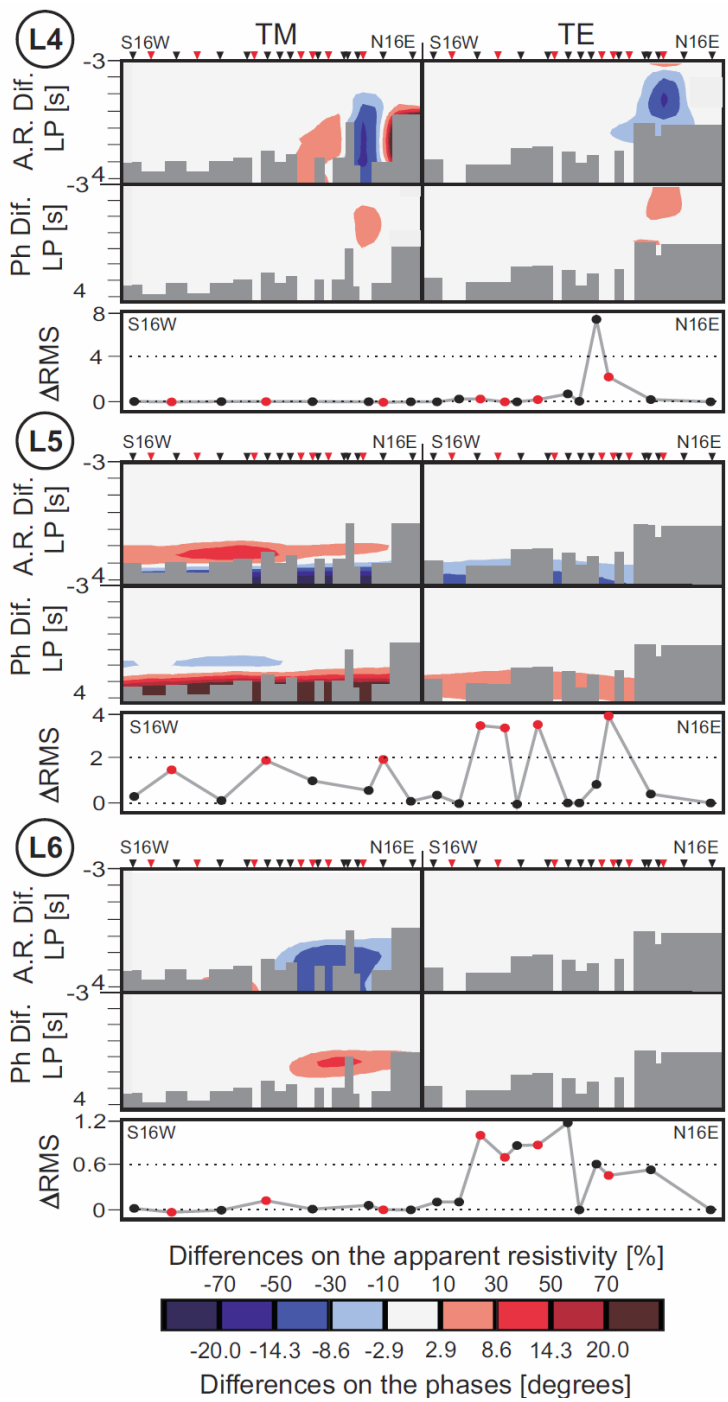

Figure 3.S4 Differences in model responses between the MT model shown in figure 3 and a modified one where geoelectrical structures (L1, L2, L3, L4, L5, L6, L7, H1 or H2) have been removed, one at a time. For each geoelectrical structure: On top, pseudosections with the observed differences in the apparent resistivity and phases for TE and TM modes (responses of the MT model shown in Fig. 3 minus responses of the modified MT model). At the bottom, variation of the rms (rms of the sites in the modified MT model minus rms of the sites in the MT model shown in Fig. 3). The electrical resistivity values used to remove the geoelectrical structures are 25 Ω·m for L1, 100 Ω·m for L2, 100 Ω·m for L3, 500 Ω·m for L4, 4000 Ω·m for L5, 3000 Ω·m for L6, 2500 Ω·m for L7, 30 Ω·m for H1 and 150 Ω·m for H2. Sites are represented by inverted triangles in the pseudosections and by circles in the rms section (in red sites with BBMT and LMT data and in black sites with BBMT data). Gray rectangles in pseudosections correspond to region without data. A.R. Dif.: Differences in apparent resistivity; Ph Dif.: Differences in phases; LP: Lg (period).

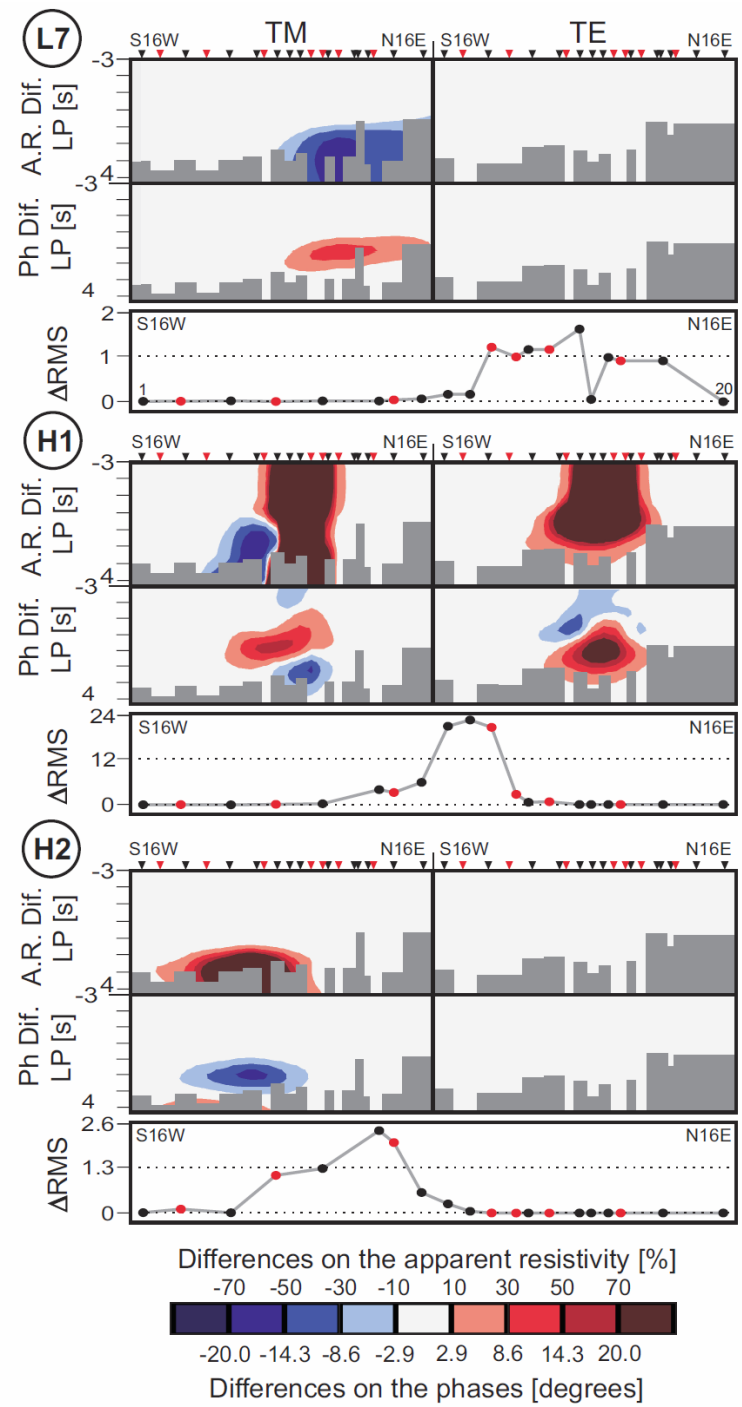

Figure 3.S4 Differences in model responses between the MT model shown in figure 3 and a modified one where geoelectrical structures (L1, L2, L3, L4, L5, L6, L7, H1 or H2) have been removed, one at a time. For each geoelectrical structure: On top, pseudosections with the observed differences in the apparent resistivity and phases for TE and TM modes (responses of the MT model shown in Fig. 3 minus responses of the modified MT model). At the bottom, variation of the rms (rms of the sites in the modified MT model minus rms of the sites in the MT model shown in Fig. 3). The electrical resistivity values used to remove the geoelectrical structures are 25 Ω·m for L1, 100 Ω·m for L2, 100 Ω·m for L3, 500 Ω·m for L4, 4000 Ω·m for L5, 3000 Ω·m for L6, 2500 Ω·m for L7, 30 Ω·m for H1 and 150 Ω·m for H2. Sites are represented by inverted triangles in the pseudosections and by circles in the rms section (in red sites with BBMT and LMT data and in black sites with BBMT data). Gray rectangles in pseudosections correspond to region without data. A.R. Dif.: Differences in apparent resistivity; Ph Dif.: Differences in phases; LP: Lg (period).

CHAPTER 4

Geophysical Journal International

Processing of Magnetotelluric data using inter-station tensor relationships

Joan Campanyà[1], Juanjo Ledo[1], Pilar Queralt[1], Alex Marcuello[1] & Alan G. Jones[2]

[1]GEOMODELS Research Insitiute, Departament de Geodinàmica i Geofísica, Universitat de Barcelona, C/Martí Franqués s/n. Barcelona 08028.
[2] Dublin Institute for Advanced Studies, Dublin, Ireland

Submitted in Geophysical Journal International: 27th November of 2012

RESUM

En el mètode magnetotel·lúric, els camps elèctrics i magnètics s'han d'enregistrar simultàniament sobre la superfície de la zona d'estudi per tal de determinar les estructures geoelèctriques del subsòl. És per això que si una de les components es torna inutilitzable les relacions tensorials del lloc d'estudi no es poden caracteritzar. Aquest problema es podria resoldre si fóssim capaços de processar les dades del lloc d'estudi utilitzant dades enregistrades per una estació veïna. En alguns casos, els camps magnètics enregistrats per una estació veïna ja s'han fet servir per determinar les relacions tensorials del lloc d'estudi, fent també referència remota, però això només es pot dur a terme si no hi han grans diferències entre els camps magnètics horitzontals dels dos llocs. Nosaltres proposem un mètode per processar les dades magnetotel·lúriques del lloc d'estudi utilitzant els camps magnètics enregistrats en una estació veïna, inclús quan hi ha diferències entre els camps magnètics horitzontals dels dos punts de mesura. Seguint el mètode proposat, les relacions tensorials del lloc d'estudi es determinen en combinar relacions tensorials entre-estacions entre els camps elèctrics i magnètics del lloc d'estudi i els camps magnètics horitzontals de l'estació veïna. Definim el paràmetre Ψ per avaluar l'aplicabilitat del mètode proposat en cada processat i per cada període. Si Ψ s'assembla a la matriu identitat, les relacions tensorials obtingudes són vàlides. Els mètode s'ha provat amb dades magnetotel·lúriques de llarg període enregistrades als Pirineus i amb dades proporcionades per observatoris magnètics, amb resultats positius. Els experiments duts a terme demostren que els resultats obtinguts seguint el mètode proposat s'ajusten al tensor d'impedàncies magnetotel·lúric i la funció de transferència geomagnètica del lloc d'estudi. També mostren que els resultats no depenen de l'estació veïna feta servir per processar les dades. A més, donada la naturalesa del mètode aquest aporta noves opcions en l'adquisició de dades magnetotel·lúriques optimitzant els aparells disponibles.

SUMMARY

In the magnetotelluric method, the electric and magnetic fields have to be simultaneously recorded on the surface of the study area to constrain the geoelectrical structures of the subsurface. From this condition, if one of the components became unusable, the tensor relationship of the local site cannot be constrained. This problem could be solved if we are able to process the data of the local site using data recorded at a neighbouring site. In some cases, the horizontal magnetic fields of a neighbouring site have been already used to constrain the tensor relationships of the local site, using remote-referencing, but it can be only applied if there are no major differences between the horizontal magnetic fields of the two sites. We propose a method to process the magnetotelluric data at the local site using the horizontal magnetic fields of a neighbouring site, even if there are differences between the horizontal magnetic fields between the two sites. Following the proposed method, the tensor relationships of the local site are constrained combining the inter-station tensor relationships between the electric and magnetic fields of the local site and the horizontal magnetic fields recorded at a neighbouring site. We define the Ψ parameter to evaluate the applicability of the proposed method for each processing and for each period. If Ψ is close to the identity matrix, the proposed relationships are valid. Long period magnetotelluric data acquired in the Pyrenees and magnetic data provided by magnetic observatories are used to test the method, with positive results. The experiments carried out demonstrate that the results obtained following the proposed method fit with the magnetotelluric impedance tensor and the geomagnetic transfer function of the local site. The experiments also show that the results obtained do not depend of the adopted neighbour horizontal magnetic fields. Furthermore, given the nature of the method it opens new ways to acquire magnetotelluric data optimizing the available instruments.

4.1 INTRODUCTION

In the magnetotelluric (MT) method, the geoelectrical structures of the subsurface are basically characterized by the MT impedance tensor (Cantwell, 1960; Rokityanski, 1961) and the geomagnetic transfer function (Parkinson, 1962; Weise, 1962). To determine these tensor relationships, the electric and magnetic time-varying fields simultaneously recorded on the surface of the study area are related in the frequency domain. If one of the recorded components becomes unusable, the tensor relationships cannot be constrained. This problem can be solved if the MT data recorded at a neighbouring site can be used to determine the tensor relationships of the local site.

In audiomagnetotellurics (AMT), where the distance between sites is typically around 200 m (i.e. Asch & Sweetkind, 2011; Falgàs et al., 2011; La Terra & Mezenes, 2011), the horizontal magnetic fields recorded at a neighbouring site can be used to process the data of the local site. This technique is already used by Mount Isa Mines' MIMDAS (Sheard, 2001) and Quantec's TITAN-24 (White & Gordon, 2003), and can be applied to constrain the MT impedance tensor of the local site if there are no main differences between the horizontal magnetic fields of the two sites. McNeice and Jones (2001) showed that especially for sub-horizontal conductors, the total magnetic fields can vary significantly between sites, so care has to be taken when using these limited acquisition methodologies.

In case of broadband magnetotelluric (BBMT) and long period magnetotelluric (LMT) data, where the distance between sites is much larger than 200 m, the MT sites can be located above different geoelectrical structures having large differences between the horizontal magnetic fields recorded on the two sites (Egbert, 2002; Habibian et al., 2010). In this case, it is not recommended to use the horizontal magnetic field of a neighbouring site to obtain the apparent resistivity and phase of the local site because the results obtained could suggest different geoelectrical structures than the ones we want to constrain.

Garcia & Jones (2005) also used the data recorded on a neighbouring site to process the data of a local site, helping to solve the problem of the AMT dead-band. They suggested a method for processing AMT data combining two tensor relationships constrained from time series recorded at a different times. The method consists in determine the quasi-magnetotelluric transfer function of a local site from the tensor multiplication of two tensor relationships: The transfer function between day time telluric channels between the local site and a base site and the night time conventional MT impedance tensor at the base site. The obtained transfer function represents the ratio of the local-telluric to base-magnetic fields obtaining the telluric-magnetotelluric (T-MT) (Hermance & Thayer, 1975) AMT transfer function of the local site. Garcia & Jones (2005) showed that it represent a reasonable approximation of the real AMT impedance tensor if there are no major differences between the horizontal magnetic fields recorded on the two sites.

In this paper we propose a method where the MT impedance tensor and the geomagnetic transfer function at a local site can be constrained using inter-station tensor relationships between the electric and magnetic fields of the local site and the horizontal magnetic fields of a neighbouring site. In this method, differences between the horizontal magnetic fields recorded at the two sites do not affect the results obtained, being able to use it when there are differences between the horizontal magnetic fields at the two sites. The inter-station tensor relationships used to constrain the MT impedance tensor of the local site represents the ratio of the local telluric to base magnetic fields and the ratio of the base magnetic to the local magnetic fields. To determine the geomagnetic transfer function the used inter-station tensor relationships represents the ratio of the local vertical magnetic to base magnetic fields and the ratio of the base magnetic to the local magnetic fields. Note that the ratio of the base magnetic to local magnetic fields is the horizontal magnetic tensor (HMT) proposed by Berdichevsky (1968), Egbert & Booker (1989) and Schmucker (1970). Although it can be used to determine geoelectrical structures, it is also employed to improve the processing of MT data detecting and removing the effect of non-stationary events (Varentsov et al., 2003; Sokolova et al., 2007).

Following the proposed method, if some of the recoded fields became unusable, the other time series can be used to calculate the inter-station tensor relationships, helping to improve the results obtained in process the MT data of the local site. As show in an example below, working with LMT data, the HMT can be constrained only using a few days of data. However, we recommend testing it in each study area to ensure that this possibility is accomplished. In a positive case, this give the opportunity to modify the logistical of a field campaign recording only a few days of magnetic time series at each site while the electric fields will be recorded all the time.

To perform this study, LMT data acquired in the Pyrenees at three different sites (*a*, *b* and *c*) were used to calculate the MT impedance tensor and the geomagnetic transfer function at site *a* in combination with the magnetic data provided by the Chambon la Forêt magnetic observatory (CLF) and the Furstenfeldbruck magnetic observatory (FUR). Both observatories are part of INTERMAGNET (http://www.intermagnet.org) (Figure 4.1).

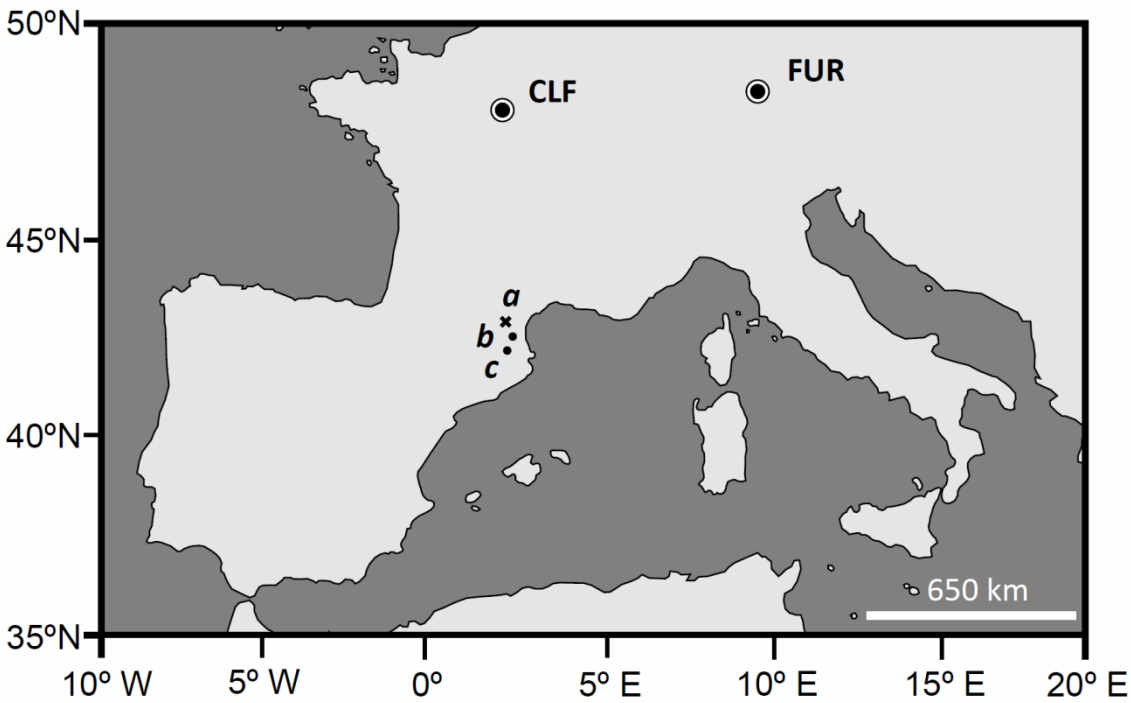

Figure 4.1 Map with the location of the LMT sites. *a*, *b* and *c* are the LMT sites recorded in the Pyrenees and CLF and FUR are the Magnetic Observatories (INTERMAGNET).

4.2 THEORY

In the proposed method, three inter-station tensor relationships are calculated to constrain the MT impedance tensor and the geomagnetic transfer functions at the local site. These tensor relationships relate the local telluric at site *a* with the neighbouring magnetic at site *b* (equation 4.1), the local vertical magnetic at site *a* with the neighbouring magnetic at site *b* (equation 4.2), and the neighbouring magnetic at site *b* with the local magnetic at site *a* (equation 4.3). In all cases dependence on frequency is assumed. The nomenclature of the tensor relationships is based on Berdichevsky & Dmitriev, (2008).

$$\boldsymbol{e}_a = \boldsymbol{Z}_{ab}\boldsymbol{h}_b \qquad (4.1)$$
$$h_z^a = \boldsymbol{S}_{ab}\boldsymbol{h}_b \qquad (4.2)$$
$$\boldsymbol{h}_b = \boldsymbol{M}_{ba}\boldsymbol{h}_a \qquad (4.3)$$

where $\boldsymbol{h}_a$ and $\boldsymbol{h}_b$ are vectors of length two comprising the two horizontal magnetic components of the sites *a* $[h_x^a, h_y^a]$ and *b* $[h_x^b, h_y^b]$, respectively. The $\boldsymbol{e}_a$ is a vector of length two comprising the horizontal electric components of the site *a* $[e_x^a, e_y^a]$ and h_z^a is the vertical component of the magnetic field recorded on *a*. $\boldsymbol{Z}_{ab}$ and $\boldsymbol{M}_{ba}$ are 2x2 complex matrix relating the two correspondent vectors and $\boldsymbol{S}_{ab}$ is a 1x2 complex vector relating h_z^a and $\boldsymbol{h}_b$.

With the aim to avoid the effect of local noise the remote reference method (Gamble et al., 1979 a,b) with a magnetic site *r* is applied when calculate $\boldsymbol{Z}_{ab}$, $\boldsymbol{S}_{ab}$ and $\boldsymbol{M}_{ba}$:

$$\boldsymbol{Z}_{ab}^{RR} = [\boldsymbol{e}_a\boldsymbol{h}_r][\boldsymbol{h}_b\boldsymbol{h}_r]^{-1} \qquad (4.4)$$
$$\boldsymbol{S}_{ab}^{RR} = [h_z^a\boldsymbol{h}_r][\boldsymbol{h}_b\boldsymbol{h}_r]^{-1} \qquad (4.5)$$
$$\boldsymbol{M}_{ba}^{RR} = [\boldsymbol{h}_b\boldsymbol{h}_r][\boldsymbol{h}_a\boldsymbol{h}_r]^{-1} \qquad (4.6)$$

where the value $[\boldsymbol{pq}]$ is the spectral density matrix for fields *p* and *q*, defined by Gamble et al. (1979b), viz.

$$[\boldsymbol{pq}] = \begin{bmatrix} \langle p_x q_x^* \rangle & \langle p_x q_y^* \rangle \\ \langle p_y q_x^* \rangle & \langle p_y q_y^* \rangle \end{bmatrix} \qquad (4.7)$$

The asterisk denotes the complex conjugate and $\langle \quad \rangle$ denotes ensemble averaging either by summation over neighbouring frequencies or by averaging different estimates at the same frequency, or both.

In case of $[h_z^a \boldsymbol{h}_r]$

$$[\boldsymbol{pq}] = [\langle p_x q_x^* \rangle \quad \langle p_x q_y^* \rangle] \quad (4.8)$$

Gamble et al. (1979b) also provide the inverse of the matrix $[\boldsymbol{pq}]$

$$[\boldsymbol{pq}]^{-1} = \frac{\begin{bmatrix} \langle p_y q_y^* \rangle & -\langle p_x q_y^* \rangle \\ -\langle p_y q_x^* \rangle & \langle p_x q_x^* \rangle \end{bmatrix}}{\langle p_x q_x^* \rangle \langle p_y q_y^* \rangle - \langle p_y q_x^* \rangle \langle p_x q_y^* \rangle} \qquad (4.9)$$

Combining equations (4.4), (4.5) and (4.6) we can obtain the MT impedance tensor and the geomagnetic transfer functions of the site *a*, $\boldsymbol{Z}_a$ and $\boldsymbol{W}_a$ respectively*:*

$$\boldsymbol{Z}_{ab}^{RR} \boldsymbol{M}_{ba}^{RR} = [\boldsymbol{e}_a \boldsymbol{h}_r][\boldsymbol{h}_b \boldsymbol{h}_r]^{-1}[\boldsymbol{h}_b \boldsymbol{h}_r][\boldsymbol{h}_a \boldsymbol{h}_r]^{-1} = [\boldsymbol{e}_a \boldsymbol{h}_r]\boldsymbol{I}[\boldsymbol{h}_a \boldsymbol{h}_r]^{-1} = \boldsymbol{Z}_a^{RR} \qquad (4.10)$$

$$\boldsymbol{S}_{ab}^{RR} \boldsymbol{M}_{ba}^{RR} = [h_z^a \boldsymbol{h}_r][\boldsymbol{h}_b \boldsymbol{h}_r]^{-1}[\boldsymbol{h}_b \boldsymbol{h}_r][\boldsymbol{h}_a \boldsymbol{h}_r]^{-1} = [h_z^a \boldsymbol{h}_r]\boldsymbol{I}[\boldsymbol{h}_a \boldsymbol{h}_r]^{-1} = \boldsymbol{W}_a^{RR} \qquad (4.11)$$

where $\boldsymbol{I}$ is the identity and $\boldsymbol{W}_a$ the geomagnetic transfer function of the site *a*.

Ensuring the applicability of the proposed method for each specific study, we define the Ψ parameter as:

$$\Psi = \boldsymbol{M}_{ba} \boldsymbol{M}_{ab} = [\boldsymbol{h}_b k][\boldsymbol{h}_a k]^{-1}[\boldsymbol{h}_a k][\boldsymbol{h}_b k]^{-1} = \boldsymbol{I} \quad (4.12)$$

Where k is the component used as a complex conjugate to constrain the tensor relationships. In the case of remote reference $k = h_r$. If the Ψ parameter differs from the identity matrix, the obtained $\boldsymbol{M}_{ba}$ is not properly relating the horizontal magnetic fields between sites *a* and *b*, and the proposed method should not be applied using

this tensor relationship. The permitted differences between the Ψ parameter and the identity matrix are suggested below.

4.3 EXPERIMENTS AND RESULTS

The data used for the experiment consist of three LMT sites recorded in the Eastern Pyrenees and the magnetic time series provided by the INTERMAGNET observatories Chambon de la Forêt (CLF) and Furstenfeldbruck (FUR) (Figure 4.1). The LMT data were recorded using the LEMI systems, designed by the Lviv Centre of the Institute of Space Research, at sites *a*, *b* and *c* between the 26th October and the 09th November of 2010 for site *b*, and between the 19th October and the 09th November of 2010 for sites *a* and *c*. In all the cases, sample rate is 1 Hz for the electric and magnetic fields. The distance between site *a* and sites *b* and *c* are 25 km and 50 km, respectively. The LMT data have been processed using the Birrp.5 program (Chave & Thompson, 2004) doing remote reference with the magnetic observatories. The same parameters have been imposed in the processing of the data, avoiding effects unrelated with the purpose of the study. When it has been necessary, error estimation has been carried out following the bootstrap method (Efron, 1979), computing a sample of 5000 bootstrapped standard deviation of 1000 samples from the analyzed parameter. The 1000 samples of the analyzed parameter have been calculated using 1000 random samples within the margin of error of each variable.

The first experiment has been developed to validate the applicability of the proposed method and consist in processing the MT data of the site *a* using different approaches. The LMT data at site *a* were processed using the magnetic data recorded at site *b*, doing remote reference with CLF, and using the magnetic data recorded on the site *c*, doing remote reference with FUR. Results obtained are compared using the *xy* and *yx* components of the MT impedance tensor and the geomagnetic transfer function. The *xx* and *yy* components of the MT impedance tensor (Figures 4.S1, 4.S2 and 4.S3 in supplementary files) are not used due as they have lower quality and do not involve differences in the final conclusions.

The first two approaches consist in processing the LMT data at site *a* doing local processing without remote reference ($\boldsymbol{Z}_a$ and $\boldsymbol{W}_a$) and local processing with remote reference with a magnetic observatory ($\boldsymbol{Z}_a^{RR}$ and $\boldsymbol{W}_a^{RR}$) (Figure 4.2). Results show the presence of local noise, which mainly affects the shorter periods of the *xy* component of the MT impedance tensor and the *Wy* component of the geomagnetic transfer function. These results suggest the necessity of undertaking remote referencing when processing the LMT data of the site *a*.

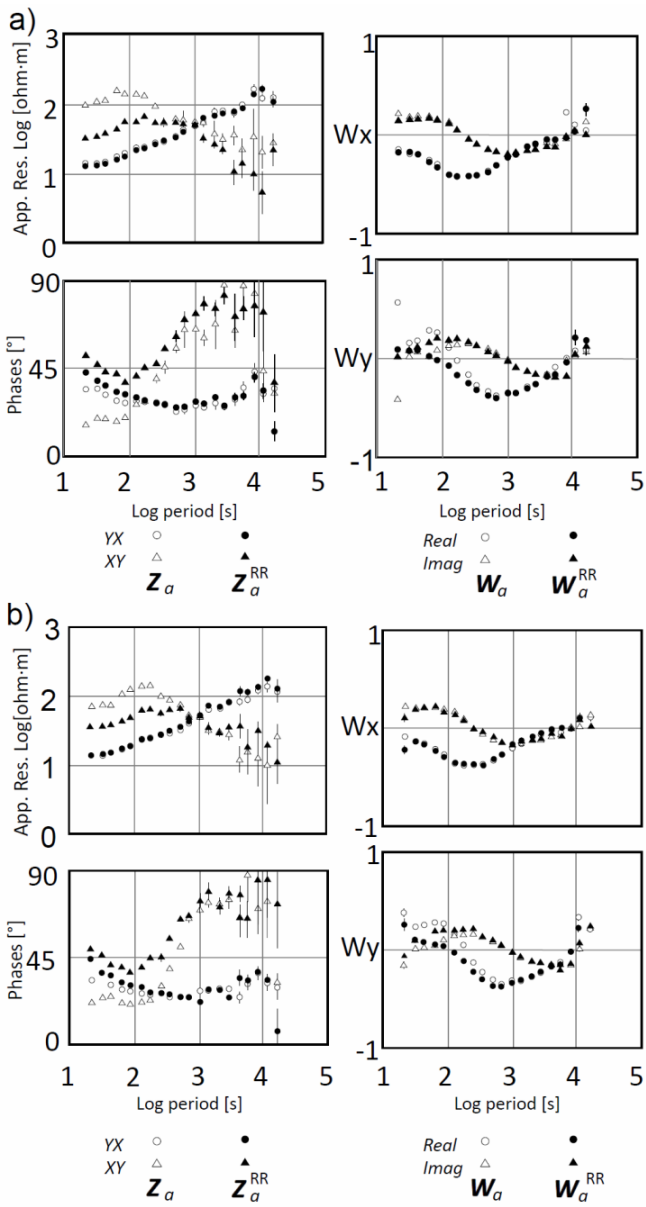

Figure 4.2 Apparent resistivity, phase and geomagnetic transfer function of the site *a* processing the data of the local site doing local processing and local processing with remote reference with CLF (a) and with FUR (b). (a) data have been acquired between the 26th October and 09th November. (b) data have been acquired between 19th October and 09th November.

Focusing on the MT impedance tensor, the next approach consists in processing the LMT data of the site *a* using the horizontal magnetic fields of sites *b* or *c* instead of those recorded at site *a*:

$$\boldsymbol{e}_a = \boldsymbol{Z}_{ab}^{RR} \boldsymbol{h}_b \qquad (4.13)$$

$$\boldsymbol{e}_a = \boldsymbol{Z}_{ac}^{RR} \boldsymbol{h}_c \qquad (4.14)$$

Finally, we calculate the MT impedance tensor of the site *a* applying the proposed method in this paper:

$$\boldsymbol{Z}_a^{RR} = \boldsymbol{Z}_{ab}^{RR} \boldsymbol{M}_{ba}^{RR} \qquad (4.15)$$

$$\boldsymbol{Z}_a^{RR} = \boldsymbol{Z}_{ac}^{RR} \boldsymbol{M}_{ca}^{RR} \qquad (4.16)$$

Equivalent steps have been followed to calculate the geomagnetic transfer function of the site *a*. Apparent resistivity, phases and the geomagnetic transfer function obtained in processing the MT data of site *a* using the horizontal magnetic fields of sites *b* and *c*, are shown in Figures 4.3 and 4.4, respectively. In all the cases, results are compared with that obtained doing local processing with remote reference ($\boldsymbol{Z}_a^{RR}$ and $\boldsymbol{W}_a^{RR}$). The results obtained using the horizontal magnetic fields of the sites *b* or *c* ($\boldsymbol{Z}_{ab}^{RR}$, $\boldsymbol{Z}_{ac}^{RR}$, $\boldsymbol{W}_{ab}^{RR}$ and $\boldsymbol{W}_{ac}^{RR}$) do not fit with the MT results of the local site ($\boldsymbol{Z}_a^{RR}$ and $\boldsymbol{W}_a^{RR}$) (Figures 4.3a and 4.4a), except when applying the horizontal magnetic tensor, $\boldsymbol{M}_{ba}^{RR}$ or $\boldsymbol{M}_{ca}^{RR}$, following the proposed method (Figures 4.3b and 4.4b). The consistence of the results obtained applying the proposed method using different horizontal magnetic fields is shown in Figure 4.5. The apparent resistivity, phase and geomagnetic transfer function values are practically the same, regardless of whether we use the horizontal magnetic fields at sites *b* or *c*.

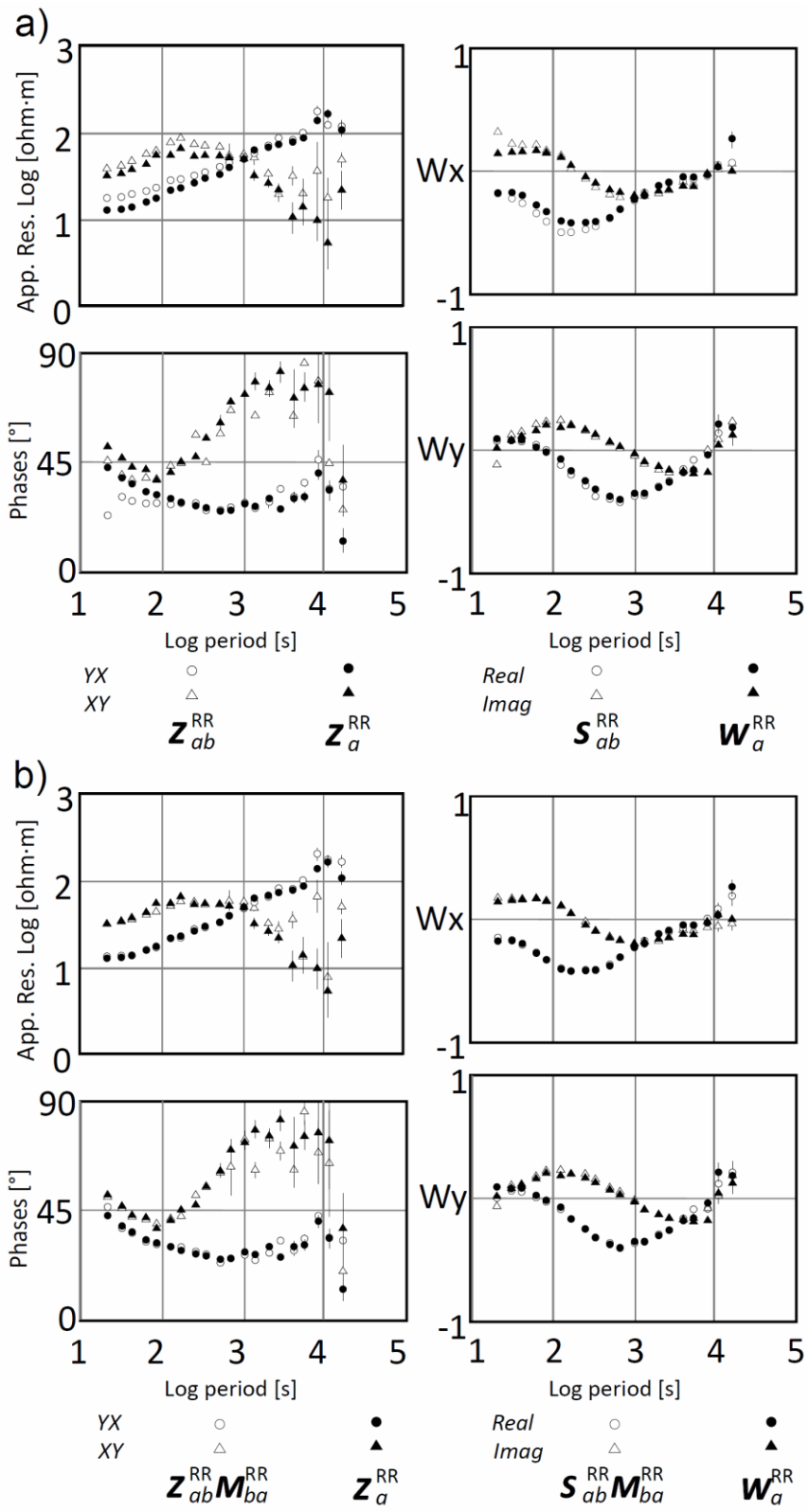

Figure 4.3 Apparent resistivity, phase and geomagnetic transfer function of the site *a* using the horizontal magnetic fields recorded on the site *b* and doing remote reference with CLF. (a) Using magnetic fields of the site *b* instead of the magnetic fields of the site *a*. (b) Following the proposed method. Results are compared with the local processing doing remote reference with CLF.

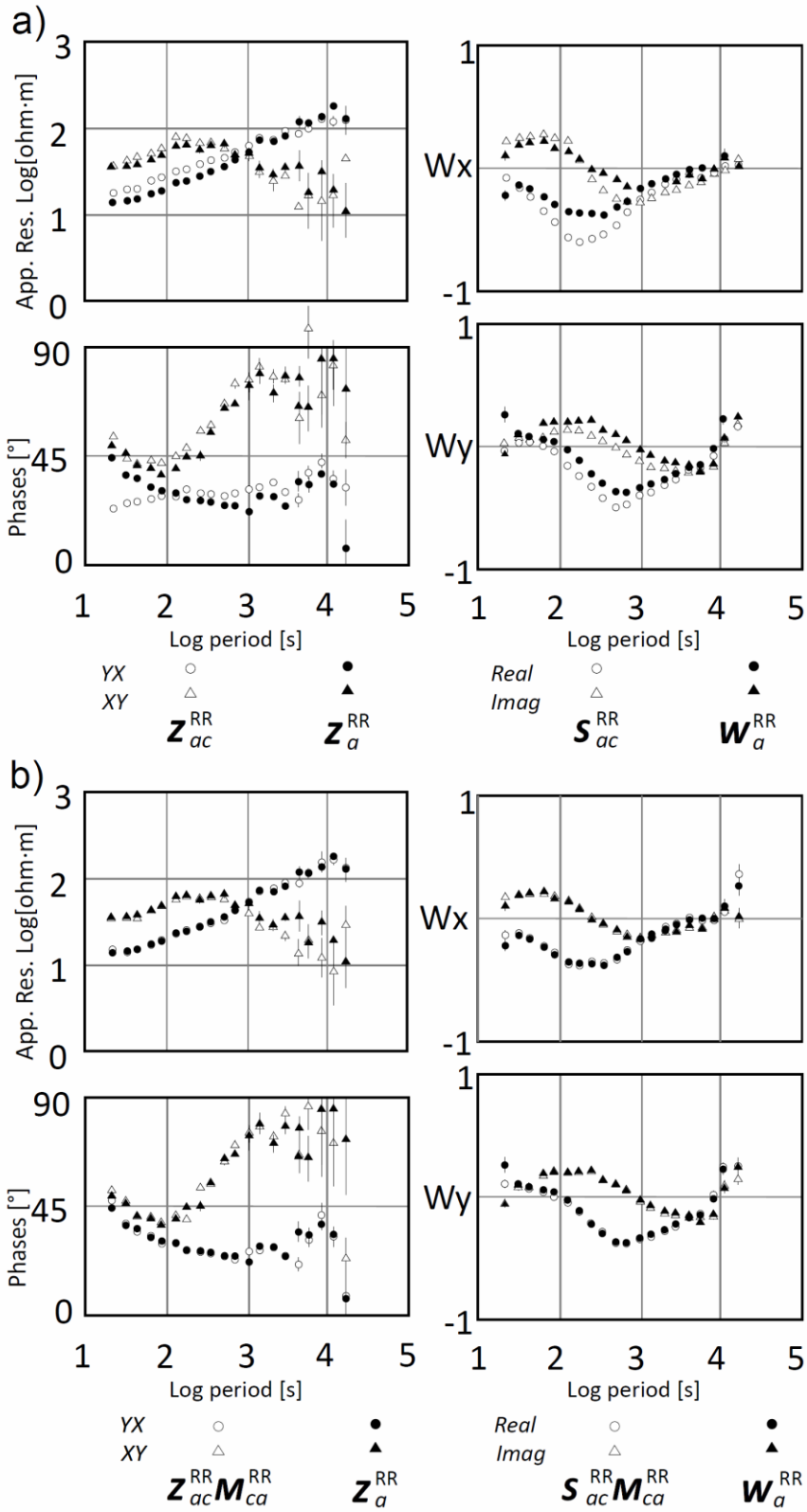

Figure 4.4 Apparent resistivity, phase and geomagnetic transfer function of the site *a* using the horizontal magnetic fields recorded on the site *c* and doing remote reference with FUR. (a) Using magnetic fields of the site *c* instead of the magnetic fields of the site *a*. (b) Following the proposed method. Results are compared with the local processing doing remote reference with FUR.

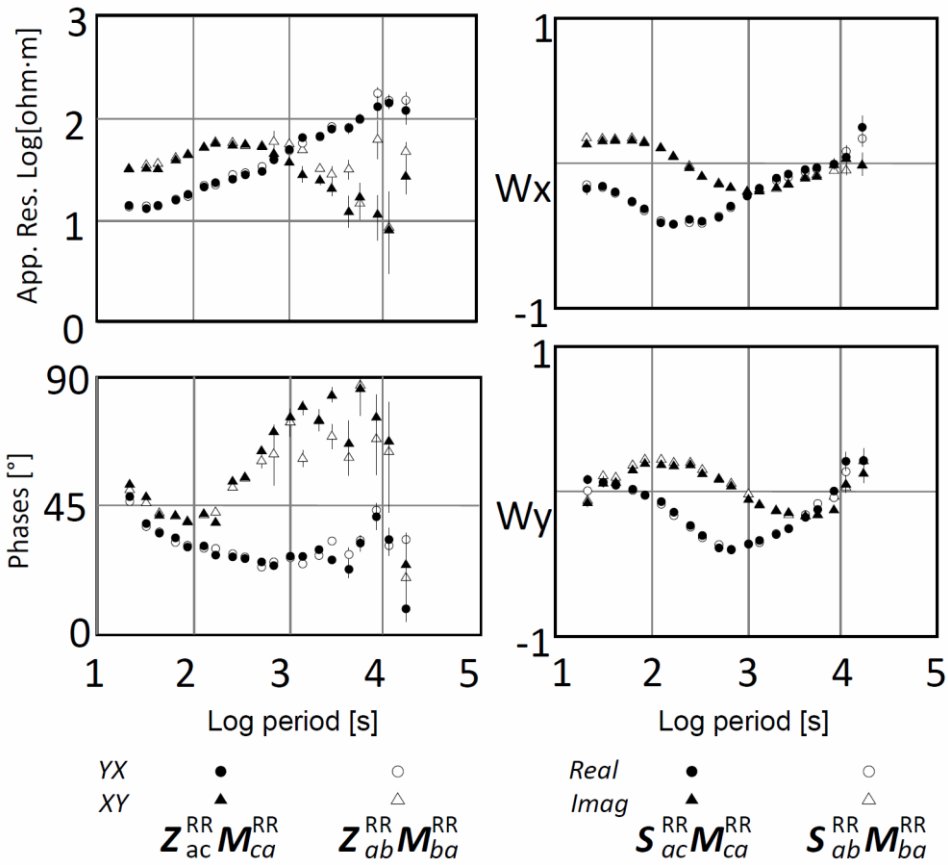

Figure 4.5 Apparent resistivity, phase and geomagnetic transfer function of the site *a* following the proposed method using the horizontal magnetic fields of the site *b* doing remote reference with CLF and using the horizontal magnetic fields of the site *c* doing remote reference with FUR.

Another experiment has been carried out to quantify the permissible differences between the parameter Ψ and the identity matrix. The experiment consisted in calculating the Ψ parameter with and without doing remote reference with a magnetic observatory. We used sites *a* and *b* doing remote reference with CLF and the sites *a* and *c* doing remote reference with FUR.

$$\Psi^{\mathrm{RR}} = \mathbf{M}_{\mathrm{ga}}^{\mathrm{RR}}\mathbf{M}_{\mathrm{ag}}^{\mathrm{RR}} \qquad (4.17)$$

$$\Psi = \mathbf{M}_{\mathrm{ga}}\mathbf{M}_{\mathrm{ag}} \qquad (4.18)$$

where *g* is *b* or *c* in each case. As shown in Figure 4.6, in case of remote referencing, the Ψ parameter better fits with the identity matrix in both cases, with differences below ±0.06. In the case of not using remote referencing, differences are up to 0.25 at shorter periods.

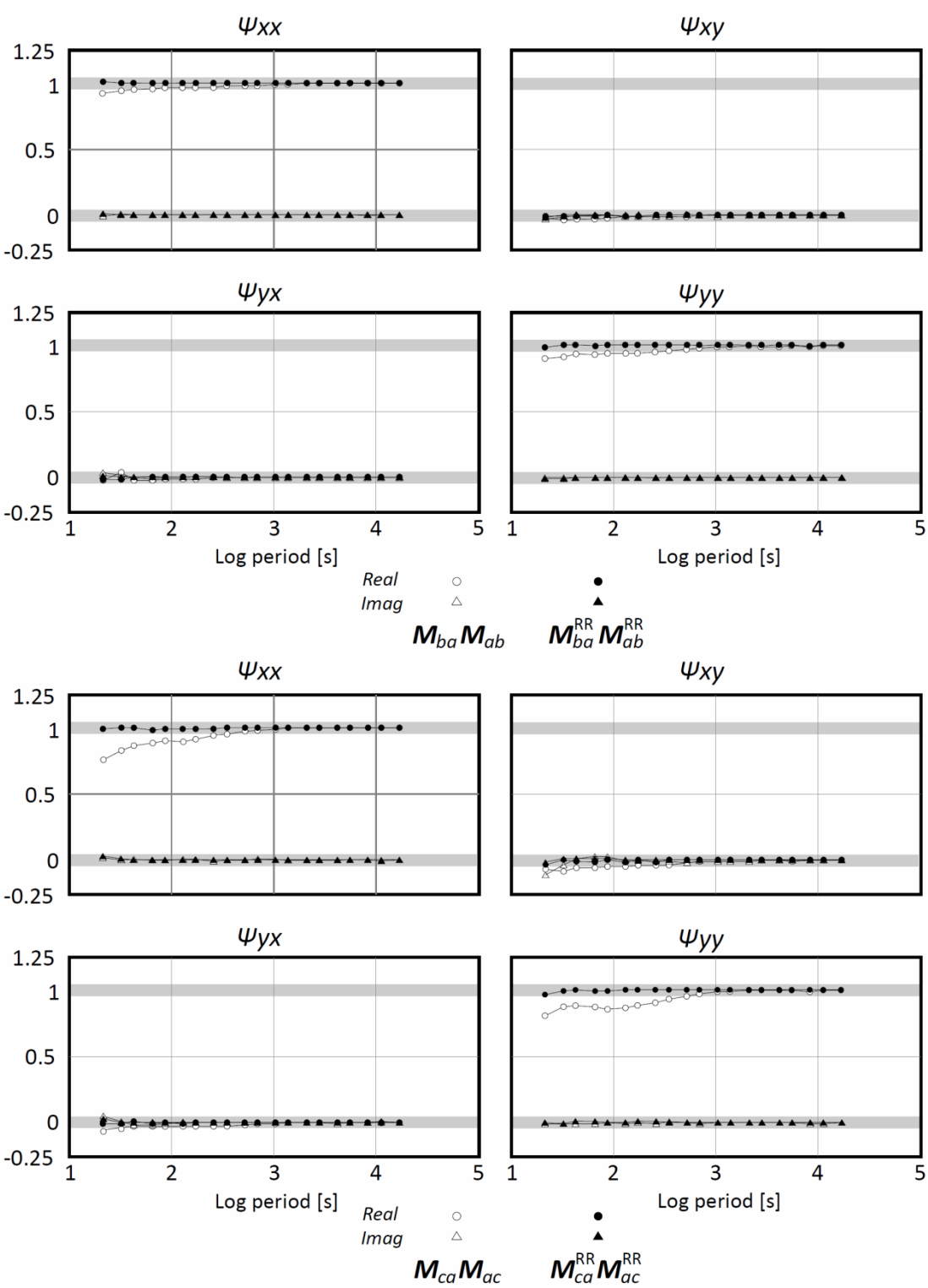

Figure 4.6 The Ψ parameter when calculate the HMT between *a* and *b* and between *a* and *c* with and without remote reference. Grey line includes the values with a difference lower than ±0.06 with the identity.

4.4 PROPERTIES AND ADVANTAGES OF THE METHOD

From the results obtained we observe that the proposed method provides practically the same results, regardless of the horizontal magnetic fields used to process the MT data of the local site (Figure 4.5). The results also corroborate the necessity to use the HMT when processing the MT data using the horizontal magnetic fields of a neighbouring site (Figures 4.3 and 4.4). The Ψ parameter, which should be the identity matrix, allows determining the periods for which the HMT properly relates the horizontal magnetic fields between two sites, suggesting the periods for which the proposed method can be used.

Below we focus on the properties of the proposed method and the associated advantages. The main property of the proposed method is that the MT impedance tensor and the geomagnetic transfer function at the local site are obtained from a combination of inter-station tensor relationships that can be constrained separately using time series recorded at different times and with different lengths. Another property is that the electric and magnetic fields recorded at the local site are not directly related, obtaining the MT impedance tensor and geomagnetic transfer function from a signal that is coherent between local, neighbour and remote sites. Taking advantage of these properties, we developed an example where the proposed method allows improving the results in the processing of the LMT data at site *a* using the horizontal magnetic fields at sites *c* and FUR. For this example, we first determine the number of days necessary to constrain the HMT between the sites *c* and *a*. As shown in Figure 4.7, two days of data is sufficient to obtain the $\boldsymbol{M}_{ca}^{RR}$.

The example consists of the hypothetical case where, having sites *c* and FUR constantly recording, after twenty days acquiring LMT data at site *a* the magnetic fields were truncated having a time series of only two days of data. With the aim of obtaining the apparent resistivity and phases at site *a*, we process the LMT data doing local processing with remote referencing. In that case, due to the electric and magnetic fields having to be recorded simultaneously, we are only able to use the LMT data recorded during the first two days (Figure 4.8a).However, using the method we are

able to calculate the inter-station tensor relationship between the electric fields recorded on *a* and magnetic fields recorded on *c*, $\boldsymbol{Z}_{ac}^{RR}$, using twenty days of data and then calculate the inter-station tensor relationship between the horizontal magnetic fields of *c* and *a*, $\boldsymbol{M}_{ca}^{RR}$, using two days of data (Figure 4.8b). The apparent resistivity curves and the phases at site *a* are improved when the method is applied, as we are able to use the twenty days of the electric field data.

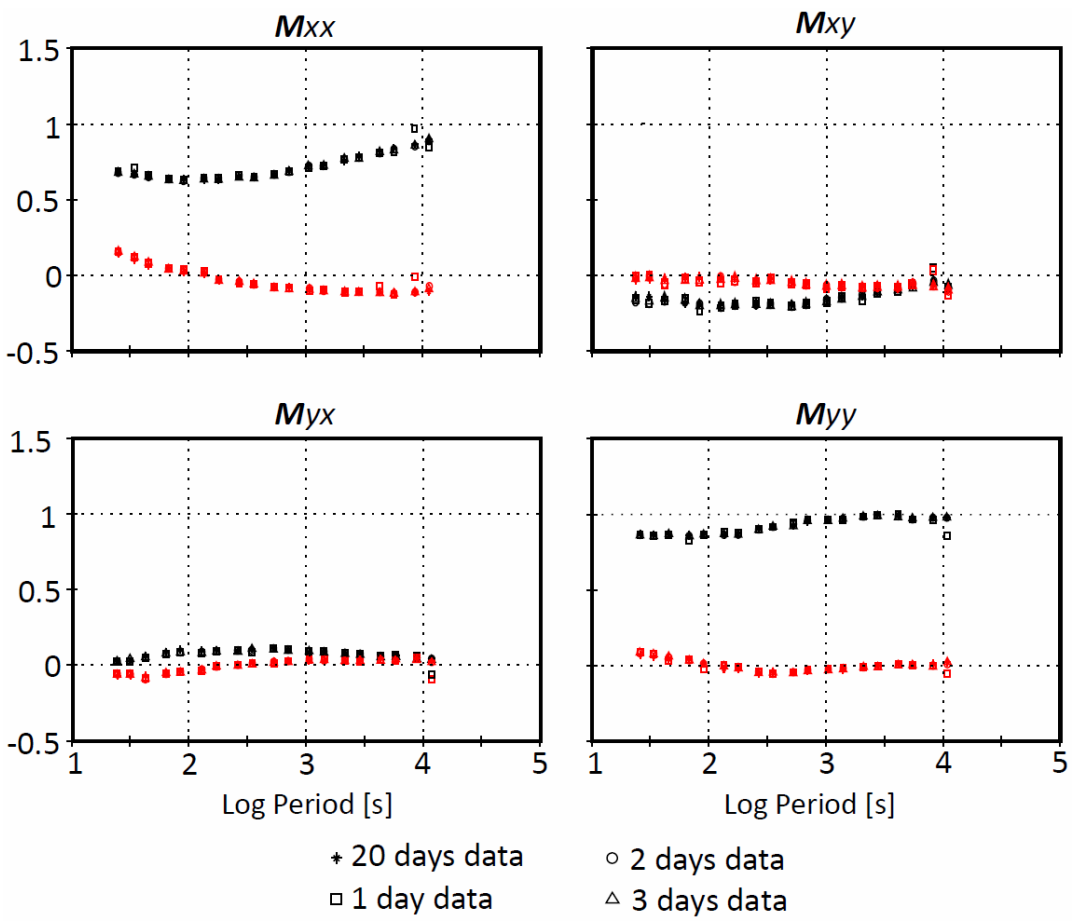

Figure 4.7 The HMT between sites *c* and *a* using time series with different length, between 1 day, the shortest, and 20 days, the longest. Remote reference has been done with FUR. Black are the real values and red are the imaginary values.

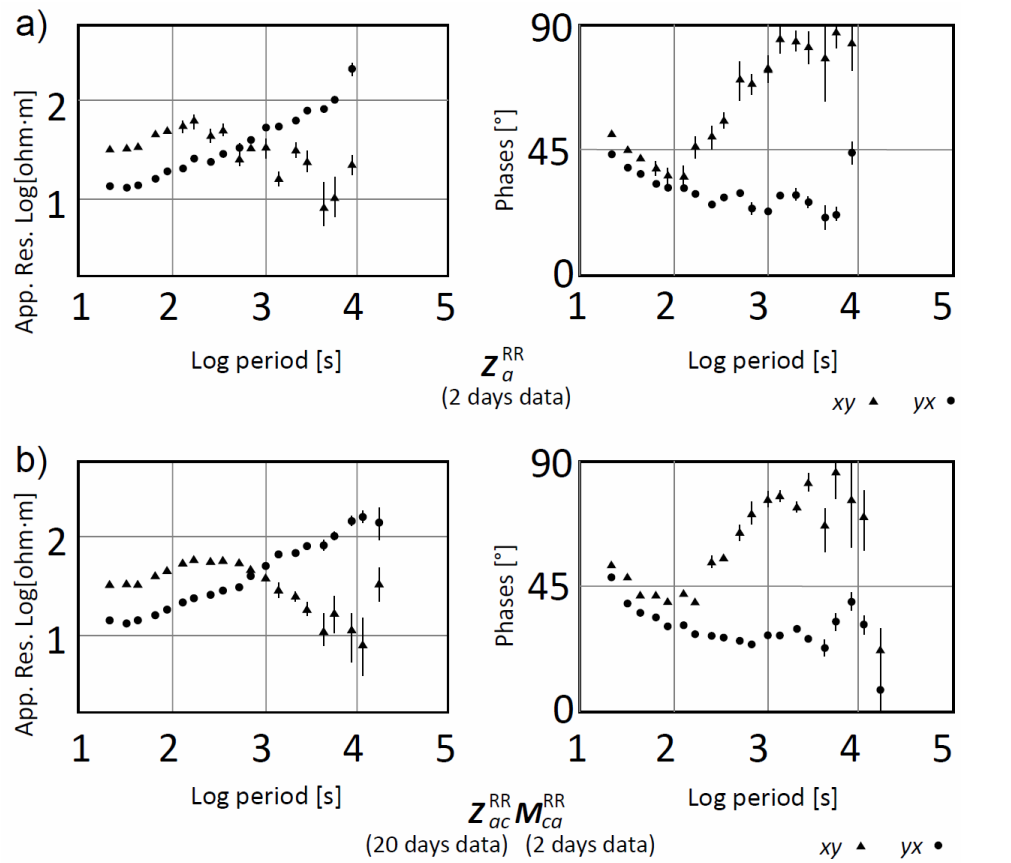

Figure 4.8 Apparent resistivity and phase of the site *a* when the magnetic fields are truncated after two days recording. (a) Doing local processing with remote reference with FUR. (b) Following the proposed method using the horizontal magnetic fields of the site *c* and doing remote reference with FUR.

4.5 CONCLUSIONS

As demonstrated, the MT impedance tensor and the geomagnetic transfer function of a local site *a* [$\boldsymbol{Z}_a(\boldsymbol{e}_a, \boldsymbol{h}_a)$ and $\boldsymbol{W}_a(h_z^a, \boldsymbol{h}_a)$] can be calculated combining inter-station tensor relationships with another site *b* [$\boldsymbol{Z}_{ab}(\boldsymbol{e}_a, \boldsymbol{h}_b)$, $\boldsymbol{S}_{ab}(h_z^a, \boldsymbol{h}_b)$ and $\boldsymbol{M}_{ba}(\boldsymbol{h}_b, \boldsymbol{h}_a)$] following the proposed method [$\boldsymbol{Z}_a = \boldsymbol{Z}_{ab}\boldsymbol{M}_{ba}$ and $\boldsymbol{W}_a = \boldsymbol{S}_{ab}\boldsymbol{M}_{ba}$]. Remote referencing to calculate all tensor relationships is recommended to avoid the effects of local noise of the different MT sites. The experiments carried out corroborate the applicability of the method and the defined Ψ parameter constrains the periods where the proposed method can be used. As only inter-station tensor relationships are used the electric and magnetic fields of the local site do not need to be recorded simultaneously and during the same time. The applicability of the proposed method opens new ways to acquire MT data getting more out of the measuring instruments.

4.6 SUPPLEMENTARY MATERIAL

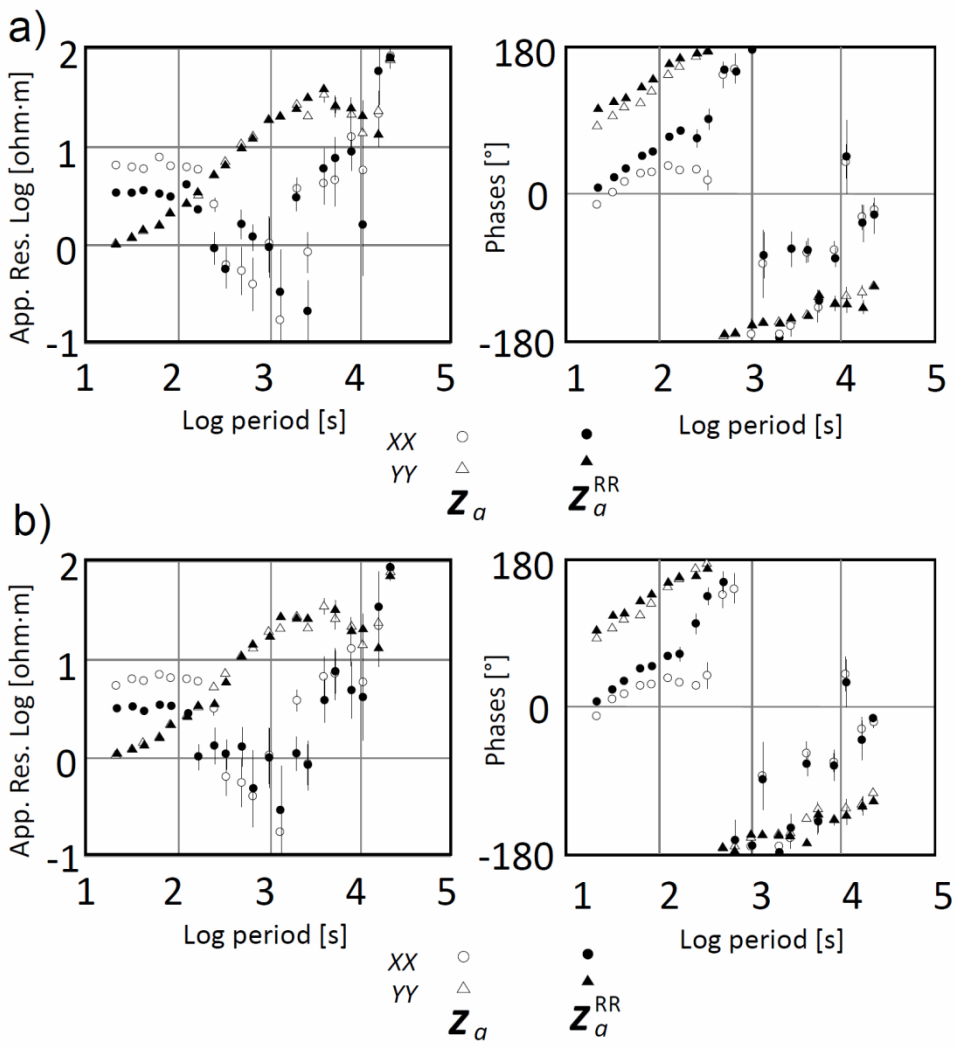

Figure 4.S1 For the *xx* and *yy* components, apparent resistivity and phase values of the site *a* processing the data of the local site doing local processing and local processing with remote reference with CLF (a) and with FUR (b). In (a) data have been acquired between the 26th October and 09th November of 2010. In (b) data have been acquired between 19th October and 09th November of 2010.

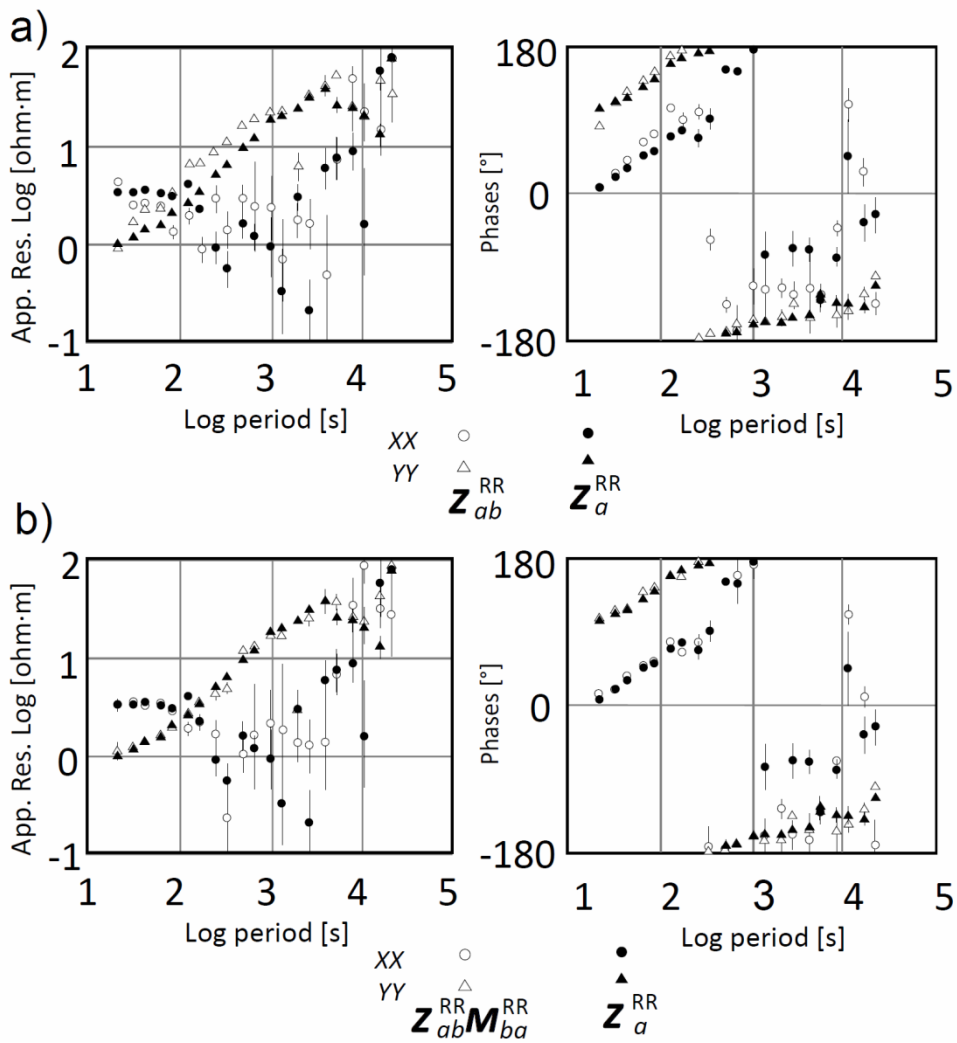

Figure 4.S2 For the *xx* and *yy* components, apparent resistivity and phase values of the site *a* using the horizontal magnetic fields recorded on the site *b* and doing remote reference with CLF. (a) Using magnetic fields of the site *b* instead of the magnetic fields of the site *a*. (b) Following the proposed method. Results are compared with the local processing doing remote reference with CLF.

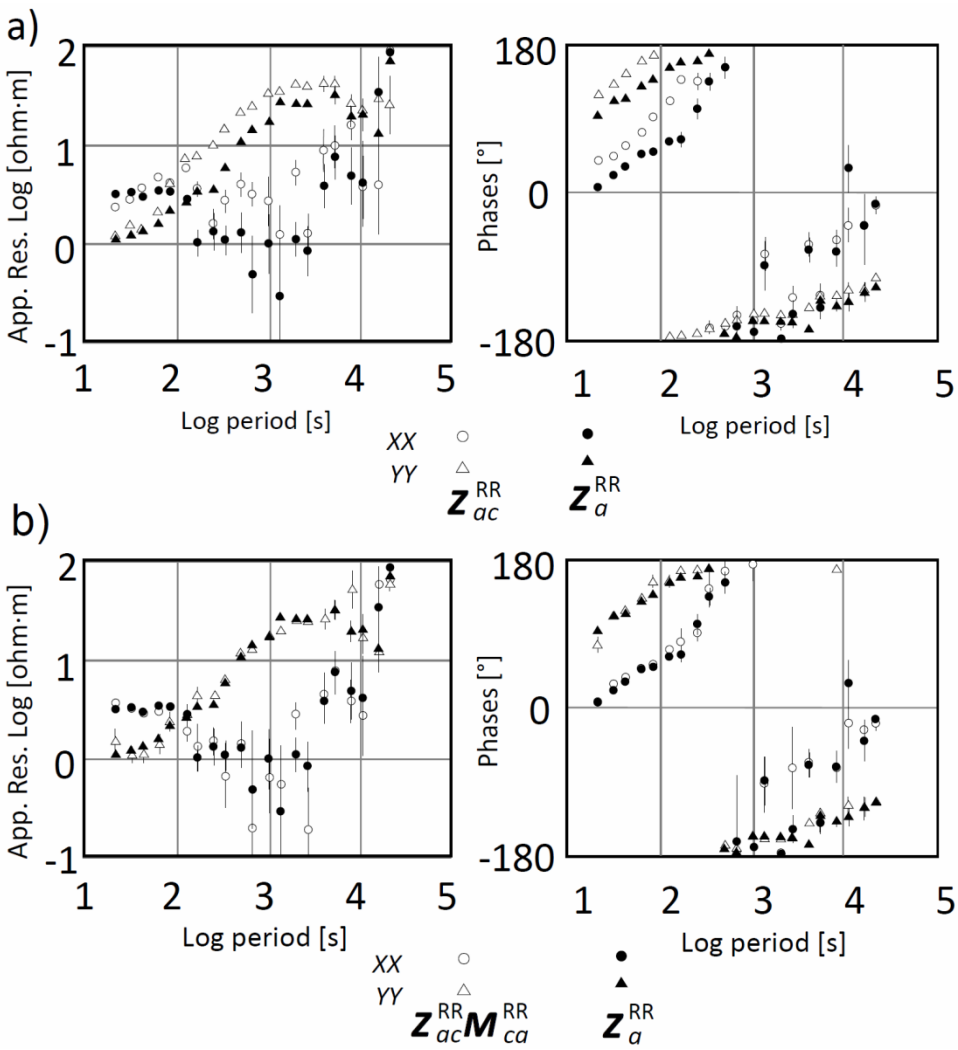

Figure 4.S3 For the *xx* and *yy* components, apparent resistivity and phase values of the site *a* using the horizontal magnetic fields recorded on the site *c* and doing remote reference with FUR. (a) Using magnetic fields of the site *c* instead of the magnetic fields of the site *a*. (b) Following the proposed method. Results are compared with the local processing doing remote reference with FUR.

5. DISCUSSION

In the discussion below, the results obtained in the West-Central Pyrenees and in the Central Pyrenees are compared with independent geophysical models of the Pyrenees and complemented with a new geoelectrical model of the Western Pyrenees, which characterize the geoelectrical structures of the region at a crustal-scale. Then the discussion is focused on the third paper exposing the validity and advantages of the proposed method for processing MT data.

5.1 GEOELECTRICAL CHARACTERIZATION OF THE PYRENEES

5.1.1 Main geoelectrical structures and evolution along the strike

The main geoelectrical structures along the Pyrenean range at lithospheric-scale are characterized comparing the results between the Central and the West-Central Pyrenees MT profiles. At crustal scale, the new geoelectrical model of the Western Pyrenees determines the geoelectrical evolution towards the West.

Figure 5.1 points out the main geoelectrical structures of the Pyrenean lithosphere from the two published papers (Campanyà et al., 2011 and Campanyà et al., 2012).The two main geoelectrical features are related with the IBSLC, structure M in figure 5.1, and with the asthenosphere, structure A in figure 5.1. Apart from these, there are also the Variscan boundary constrained below the Ebro basin in the West-Central Pyrenees, structure V in figure 5.1, and the low electrical resistivity structure associated with fluids and Silurian sediments, structure S in figure 5.1. All these structures are associated with low electrical resistivity values.

Focusing on the IBSLC, the associated geoelectrical structure is dipping north in both cases and its top is at around 30 km depth, although a bit shallower in the West-Central Pyrenees. The electrical resistivity values associated with the IBSLC below the Central Pyrenees and the West-Central Pyrenees, to a depth of 50 km, are between 2 Ω·m and 6 Ω·m. The geochemical analysis developed in chapter 2 using the geotherms proposed by Glover et al. (2000) and Vacher and Souriau (2001) and the influence of the water on the melt temperature for a typical crustal rock (Thompson, 1992) suggests that conditions of the IBSLC are suitable for partial melting (Figure 5.2). Partial melting by dehydration melting of muscovite and biotite has been assumed as the hypothesis that better explain the geophysical results associated with the IBSLC.

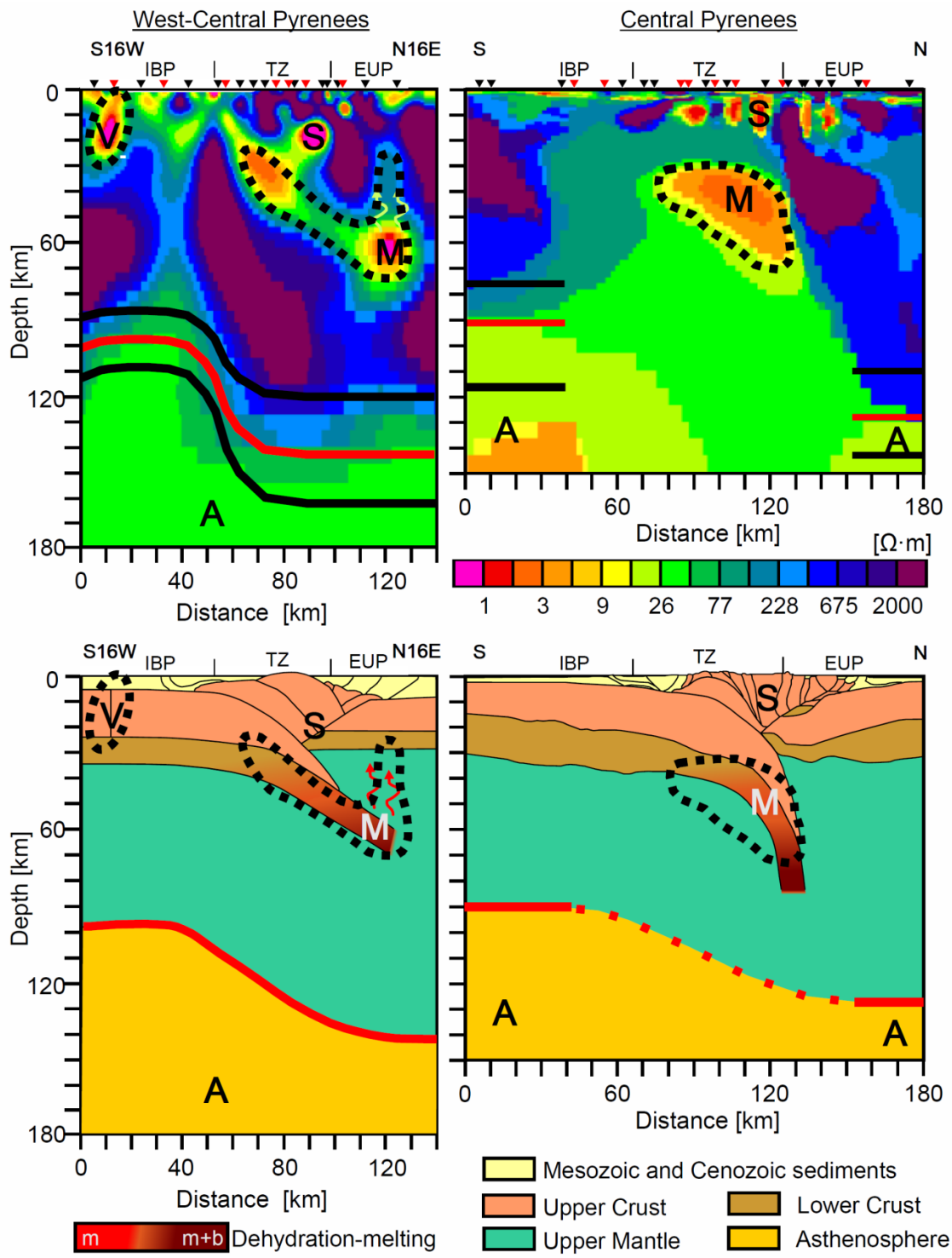

Figure 5.1 (TOP) West-Central Pyrenees MT model (left) and Central Pyrenees MT model (right). Black dashed contours the main geoelectrical structures. Red line: LAB suggested by MT results. Black lines: resolution constraining the LAB. (BOTTOM) Cartoon geological sections of the West-Central and the Central Pyrenees with our interpretation of the partial-melting region and the LAB. In the dehydration melting: *m* when muscovite produces dehydration melting and *m+b* when muscovite and biotite produce dehydration melting. Red dashed interpolated LAB below Central Pyrenees, due no resolution in this region. Major geoelectrical structures: M, Partial melting of the IBSLC; A, asthenosphere; S, fluids and Silurian sediments; V, Variscan boundary.(Modified from Campanyà et al. 2012).

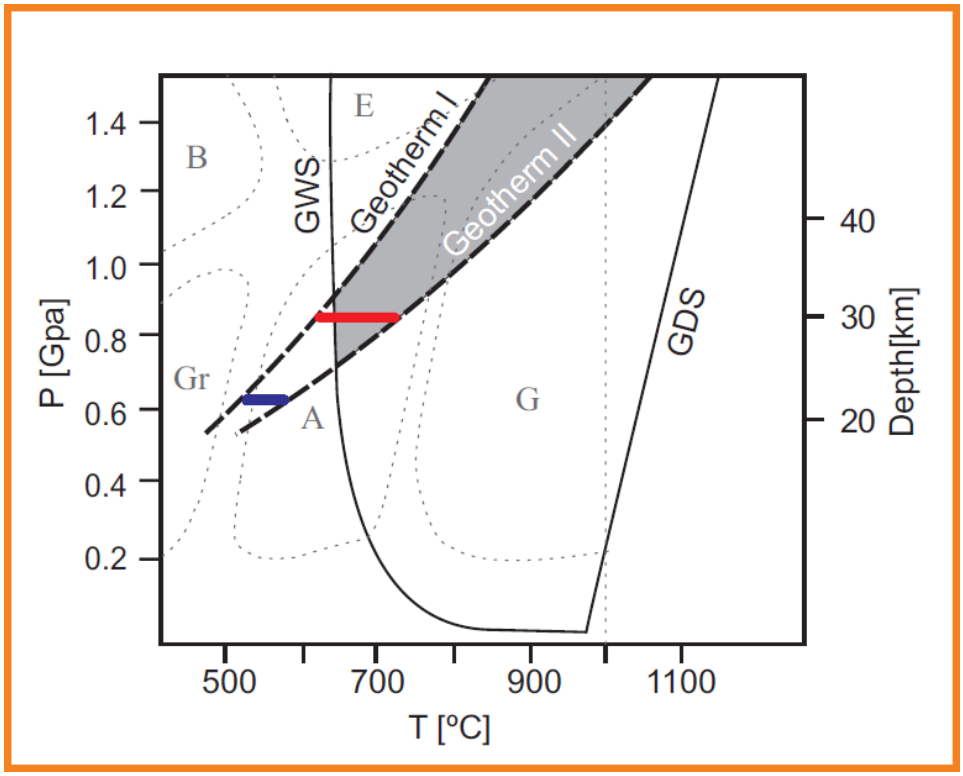

Figure 5.2 Influence of the water on the melt temperature of the granite (common crustal rock). Geotherm I from Vacheur and Souriau (2001). Geotherm II from Glover et al. (2000). Grey zone is region where we have the appropriate conditions to obtain partial melting if presence of water. Red line and blue line indicate the depth of the top of the geoelectrical structure suggested by in this thesis and the suggested by Ledo (1996) and Pous et al. (1995a). Smooth dashed lines are the metamorphic facies of a mafic crustal rock (Modified of Buscher and Frey, 1994). GWS, Granite wet solidus; GDS, Granite dry solidus; A, Amphibolite; B, Blueschist; E, Eclogite; G, Granulite and Gr, Greenschist. Modified from Thompson (1992).

Following the Modified Brick Layer Model (MBLM) proposed by Partzsch et al. (2000), a percentage of partial melting between 4 % and 15 % of melt explain the low electrical resistivity values associated with the IBSLC in the West-Central and the Central Pyrenees until 50 km depth.

At a depth greater than 50 km, there are major differences between the two profiles. In the Central Pyrenees the 80° dip of the IBSLC screens the geoelectical properties associated with the bottom of this formation. In the West-Central Pyrenees, due to the dip of 35°, the geoelectrical properties of the IBSLC can be constrained until 70 km depth, also observing dehydration melting of biotite at the bottom of the IBSLC. In this case the MBLM have determined an amount of partial melting between 15% and 25% of melt. Arzi (1978) suggest that these values of partial melting can produce melt

migration, which would explain the decrease of the electrical resistivity values of the European upper mantle above the IBSLC.

Another major geoelectrical structure has been constrained at the bottom of both MT models, with electrical resistivity values between 10 Ω·m and 70 Ω·m (Structure A in figure 5.1). This structure has been associated with the asthenosphere and their top with the LAB. The absence of main geoelectrical differences between the two profiles associated with structure A suggests an asthenosphere with similar properties below the two MT profiles. Focusing on the LAB, the geoelectrical models suggest an European plate thicker than the Iberian plate, close to the collision zone, locating the LAB at around 90 km depth below the Iberian plate and at around 130 km depth below the European plate. Beneath the collision zone, the LAB has been only constrained in the West-Central Pyrenees, with similar depth than the obtained below the European plate. In the Central Pyrenees, the LAB below the IBSLC cannot be accurately determined due to the screening effect of the low electrical resistivity structure associated with the IBSLC.

The low electrical resistivity structure completely buried below the Ebro basin at upper and middle crustal depths has been only observed in the West-Central Pyrenees MT profile (Structure V in figure 5.1). As there is no structures affecting the sedimentary infilling of the Ebro Basin above this structure, it has been associated with previous Variscan tectonic events. According to the subdivision of the Variscan belt (see Martinez Catalán et al., 2007 for further information) it could correspond to the prolongation of the limit between the Western Asturian Leonese and the Central Iberian zone below the Ebro Basin (Figure 5.3).

Due to the similarity of structure V with other Variscan boundaries characterized in the South-Western part of the Iberian plate (Da Silva et al., 2007; Muñoz et al., 2008; Pous et al., 2004, 2011), the electrical resistivity values of structure V have been associated with the presence of graphite along a major Variscan tectonic boundary.

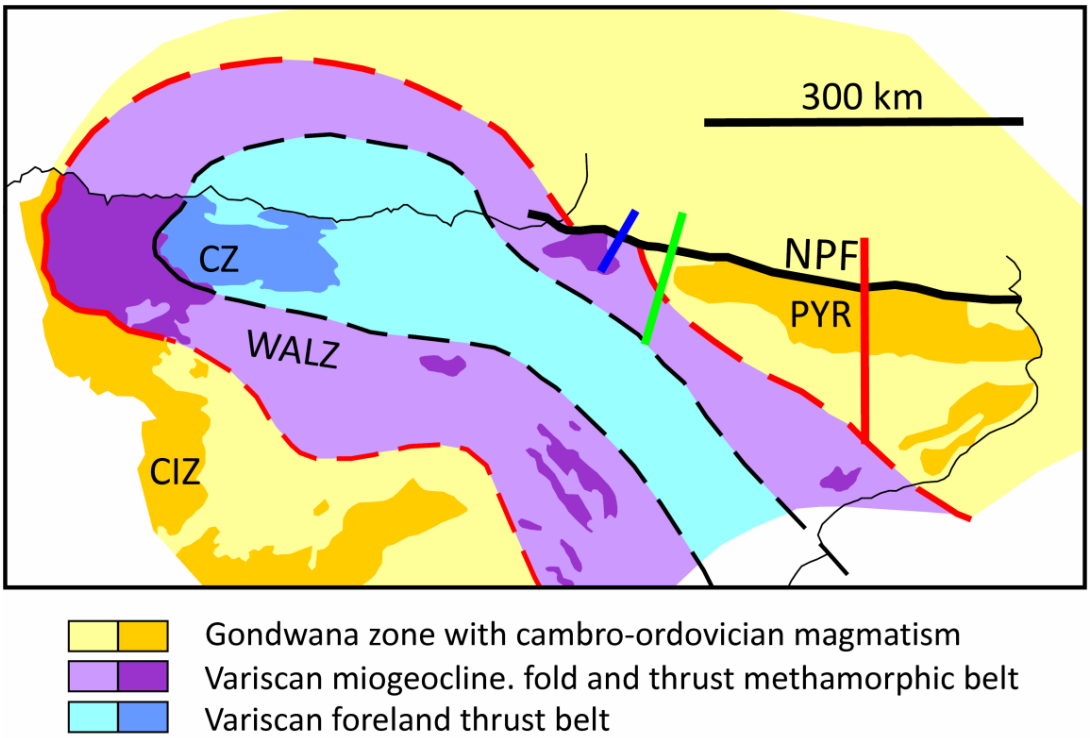

Figure 5.3 Subdivision of the Variscan belt. Red dashed line: Propagation of the boundary between CIZ and WALZ below sediments. Red line: Central Pyrenees MT profile. Green line: West-Central Pyrenees MT profile. Blue line: Western Pyrenees MT profile. Abbreviations: CIZ: Central Iberian zone; CZ: Cantabrian zone; NPF: North Pyrenean fault; PYR: Pyrenees; WALZ: Western-Asturian Leonese zone. Modified from Martinez Catalán et al., (2007).

To analyse the geoelectrical structures at crustal depths above the collision zone, the BBMT sites acquired in the Western Pyrenees have been modelled obtaining a geoelectrical model of the region (Figure 5.4a). Figure 5.4b compares the data used for the inversion and the model responses in pseudosection format for the apparent resistivity and phases for TE and TM modes. A similar procedure has been followed to obtain this geoelectrical model than the one in the West-Central Pyrenees MT profile. In this case, according to the results shown in figures 1.20 and 1.22, the MT profile have a N30E direction, perpendicular to the E30S strike direction of the geoelectrical structures. The static shift has been corrected using the depth of the contact between the Mesozoic and Palaeozoic basement obtained by Lanaja and Querol (1987). The MT impedance tensor of each site has been rotate 30° clockwise before the inversion, defining the TE and TM modes used for the two-dimensional inversion (Rodi and Mackie, 2001).

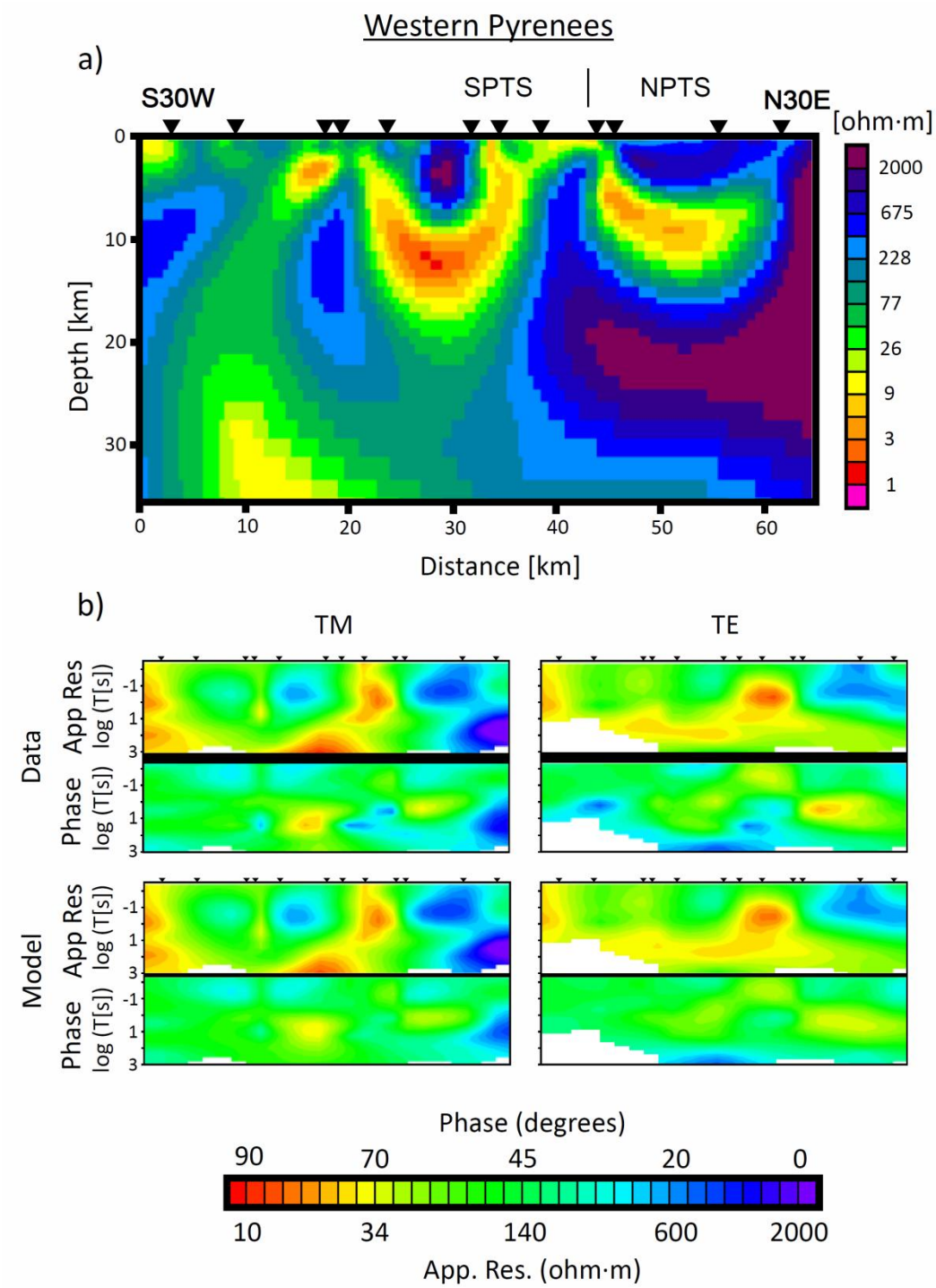

Figure 5.4 a) Geoelectrical model of the Western Pyrenees. Sites are represented by inverted triangles. b) Comparison between the model response and the data in pseudosection format for the apparent resistivity and phase for TM and TE modes. Misfit between model response and data has an RMS of 1.6. SPTS, South Pyrenean Thrust Sheets; NPTS, North Pyrenean Thrust Sheets.

Comparison of the geoelectrical structures between the three MT profiles at crustal depths shows the propagation of the M geoelectrical structure to the West, associated with partial melting of the IBSLC (figure 5.5).

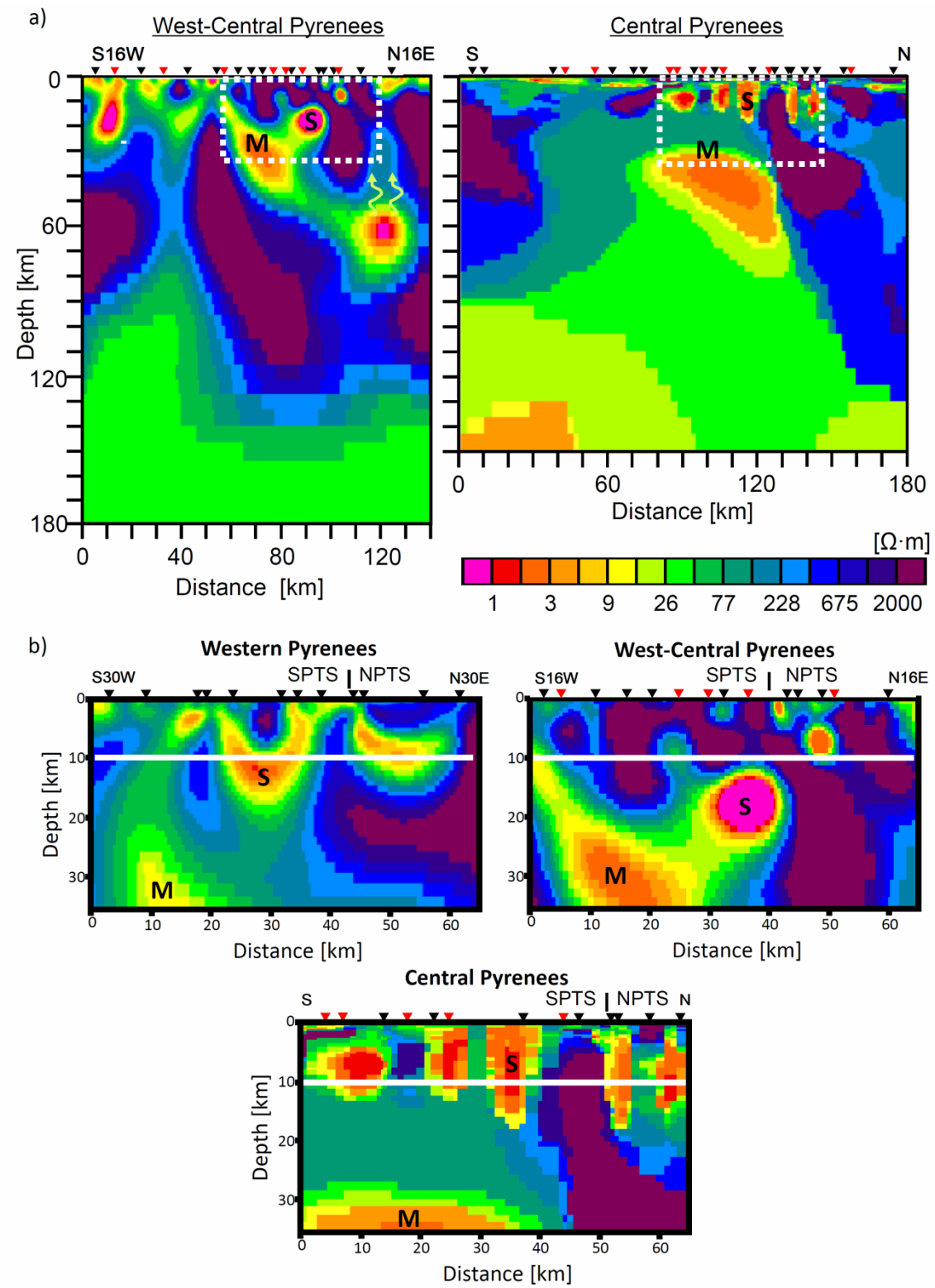

Figure 5.5 a) Geoelectrical model of the West-Central Pyrenees (Campanyà et al., 2012) and the Central Pyrenees (Campanyà et al., 2011). White dashed line limits the equivalent region between the Western Pyrenees and the Central and West-Central Pyrenees MT profiles, at crustal depths. b) Geoelectrical models of the equivalent region below the three MT profiles at crustal depths. S is the geoelectrical structure associated with fluids and Silurian sediments. M the geoelectrical structure associated with partial melting of the IBSLC. SPTS, South Pyrenean Thrust Sheets; NPTS, North Pyrenean Thrust Sheets. White line indicates ten kilometres depth. Inverted triangles are MT sites (Black: BBMT data; Red: BBMT+LMT data).

Focusing on bit shallower geoelectrical structures, in the three MT geoelectrical models there is a low electrical resistivity structure associated with fluids and Silurian sediments (S in figures 5.5). In the Central Pyrenees is located between sub-vertical faults of the Axial zone, at around 10 km depth, while in the West-Central Pyrenees is located between 10 km and 20 km depth and is associated with the Gavarnie thrust, which is branching with the North Pyrenean sole thrust. In the Western Pyrenees MT profile the S structure is also located below 10 km depth, but shallower than in the West-Central Pyrenees. The dip of the structures to the West, preserving higher structural levels in the West-Central Pyrenees than in the Central Pyrenees, and the related westward termination of the Axial zone antiformal stack of the Central Pyrenees would explain the different depth of the S structure between the Central Pyrenees MT profile and the West-Central and Western Pyrenees MT profiles.

5.1.2 Comparison with independent geophysical studies

As shown in chapters 2 and 3, comparison of the geoelectrical models with other geophysical results, focused on different physical properties, helps determine the physical and chemical processes of the subsurface, as well as the geological structures.

5.1.2.1 Comparison with deep seismic profiles

The deep seismic profiles carried out in the Central Pyrenees and in the West-Central Pyrenees interpreted by Muñoz (1992) and Muñoz (2002), respectively, characterize the geological structures at crustal depths. Comparison of these results with the obtained from the MT profiles helps associate the geoelectrical anomalies with geological structures of the subsurface (Figure 5.6). This association is particularly clear if focus on the IBSLC suggested from the deep seismic profiles, which is coincident with the low electrical resistivity structure characterized below the collision zone at lower-crustal and upper-mantle depths.

Moreover, the results obtained from MT data can also constrain the geological structures in regions where the deep seismic profile has poor resolution, as happened in the West-Central Pyrenees. The MT results have proposed extend the IBSLC until 70 km depth and increase the dip of the Gavarnie thrust (white dashed lines in Figure 5.6).

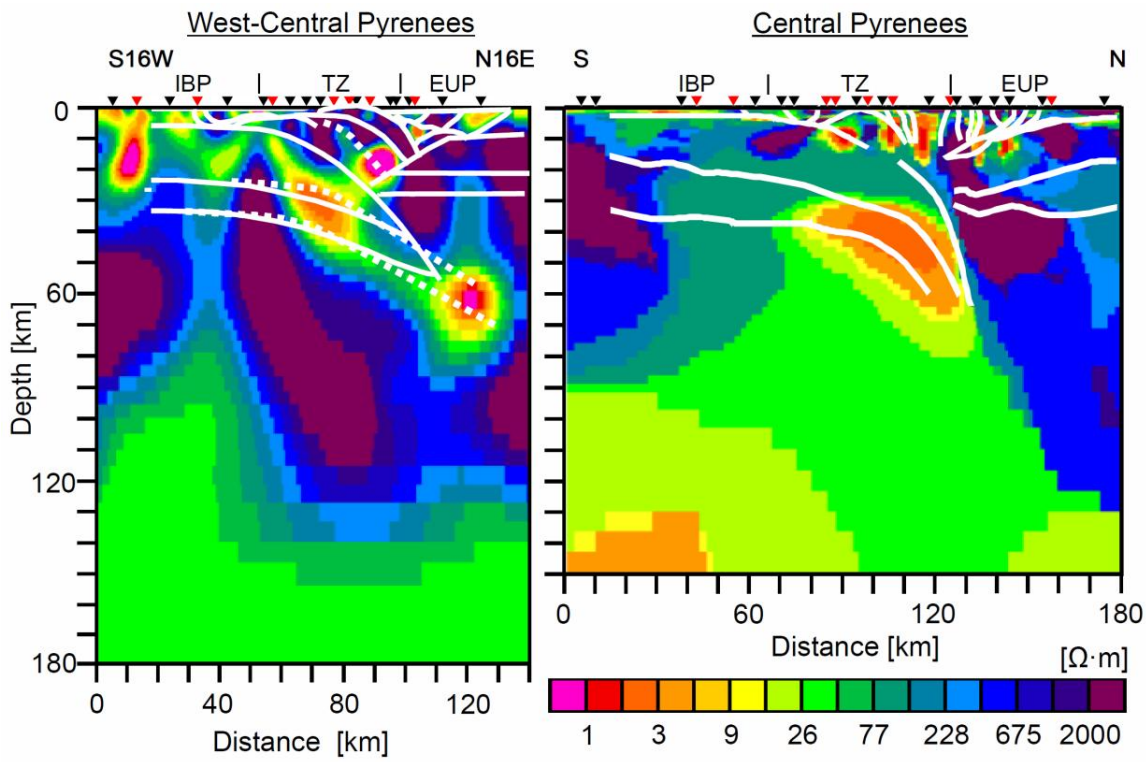

Figure 5.6. Geoelectrical models obtained by Campanyà et al. (2011) and Campanyà et al. (2012) in the Central and West-Central Pyrenees, respectively. White lines, geological models proposed by Muñoz (1992) in the Central Pyrenees and by Muñoz (2002) in the West-Central Pyrenees. White dashed lines: Modifications of the geological model in the West-Central Pyrenees from the MT results. EUP: European plate; IBP: Iberian plate; TZ: Transition zone.

5.1.2.2 Comparison with seismic tomography models

Various seismic tomography models constrain the upper-mantle velocity anomalies below the Pyrenees. Figure 5.7 superimpose the geoelectrical structure associated with the IBSLC and with the electrical LAB on the seismic tomography models suggested by Amaru et al. (2008), Koulakov et al. (2009) and Souriau et al. (2008) in the Central Pyrenees and the West-Central Pyrenees. Seismic tomography models

proposed by Koulakov et al. (2009) and Amaru et al. (2008) are similar between them, but this is not the case of the results proposed by Souriau et al. (2008), especially in the West-Central Pyreenes. In the following analysis we will focus on the results proposed by Koulakov et al. (2009) and Amaru et al. (2008), which are also more consistent with the geoelectrical models.

From figure 5.7, the low electrical resistivity structure associated with the IBSLC coincide with a decrease of the P-waves and the S-waves velocity and, except in the S-wave model of the Central Pyrenees proposed by Koulakov et al. (2009), the IBSLC is also associated with negative velocity anomalies. The low electrical resistivity values and the decrease of the seismic velocity waves are consistent with the hypothesis of partial melting of the IBSLC. In addition, the bottom of the low electrical resistivity structure associated with the IBSLC in the West-Central Pyrenees agrees with the bottom of the S-waves anomaly (Figure 5.7a) corroborating an IBSLC until the depth of 70 km. In the models proposed by Souriau et al. (2008) below the Central Pyrenees (Figure 5.7h), the IBSLC is also associated with a decrease of the velocity anomaly, but not with negative values.

At greater depths, the S-waves seismic tomography models suggested by Koulakov et al. (2009), shows a negative V_s anomaly at the bottom of the models that can be associated with the asthenosphere and their top with the seismic LAB. Comparing the electrical LAB with the seismic LAB (Figure 5.7 a,b), results are similar below the Iberian and the European plates in the Central Pyrenees and below the European plate and the collision zone in the West-Central Pyrenees. Below the Iberian plate in the West-Central Pyrenees the variations of V_s anomalies are smooth and the V_s seismic LAB is not well constrained.

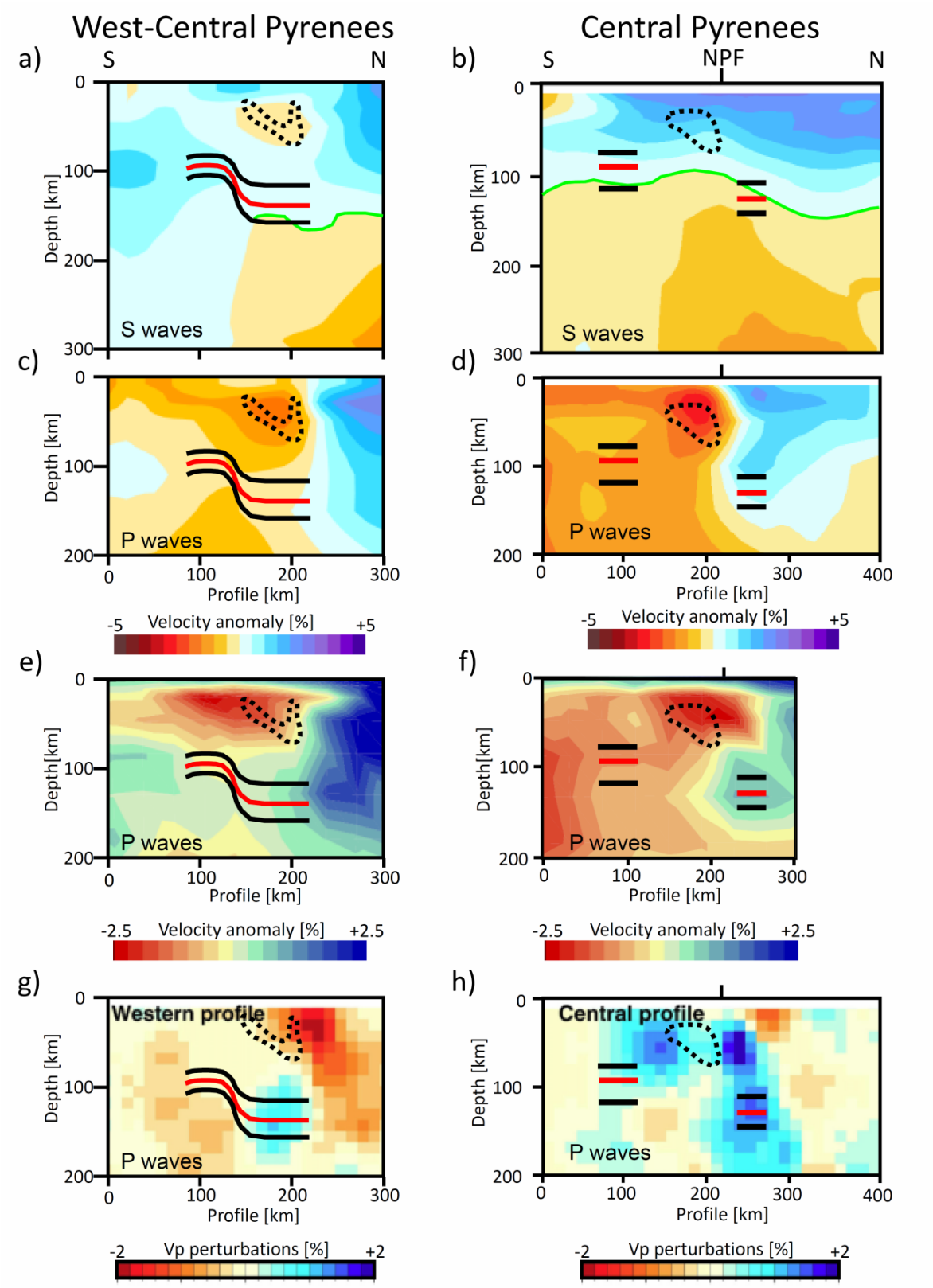

Figure 5.7 Seismic tomography models suggested by Koulakov et al. (2009) (*a,b,c* and *d*). Seismic tomography models suggested by Amaru et al. (2008) (*e* and *f*) and by Souriau et al. (2008) (*g* and *h*). Superimposed on the six models: Contour of partial melting region (black dashed line) and electrical LAB (red and black lines). Green line: seismic LAB. NPF: North Pyrenean Fault.

5.1.2.3 Comparison with studies based on thermal and gravity data

The low electrical resistivity values associated with the IBSLC have been explained following the geotherms proposed by Zeyen and Fernández (1994) and Glover et al. (2001) in the analysis of a representative rock of the IBSLC. Partial melt by dehydration melting of muscovite and biotite has been suggested as the most probable phenomena to explain the electrical resistivity values of the IBSLC below the Central Pyrenees. Results proposed by Tesauro et al. (2009), showing no thermal anomalies between the Central and West-Central Pyrenees (Figure 1.8 a), allows the use of the thermal analysis developed in the Central Pyrenees also in the West-Central Pyrenees.

At greater depths, the thermal results proposed by Tesauro et al. (2009), which associate the thermal LAB with the geotherm of 1200 ^{o}C, constrain the LAB between the Central and the West-Central Pyrenees at around 120 km depth (Figure 1.8 b), being consistent with the seismic and the electrical LABs (Figure 5.7 a,b).

The models based on gravity data of the Central and the West-Central Pyrenees propose different density distribution of the subsurface (Figures 1.6 and 1.7). However, despite the differences between them all the results agree with the presence of the IBSLC. The high density body observed at upper and middle crustal depths below the NPTS in the West-Central Pyrenees is not associated with a electrical anomaly in the MT models. In this case, the geoelectrical results cannot help to differentiate between the two main hypothesis associate with this gravimetric anomaly: the presence of lower-crustal or upper-mantle rocks at upper and middle crustal depths (Casas et al., 1997; Jammes et al., 2010; Pedreira et al., 2007; Vacheur and Souriau, 2001).

5.2 IMPROVING MT DATA PROCESSING

A new method has been proposed for processing the MT data of a local site using inter-station tensor relationships between the electric and magnetic fields of the local site and the horizontal magnetic fields recorded at a neighbouring site. The proposed method determines the MT impedance tensor and the geomagnetic transfer function

of a local site a [$\boldsymbol{Z}_a(\boldsymbol{e}_a, \boldsymbol{h}_a)$ and $\boldsymbol{W}_a(h_z^a, \boldsymbol{h}_a)$] combining inter-station tensor relationships with another site b [$\boldsymbol{Z}_{ab}(\boldsymbol{e}_a, \boldsymbol{h}_b)$, $\boldsymbol{S}_{ab}(h_z^a, \boldsymbol{h}_b)$ and $\boldsymbol{M}_{ba}(\boldsymbol{h}_b, \boldsymbol{h}_a)$] following the proposed method [$\boldsymbol{Z}_a = \boldsymbol{Z}_{ab}\boldsymbol{M}_{ba}$ and $\boldsymbol{W}_a = \boldsymbol{S}_{ab}\boldsymbol{M}_{ba}$].

After the theoretical development, various tests have been done evaluating its applicability. Results confirm the reliability of the method to determine the impedance tensor and the geomagnetic transfer function of the local site, independently of the neighbouring site used for processing the MT data. Moreover, the horizontal magnetic fields of the neighbouring site cannot be used instead of the horizontal magnetic fields of the local site to determine the tensor relationships of the local site. The defined Ψ parameter constrain the periods where the proposed method can be used.

The proposed method has the advantage that the electric and magnetic fields of the local site do not have to be simultaneously recorded. As shown in chapter 4, this property allows improving the processing of MT data when the time series of the magnetic fields have been truncated. Moreover, the proposed method can also modify the MT surveys reducing the number of magnetic sensors. From the LMT data processed in the Pyrenees, we can assume that twenty days recording the electric fields of the local site and four days recording the horizontal magnetic fields of the local site are enough to determine the inter-station tensor relationships with the horizontal magnetic fields of a neighbouring site. Taking advantage of the proposed method, we can reduce the number of magnetic sensors by five and still obtain equivalent results as if the electric and magnetic fields are simultaneously recording for twenty days in each site. Figure 5.8 shows the layout of a hypothetical LMT survey where the proposed method is used to reduce the number of magnetic sensors.

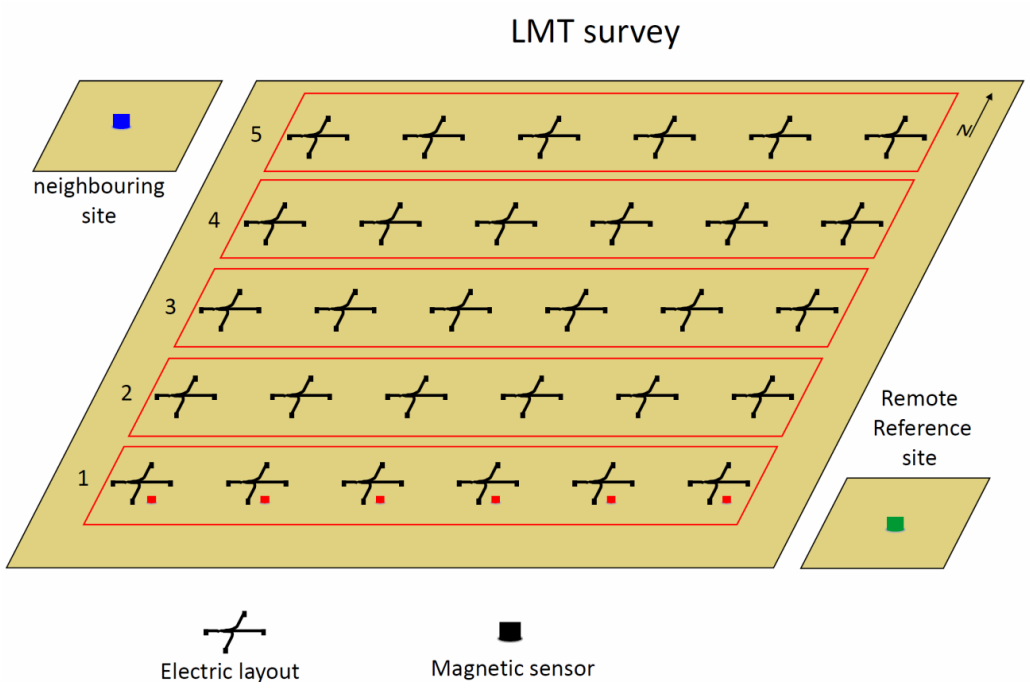

Figure 5.8 Layout of a hypothetical LMT survey. Red magnetic sensors: Magnetic sensors recording on a LMT site. Green magnetic sensor: Magnetic sensor used for remote reference. Blue magnetic sensor: Magnetic sensor used as a neighbouring site in the proposed method. Red rectangle surrounding LMT sites: Group of LMT sites simultaneously recording with red magnetic sensors. After four days recording, the magnetic sensors are moved from 1 to 2, and then from 2 to 3 and so on until record the magnetic fields in all the sites of the LMT survey. In each site the electric fields are recording all the time.

Following this scheme, the electric field is constantly recorded at each site, as well as the magnetic fields of the neighbouring and the remote reference sites. The magnetic fields of the study area are recorded at each site only for four days and then moved to the next line. With this method six magnetic sensors, plus one remote reference and another neighbouring site, have to be used to record thirty LMT sites in twenty days. Following the usual way of recording LMT data we will need thirty magnetic sensors, plus one remote reference, to obtain equivalent results within the same number of days.

6. CONCLUSIONS
and perspective of advance

The aims of the thesis associated with the geoelectrical characterization of the Pyrenean lithosphere and the development of a method to improve the processing of the MT data have been accomplished within the three papers. The proposed results not only represent a breakthrough in the studied subjects, but also open new lines of research to further improve the characterization of the lithosphere using MT data, particularly in the Pyrenees.

In the Pyrenees forty two new BBMT sites and twenty nine new LMT sites were acquired between 2009 and 2010. These data, jointly with previous BBMT sites, have been used to determine the geoelectrical structures of the subsurface. The two new geoelectrical models, already published in a scientific journal indexed in the Journal Citation Reports (ISI), determine the electrical lithosphere below the Central and the West-Central Pyrenees. In this thesis, also a non published MT model in the Western Pyrenees characterizes the geoelectrical structures at crustal-scale.

One of the main geoelectrical structures constrained below the three MT profiles is the Iberian subducted lower crust (IBSLC). The new characterization of the IBSLC presents some differences with the previous MT studies (Ledo, 1996; Ledo et al., 2000 and Pous et al, 1995a). Below the Central Pyrenees the most important difference is related to the top of the low electrical resistivity structure associated with the IBSLC. In this thesis the top has been determined 9 km deeper than previous MT studies, better fitting with the hypothesis of partial melting. In the West-Central Pyrenees the new MT profile obtained using twenty BBMT sites, seven of them with LMT data, instead of the four BBMT sites previously used by Ledo et al. (2000), shows for first time in the Pyrenees

three different phases associated with partial melting of the IBSLC: Partial melting by dehydration melting of muscovite, partial melting by dehydration melting of muscovite and biotite and melt migration released from the bottom of the IBSLC. From the results obtained in the West-Central Pyrenees, the coincidence of the bottom of the low electrical resistivity structure associated with the IBSLC with the bottom of a negative Vs anomaly (Koulakov et al., 2009) and the presence of seismic activity in this region (Koulakov et al., 2009) suggest extending the IBSLC to the depth of 70 km. In the Western Pyrenees the top of the IBSLC has been also constrained at around 30 km depth showing similar electrical resistivity values than the characterized below the Central and the West-Central Pyrenees. Comparing the IBSLC below the Central and the West-Central Pyrenees at upper-mantle depths, a major difference between the dip of the IBSLC is observed indicating greater shortening in the Central Pyrenees.

Referent to the crustal geoelectrical structures, the low electrical resistivity values observed below the Ebro basin at upper–crustal and middle-crustal depths in the West-Central Pyrenees have been associated with the presence of graphite in a major Variscan tectonic boundary zone. In the transition zone between plates, at crustal depths, a low electrical resistivity structure associated with the presence of fluids and Silurian sediments has been observed below the three MT profiles, but at different depths. These differences in the location of the Silurian sediments, preferentially located along major faults, have been explained by the west plunge of the basement-involved thrusts observed in the core of the Pyrenees.

The asthenosphere has been determined below the Central Pyrenees and the West-Central Pyrenees with electrical resistivity values between 10 Ω·m and 70 Ω·m, having no main differences between the two MT profiles. Their top has been associated with the LAB, at around 130 km depth below the European plate and at around 90 km depth below the Iberian plate. This results suggest and European plate thicker than the Iberian one close to the collision zone.

Comparison of the MT results obtained in the Pyrenees with independent geological and geophysical studies have allowed associate the geoelectrical structures with

crustal geological structures, evaluate the hypothesis of partial melting to explain the low electrical resistivity values associated with the IBSLC, associate with graphite the electrical anomaly located below the Ebro basin in the West-Central Pyrenees and corroborate the depth of the electric LAB comparing with the seismic and the thermal LABs.

As a perspective of advance, there are two lines related to the MT method and the Pyrenees that could be done in the near future. Firstly, it would be interesting to model the BBMT and LMT data acquired in the Eastern Pyrenees using a three dimensional inversion code including the effect of the seawater, or carry out a three dimensional model from the Mediterranean See to the Atlantic Ocean using the 82 MT sites already acquired along the Pyrenees. Secondly, it would be also interesting to determine the lateral propagation of the unexpected geoelectrical structure observed below the Ebro Basin associated with the presence of a Variscan boundary completely buried below the sediments. New MT profiles can be done, gradually moving away from the West-Central Pyrenees MT profile, determining the evolution of this structure below the Ebro basin.

Focusing on the methodological improvement, we have proposed a new method for processing MT data of a local site using inter-station tensor relationships with a neighbouring site, without simultaneously record the electric and magnetic time-varying fields of the local site. Different tests have been done corroborating the viability and the reliability of the proposed method. Also a parameter has been defined constraining the applicability of the method in each specific study for each analysed period. From the properties of the proposed method exposed in chapter 4 and in the Discussion there are two major advantages associated with the processing of old and new MT data and the acquisition of future MT data. Firstly, the proposed method allows improves the processing of the MT data when the time series of the magnetic fields have been truncated. Secondly, the suggested method allows modify the future MT surveys getting more out of the measuring instruments.

REFERENCES

Amaru, M.; Spakman, W.; Villaseñor, A.; Sandoval, S. and Kissling, E., 2008. A new absolute arrival time data set for Europe. *Geophys. J. Int.* 173, 465-472.

Arzi, A.A., 1978. Critical phenomena in the rheology of partially melted rocks. *Tectonophysics*, 44, 173-184.

Asch, T.H. and Sweetkind, D.S., 2011. Audiomagnetotelluric characterisation of range-front faults, Snake Range, Nevada. *Geophys*., 76 (1), B1-B7.

Avdeeva, A., 2008. Three-dimensional Magnetotelluric inversion. PhD Theses. National University of Ireland. (Ireland).

Baba, K.; Chave, A.D.; Evans, R.L.; Hirth, G. and Mackie, R.L., 2006. Mantle dynamics beneath the East Pacific Rise at 17S: insights from the Mantle Electomagnetic and Tomography (MELT) experiment. *J. Geophys. Res*., 111, B02101, doi:10.1029/2004JB003598.

Bahr, K., 1988. Interpretation of the magnetotelluric impedance tensor: regional induction and local telluric distortion. *J. Geophys*., 62, 119-127.

Bailey, R.C., 1990. Trapping of aqueous fluids in the deep crust. *Geophys. Res. Lett*., 17, 1129-1132.

Beamish, D. and Travassos, J.M., 1992. The use of the D+ solution in magnetotelluric interpretation. *J. Appl. Geophys*., 29, 1-19.

Beaumont, C.; Muñoz, J.A.; Hamilton, J. and Fullsack, P., 2000. Factors controlling the Alpine evolution of the central Pyrenees inferred from a comparison of observations and geodynamical models. *J. Geophys. Res*., 105, 8121-8145.

Berdichevsky, M.N., 1968. Electrical prospecting by the method of Magnetotelluric Profiling, Nedra, Moscow.

Berdichevsky, M.N. and Dmitriev V.I., 1976. Basic principles of interpretation of magnetotelluric sounding curves. In: A. Adam (Editor), Geoelectric and Geothermal studies. KAPG Geophys. Monogr., Akademiai Kiado, Budapest, 165-221.

Berdichevsky M.N. and Dmitriev V.I., 2008. Models and Methods of Magnetotellurics. Springer-Verlag Berlin Heidelberg.

Bucher, K. and Frey, M., 1994. Petrogenesis of Metamorphic Rocks, 6th edn, Srpinger-Verlag, Berlin.

Cagniard, L., 1953. Basic theory of the magnetotelluric method of geophysical prospecting. *Geophys.*, 18, 605-635.

Caldwell, T.G.; Bibby, H.M. and Brown, C., 2004. The magnetotelluric phase tensor. *Geophys. J. Int*., 158, 457-469.

Campanyà, J.; Ledo, J.; Queralt, P.; Marcuello, A.; Liesa, M. and Muñoz, J.A. 2011. Lithospheric characterization of the Central Pyrenees based on new magnetotelluric data. *Terra Nova*, 23, 213 - 219. doi: 10.1111/j.1365-3121.2011.01001.x.

Campanyà, J.; Ledo, J.; Queralt, P.; Marcuello, A.; Liesa, M. and Muñoz, J.A. 2012. New geoelectrical characterization of a continental collision zone in the West-Central Pyrenees: Constraints from long period and broadband magnetotellurics. *Earth Planet. Sci. Lett.*, 333-334, 112-121.

Cantwell, T., 1960. Detection and analysis of low frequency magnetotelluric signals. Ph.D thesis. M.I.T.

Carrasquilla, A. And Rijo, L., 1998. Analysis of electrojet-distorted magnetotelluric sounding curves. *J. Appl. Geophys.*, 40, 187-204.

Casas, A.; Kearey, P.; Rivero, L. and Adam, C.R., 1997. Gravity anomaly map of the Pyrenean region and a comparison of the deep geological structure of the western and eastern Pyrenees. *Earth Planet. Sci. Lett.*, 150, 65-78.

Chandrasekhar, E.; Mathew, G. and Harinarayana, T., 2012. A new hypothesis for the deep subsurface structures near the Bhuj 2001 earthquake (Mw 7.6) hypocentre zone and its tectonic implications. *Geophys. J. Int.,* 190, 761-768.

Chave, A.D., Thompson, D.J. and Ander, M.E., 1987. On the Robust Estimation of Power Spectra, Coherences, and Transfer Functions. *J. Geophys. Res*., 92, B1,633-648.

Chave A.D. and Smith, J.T., 1994. On electric and magnetic galvanic distortion tensor decompositions. *J. Geophys*., Res., 99, B3, 4669-4682.

Chave, A.D. and Thompson, D.J., 2004. Bounded influence estimation of magnetotelluric response functions. *Geophys. J. Int.,* 157, 988-1006.

Chave, A.D. and Jones, A.G., 2012. The Magnetotelluric Method. Cambridge University press. United Kingdom.

Choukroune and Ecors-Pyrenees Team (1989): The ECORS Pyrenean deep seismic profile: reflection data and the overall structure of the orogenic belt. *Tectonics*, 8, 23-39.

Clemens, J. D., 2006. Melting of the continental crust: fluid regimes, melting reactions and source-rock fertility. In: Evolution and Differentiation of the Continental Crust (M. Brown and T. Rushmer, eds), Cambridge University Press, 296-327.

Cloetingh, S.; van Wees, J.D.; Ziegler, P.A.; Lenkey, L. ; Beekman, F.; Tesauro, M.; Förster, A.; Norden, B.; Kaban, M.; Hardebol, N.; Bonté, D.; Genter, A.; Guillou-Frottierg, L.; Ter Voorde, M.; Sokoutis, D.; Willingshofer, E.; Cornu, T.; Worum, G., 2010. Lithosphere tectonics and thermo-mechanical properties: An integrated modelling approach for Enhanced Geothermal Systems exploration in Europe. *Earth-Science Reviews*, 102 (3-4), 159-206.

Da Silva, N.V.; Mateus, A.; Santos, F.A.M.; Almeida, E.P. and Pous, J., 2007. 3-D electromagnetic imaging of a Palaeozoic plate-tectonic boundary segment in SW Iberian Variscides (S Alentejo, Portugal. *Tectonophysics*, 445, 98-115.

Daignières, M., Séguret, M., Specht, M., ECORS team,1994. The Arzacq–Western Pyrenees ECORS deep seismic profile. *Publ. Eur. Assoc. Pet. Geol*. 4, 199–208.

deGroot-Hedlin, C. and Constable, S., 1990. Occam's inversion to generate smooth, two-dimensional models from magnetotelluric data. *Geophys.*, 55, 1613-1624.

ECORS-Pyrenees Team, 1988. The ECORS deep reflection seismic survey across the Pyrénées. *Nature,* 331,508–510.

Efron, B., 1979. Bootstrap methods: Another look at the jackknife. *Annals of Statistics*, 7, 1-26

Egbert, G.D. and Booker, J.R., 1986. Robust estimation of geomagnetic transfer functions. *Geophys. J.R. astr. Soc*., 87, 173-194.

Egbert, G.D. and Booker, J.R.: 1989, Multivariate analysis of geomagnetic array data, The response space, *J. Geophys. Res*. 94, 14,227–14,248.

Egbert, G.D., 2002. Processing and interpretation of the electromagnetic induction array data. *Surv. in Geophys*., 23, 207-249.

Egbert, G.D. and Kelbert, A., 2012. Computation recipes for electromagnetic inverse problems. *Geophys. J. Int.*, 189,251-267.

Ekström, G. and A.M., Dziewonski, 1998. The unique anisotropy of the Pacific upper mantle, *Nature*, 394, 168-172.

Falgàs, E.; Ledo, J.; Benjumea, B. and Queralt, P., 2011. Integrating Hydrogeological and Geophysical Methods for the Characterization of a Deltaic Aquifer System, *Surv Geophys*. doi:10.1007/s10712-011-9126-2.

Fernández-Viejo,G.; Gallart, J.; Pulgar, J. A.; Gallastegui, J.; Dañobeitia, J. J. and Córdoba, D., 2000. Seismic signature of Variscian and Alpine tectonics in NW Iberia: Crustal structure of the Cantabrian Mountains and Duero basin. *J. Geophys. Res.,* 105, 3001–3018

Ferrer, O.; Roca, E.; Benjumea, B.; Muñoz, J. A.; Ellouz, N. and the MARCONI Team, 2008. The deep seismic reflection MARCONI-3 profile: Role of extensional Mesozoic structure during the Pyrenean contractional deformation at the eastern part of the Bay of Biscay. *Mar. Pet. Geol*. 25(8), 714–730.

Ferrer O., 2012. Salt tectonics in the Parentis Basin (eastern Bay of Biscay): Origin and kinematics of salt structures in a hyperextended margin affected by subsequent contractional deformation. Ph.D Thesis. Universitat de Barcelona (Spain).

Fowler, C.M.R., The Solid Earth: an introduction to global geophysics, Cambridge University Press, United Kingdom, 1994 (2nd edition, 2005)

Friedrichs, B., 2003. Mapros, Magnetotelluric Processing Software (Metronix). User Manual.

Frizon de Lamotte, D.; Crespo-Blanc, A.; Saint-Bezar, B.; Fernàndez, M.; Zeyen, H. and Ayarza, P., 2004. TRANSMED-TRANSECT I [Betics, Alboran Sea, Rif, Moroccan Meseta, High Atlas, Jbel Saghro, Tindouf basin]. edited by R. W. Cavazza, F., Spakman, W., Stampfli, G. and Ziegler, P.A., /Springer-Verlag/.

Gabàs, A. and Marcuello, A., 2003. The relative influence of different types of magnetotelluric data on joint inversions. *Earth, Planets and Space*. 55 (5), 243-248.

Gamble, T.D.; Goubau, W.M. and Clarke, J. , 1979a. Magnetotellurics with a remote reference. *Geophys.*, 44, 53-68.

Gamble, T.D.; Goubau, W.M. and Clarke, J., 1979b. Error analysis for remote reference magnetotellurics. *Geophys*., 44, 959-968.

Garcia X. and Jones, A.G., 1999. Extended decomposition of MT data. In Second Int. Symp. On Three-Dimensional Electromagnetics, Salt Lake City, Utah.

Garcia X. and Jones, A.G.,2002. Extended decomposition of MT data. In three-Dimensional electromagnetic, ed. M. S. Zhdanov and P.E. Wannamaker. Amsterdam: Elsevier, pp. 235-250.

Garcia, X. and Jones, A.G., 2005. A new methodology for the acquisition and processing of audio-magnetotelluric (AMT) data in the AMT dead band. *Geophys*., 70 (5), G119-G126. doi: 10.1190.2073889.

García-Mondejar, J. (1989) Strike-slip subsidence of the Basque-Cantabrian Basin of Northern Spain and its relationships to Aptian-Albian opening of Bay of Biscay. In: Tankard, A.J. and Balkwill, H.R. (eds.). Extensional Tectonics and Stratigraphy of the North Atlantic Margins, *American Association of Petroleum Geologists Memoir*, 46, 395–409, Tulsa, Okla.

Glover, P.W.J.; Pous, J.; Queralt, P.;Muñoz, A.; Liesa, M. and Hole, M.J., 2000. Integrated two dimensional lithospheric conductivity modelling in the Pyrenees using field-scale and laboratory measurements. *Earth Planet. Sci. Lett.*, 178, 59-72.

Groom, R. W. and Bailey, R. C., 1989. Decomposition of magnetotelluric impedance tensor in the presence of local three-dimensional galvanic distortion. *J. Geophys. Res.*, 94, 1913-1925.

Gunnell, Y.; Zeyen, H. and Calvet, M., 2008. Geophysical evidence of a missing lithospheric root beneath the Eastern Pyrenees: Consequences for post-orogenic upflit and associated geomorphic signatures. *Earth Planet. Sci. Lett.*, 276, 302-313.

Haak, V. and Hutton, V.RS., 1986. Electrical resistivity in continental lower crust. In: J.B. Dawson, D.A. Carswell, J. Hall and K.H. Wedepohl (Editors), The Nature of the Lower Continental Crust. Geo\. Soc. London, Spec. Pub., 24: 35-49.

Habibian, B.D.; Brasse, H.; Oskooi, B.; Ernst, T.; Sokolova, E.; Varentsov, Iv. and EMTESZ Working Group, 2010. The conductivity structures across the Trans-European Suture Zone from magnetotelluric and magnetovariational data modeling. *Phys. Earth Planet. Int*., 183,377-386.

Hatakeyama,H. and Hirayama, M., 1934. On the phase difference between the pulsation of terrestrial magnetism and of the earth current. *J. Meteorol. Soc. Japan*, 12, 449-459.

Heinson, G., 1999. Electromagnetic Studies of the Lithosphere and Asthenosphere. *Surv. in Geophys*., 20, 229-255.

Heinson, G.S.; Constable, S.C.; White, A., 2000. Episodic melt transport at mid-ocean ridges inferred from magnetotelluric sounding. *Geophy. Res. Lett*., 27, 2317-2320.

Hermance, J. F. and Thayer, R.E.,, 1975. The telluric-magnetotelluric method. *Geophys*., 40, 664-668.

Hirayama, M., 1934. On the relations between the variations of the earth potential gradient and terrestrial magnetism. *J. Meteorol. Soc. Japan*, 12, 16-22.

Hogan P.J. and Burbank D.,W., 1996. Evolution of the Jaca piggyback basin and emergence of the External Sierras, southern Pyrenees, P. Friend, C. Dabrio, Editors , Tertiary Basins of Spain: the Stratigraphic Record of Crustal Kinematics 6, Cambridge University Press, Cambridge, pp. 153–160.

Jammes, S.; Manatschal, G.; Lavier, L. and Masini, E., 2009. Tectonosedimentary evolution related to extreme crustal thinning ahead of a propagating ocean: the example of the western Pyrenees. *Tectonics*, 28, TC4012.

Jammes, S.; Lavier, L.; Manatschal, G., 2010. Extreme crustal thinning in the Bay of Biscay and the Western Pyrenees: From observations to modeling. *Geochemistry geophysics geosystems*, 11, Q10016.

Jegen, M.D.; Hobbs, R.W.; Tarits, P.; Chave, A., 2009. Joint inversion of marine magnetotelluric and gravity data incorporating seismic constraints Preliminary results of sub-basalt imaging off the Faroe Shelf. *Earth Planet. Sci. Lett.*, 282, 47-55.

Jiracek, G., 1990. Near-surface and topographic distortions in electromagnetic induction. *Surv. Geophys*., 11, 163-203.

Jones, A.G., 1988. Static shift of magnetotelluric data and its removal in a sedimentary basin environment. *Geophys.*, 53, 967-978.

Jones, A.G.; Plomerova, J.; Korja, T.; Sodoudi, F. and Spakman, W., 2010. Europe from the bottom up: A statistical examination of the central and northern European

lithosphere-asthenosphere boundary from comparing seismological and electromagnetic observations. *Lithos*, 120, 14-29.

Junge, A., 1992. On the effective number of degrees of freedom in magnetotelluric transfer function estimation. In Protokoll Kolloquium Elektromagnetische Tiefenforschung, pp. 139-158, eds Haak, V. and Rodemann, H., DGG, Borkheide, Germany (in German).

Junge, A., 1996. Characterization of and Correction for Cultural Noise. *Surv. in Geophys.*, 17, 361-391.

Kato, Y. and Kikuchi, T., 1950a. On the phase difference of earth current induced by the changes of the earth's magnetic field, part 1. Sci. Rep. Tohoku Univ., 5th Ser., 2, 139-141.

Kato, Y. and Kikuchi, T., 1950b. On the phase difference of earth current induced by the changes of the earth's magnetic field, part 2. Sci. Rep. Tohoku Univ., 5th Ser., 2, 142-145.

Kaufman, A.A., 1988. Reduction of the geological noise in magnetotelluric soundings. *Geodex*, 25, 145-161.

Kelbert, A.; Egbert, G.D. and deGroot-Hedlin, C., 2012. Crust and upper mantle electrical conductivity beneath the Yellowstone Hotspot Track. *Geology*, 40, 477-450. Doi:10.1130/G32655.1

Korja, T., 2007. How is the European Lithosphere Imaged by Magnetotellurics? *Surv. Geophys*., 28, 239-272. Doi: 10.1007/s10712-007-9024-9

Koulakov, I.; Kaban, M.K.; Tesauro, M. and Cloetingh, S., 2009. P and S velocity anomalies in the upper mantle beneath Europe from tomographic inversion of ISC data.*Geophys.J.Int.*,179(1),345-366. doi:10.1111/j.1365246X.2009.04279.x

Kusi, R., Electromagnetic induction studies in the Eyre Peninsula, South Australia, PhD Thesis, Flinders University, Australia, 1997. pp263.

La Terra, E.F. and Menezes, P.T.L., 2012. Audiomagnetotelluric 3D imaging of the Regis kimberlite pipe, Minas Gerais, Brazil. *J. of Appl. Geophys*., 77, 30-38.

Lanaja, J. M. and Querol, R., 1987. (Ed.) Contribución de la exploración petrolífera al conocimiento de la geología de España Instituto Geológico y Minero de España, 465pp.

Le Pape, F.; Jones, A.G.; Vozar, J. and Wenbo, W.; 2012. Penetration of cristal melt beyond the Kunlun Fault into northern Tibet. *Nature Geoscience*, 5, 330-335.

Ledo, J., 1996. Aplicación del método magnetotelúrico al estudio de la estructura Litosférica de los Pirineos. Ph.D thesis. Universitat de Barcelona, Spain.

Ledo, J.; Queralt, P. and Pous, J., 1998. Effects of galvanic distortion on magnetotelluric data over three dimensional structure, *Geophys. J. Int.,* 132, 295-301.

Ledo, J.; Ayala, C.; Pous, J.; Queralt, P.; Marcuello, A. and Muñoz, J.A., 2000. New geophysical constrains on the deep structure of the Pyrenees. *Geophys. Res. Lett.*, 27, 1037-1040.

Ledo, J.; Gabàs, A. and Marcuello, A, 2002. Static shift levelling using geomagnetic transfer functions. *Earth Planets Space*, 54, 493-498.

Ledo, J. and Jones, A.G., 2005. Upper mantle temperature determined from combining mineral composition, electrical conductivity laboratory studies and magnetotelluric field observations: application to the Intermontane Belt,Northern Canadian Cordillera. Earth Planet. Sci. Lett., 236, 258–268.

Ledo, J.; Jones, A.G.; Siniscalchi, A.; Campanyà, J.; Kiyan, D.; Romano, G.; Rouai, M.; TopoMed MT Team, 2011. Electrical signature of modern and ancient tectonic processes in the crust of the Atlas mountains of Morocco. *Phys. Earth Planet. Int.*,185, 82-88,

Lezaeta P., Haak, V., 2003. Beyond magnetotelluric decomposition: Induction, current channelling, and magnetotelluric phases over 90°. *J. Geophys. Res.*, 108, B6, 2305. Doi:10.1029/2001JB000990.

Liang, X.; Sandvol, E.; Chen, Y.J.; Hearn, T.; Ni, J.; Klemperer, S.; Shen, Y. and Tilmann, F., 2012. A complex Tibetan upper mantle: A fragmented Indian slab and no south-verging subduction of Eurasian lithosphere. *Earth Planet. Sci. Lett.* ,333-334, 101-111.

Mackie, R. L. and Madden, T. R. (1993). Three dimensional magnetotelluric inversion using conjugate gradients. *Geophys. J. Int*., 115, 215-229.

Martí, A., 2006. A Magnetotelluric Investigation of Geoelectrical Dimensionality and Study of the Central Betic Crustal Structure. Ph.D. Thesis. Universitat de Barcelona (Spain).

Martí, A.; Queralt, P.; Roca, E.; Ledo, J. and Galindo-Zaldívar, J., 2009a. Geodynamic implications for the formation of the Betic–Rif orogen from magnetotelluric studies. *J. Geophys. Res*., 114, B01103, doi:10.1029/2007JB005564

Martí, A.; Queralt, P. and Ledo, J., 2009b. WALDIM: A code for the dimensionality analysis of magnetotelluric data using the rotational invariants of the magnetotelluric tensor. *Computers and Geosciences*, 35 (12), 2295-2303

Martínez Catalán, J.R.; Arenas, R.; Díaz García, F.; Gómez Barreiro, J.; González Cuadra, P.; Abati, J.; Castiñeiras, P.; Fernández-Suárez, J.; Sánchez Martínez, S.; Andonaegui, P.; González Clavijo, E.; Díez Montes, A.; Rubio Pascual, F.J. and Valle Aguado, B., 2007: Space and time in the tectonic evolution of the northwestern Iberian Massif. Implications for the comprehension of the Variscan belt. In: R.D. Jr. Hatcher, M.P. Carlson, J.H. McBride and J.R. Martínez Catalán (Eds.). 4-D Framework of Continental Crust. *Geological Society of America Memoir*, 200, 403-423. Boulder, Colorado.

Martínez Catalán, J.R.; Arenas, R.; Abati, J.; Sánchez Martínez, S.; Díaz García F.; Fernández-Suárez, J.; González Cuadra, P.; Castiñedas, P.; Gómez Barreiro, J.; Díez Montes, A.; González Clavijo, E.; Rubio Pascoal, F.; Andonaegui, P.; Jefferies, T.E.; Alcock, J.E.; Díez Fernández, R.; and López Carmona, A., 2009. A rootless suture and the loss of the roots of a mountain chain: The Variscan Belt of NW Iberia. C.R. *Geocience*, 341(2-3), 114-126.

McNeice, G. and Jones, A.G., 2001. Multisite, multifrequency tensor decomposition of magnetotelluric data. *Geophys. J. Int*., 163, 38-41.

McPherron, R.L., 2005. Magnetic pulsations: Their sources and relation to solar wind and geomagnetic activity. *Surv. In Geophys*., 26, 545-592.

Millán, H., 1996. Estructura del frente de cabalgamiento surpirenaico en las Sierras Exteriores Aragonesas. PhD Thesis, Univ. de Zaragoza.

Muller, M.R.; Jones, A.G.; Evans, R.L.; Grutter, H.S.; Hatton, C.; Garcia, X.; Hamilton, M.P.; Miensopust, M.P.; Hutchins, D.; Fourie, C.J.; Jelsma, H.A.; Evans, S.F.; Aravanis, T.; Pettit, W.; Webb, S.J. and Wasborh, J., 2009. Lithospheric structure, evolution and diamond prospectivity of the Rehoboth Terrane and western Kaapvaal Craton, southern Africa: Constraints from broadband magnetotellurics. *Lithos*, 112, 93-105.

Muñoz, J.A., 1992. Evolution of a continental collision belt: ECORS-Pyrenees cristal balanced cross-section. In: K.R. McClay (Editor) In: Thrust Tectonics. Chapman and Hall, London, p. 235-246.

Muñoz, J. A., 2002. The Pyrenees, in The Geology of Spain, edited by W. Gibbons and T. Moreno, pp. 370-385, *Geological Society of London*, London.

Muñoz, G.; Mateus, A.; Pous, J.; Heise, W.; Santos, F.M, Almeida, E., 2008. Unraveling middle-crust conductive layers in Paleozoic Orogens through 3D modeling of magnetotelluric data: the Ossa-Morena Zone case study (SW Iberian Variscides) *Journal of Geophysical research-solid* 113, B6.

Neves, A.S.D., 1957. The generalized magneto-telluric method. Ph.D., thesis, Massachusetts Institute of Technology.

Padilha, A.L., Vitorello, I. and Rijo, L., 1997. Effects of the equatorial electrojet on magnetotelluric surveys: field results from Northwest Brazil. *Geophys. Res. Lett.*, 24, 89-92.

Osipova, I.L., Hjelt, S.E. and Vanyan, L.L. (1989). Source field problems in northern parts of the Baltic Shield. Phys. Earth Planet. Inter., 53, 337-342.

Olivet, J.L., 1996. La cinematique de la plaque Iberique. Bull. Centres Res. Explor. Prod. Elf Aquitanie 20, 131-195.

Parkinson, W.D., 1962. The influence of the continents and oceans on geomagnetic variations. *Geophys. J.R. Astron. Soc.*, 80, 177-194.

Partzsch, GM.; Schilling, F.R. and Arndt, J., 2000. The influence of partial melting on the electrical behavior of the crustal rocks: laboratory examinations, model calculations and the geological interpretations Tectonophysics, 317, 189-203.

Patiño Douce, A.E. and Harris, N., 1998. Experimental constraints on Himalayan Anatexis. *Journal of Petrology*. 39, 689-710.

Pedreira, D.; and Pulgar, J.A.; Gallart, J.; Díaz, J., 2003. Seismic evidence of Alpine crustal thickening and wedging from the western Pyrenees to the Cantabrian Mountains (north Iberia) *J. Geophys. Res.*, 108, B4, 2204. doi:10.1029/2001JB001667.

Pedreira, D.; Pulgar, J.A.; Gallart, J. and Torne, M., 2007. Three-dimensional gravity and magnetic modeling of crustal indentation and wedging in the western

Pyrenees-Cantabrian Mountains. *Journal of geophysical research-solid*, 112, B12.

Pinto, LGR.; de Padua, MB.; Ussami, N.; Vitorello, I.; Padilha, A.L. and Braitenberg, C., 2010. Magnetotelluric deep soundings, gravity and geoid in the south Sao Francisco craton: Geophysical indicators of cratonic lithosphere rejuvenation and crustal underplating. *Earth Planet. Sci. Lett.*, 297, 423-434.

Pous, J.; Ledo, J.; Marcuello, A. and Daignières, M., 1995a. Electrical resistivity model of the crust and upper mantle from a magnetotelluric survey through the Central Pyrenees. *Geophys. J. Int*., 121, 750-762.

Pous, J.; Muñoz, J.A.; Ledo, J. and Liesa, M., 1995b. Partial melting of the subducted continental lower crust in the Pyrenees*, J. Geol. Soc. London*, 152, 217-220.

Pous J.; Queralt, P. and Marcuello, A., 2001. Magnetotelluric signature of the Western Cantabrian Mountains. *Geophys. Res. Letters*, 28, 1795-1798.

Pous, J.; Muñoz, G.; Heise, W.; Melgarejo, J.C. and Quesada, C., 2004. Electromagnetic imaging of Variscan cristal structures in SW Iberia: the role of interconnected graphite. *Earth Planet. Sci. Lett.*, 217, 435-450.

Pous, J.; Poyatos, DM.; Heise, W.; Santos, FM.; Galindo-Zaldivar, J.; Ibarra, P.; Pedrera, A.; Ruiz-Constan, A.; Anahnah, F.; Goncalves, R. and Mateus, A., 2011. Constrains on the crystal structure of the internal Variscan Belt in SW Europe: A magnetotelluric transect along the eastern part of Central Iberian Zone, Iberian Massif. *Journal of Geophysical Research-Solid Earth*, 116, B02103.

Pulgar, J. A.; Gallart, J.; Fernández-Viejo, G.; Pérez-Estaún, A.; Álvarez-Marrón, J. and the ESCI Group, 1996. Seismic image of Cantabrian Mountains in the western extension of the Pyrenean belt from integrated reflection and refraction data. *Tectonophysics*, 264, 1–19.

Rigo, A.; Souriau, A.; Dubos, N.; Sylvander, M. and Ponsolles, C., 2005. Analysis of the seismicity in the central part of the Pyrenees (France), and tectonic implications. *Journal of Seismology*, 9, 211-222.

Rikitake, T., 1948. Note on the electromagnetic induction within the earth. Bull Earthq. Res. Inst., Univ. Tokyo, 24, 1-9.

Rikitake, T., 1951. Changes in earth current and their relation to the electrical state of the earth's crust. Bull. Earthq. Res. Ins., Univ. Tokyo, 29, 271-276.

Roca, E.; Muñoz, J. A.; Ferrer, O. and Ellouz, N., 2011. The role of the Bay of Biscay Mesozoic extensional structure in the configuration of the Pyrenean orogen: Constraints from the MARCONI deep seismic reflection survey. *Tectonics*, 30, TC2001.

Rodi, W. And Mackie, R.L., 2001. Nonlinear conjugate gradients algorithm for 2-D magnetotelluric inversion. *Geophysics,* 66, 174-187.

Rokityanski, I.I., 1961. On the application of the magnetotelluric method to anisotropic and inhomogeneous masses. *Izvestia*, 11, 1607-1613.

Rosell, O.; Martí, A.; Marcuello, A.; Ledo, J.; Queralt, P.; Roca, E. and Campanyà, J., 2011. Deep electrical resistivity structure of the northern Gibraltar Arc (western Mediterranean): evidence of lithospheric slab break-off. *Terra Nova*, 23, 179-186.

Rosenbaum, G.; Lister, G. S. and Duboz, C. 2002. Reconstruction of the tectonic evolution of the western Mediterranean since the Oligocene. In:Rosenbaum, G. and Lister, G. S. 2002. Reconstruction of the evolution of the Alpine-Himalayan Orogen. *Journal of the Virtual Explorer*, 8, 107 - 130.

Ruiz, M.; Gallart, J.; Díaz, J.; Olivera, C.; Pedreira, D.; López, C.; González-Cortina, J.M., Pulgar, J.A., 2006. Seismic activity at the western Pyrenean edge. *Tectonophysics*, 412, 217-235.

Savostin, L.A.; Sibuet, J.C.; Zonenshain, L.P.; Le Pichon, X. and Roulet, M.J. (1986) Kinematic evolution of the Tethys belt from the Atlantic Ocean to the Pamirs since the Triassic. *Tectonophysics*, 123, 1–35.

Schmucker, U., 1970. Anomalies of geomagnetic variations in the Southwestern United States*. J. Geomagn. Oceanogr*., Univ. of California Press, Berkeley.

Schmucker, U., 1985. Numerical Data and Functional relationships in Science and Technology, vol. 2, chap. Geophysics of the Solid Earth, the Moon and the Planets, pp. 31-73, K. Uchs and H.Soffel ed., Springer-Verlag, Berlin-Heidelberg, 1985

Schwabe, H., 1844, “Sonnen-Beobachtungen im Jahre 1843”, Astron. Nachr., 21(495), 233–236.

Selway, K.; Hand, M.; Heinson, G.S. and Payne, J.L., 2009. Magnetotelluric constrains on subduction polarity: Reversing reconstruction models for Proterozoic Australia. *Geology*, 37 (9), 799-802. doi: 10.1130/G30175A.1.

Sheard, N., 2001. The values of advanced geophysical technology in modern exploration. Bulletin of the Australian Institute of Geoscientists, 35, 53-56.

Simpson, F. and Bahr, K., 2005. Practical Magnetotellurics. Cambridge University press. United Kingdom.

Siniscalchi, A.; Tiripaldi, S.; Neri, M. ; Balasco, M. ; Romano, G.; Ruch, J. and Schiavone, D., 2012. Flank instability structure of Mt. Etna inferred by a magnetotelluric survey. *Jour. Geophys. Res.*, 117, B03216, 14 PP.

Siripunvaraporn, W. and Egbert, G., 2000. An efficient data-subspace inversion method for 2-D magnetotelluric data. *Geophys.,* 65,791-803.

Siripunvaraporn, W.; Egbert, G.; Lenbury, Y. and Uyeshima, M. (2005). Three-dimensional magnetotelluric inversion: data space method, *Phys. Earth Planet. Interior.,* 150, 3–14.

Smith, J.T. and Booker, J.R., 1991. Rapid inversion of two- and three- dimensional magnetotelluric data. *J. Geophys. Res*., 96, 3905-3922.

Smith, J.T., 1995. Understanding telluric distortion matrices*, Geophys. J. Int*., 122, 219-226.

Sokolova, E.Yu. and Varentsov, Iv.M. and BEAR Working Group, 2007. Deep array electromagnetic sounding on the Baltic Shield: External excitation model and implications for upper mantle conductivity studies, Tectonophysics, 445, 3-25.

Souriau, A. and Granet, M., 1995. A tomographic study of the lithosphere beneath the Pyrenees from local and teleseismic data. *J. Geophys. Res.,* 100(B9), 18117–18134.

Souriau, A.; Chevrot, S. and Olivera, C., 2008. A new tomographic image of the lithosphere beneath the Pyrenees from local and teleseismic data. *Tectonophysics*, 460, 206-214.

Srivastava, S.P.; Roest, W.R.; Kovacs, L.C.; Oakey, G.; Lévesque, S.; Verhoef, J. and Macnab, R. (1990) Motion of Iberia since the Late Jurassic : Results from detailed aeromagnetic measurements in the Newfoundland Basin. *Tectonophysics*, 184, 229-260.

Teixell, A., 1996. The Ansó transect of the southern Pyrenees: basement and cover thrust geometries. Journal of the Geological Society of London, 153, 301-310.

Teixell, A., 1998. Crustal structure and orogenic material budget in the west central Pyrenees. *Tectonics*, 17, 395-406.

Tesauro, M.; Kaban, M.K. and Cloetingh, S.A.P.L., 2009. A new termal and rheological model of the European lithosphere. *Tectonophysics*, 476, 478-495.

Thompson, A.B., 1992. Understanding the Earth. (G.C. Brown, C.J. Hawkesworth and R.C.L. Wilson, eds) Cambridge University press, 551 pp.

Thompson, A.B. and Connolly, J.A.D., 1995. Melting of the continental crust: Some termal and petrological constraints on anatexis in continental collision zones and other tectonic settings. *Jour. Geophys. Res*., 100,15565-15579.

Tikhonov, A.N., 1950. On determination of electric characteristics of deep layers of the earth's crust. Dokl. Acad. Nauk SSSR, 151, 295-297.

Torné, M.; De Cabissole, B., Bayer, R. ; Casas, A., Daignières, M. and Rivero, A., 1989. Gravity constraints in the deep structure of the Pyrenean Belt along the ECORS profile. *Tectonophysics*, 165, 105-116.

Tucholke, B.E.; Sawyer, D.S. and Sibuet, J.C. (2007) Breakup of the Newfoundland-Iberia rift. In: Karner, G.D., Manatschal, G. And Pinheiro, L.M. (eds.). Imaging, Mapping and Modelling Continental Lithosphere Extension and Breakup. *Geological Society Special Publications*, 282, 9–46.

Türkoğlu, E.; Unsworth, M.; Çağlar, I.; Tuncer, V. and Avşar, Ü., 2008. Lithospheric structure of the Arabia-Eurasia collision zone in eastern Anatolia: Magnetotelluric evidence for widespread weaking by fluids? *Geology*, 36(8), 619-622. doi:10.1130/G24683A.1.

Unsworth, M., 2009. Magnetotelluric Studies of Active Continent–Continent Collisions. *Surv. Geophys*, 31, 137-161.

Utada H. and Munekane H. 2000 On galvanic distortion of regional three-dimensional magnetotelluric impedances. *Geophys. J. Int*., 140 (2), 385-398.

Varentsov, Iv.M.; Sokolova, E.Yu. and BEAR WG, 2003. Diagnostics and suppression of auroral distortions in the transfer operators of the EM field in the BEAR experiment, *Izv., Phys. Solid Earth*, 39, 4: 283–307.

Vacher, P. And Souriau, A., 2001. A three-dimensional model of the Pyrenean deep structure basen on gravity modelling, seismic images and petrological constraints. *Geophys. J. Int*., 145, 460-470.

Vergés, J.; Millán, H.; Roca, E.; Muñoz, J.A.; Marzo, M.; Cirés, J.; Den Bezemer, T.; Zoetemeijer, R. and Cloetingh, S. 1995. Eastern Pyrenees and related foreland basins: pre-, syn- and post-collisional crustal-scale cross-sections. *Marine and Petroleum Geology.* 12, 893-915.

Vergés, J. and García-Senz, J. (2001) Mesozoic evolution and Cainozoic inversión of the Pyrenean Rift. In: Ziegler, P.A.; Cavazza, W.; Robertson, A.H.F. and Crasquin-Soleau, S. (eds.). Peri-Tethyan Memoir 6: Peri-Tethyan Rift/Wrench Basins and Passive Margins. Memoires du Museum National d'Histoire Naturelle, 186, 187–212.

Vergés, J.; Fernàndez, M. and Martínez, A. (2002) The Pyrenean orogen: Pre-, syn-, and postcollisional evolution. In: Rosenbaum, G. and Lister, G.S. (eds.). Reconstruction of the Evolution of the Alpine-Himalayan Orogen.Journal of the Virtual Explorer, 8, 57-76.

Vielzeuf, D., 1984. Relations de phases dans les facies granulite et implications géodynamiques. L'éxemple des granulites des Pyrénéés. Thèse Doctorat d'État, Clermont-Ferrand, 288 pp.

Vielzeuf, D. and Holloway, J.R., 1988 Experimental determination of the fluid-absent melting relations in the pelitic system. Consequences for crustal differentiation. Contributions to Mineralogy and Petrology, 98 (1988), pp. 257–276.

Vozoff, K., 1972, The magnetotelluric method in the exploration of sedimentary basins. *Geophysics,* 37, 98-142.

Vozoff, K., 1991., The magnetotelluric method, Electromagneitc methods in applied geophysics –Aplications, Chapter 8, 1991.

Waldhauser, F.; Lippitsch, R.; Kissling, E. and Ansorge, J., 2002. High resolution teleseismic tomography of upper mantle structure using an a priori three-dimensional crustal model. *Geophys. J. Int*. 150, 403–414.

Weaver, J.T.; Agarwall, A.K. and Lilley, F.E.M., 2000. Characterisation of the magnetotelluric tensor in terms of its invariants. *Geophys. J. Int*., 141, 321-336.

Wei, W.B.; Unsworth, M.; Jones, A.; Booker, J.; Tan, H.D.; Nelson, D.; Chen, L.S.; Li, S.H.; Solon, K.; Bedrosian, P.; Jin, S.; Deng, M.; Ledo, J.; Ray, D. and Roberts, B., 2001. Detection of widespread fluids in the Tibetan crust by magnetotelluric studies. *Science*, 292, 716-718.

Weise, H., 1962. Geomagnetische Tiefentellurik. *Geophys. Pure Appl*. 52, 83-103.

White, M. and Gordon, R., 2003. Deep imaging: New technology lowers cost discovery, *Canadian Mining Journal*, 27-28.

Wolf, R., 1877, Geschichte der Astronomie, vol. 16 of Geschichte der Wissenschaften in Deutschland.Neuere Zeit, Oldenbourg, M¨unchen. Related online version (cited on 2010): http://ebooks.ethbib.ethz.ch/fulltext/Rara/1681.pdf

Zhang, P.; Roberts, R.G., and Pedersen, L.B., 1987. Magnetotelluric Strike Rules. *Geophysics*, 52, 267-278.

Zhao, G.; Unsworth, M.J.; Zhan, Y.; Wang, L.; Chen, X.; Jones, A.G.; Tang, J.; Xiao, Q.; Wang, J.; Cai, J.; Li, T.; Wang, Y and J. Zhang, 2012. Crustal structure and rheology of the Longmenshan and Wenchuan Mw 7.9 earthquake epicentral area from magnetotelluric data. *Geology* (in press).

Zeyen, H. and Fernández, M., 1994. Integrated lithospheric modeling combining termal, gravity, and local isostasy analysis: Aplication to the NE Spanish Geotransect. *Jour. Geophys. Res*., 99, 18089-18102.

ANNEX

Published and submitted papers

1. Campanyà, J.; Ledo, J.; Queralt, P.; Marcuello, A.; Liesa, M.; Muñoz, J.A. 2011. Lithospheric characterization of the Central Pyrenees based on new magnetotelluric data. *Terra Nova*. **23**, 213 - 219. doi: 10.1111/j.1365-3121.2011.01001.x.

2. Campanyà, J.; Ledo, J.; Queralt, P.; Marcuello, A.; Liesa, M.; Muñoz, J.A. 2012. New geoelectrical characterization of a continental collision zone in the West-Central Pyrenees: Constraints from long period and broadband magnetotellurics. *Earth and Planetary Science Letters*, **333-334**, 112-121. doi: 10.1016/j.epsl.2012.04.018.

3. Campanyà, J.; Ledo, J.; Queralt, P; Marcuello, A; Jones, A.G., 2013. Processing of Magnetotelluric data using inter-station tensor relationships. *Geophysical Journal International* (Under review).

Paper 1

Campanyà, J.; Ledo, J.; Queralt, P.; Marcuello, A.; Liesa, M.; Muñoz, J.A. 2011. Lithospheric characterization of the Central Pyrenees based on new magnetotelluric data. *Terra Nova*. **23**, 213 - 219. doi: 10.1111/j.1365-3121.2011.01001.x.

Terra Nova

doi: 10.1111/j.1365-3121.2011.01001.x

Lithospheric characterization of the Central Pyrenees based on new magnetotelluric data

Joan Campanyà,[1] Juanjo Ledo,[1] Pilar Queralt,[1] Alex Marcuello,[1] Montserrat Liesa[2] and Josep A. Muñoz[1]

[1]*Institut Geomodels, Departament de Geodinàmica i Geofísica, Universitat de Barcelona, C/Martí Franqués s/n Barcelona, 08028, Spain;*
[2]*Departament de Geoquímica, Petrologia i Prospecció Geològica, Universitat de Barcelona, C/Martí Franqués s/n Barcelona, 08028, Spain*

ABSTRACT

The Pyrenees resulted from the continent–continent collision between the Iberian and European plates during the Alpine orogeny. Although the subduction of the Iberian lower crust is currently accepted, the physical processes that occur at the boundary between the plates are still a topic of open discussion today, as illustrated by the debate about the presence or absence of partial melting in the Iberian Subducted Lower Crust. Long Period Magnetotelluric data acquired for the first time in the Central Pyrenees constrain the low electrical resistivity structure in the Iberian Subducted Lower Crust better than previous studies, plotting their upper limit 9 km deeper. This new upper limit reinforces the hypothesis of partial melting. Additionally, Long Period Magnetotelluric data constrain the lithosphere–asthenosphere boundary at 90 and 130 km deep below the Iberian and European plates, respectively, and are compatible with electrical resistivity values between 10 and 18 ohm·m for the asthenosphere.

Terra Nova, 23, 213–219, 2011

Introduction

Continent–continent collision is a fundamental tectonic process that plays a primary role in the development of continents. The electromagnetic signature of continent–continent collision zones depends on the age of the collision and usually presents a major low electrical resistivity structure at crustal or upper-mantle depths associated with water, melt, sulphides or graphite (i.e. Wei *et al*., 2001; Türkoğlu *et al*., 2008; Martí *et al*., 2009a; and Selway *et al*., 2009). In active collisions the low electrical resistivity structure appears, usually, in the middle crust. In contrast, when it becomes more stable they appear at lower-crustal and upper-mantle depths (see Unsworth, 2009 for a review). Within the Alpine–Himalayan mountain belt, the collision between the Iberian and the European plates from the Late Cretaceous to the Early Miocene resulted in the formation of the Pyrenees (Muñoz, 1992). This mountain range offers a unique opportunity to study orogenic processes due to the well-constrained geological evolution and the significant amount of geophysical data available (see Muñoz, 2002 for a review).

We present a joint interpretation of the available geophysical and geological data together with the first Long Period Magnetotelluric (LMT) data collected in the Pyrenees. These new data confirm the hypothesis of partial melting in the Iberian Subducted Lower Crust (IBSLC) and constrain the lithosphere–asthenosphere boundary (LAB) and the electrical resistivity of the asthenosphere. The geoelectrical characterization of the Pyrenean lithosphere will help us to gain insight into the evolution of the lithosphere in continental-collision zones.

Geological setting and previous studies

The Central Pyrenees is a double-wedge orogenic system bounded by two foreland basins: the Ebro Basin (EB) southwards, and the Aquitaine Basin (AB) northwards (Fig. 1). The south Pyrenean wedge consists of south directed thrust sheets involving Mesozoic and Palaeogene sedimentary successions (SPTS). Northwards, the basement rocks initially located underneath the cover successions of the South Pyrenean Thrust Sheets were synchronously underthrusted and piled into an antiformal stack. These south Pyrenean basement thrust sheets only involve upper-crustal rocks which crop out along the central part of the Pyrenees and have been historically referred as the Axial Zone (AZ). The North Pyrenean Thrust Sheets (NPTS) involve a complete crustal section of cover and basement rocks. Restoration of the Pyrenean thrust sheets gives a minimum shortening of 150–160 km across the Central Pyrenees (Muñoz, 1992; Beaumont *et al*., 2000).

Several refraction and deep reflection seismic profiles constrain the crustal thickness in the Pyrenean domain (Muñoz, 2002).The depth of the European Moho varies between 30 and 35 km. The depth of the Iberian one increases progressively from south to north from 35 to 60 km (ECORS-Pyrenees team, 1988; Choukroune and ECORS-Pyrenees Team, 1989). These differences are related to the limited subduction of the Iberian lower crust below the European one and the stacking of basement thrust sheets in the southern Pyrenees (Muñoz, 1992).

A tomographic model from teleseismic P-waves travel times (Souriau and Granet, 1995) showed a negative V_p anomaly below the Central Pyrenees which pointed to the subduction of the Iberian lower crust down to 80–100 km depth. A recent tomographic model from teleseismic P and PKP-waves travel times (Souriau *et al*., 2008) include crustal corrections before inversion and the negative V_p anomaly disappear, suggesting that it was an artefact. Authors alleged that the data are not at odds with the subduction hypothesis, although did

Correspondence: Mr Joan Campanyà, Institut Geomodels, Departament de Geodinàmica i Geofísica, Universitat de Barcelona, C/Martí Franqués s/n Barcelona, 08028, Spain. Tel.: +34600357196; e-mail: jcampanya@ub.edu

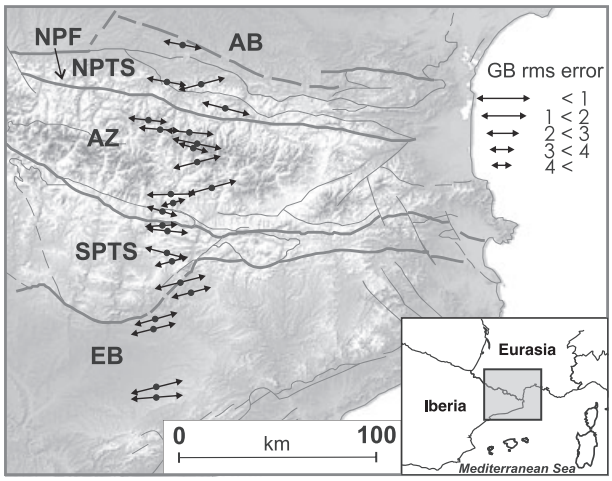

Fig. 1 Location of the MT stations (Black spots) in a structural sketch of the study area on a topographical map of the Pyrenees. The arrows indicate the strike direction of each site and their lengths are associated with the compatibility of the data to assume two-dimensional data in the suggested strike direction. EB, Ebro Basin; SPTS, South Pyrenean Thrust Sheets; AZ, Axial Zone; NPTS, North Pyrenean Thrust Sheets; AB, Aquitaine Basin; NPF, North Pyrenean Fault. Thick lines divide the main geological units and thin lines are the internal divisions.

not confirm it. Nevertheless, a new tomographic model (Koulakov *et al.*, 2009), also including crustal corrections, has obtained a negative V_p anomaly beneath the Central Pyrenees. Koulakov *et al.* (2009) also show an S-waves model without a major V_s anomaly associated with the IBSLC.

Ledo (1996) and Ledo *et al.* (2000) obtained a three-dimensional electrical resistivity model for the Central and Western Pyrenees using Broad Band Magnetotelluric (BBMT) data. The three-dimensional model validated a previous two-dimensional model of the Central Pyrenees (Pous *et al.*, 1995a) and corroborated the validity of considering the behaviour of Central Pyrenees resistivity structure as two-dimensional (Pous *et al.*, 1995a). All these models, obtained by trial-and-error fitting of the data, show a low electrical resistivity anomaly in the Iberian lower crust associated with the subduction of the Iberian plate and attributed to a small portion of partial melting (Pous *et al.*, 1995b; Glover *et al.*, 2000; Ledo *et al.*, 2000).

Gravity and geoid anomaly models are compatible with the subduction of the Iberian lower crust (Ledo *et al.*, 2000; Vacher and Souriau, 2001) and so does a recent work integrating heat flow, gravity, geoid anomaly and topography data (Gunnell *et al.*, 2008). Heat flow related studies (Zeyen and Fernández, 1994; Glover *et al.*, 2000; Tesauro *et al.*, 2009) constrain the geotherms below the Pyrenees at lithospheric scale, without observing any anomaly associated to the subduction of the Iberian lower crust, suggesting that thermal re-equilibration has already ended.

Subduction of the Iberian lower crust below the European one is currently accepted but the physical processes that occur in the boundary between the plates are still an open discussion, as illustrated by the debate about the existence of partial melting in the subducted slab (Pous *et al.*, 1995b; Vacher and Souriau, 2001; Souriau *et al.*, 2008).

Magnetotelluric data

The previous magnetotelluric (MT) data were acquired along a 180 km North–South profile, parallel to ECORS-Pyrenees seismic profile, and were composed of 16 BBMT sites (Pous *et al.*, 1995a; Ledo, 1996) collected between 1992 and 1993.

In 2009, new BBMT and LMT data were acquired in eight new sites along the ECORS profile. BBMT data were recorded using a Metronix ADU06 system and were processed using Metronix software (Friedrichs, 2003). LMT data were recorded using a LEMI system designed by the Lviv Centre of Institute of Space Research and processed using Birrp.5 (Chave and Thompson, 2004). The combination of BBMT and LMT data allows us to cover a period range between 0.001 and 20 000 s.

In order to determine the dimensionality of the regional structures and to obtain the regional impedance tensor we applied the Groom and Bailey (1989) method following the scheme of McNeice and Jones (2001). Geoelectric strike directions of individual sites were estimated from the MT impedance tensors at each site for all the periods with an error floor of 5% on the impedance tensor components

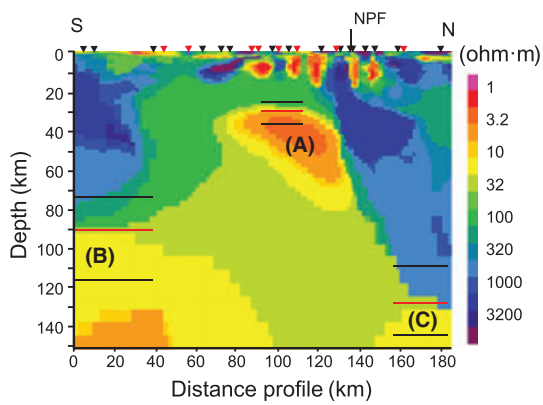

Fig. 2 Two-dimensional electrical resistivity model obtained from the joint inversion TE- and TM-mode for apparent resistivity and phases. Red lines show the position of the upper limit of A, B and C structures suggested in this work. Black lines show the possible variations of the upper limits, resulted from the sensitivity test, for structures A, B and C. Sites are represented by inverted triangles (red sites have BBMT and LMT data and black sites have BBMT data). NPF, North Pyrenean Fault.

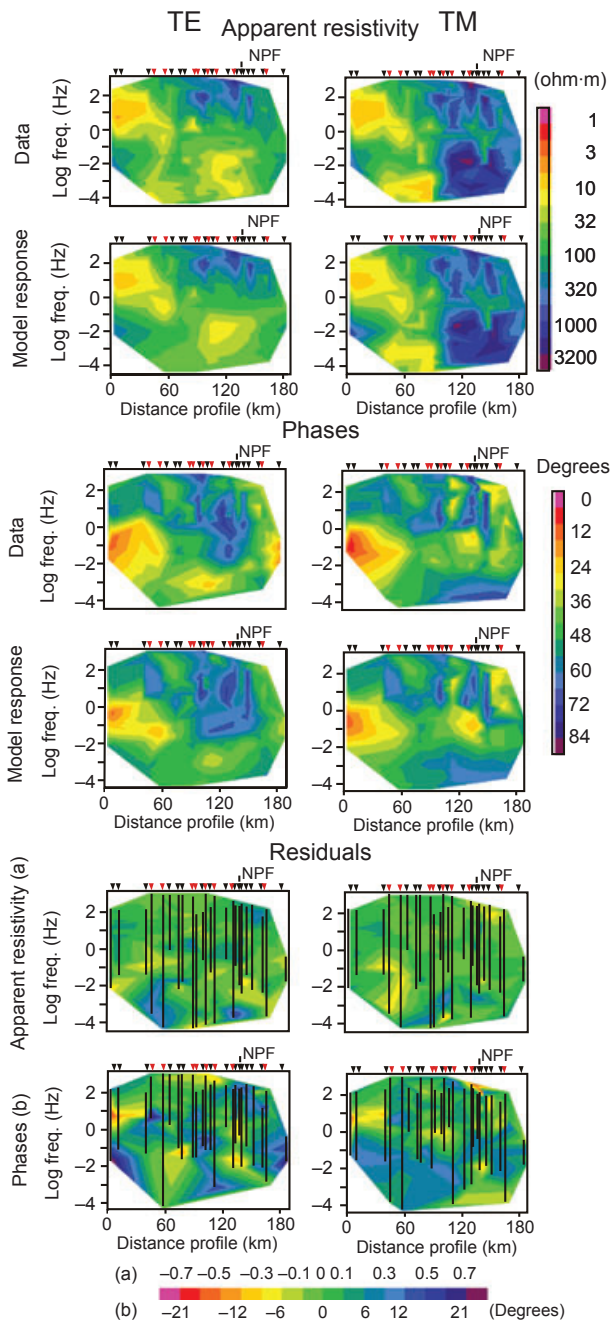

Fig. 3 Comparison between the observed data and the model responses. At the top the pseudosection of the apparent resistivity. At the middle the pseudosection of the phases. At the bottom the pseudosection of the residuals for the apparent resistivity (Model responses minus raw data divided by raw data) and the phases (Model responses minus raw data). In both cases for TE and TM mode (left and right respectively). Sites are represented by inverted triangles (red sites have BBMT and LMT data and black sites have BBMT data). Black lines in the residual pseudosection show the range of periods used for each site for the inversion. The misfit between the data and the model responses has an RMS value of 3.1.

(Fig. 1). Two-dimensional data dimensionality is assumed with a dominant East–West strike direction. These results were confirmed by the rotational invariants (Weaver *et al.*, 2000) using the WALDIM code (Martí *et al.*, 2009b). The static shift was corrected using seismic and well data (Lanaja and Querol, 1987) to fix the contact between the Mesozoic and the Palaeozoic basement following the method of Jones (1988).

Two-dimensional inversion

Two-dimensional inversion of the data was done using the algorithm of Rodi and Mackie (2001) using the TE- and the TM-mode of the apparent resistivity and phases. We fitted the logarithm of the apparent resistivity data to within 10% and the phases to within 2.86°. The model obtained is shown in Fig. 2. The residuals between the observed data and the model responses are random and no strong feature in the data is unexplained (Fig. 3).

The most striking features of the electrical resistivity model (Fig. 2) have been labelled A (associated to the IBSLC), B and C (associated to the asthenosphere below the Iberian and European plates, respectively). Nonlinear sensitivity tests (Ledo and Jones, 2005) were carried out to determine their upper and lower electrical resistivity bounds and the bounds on their top depths. Thus, the electrical resistivity for structure A should range between 3.2 and 5.6 ohm·m and its upper limit between 25 and 38 km depth. The electrical resistivity for structures B and C, assuming structures with homogeneous electrical resistivity, should range between 10 and 18 ohm·m. The upper limit of structure B should be between 75 and 115 km depth and between 110 and 145 km depth for C (Fig. 2). The low electrical resistivity values of structure A screen the structures below it but the nonlinear sensitivity test gave a minimum value of 30 ohm·m for the region below.

Discussion and conclusions

Subduction of the Iberian lower crust

Some authors have proposed the presence of partial melting in the IBSLC (Pous *et al.*, 1995b; Glover *et al.*, 2000; Ledo *et al.*, 2000; Partzsch *et al.*, 2000). Conversely, Vacher and Souriau (2001) suggest the presence of free water released from metamorphic reactions in the amphibolite to eclogite facies transition. This facies change could also account for the density

increase of the subducted slab. Gravimetric and geoid anomaly data accept both homogeneous and increasing density gradient of the subducted slab (Ledo *et al.*, 2000; Vacher and Souriau, 2001).

Our results suggest that the top of structure A is located at 30 km depth, 9 km deeper than the previous MT models (Pous *et al.*, 1995a; Ledo, 1996). This limit coincides with the lower–upper crust limit suggested by Muñoz (1992) (Fig. 4). At this depth, the geotherms calculated by Vacher and Souriau (2001) and Glover *et al.* (2000) intersect the granite wet solidus curve at ~630 °C (Fig. 5). Figure 5 also shows that the rocks of structure A would be in amphibolite facies and at temperatures high enough to melt if the rock composition is favourable and provided an aqueous fluid phase is present (Thompson and Connolly, 1995). The new characterization of structure A solves the problem associated with the hypothesis of partial melting present in the previous MT model (Fig. 5).

Geological data suggest that in high-grade metamorphic events, fluid-undersaturated conditions prevail (Clemens, 2006) as free water expelled by metamorphic reactions escapes (Bailey, 1990). When temperature conditions are high enough to cause partial melting, dehydration-melting reactions of hydrous minerals such as muscovite and biotite are the main reactions producing melts. Muscovite dehydration-melting takes place at temperatures near the granite wet solidus. This reaction releases a small amount of melt which does not migrate as the critical melt percentage is not achieved. Extensive melting only occurs at temperatures over 800 °C, generally associated with dehydration-melting reactions of biotite. The deeper levels outcropping in the North Pyrenean and Axial Zone suggest that the Pyrenean middle and lower crust is formed by pelites and greywackes metamorphosed during Variscan orogeny to amphibolite and granulite facies (Vielzeuf, 1984). Thus, the rocks contain a limited amount of water in their structures stored in the hydrous phases, mainly in muscovite and biotite at lower temperatures (amphibolite facies) and biotite at higher temperatures (granulite facies). If temperature is high enough to produce partial melting, as shown in Fig. 5, an undersaturated melt will be stable and the fluid will migrate to the melt as soon as it is formed.

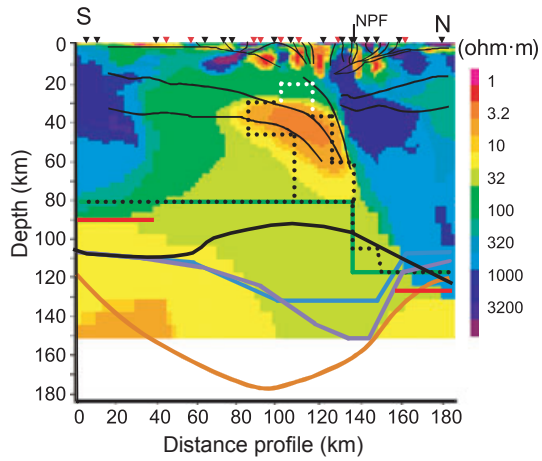

Fig. 4 Cross-section showing the main structural lithospheric features superimposed on the electrical resistivity model of Fig. 2. In the upper part, we have superimposed a simplification of the geological interpretation realized by Muñoz (1992). In the lower part, we have included the LAB suggested by different geophysical studies: Ledo *et al.* (2000) (green), Gunnell *et al.* (2008) (orange), Zeyen and Fernández (1994) (blue), Frizon de Lamotte *et al.* (2004) (purple). Black line is the LAB obtained from the S-waves model provided by Koulakov *et al.* (2009). Red lines are the LAB suggested in this work from BBMT and LMT data. Black points represent the equivalent of the structure A and the LAB obtained by Pous *et al.* (1995a) and Ledo (1996). White dashed line shows the difference of the upper limit of structure A between the previous and the new MT model.

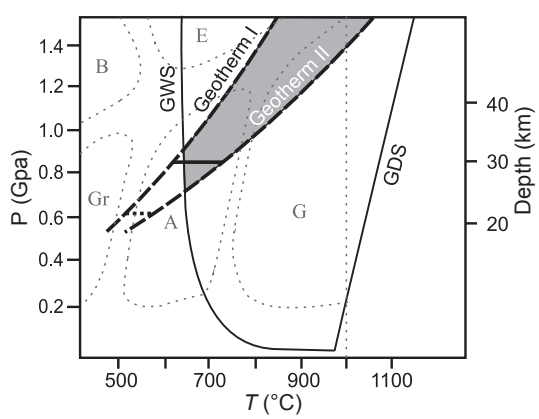

Fig. 5 Influence of the water on the melt temperature of the granite (common crustal rock). Geotherm I: Geotherm suggested by Vacher and Souriau (2001) based on the data and calculations of Zeyen and Fernández (1994). Geotherm II: Geotherm suggested by Glover *et al.* (2000). The grey zone gives the range of pressure and temperature where we have the appropriate conditions to obtain partial melting of a granite rock in the presence of free water. The dotted thick line and continuous thick line indicate the depth at which the previous MT model (Pous *et al.*, 1995a; Ledo, 1996) and the model obtained in this work, respectively, have the upper limit of the low electrical resistivity structure associated with the partial melting zone. Smooth dashed lines represent the main metamorphic facies of mafic crustal rocks (Modifies of Bucher and Frey, 1994). GWS, Granite wet solidus; GDS, Granite dry solidus; A, Amphibolite; B, Blueschist; E, Eclogite; G, Granulite and Gr, Greenschist. Modified from Thompson (1992).

Using the Modified Brick Layer Model (MBLM) suggested by Partzsch *et al.* (2000), the amount of

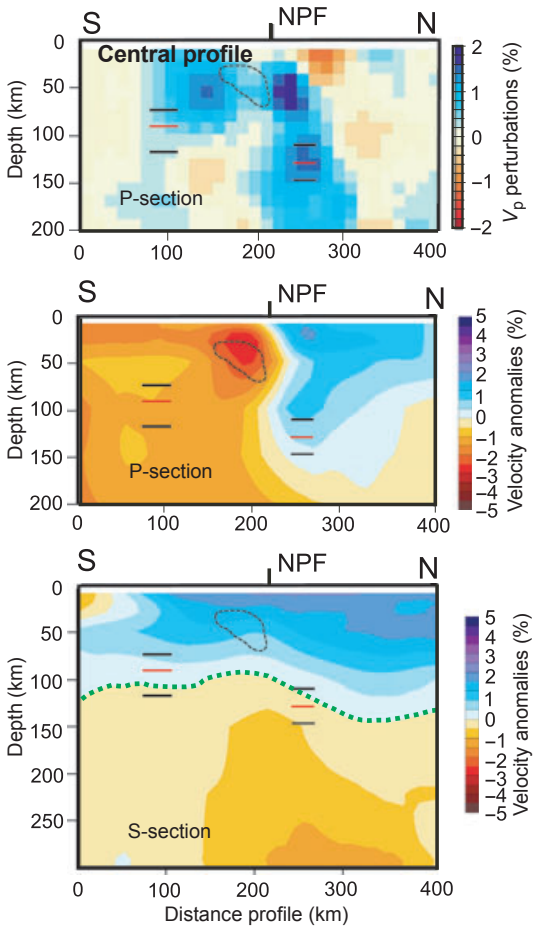

Fig. 6 Seismic tomography models from P-waves obtained by Souriau *et al.* (2008) (top) and Koulakov *et al.* (2009) (middle) and the S-wave model obtained by Koulakov *et al.* (2009) (bottom). Superimposed on the three models: the contour of the structure A, the low electrical resistivity structure associated with the IBSLC (black dashed line), and the LAB beneath Iberian and European plates (black and red lines) obtained in this work. In the S-waves model, the upper limit of the negative V_s anomaly associated with the LAB (green dashed line).

partial melting necessary to explain the low electrical resistivity of structure A is between 2.5 and 9 vol.%. This volume is far below the critical melt percentage (20 vol.%) necessary to migrate and rise to the surface.

Despite the disagreement between the two most recent studies from seismic tomography (Souriau *et al.*, 2008; Koulakov *et al.*, 2009) it should be noted that in both cases there is a local minimum of the V_p anomaly corresponding to structure A (Fig. 6), a structure associated with the IBSLC and the presence of partial melting. The absence of a major V_s anomaly in the S-waves model (Koulakov *et al.*, 2009) associated with structure A (Fig. 6) could be related to the small amount of partial melting and to the absence of a thermal anomaly in this region.

Lithosphere–Asthenosphere Boundary below the Iberian and the European plates

The electrical resistivity and the upper limit of structures B and C, associated with the asthenosphere, are consistent with the results obtained in other areas (Heinson, 1999; Korja, 2007; Jones *et al.*, 2010). The LAB below the IBSLC cannot be accurately determined due to the screening effect of the low electrical resistivity associated with partial melting.

Different geophysical studies have been done to constrain the LAB beneath Central Pyrenees, among them: topography, Bouguer anomaly and heat flow data (Zeyen and Fernández, 1994), BBMT data (Pous *et al.*, 1995a; Ledo, 1996), BBMT, geoid anomaly and Bouguer anomaly data (Ledo *et al.*, 2000) and topography, geoid anomaly, gravity and heat flow data (Gunnell *et al.*, 2008). Figure 4 shows the LAB suggested by these studies, jointly with the LAB suggested by Frizon de Lamotte *et al.* (2004) and by Koulakov *et al.* (2009) and they are all superposed on the MT model obtained in this work. The thermal and rheological model suggested by Tesauro *et al.* (2009) gives values in the order of 120 km for the LAB in the area. It is worth nothing that MT models show a European plate thicker than the Iberian one in agreement with the LAB observed in Koulakov *et al.* (2009) (Figs 4 and 6).The proposed depths for the LAB below the Iberian and European plates are similar in all the models. However, they significantly differ below the IBSLC up to 100 km, emphasizing the poor characterization of the LAB at the plate boundary.

In summary, the better characterization of the upper limit of the low electrical resistivity structure beneath the Central Pyrenees, structure A, jointly with the available geophysical and geological data of the region, allow us to reinforce the presence of partial melting in the IBSLC. In addition, structures B and C show a European plate thicker than the Iberian one and an asthenosphere with an electrical resistivity between 10 and 18 ohm·m.

Acknowledgements

We sincerely thank Professor Carlo Doglioni, Dr Toivo Korja, an anonymous reviewer and the Associate Editor for their useful comments on the manuscript. This research was funded by MAGBET (CGL2006-101660), PIER-CO2 (CGL2009-07604), MODES4D (CGL2007-66431-C02-02/BTE), INTEC-TOSAL (CGL2010-21968-C02-01) projects, Grup de Recerca de Geodinàmica i Anàlisi de Conques (2009SRG1198) and the Departamento de Universidades, Investigación y Sociedad de la Información de la Generalitat de Catalunya. We are

grateful to DIAS (Dublin Institute for Advanced Studies) for lending the LEMI equipments, to Dr Ivan Koulakov for providing the tomographical profiles and to the assistants in fieldwork, especially Victor Salinas.

References

Bailey, R.C., 1990. Trapping of aqueous fluids in the deep crust. *Geophys. Res. Lett.*, **17**, 1129–1132.

Beaumont, C., Muñoz, J.A., Hamilton, J. and Fullsack, P., 2000. Factors controlling the Alpine Evolution of the Central Pyrenees inferred from a comparison of observations and geodynamical models. *J. Geophys. Res.*, **105**(B4), 8121–8145.

Bucher, K. and Frey, M., 1994. *Petrogenesis of Metamorphic Rocks*, 6th edn. Srpinger-Verlag, Berlin.

Chave, A.D. and Thompson, D.J., 2004. Bounded influence estimation of magnetotelluric response functions. *Geophys. J. Int.*, **157**, 988–1006.

Choukroune, P. and ECORS-Pyrenees Team, 1989. The ECORS Pyrenean deep seismic profile reflection data and the overall structure of an orogenic belt. *Tectonics*, **8**(1), 23–39.

Clemens, J.D., 2006. Melting of the continental crust: fluid regimes, melting reactions and source-rock fertility. In: *Evolution and Differentiation of the Continental Crust* (M. Brown and T. Rushmer, eds), pp. 296–327. Cambridge University Press, Cambridge, UK.

ECORS-Pyrenees Team, 1988. The ECORS deep reflection seismic survey across the Pyrénées. *Nature*, **331**, 508–510.

Friedrichs, B., 2003. Mapros, Magnetotelluric Processing Software (Metronix). User Manual.

Frizon de Lamotte, D., Crespo-Blanc, A., Saint-Bezar, B., Fernàndez, M., Zeyen, H. and Ayarza, P., 2004. TRANSMED-TRANSECT I [Betics, Alboran Sea, Rif, Moroccan Meseta, High Atlas, Jbel Saghro, Tindouf basin]. In: *The TRANSMED Atlas - The Mediterranean Region from Crust to Mantle* (W. Cavazza, F. Roure, W. Spakman, G.M Stampfli and P.A. Ziegler eds), pp. 91–97. Springer, Berlin-Heidelberg.

Glover, P.W.J., Pous, J., Queralt, P., Muñoz, A., Liesa, M. and Hole, M.J., 2000. Integrated two-dimensional lithospheric conductivity modelling in the Pyrenees using field-scale and laboratory measurements. *Earth Planet. Sci. Lett.*, **178**, 59–72.

Groom, R.W. and Bailey, R.C., 1989. Decomposition of magnetotelluric impedance tensor in the presence of local three-dimensional galvanic distortion. *J. Geophys. Res.*, **94**, 1913–1925.

Gunnell, Y., Zeyen, H. and Calvet, M., 2008. Geophysical evidence of a missing lithospheric root beneath the Eastern Pyrenees: consequences for post-orogenic upflit and associated geomorphic signatures. *Earth Planet. Sci. Lett.*, **276**, 302–313.

Heinson, G., 1999. Electromagnetic studies of the lithosphere and asthenosphere. *Surv. Geophys.*, **20**, 229–255.

Jones, A.G., 1988. Static shift of magnetotelluric data and its removal in a sedimentary basin environment. *Geophysics*, **53**, 967–978.

Jones, A.G., Plomerova, J., Korja, T., Sodoudi, F. and Spakman, W., 2010. Europe from the bottom up: a statistical examination of the central and northern European lithosphere-asthenosphere boundary from comparing seismological and electromagnetic observations. *Lithos*, **120**, 14–29.

Korja, T., 2007. How is the European lithosphere imaged by magnetotellurics? *Surv. Geophys.*, **28**, 239–272, doi: 10.1007/s10712-007-9024-9.

Koulakov, I., Kaban, M.K., Tesauro, M. and Cloetingh, S., 2009. P and S velocity anomalies in the upper mantle beneath Europe from tomographic inversion of ISC data. *Geophys. J. Int.*, **179**, 345–366, doi:10.1111/j.1365246X.2009.04279.x.

Lanaja, J.M. and Querol, R., (Eds), 1987. *Contribución de la Exploración Petrolífera al Conocimiento de la Geología de España*. Instituto Geológico y Minero de España, Madrid, 465pp.

Ledo, J., 1996. *Aplicación del Método Magnetotelúrico al Estudio de la Estructura Litosférica de los Pirineos*. PhD thesis, Universitat de Barcelona, Spain, 196 pp.

Ledo, J. and Jones, A.G., 2005. Upper mantle temperature determined from combining mineral composition, electrical conductivity laboratory studies and magnetotelluric field observations: application to the Intermontane Belt, Northern Canadian Cordillera. *Earth Planet. Sci. Lett.*, **236**, 258–268.

Ledo, J., Ayala, C., Pous, J., Queralt, P., Marcuello, A. and Muñoz, A., 2000. New geophysical constrains on the deep structure of the Pyrenees. *Geophys. Res. Lett.*, **27**, 1037–1040.

Martí, A., Queralt, P., Roca, E., Ledo, J. and Galindo-Zaldívar, J., 2009a. Geodynamic implications for the formation of the Betic–Rif orogen from magnetotelluric studies. *J. Geophys. Res.*, **114**, B01103, doi:10.1029/2007JB005564.

Martí, A., Queralt, P. and Ledo, J., 2009b. WALDIM: a code for the dimensionality analysis of magnetotelluric data using the rotational invariants of the magnetotelluric tensor. *Comput. Geosci.*, **35**, 2295–2303.

McNeice, G. and Jones, A.G., 2001. Multisite, multifrequency tensor decomposition of magnetotelluric data. *Geophys. J. Int.*, **163**, 38–41.

Muñoz, J.A., 1992. Evolution of a continental collision belt: ECORS-Pyrenees cristal balanced cross-section. In: *Thrust Tectonics* (K.R. McClay, ed.), pp. 235–246. Chapman & Hall, London.

Muñoz, J.A., 2002. The Pyrenees. In: *The Geology of Spain*, (W. Gibbons and T. Moreno, eds), pp. 370–385, Geological Society of London, London.

Partzsch, G.M., Schilling, F.R. and Arndt, J., 2000. The influence of partial melting on the electrical behavior of the crustal rocks: laboratory examinations, model calculations and the geological interpretations. *Tectonophysics*, **317**, 189–203.

Pous, J., Ledo, J., Marcuello, A. and Daignières, M., 1995a. Electrical resistivity model of the crust and upper mantle from a magnetotelluric survey through the central Pyrenees. *Geophys. J. Int.*, **121**, 750–762.

Pous, J., Muñoz, A., Ledo, J. and Liesa, M., 1995b. Partial melting of subducted continental lower crust in the Pyrenees. *J. Geol. Soc. London*, **152**, 217–220.

Rodi, W. and Mackie, R.L., 2001. Non linear conjugate gradients algorithm for 2D magnetotelluric inversión. *Geohysics*, **66**, 174–187.

Selway, K., Hand, M., Heinson, G.S. and Payne, J.L., 2009. Magnetotelluric constrains on subduction polarity: reversing reconstruction models for Proterozoic Australia. *Geology*, **37**, 799–802, doi: 10.1130/G30175A.1.

Souriau, A. and Granet, M., 1995. A tomographic study of the lithosphere beneath the Pyrenees from local and teleseismic data. *J. Geophys. Res.*, **100**(B9), 18117–18134.

Souriau, A., Chevrot, S. and Olivera, C., 2008. A new tomographic image of the Pyrenean lithosphere from teleseismic data. *Tectonophysics*, **460**, 206–214.

Tesauro, M., Kaban, M.K. and Cloetingh, S.A.P.L., 2009. A new termal and rheological model of the European lithosphere. *Tectonophysics*, **476**, 478–495.

Thompson, A.B., 1992. Metamorphism and Fluids. In: *Understanding the Earth* (G.C. Brown, C.J. Hawkesworth and R.C.L. Wilson, eds), pp 222–248 . Cambridge University Press, Cambridge, UK.

Thompson, A.B. and Connolly, J.A.D., 1995. Melting of the continental crust: some thermal and petrological constraints on anatexis in continental collision zones and other tectonic settings. *J. Geophys. Res.*, **100**, 15565–15579.

Türkoğlu, E., Unsworth, M., Çağlar, I., Tuncer, V. and Avşar, Ü., 2008. Litho-

spheric structure of the Arabia-Eurasia collision zone in eastern Anatolia: magnetotelluric evidence for widespread weaking by fluids? *Geology*, **36**, 619–622, doi:10.1130/G24683A.1.

Unsworth, M., 2009. Magnetotelluric studies of active continent–continent collisions. *Surv. Geophys.*, **31**, 137–161.

Vacher, P. and Souriau, A., 2001. A three-dimensional model of the Pyrenean deep structure based on gravity modelling, seismic images and petrological constraints. *Geophys. J. Int.*, **145**, 460–470.

Vielzeuf, D., 1984. *Relations de phases dans les facies granulite et implications géodynamiques. L'*éxemple des granulites des Pyrénéés. Thèse Doctorat d'État, Université Blaise Pascal, Clermont-Ferrand, France, 288 pp.

Weaver, J.T., Agarwall, A.K. and Lilley, F.E.M., 2000. Characterisation of the magnetotelluric tensor in terms of its invariants. *Geophys. J. Int.*, **141**, 321–336.

Wei, W.B., Unsworth, M., Jones, A., Booker, J., Tan, H.D., Nelson, D., Chen, L.S., Li, S.H., Solon, K., Bedrosian, P., Jin, S., Deng, M., Ledo, J., Ray, D. and Roberts, B., 2001. Detection of widespread fluids in the Tibetan crust by magnetotelluric studies. *Science*, **292**, 716–718.

Zeyen, H. and Fernández, M., 1994. Integrated lithospheric modeling combining termal, gravity, and local isostasy analysis: application to the NE Spanish Geotransect. *J. Geophy. Res.*, **99**, 18089–18102.

Received 22 December 2010; revised version accepted 25 March 2011

Paper 2

Campanyà, J.; Ledo, J.; Queralt, P.; Marcuello, A.; Liesa, M.; Muñoz, J.A. 2012. New geoelectrical characterization of a continental collision zone in the West-Central Pyrenees: Constraints from long period and broadband magnetotellurics. *Earth and Planetary Science Letters*, **333-334**, 112-121. doi: 10.1016/j.epsl.2012.04.018.

Earth and Planetary Science Letters 333–334 (2012) 112–121

Contents lists available at SciVerse ScienceDirect

Earth and Planetary Science Letters

journal homepage: www.elsevier.com/locate/epsl

New geoelectrical characterisation of a continental collision zone in the West-Central Pyrenees: Constraints from long period and broadband magnetotellurics

Joan Campanyà [a,*], Juanjo Ledo [a], Pilar Queralt [a], Alex Marcuello [a], Montserrat Liesa [b], Josep A. Muñoz [a]

[a] Institut Geomodels, Departament de Geodinàmica i Geofísica, Universitat de Barcelona, C/Martí Franqués s/n, Barcelona 08028, Spain
[b] Departament de Geoquímica, Petrologia i Prospecció Geològica, Universitat de Barcelona, C/Martí Franqués s/n, Barcelona 08028, Spain

ARTICLE INFO

Article history:
Received 14 January 2012
Received in revised form
10 April 2012
Accepted 13 April 2012
Editor: P. Shearer

Keywords:
magnetotelluric
continental collision
lithosphere–asthenosphere boundary
Pyrenees
Variscan orogeny
partial melting

ABSTRACT

Continental collision dominates the development of a large number of mountain ranges on Earth. Although the geological evolution of these regions is highly studied, lithospheric-scale physical processes are less well characterised and their interpretations frequently differ. A new magnetotelluric profile crossing the West-Central Pyrenees with broadband and long period magnetotelluric data constrains the geoelectrical features of this continental collision zone confining the geological and physical processes that take place at a lithospheric scale. Three geoelectrical structures associated with partial melting and its melt migration are imaged for the first time in the West-Central Pyrenees suggesting an Iberian subducted lower crust reaching the depth of 70 km. This result, supported by an analysis of the thermal evolution of the Iberian subducted lower crust, reinforces the hypothesis of partial melting in this region. From the long period magnetotelluric data, the asthenosphere has been imaged as a geoelectrical structure with electrical resistivity values between 20 Ω m and 70 Ω m. The lithosphere–asthenosphere boundary close to the collision zone has been constrained between 90 km and 110 km depth below the Iberian plate and between 120 km and 160 km depth below the transition zone between plates and the European plate, in agreement with the previous geophysical data. Additionally, other geoelectrical anomalies imaged have been associated with an unexpected major Variscan boundary located below the Ebro basin, Silurian sediments and free fluids in the Gavarnie thrust, and with a thick sequence of Jurassic and Early Cretaceous sediments situated below the North Pyrenean Thrust Sheet.

1. Introduction

Tectonic processes dominate the development of the outermost layer of the Earth creating, shaping and destroying the lithosphere over millions of years. Continent–continent collision systems, responsible for the formation of large mountains ranges like the Himalaya and Alps, play a primary role in the development of the continents. To comprehend the physical and geological properties associated, several magnetotelluric (MT) studies have been made constraining their electrical resistivity (see Korja, 2007; Unsworth, 2009 for reviews). The use of broadband magnetotelluric (BBMT) and long period magnetotelluric (LMT) data allows characterising the geoelectrical structures at a lithospheric scale (i.e. Campanyà et al., 2011; Muller et al., 2009; Rosell et al., 2011).

A particular case of continental collision resulted in the Pyrenees during the Alpine orogeny. The significant amount of available geophysical data and the highly studied geological evolution make this mountain chain an ideal area to study continental collision systems (see Muñoz, 2002 for a review). However, two main questions concerning the lithospheric structure and its physical stage are still open: (i) the presence of partial melting in the Iberian Subducted Lower Crust (IBSLC) (Campanyà et al., 2011; Glover et al., 2000; Ledo 1996; Pous et al., 1995; Vacher and Souriau, 2001); (ii) the cause of the positive gravimetric anomaly observed below the North Pyrenean Thrust Sheets (NPTS) in the West-Central Pyrenees (Casas et al., 1997; Jammes et al., 2010; Pedreira et al., 2007; Vacher and Souriau, 2001). In addition, the lithosphere–asthenosphere boundary (LAB) in this region has been not accurately determined.

The geoelectrical information obtained from MT data is independent of other physical properties typically analysed in lithospheric studies like density, velocity anomaly and temperature (i.e. Gunnell et al., 2008; Koulakov et al., 2009; Tesauro et al., 2009).

* Corresponding author. Tel.: +34 93 4035913.
E-mail addresses: jcampanya@ub.edu, joancampillov@gmail.com (J. Campanyà).

0012-821X/$ - see front matter © 2012 Elsevier B.V. All rights reserved.
http://dx.doi.org/10.1016/j.epsl.2012.04.018

Comparison of the MT data with independent available geological and geophysical data better determines the geological and physical processes of the study area (i.e. Jegen et al., 2009; Jones et al., 2010; Pinto et al., 2010).

The new BBMT and LMT data collected in the West-Central Pyrenees, jointly with the latest results obtained in the Central Pyrenees by Campanyà et al. (2011) and the available geological and geophysical data, are used to constrain the geological and geophysical processes of the West-Central Pyrenees and the lateral variations along the strike in the Pyrenees. More specifically, this study has the aim to characterise the physical properties and the depth of the partial melting region associated with the IBSLC, the LAB and the electrical resistivity of the asthenosphere. At crustal depths, we constrain the geoelectrical structures related with the presence of fluids, sediments and graphite, associating them with the respective geological processes. The results obtained in the West-Central Pyrenees help us to deepen our understanding about the continental collisions and the related physical properties.

2. Geological setting

The Pyrenees resulted from the convergence between the Iberian and European plates from Late Cretaceous to Middle Eocene times (Olivet, 1996; Rosenbaum et al., 2002). The Pyrenean orogen extends from the western Mediterranean to the Atlantic Ocean along northern Iberia. Its shows significant along-strike differences in the structural style at a crustal scale, which resulted from the inversion of a previous segmented rift system in continuation with the Bay of Biscay (Beaumont et al., 2000; Muñoz, 2002; Roca et al., 2011). In spite of such differences, the Iberian continental crust subducted below the European crust, even in the Cantabrian region where the Pyrenean orogenic system is adjacent to oceanic crust of the Bay of Biscay. Crustal structure has been imaged by the numerous deep reflection and wide angle seismic profiles acquired all along the orogen since the 80s (Choukroune et al., 1989; Fernández Viejo et al., 2000; Ferrer et al., 2008; Pulgar et al., 1996; Roca et al., 2011). Among them, the best known crustal section is the ECORS profile across the Central Pyrenees (Choukroune et al., 1989; Muñoz, 1992). In that section, the crustal structural geometry consists of an asymmetric double-wedge orogenic system with the southern Pyrenees being wider and involving more than 100 km of the shortening of the total estimated shortening of 165 km across the entire orogen (Beaumont et al., 2000). In the West-Central Pyrenees, the structural style changes with respect the ECORS section. Here, the basement thrust sheets of the interior part of the chain are imbricated instead of being piled on the top of each other to form an antiformal stack, as observed in the ECORS section (Muñoz, 2002; Teixell, 1998). Crustal structure is not so well constrained, as the only existing deep reflection seismic profile (ECORS-Arzacq) only registered the northern part of the orogen (Teixell, 1998). Southwards, the south directed imbricated basement thrust sheets forming the middle and higher part of the orogen, the southern Pyrenees are characterised by a wide sinclynorium. This sinclynorium supports the Paleogene piggy-back basin filled by an up to 8 km thick succession from the Middle Eocene turbidites to the Upper Oligocene continental conglomerates (Hogan and Burbank, 1996; Teixell, 1996). These sediments, together with a prekinematic succession of the Upper Cretaceous-Middle Eocene limestones, were detached into the Triassic evaporites and transported southwards on top of the Palogene to lower Miocene sediments of the Ebro foreland basin (Millán, 1996). The West-Central Pyrenees MT profile, herein presented, traverses the western part of the Palaeozoic basement-involved Gavarnie thrust sheet, which is the upper unit of the basement stack of thrust sheets (also referred as the Axial Zone). Northwards, south-directed thrusts inverted Early Cretaceous extensional basins which were floored by an exhumed continental mantle (Jammes et al., 2009, 2010). North-directed thrust structures are restricted, along the MT profile, to the north-Pyrenean thrust front which transported northwards the Mauleon basin on top of the Arzacq basin, part of the Aquitanian foreland (Teixell, 1998).

To comprehend the geological and geophysical features observed in the West-Central Pyrenees, two main tectonic processes prior to the continental collision between the Iberian and European plates should be taken into account. Firstly, the opening of the Bay of Biscay during the Early Cretaceous rifting, which caused extreme crustal thinning and the rise of lower crustal and/or upper mantle rocks to upper and middle crustal depths (Jammes et al., 2010; Pedreira et al., 2007). Secondly, the Variscan orogenic and post-orogenic events that yielded a structural grain to the Iberian crust before the Cretaceous extensional event (Martínez Catalán et al., 2009).

3. Previous geophysical studies

Several geophysical studies have been taken into account to interpret the geoelectrical structures observed in the West-Central Pyrenees MT profile.

3.1. ECORS Arzac deep seismic profile

ECORS Arzac deep seismic profile was undertaken close to the northern part of the West-Central Pyrenees MT profile (Fig. 1). The geological interpretations of this profile (Muñoz, 2002; Teixell, 1998) are similar between them for the upper and middle crust and suggest a similar depth for the Moho. The Moho depth is 30 km to 35 km below the European crust and 30 km to 50 km below the Iberian crust, deepening progressively from south to north. These differences are related with the IBSLC and the stacking of the basement thrust sheets in the Southern Pyrenees (Muñoz, 2002). The main discrepancies between the two geological interpretations (Muñoz, 2002; Teixell, 1998) are in

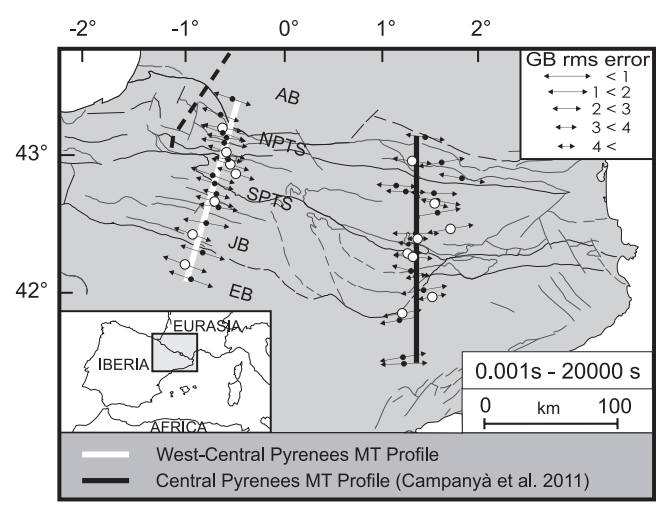

Fig. 1. Location of the MT stations in a structural sketch of West-Central and Central Pyrenees. Black spots correspond to stations with BBMT data and white spots stations with BBMT and LMT data. The arrows indicate the strike direction of each site. The lengths of the arrows indicate the compatibility of the data to the assumed two-dimensional strike direction. Strikes for Central Pyrenees from Campanyà et al. (2011). Black dashed line corresponds to the ECORS Arzac deep seismic profile. EB, Ebro Basin; JB, Jaca Basin; SPTS, South Pyrenean Thrust Sheets; NPTS, North Pyrenean Thrust Sheets; AB, Aquitaine Basin. Thin lines divide the main geological units of the region.

constraining the geological structures located in the transition zone between plates, and the depth of the IBSLC.

3.2. Tomographic models and seismic activity

A recent tomographic model from teleseismic P-waves travel times (Amaru et al., 2008), including crustal corrections before the inversion, suggests the presence of a negative V_p anomaly associated with the transition zone between the Iberian and European plates as well as below the Iberian plate. The tomographic model of Souriau et al. (2008) which includes crustal corrections, also suggests the presence of a low V_p anomaly associated with the transition between the Iberian and European plates below the West-Central Pyrenees MT profile. Similarly, a new tomographic model (Koulakov et al., 2009), including crustal corrections, has obtained a negative V_p anomaly beneath the West-Central Pyrenees. Koulakov et al. (2009) also shows an S-waves model of the region with a negative V_s anomaly in the transition zone between the Iberian and European plates and a negative V_s anomaly at the deeper parts which could be related with the asthenosphere.

The seismic activity in the West-Central Pyrenees is basically located at upper and middle crustal depths, down to 20 km depth, below the northern Pyrenees although seismic activity is occasionally registered at greater depths (Koulakov et al., 2009; Rigo et al., 2005; Ruiz et al., 2006).

3.3. Geoelectrical models

Using BBMT data, Ledo (1996) and Pous et al. (1995) showed a two-dimensional geoelectrical model of the Central Pyrenees and Ledo et al. (2000) obtained a three-dimensional electrical resistivity model of the Central and West-Central Pyrenees. The three models were obtained by trial-and-error fitting of the data. Although there were numerous BBMT sites located in the Central Pyrenees there were only three in the West-Central Pyrenees. Recently, Campanyà et al. (2011), constrain the geoelectrical structures of the Central Pyrenees, from BBMT and LMT data, using a two dimensional inversion code. All the MT models show a low electrical resistivity structure associated with the IBSLC and various studies (Campanyà et al., 2011; Glover et al., 2000; Ledo, 1996; Pous et al., 1995) support the hypothesis of partial melting to explain the low electrical resistivity values associated with the IBSLC. At the deepest part of the models, a low electrical resistivity structure is related with the asthenosphere and therefore maps the lithosphere–asthenosphere boundary (LAB) below the Iberian and European plates, suggesting a thicker European plate close the collision zone.

3.4. Gravity data

Several gravity studies have been made in the West-Central Pyrenees (Casas et al., 1997; Jammes et al., 2010; Pedreira et al., 2007; Vacher and Souriau, 2001). In all cases, the presence of high density bodies located at upper and middle crustal depths below the NPTS is constrained but whether these bodies represent lower crustal or upper mantle rocks is still a matter of debate. Gravity models are compatible with the IBSLC, but the studies do not agree with the physical processes associated, in particular with the presence or absence of partial melting.

3.5. Thermal studies

There are no specific thermal studies done in the West-Central Pyrenees. In a large scale, Tesauro et al. (2009) obtained the geotherms of the European lithosphere from 60 km to greater depths. They show no significant thermal differences between the Central and West-Central Pyrenees. Zeyen and Fernández (1994) suggest that the thermal equilibration below the Central Pyrenees has already ended. Due to the proximity of the MT profiles, it is assumed that the geotherms used by Campanyà et al. (2011) in the Central Pyrenees are approximately valid for the West-Central Pyrenees.

For the deepest parts of the lithosphere, Tesauro et al. (2009) show a slight increase in the temperature at the southern part of the West-Central Pyrenees which could be interpreted as the thinning of the lithosphere.

Taking into account the previous geophysical information two main debates are open in the West-Central Pyrenees. Firstly, the IBSLC below the West-Central Pyrenees is currently accepted by the geological and geophysical communities but the depth of the crustal root and the associated physical processes are still in debate. Secondly, the source of the high density body at upper/middle crustal depths observed below the NPTS. About the LAB, prior MT and thermal studies not accurately constrain it below the West-Central Pyrenees suggesting an European plate thicker than the Iberian plate, close to the collision zone.

4. New magnetotelluric data

New MT data were acquired in the summer 2010 at 20 sites along a 140 km profile crossing the West-Central Pyrenees. The BBMT data were recorded in all the sites and LMT data at seven of the BBMT sites. On average, the distance between the sites with BBMT data and between the sites with BBMT+LMT data is 6.5 km and 15 km, respectively. Recording times were at least three days for sites with BBMT data and fifteen days for sites with LMT data.

The BBMT data were recorded using a Metronix ADU06 and ADU07 systems and processed using Metronix software (Friedrichs, 2003). The LMT data were recorded using a LEMI system designed by the Lviv Center of the Institute of Space Research and processed using Birrp.5 (Chave and Thompson, 2004). Remote reference has been used between sites located in the northern half of the profile and sites located in the southern half of this in order to avoid the effect of a possible local noise. The combination of BBMT and LMT data allows us to cover a period range between 0.001 s and 20,000 s. The LEMI stations allow us to also constrain the induction arrows for the LMT data, covering a period range between 50 s and 20,000 s. Anomalous phases, $>90^\circ$, have been observed in the TE mode for periods longer than 10 s (see sites 15, 17, 18, 19 in Fig. S1) in the sites located at the NPTS. To explain these anomalous data we use the arguments suggested by Lezaeta and Haak (2003). They demonstrate that in a 2D/3D geoelectrical model the presence of current channelling affects the magnetotelluric data on the TE mode causing phases greater than 90° as happen in the anomalous data observed in the West-Central Pyrenees. Current channelling in this region can be explained by low electrical resistivity structures associated with the shear zones presents in the NPTS. These data were not considered during the inversion procedure.

Geoelectric strike direction was computed from the MT impedance tensors at each site for all the periods applying the Groom and Bailey (1989) method, following the scheme of McNeice and Jones (2001). A 5% error floor on the impedance tensor components is applied. The rotational invariants (Weaver et al., 2000) using the WALDIM code (Martí et al., 2009) have been used to corroborate the results. Two-dimensional data is constrained with a 106°, clockwise from North, strike direction. Fig. 1 shows the fit of the data in assume a geoelectrical strike direction close to 106° for each site for all period bands and compare with the strike obtained in the Central Pyrenees by Campanyà et al. (2011). Fig. S2 shows the geoelectrical strike direction split in two period bands (BBMT: 0.001–100 s and LMT: 10–20,000 s). In both cases two dimensional geoelectrical structures

with a 106° strike direction is constrained. In addition, the induction arrows obtained from the LMT data corroborate this strike (Fig. 2). The static shift was corrected using the depth of the contact between the Mesozoic and Palaeozoic basement obtained from Lanaja and Querol (1987) which is observed as an important increase of the electrical resistivity in the TM mode. In 80% of the cases the static shift values are less than half decade and in no case exceed a decade and a half.

5. Two-dimensional inversion

Two-dimensional inversion of the TE and TM mode apparent resistivity and phase data was made using the algorithm of Rodi and Mackie (2001). An error of 10% for the apparent resistivity and 2.86° for the phases has been used for the inversion process giving equal weight to all data type (Gabàs and Marcuello, 2003). The MT model was obtained using smooth curves with 10% $D+$ values (Beamish and Travassos, 1992). This type of smoothing force the curves to have coherence between apparent resistivity and phases. Fig. S3 shows the obtained smooth curves superimposed on the raw data. The smooth curves have been used in the two-dimensional inversion process with the aim to avoid unnecessary structures as much as possible and fill the gap in sites where some periods have no data (Fig. S1). These periods without data are usually related with low natural signal.

The two-dimensional inversion process using BBMT and LMT data does not clearly obtain geoelectrical structures at the bottom of the model, below the white dashed line in Fig. 3. To better constrain this region we fixed the obtained electrical resistivity values until 110 km depth and inverted using only LMT data (between 1000 s and 20,000 s). The MT model of the West-Central Pyrenees profile, obtained from the two inversion process, is shown in Fig. 3.

To compare data and model responses, in all the cases we use the responses of the final model shown in Fig. 3. Fig. 4 compares the smooth data used for the inversion and model responses in pseudosection format for the apparent resistivities and phases and shows the misfit between them. Fig. S1 shows the curves of the raw data and the model responses. The misfit between the data and the model responses has an RMS value of 1.6 for the smooth curves and 2.3 for raw data. The RMS of the second inversion process, using only periods between 1000 s and 20,000 s, decrease from 4.1, MT model obtained from the first inversion process, to 2.7, definitive MT model.

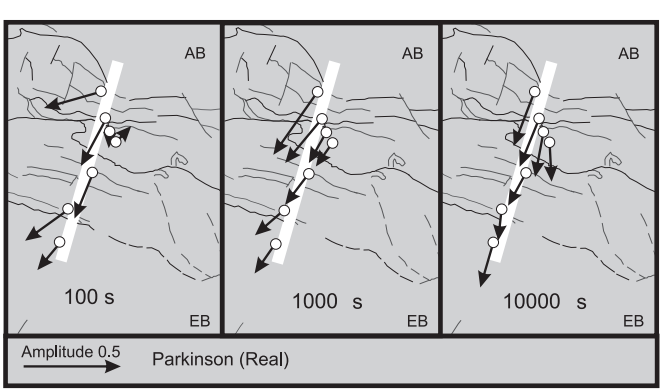

Fig. 2. Structural sketch of the West-Central Pyrenees profile showing the transfer functions for the sites with LMT data for periods of 100 s, 1000 s and 10,000 s. Parkinson (real) arrow point to the low electrical resistivity structure observed from the site.

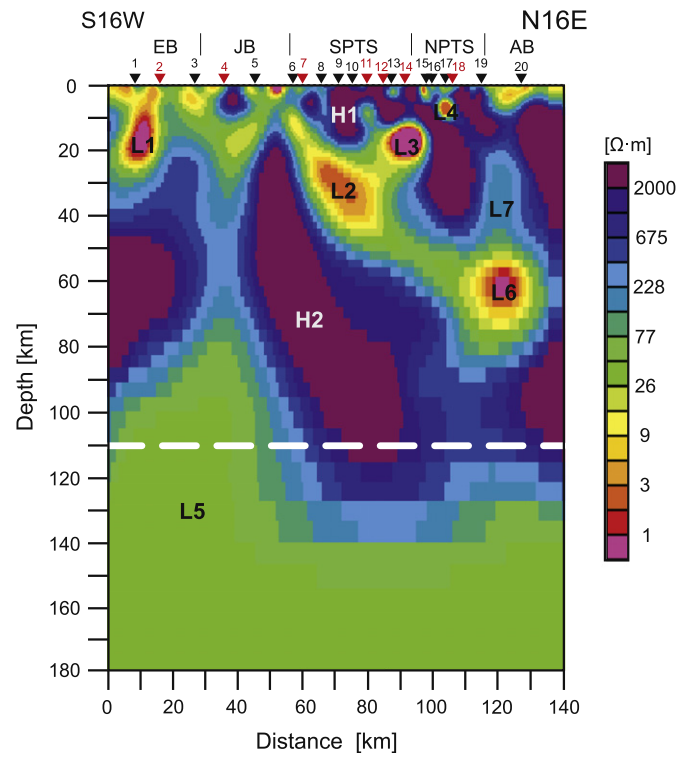

Fig. 3. Two-dimensional electrical resistivity model obtained from the joint inversion of the TE and TM modes for apparent resistivities and phases. Sites are represented by inverted triangles (in red sites with BBMT and LMT data and in black sites with BBMT data). The white dashed line delineates the region of the MT model obtained using only long period data and fixing the electrical resistivity of model above. EB, Ebro Basin; JB, Jaca Basin; SPTS, South Pyrenean Thrust Sheets; NPTS, North Pyrenean Thrust Sheets; AB, Aquitaine Basin. Labels L1–L7 and H1, H2 denote model features discussed and interpreted in text. (For interpretation of the references to color in this figure legend, the reader is referred to the web version of this article.)

5.1. Electrical resistivity structures

The main geoelectrical features have been labelled "L" for low electrical resistivity structures and "H" for high electrical resistivity structures (Fig. 3). The model contains seven main low electrical resistivity structures. Features L1, L3 and L4 are associated with upper and mid-crustal structures while features L2, L6 and L7 are located at lower crustal and upper mantle depths. L5 structure is related with the asthenosphere. Two main high electrical resistivity structures are observed in the model, H1 located at crustal depth and H2 located on the transition zone between the Iberian and European plates. The areas with high electrical resistivity values at the edges of the MT model are associated to the Iberian (south) and European (north) lithospheres.

5.2. Non-linear sensitivity test

A non-linear sensitivity test was carried out to justify the presence of the geoelectrical structures and appraise the resolution of the MT model. The test consists on comparing the differences between the final MT model (Fig. 3) and a modified model, where some properties of the studied feature have been changed such as the geometry of the structures or their electrical resistivities. If the difference between the MT model responses is greater than 10% on the apparent resistivity or 2.86° on the phase the modification is excluded. Conversely, if the differences are lower than the values exposed we assume that the data have no resolution to constrain between the final MT model and the

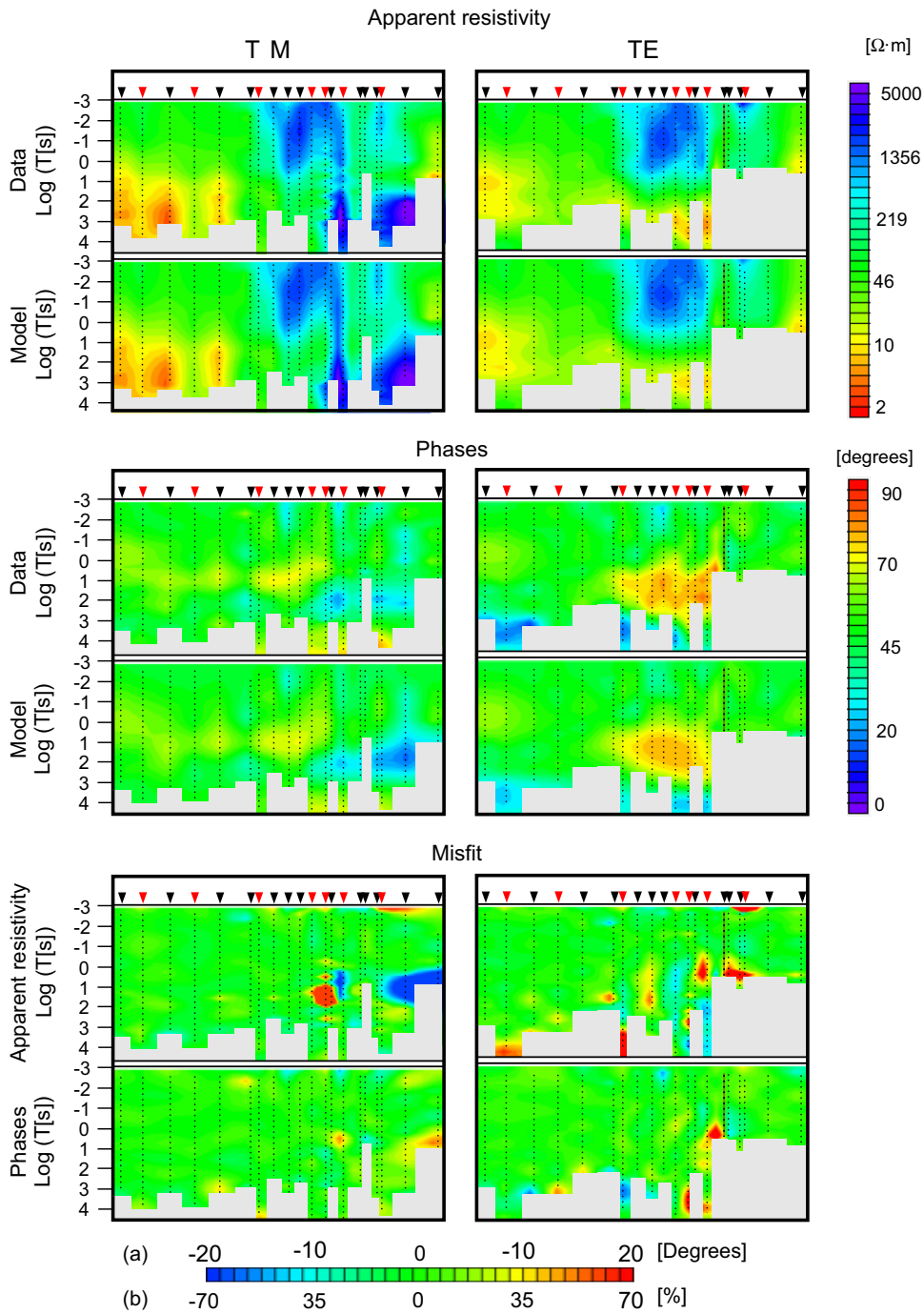

Fig. 4. Comparison between the smoothed data and the model responses in pseudosection format for the apparent resistivity (top) and phases (middle). The misfit between smoothed data and model responses is shown in pseudosection format to the bottom. In both cases for TM and TE mode (left and right respectively). Sites are represented by inverted triangles (in red sites with BBMT and LMT data and in black sites with BBMT data). Tiny black dots are smooth data points used for the inversion. (For interpretation of the references to color in this figure legend, the reader is referred to the web version of this article.)

modified model and the change is accepted due we have no resolution to differentiate between the two models.

Firstly, the requirement of all the main geoelectrical structures obtained by the inversion procedure has been examined. The main geoelectrical structures have been removed changing their electrical resistivity values by the neighbour's electrical resistivity values. Differences in model responses are in all the cases greater than 10% on the apparent resistivity and/or great than 2.86° on the phases and we observe a significant increase of the RMS in some sites suggesting that all the structures here analysed are necessary to explain the data (Fig. S4). Fig. S4 also shows which sites and periods are sensitive to the main geoelectrical structures.

Secondly, once we know which structures are necessary to explain the data, we use the sensitivity test to constrain the resolution we have on these structures. The sensitivity test constrains that the electrical resistivity values of L1 should range between 0.6 Ω m and 0.8 Ω m, their upper boundary between 9 km and 11 km depth and the lower boundary between 19 km and 24 km depth. This test also suggests that structure L1 has no lateral continuity. The electrical resistivity of L2 should range between 2 Ω m and 6 Ω m and their upper boundary between 21 km and 28 km depth. Assuming a

homogeneous electrical resistivity of 2 Ω m for L2 structure the sensitivity test constrain that the lower boundary of L2 could reach 65 km depth, connecting with L6. L3 electrical resistivity should range between 0.1 Ω m and 0.2 Ω m and its upper boundary between 13 km and 15 km depth. The electrical resistivity values of L4 should range between 2 Ω m and 6 Ω m. The electrical resistivity values of L5 should range between 20 Ω m and 70 Ω m and its upper boundary should be located between 90 km and 110 km depth below the Iberian plate and between 120 km and 160 km depth below the transition zone between plates and the European plate. The electrical resistivity values of L6 should range between 1 Ω m and 20 Ω m. L7 structure has electrical resistivity values between 90 Ω m and 250 Ω m and its upper boundary should range between 22 km and 28 km depth. This large range of electrical resistivity values for structures L6 and L7 is associated with the lack of long periods for the TE data on the stations located above them.

For the high electrical resistivity features the non-linear sensitivity test suggests values of the electrical resistivity between 5000 Ω m and 15,000 Ω m for H1 and between 6000 Ω m and 20,000 Ω m for H2. It also indicates that the upper boundary of H2 should be between 15 km and 17 km depth.

6. Discussion

6.1. Interpretation of the main geoelectrical structures

6.1.1. Low electrical resistivity structure below Ebro Basin (L1)

The L1 feature is a sub-vertical low electrical resistivity structure completely buried below the Ebro Basin at upper and middle crustal depths. As there is not any structure affecting the sedimentary infilling of the Ebro Basin above this electrical resistivity structure, it could be associated with the previous Variscan tectonic events. According to the subdivision of the Variscan belt (see Martínez Catalán et al., 2007 for further information) it could correspond to the prolongation of the limit between the Western Asturian Leonese and Central Iberian zones below the Ebro Basin. In the southwester part of the Iberian plate, the Variscan boundaries between the different geological units (the Ossa Morena Zone (OMZ) and the South Portugese Zone, (SPZ) and between the Ossa Morena and the Central Iberian Zones (CIZ)) have been imaged by MT data (Da Silva et al., 2007; Muñoz et al., 2008; Pous et al., 2004, 2011). These boundaries appear as sub-vertical low electrical resistivity structures located in the upper and middle crust, similar to the L1 structure, and are associated with graphite. In the Cantabrian mountains, Pous et al. (2001) also associate a low electrical resistivity structure located at lower crustal depths with graphite as a signature of the Variscan convergence. Due to the geoelectrical similarities within the Variscan boundaries constrained in the Iberian plate and the geoelectrical similarities with L1, we suggest the presence of graphite along a major Variscan tectonic boundary to explain the low electrical resistivity values of the structure L1. Nevertheless, more geophysical studies should be done to better constrain this buried structure which has not been previously observed below the Ebro Basin.

6.1.2. Iberian subducted lower crust (L2, L6 and L7).

From the non-linear sensitivity test, L2 and L6 structures can be connected suggesting that they can be associated with the same geological processes. Comparison of the MT model with the geological models of Muñoz (2002) and Teixell (1998) suggests that L2 and L6 structures are related with the IBSLC (Fig. 5). The top of the L2 structure coincides with the top of the low electrical resistivity structure constrained by Ledo et al. (2000).

As suggested by Campanyà et al. (2011), Glover et al. (2000), Ledo et al. (2000) and Pous et al. (1995), partial melting could be the cause of the low electrical resistivity values observed in the IBSLC. Following the analysis of Campanyà et al. (2011), a percentage of partial melting between 4% and 15% melt from dehydration-melting of muscovite, which take place at temperatures of 650 °C or higher, can explain the low electrical resistivity values observed in L2 (Partzsch et al., 2000). At the position of L6, Tesauro et al. (2009) suggest a temperature around 900 °C. This temperature is sufficiently high to produce dehydration-melting of muscovite and also of biotite, which produce extensive melting (Patiño Douce and Harris, 1998; Vielzeuf and Holloway, 1988). From the Modified Brick Layer Model of Partzsch et al. (2000), the amount of partial melting necessary to explain the electrical resistivity range of L6 obtained from the non-linear sensitivity test is between 3% and 27%, being between 15% and 25% to explain the electrical resistivity values which better fit the data, between 1.3 Ω m and 2 Ω m. From Arzi (1978), melt percentage of 20% or higher can be associated with melt migration, suggesting 20% melting as the critical melt percentage to have melt migration. The melt values obtained in L6 can exceed the 20%, suggesting that melt migration is possible as the critical melt percentage can be exceeded. A small amount of melt could have migrated upwards from the IBSLC explaining the decrease of the electrical resistivity values in the European upper mantle associated with L7 structure.

As we know that convergence of the Pyrenees stopped 20 million years ago, we have calculated the thermal evolution of the IBSLC (Fowler, 2005, p. 283) in order to estimate the time needed to heat the structure L6 at a temperature over 850 °C. According to Fig. 5, the Iberian subducted lower crust is represented by a 10 km thick layer (Pedreira et al., 2003) at an initial temperature of 500 °C (Zeyen and Fernández, 1994). In the deeper parts, the IBSLC is located in the European upper mantle between 60 km and 70 km depth. The European upper mantle temperatures at these depths are 900 °C and 1000 °C, respectively (Tesauro et al., 2009).

From these parameters, temperatures above 850 °C for the structure L6 would be achieved between 3 Ma and 16 Ma after the end of the orogeny. This means that, at present there could be melt mostly produced by dehydration melting of biotite, which occurs at a temperature higher than 850 °C (Vielzeuf and Holloway, 1988). This result agrees with the idea of assuming magmatic activity in order to explain the decrease of electrical resistivity observed in L7. The presence of earthquakes located around structure L7 is consistent with this hypothesis (Fig. 5).

The low electrical resistivity structures L2, L6 and L7 coincide with the negative velocity anomaly of P and S waves observed in the different tomographic models (Amaru et al., 2008; Koulakov et al., 2009; Souriau et al., 2008) (Fig. 6). The decrease of the P and S velocity anomalies is consistent with the presence of partial melting in the IBSLC.

The location of the geoelectrical structure L6 also agrees with the deep seismic activity, suggesting that the IBSLC was subducted down until the depth of 70 km (Fig. 5). These results are consistent with the lower boundary of the negative S-wave velocity anomaly suggested by Koulakov et al. (2009) (Fig. 6).

6.1.3. Intersection between major faults (L3)

L3 structure is located at the transition zone between the Iberian and European plates, close to the intersection between the Gavarnie thrust and the North Pyrenean sole thrust as suggested by the geological models (Fig. 5). Observing the low electrical resistivity area dipping north above structure L3 we suggest to modify the geometry of the Gavarnie thrust at depth with respect to the previous geological models increasing its dip and associating L3 with the branching between the Gavarnie and the sole thrusts (Fig. 5). The presence of the Silurian sediments, previously

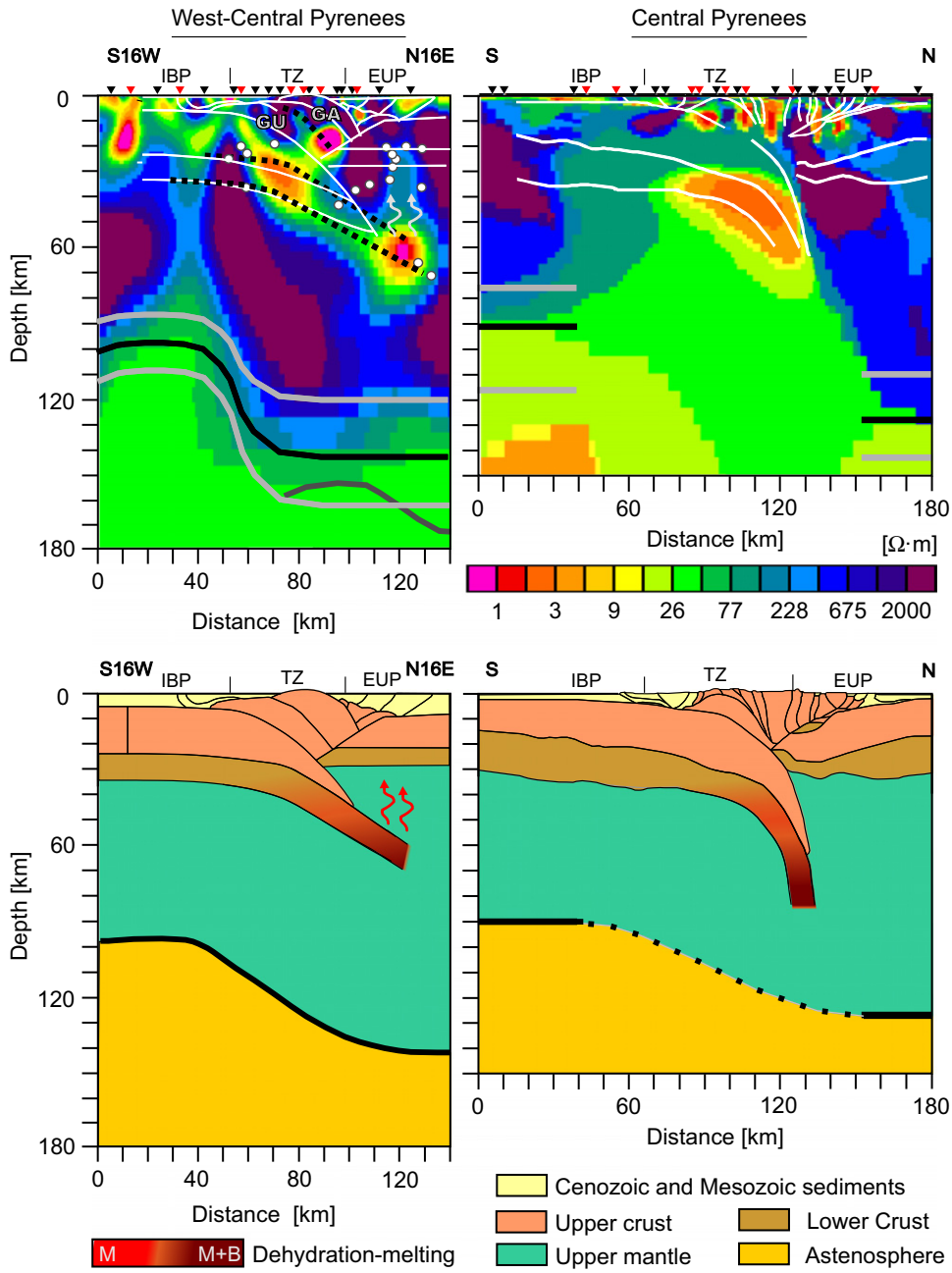

Fig. 5. (Top) West-Central Pyrenees MT model (left) compared with Central Pyrenees MT model (right) obtained by Campanyà et al. (2011). White lines correspond to the geological model suggested by Muñoz (2002) in West-Central Pyrenees and by Muñoz (1992) in Central Pyrenees. Black dashed lines are modifications on the geological models suggested by MT results. White–red spots are the earthquakes recorded below 20 km depth from Koulakov et al. (2009). Green arrows indicate melt migration. Black line: lithosphere–asthenosphere boundary suggested by MT results. Grey lines: resolution constraining the lithosphere asthenosphere boundary from the sensitivity test. Red line: lithosphere–asthenosphere boundary from Koulakov et al. (2009) in West-Central Pyrenees. GA, Gavarnie thrust; GU, Guarga thrust. (Bottom) Cartoon geological sections of the West-Central and the Central Pyrenees with our interpretation of the partial-melting region and the LAB. In the dehydration melting process: M when Muscovite produce dehydration melting and M+B when Muscovite and Biotite produce dehydration melting. Black dashed interpolated LAB below Central Pyrenees due no resolution in this region. (For interpretation of the references to color in this figure legend, the reader is referred to the web version of this article.)

deformed by the Variscan orogeny, together with the presence of fluids explains the low electrical resistivity values observed in L3.

6.1.4. Jurassic and Early Cretaceous sediments (L4)

The low electrical resistivity values of L4 are explained by the presence of a great amount of Jurassic and Early Cretaceous sediments preserved in the Lower Cretaceous extensional basins that resulted from the opening of the Bay of Biscay, and were subsequently inverted during the continental collision. The anomalous phases observed for the sites located in this area (sites 15, 17, 18 and 19), see Fig. S1, delineate a region which is coincident with the positive gravimetric anomaly observed in the West-Central Pyrenees (Casas et al., 1997; Jammes et al., 2010; Pedreira et al., 2007; Vacher and Souriau, 2001), but no evidences directly relate both anomalies with the same cause.

6.1.5. Lithosphere–asthenosphere boundary, LAB (L5)

The MT model obtained suggests a LAB between 90 km and 110 km depth below the Iberian plate and between 120 km and 160 km depth below the transition zone between plates and the

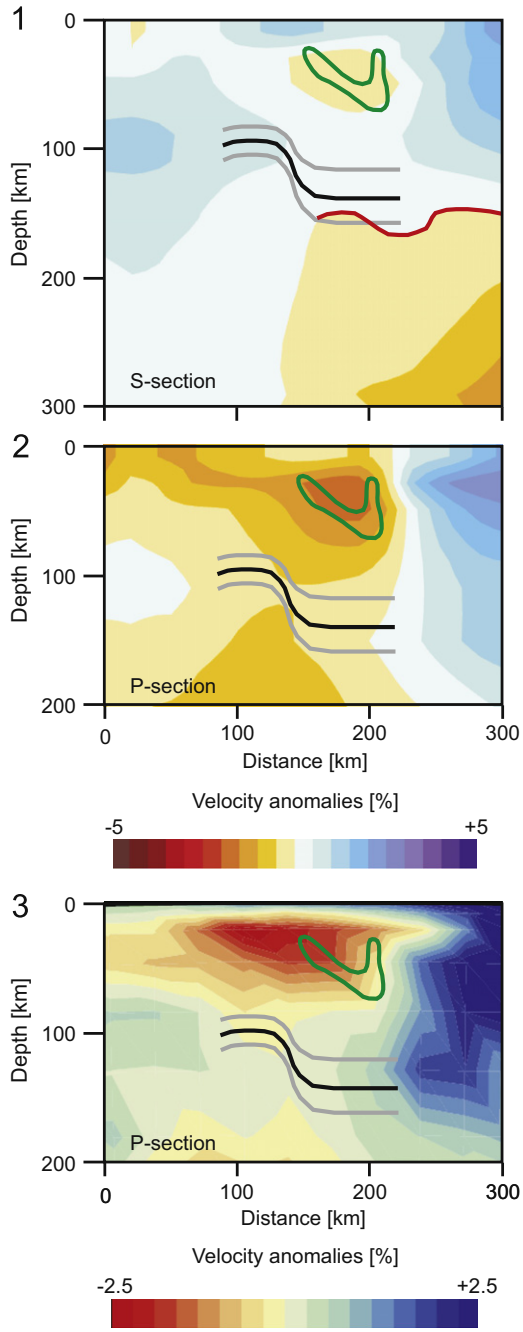

Fig. 6. Seismic tomography model from S-waves obtained by Koulakov et al. (2009) (1). Seismic tomography models from P-waves obtained by Koulakov et al. (2009) (2) and Amaru et al. (2008) (3). Superimposed on the three models: contour of the partial melting region (green line) and geoelectrical lithosphere–asthenosphere boundary (black and grey lines) obtained in this work. In panel (1), the upper boundary of the negative *Vs* anomaly is associated with the seismic lithosphere–asthenosphere boundary (red line). (For interpretation of the references to color in this figure legend, the reader is referred to the web version of this article.)

European plate close to the collision zone. The electrical resistivity values of the asthenosphere have been constrained between 20 Ω m and 70 Ω m. These values are consistent with the results obtained in other areas (Heinson, 1999; Jones et al., 2010; Korja, 2007). The S-wave model of Koulakov et al. (2009) suggests a deep negative V_s anomaly that can be associated with the asthenosphere. The V_s seismic LAB below the transition zone between plates and below the European plate agrees with the geoelectrical LAB observed in the MT model. Below the Iberian plate, the variations of the V_s anomalies are smooth and the V_s seismic LAB is not well constrained (Fig. 6). In Tesauro et al. (2009), the thermal LAB below the West-Central Pyrenees associated with the geotherm of 1200 °C is approximately at the depth of 130 km, a bit shallower below the Iberian plate, being also consistent with the geoelectrical LAB obtained in this study.

6.1.6. High electrical resistivity structures H1 and H2

The H1 high electrical resistivity structure is located at the shallower depths of the transition zone between plates and is associated with the basement-involved Guarga and Gavarnie thrust sheets. These thrust sheets are separated by a low electrical resistivity region dipping north associated with the Gavarnie thrust. The H2 high electrical resistivity structure is located below L3 structure showing that in West-Central Pyrenees our MT model has enough resolution to constrain the bottom of the partial melting area. The H2 structure is related with rocks from the Iberian lower crust and upper mantle without the presence of partial melting.

6.2. Comparison between the West-Central and Central Pyrenees MT models

Comparison between the two models will be carried out following the main five regions in which the sections have been divided: the Iberian subducted lower crust, the Iberian plate, the European plate, the structures located at the transition zone between plates at upper and middle crustal depths and the lithosphere–asthenosphere boundary. The West-Central and the Central Pyrenees MT models with the same electrical resistivity colour scale are shown in Fig. 5.

6.2.1. Iberian subducted lower crust

In this region, the main difference between the two models is the dip of the low electrical resistivity structure associated with the partial melting of the IBSLC. In Central Pyrenees, the maximum dip of the IBSLC is 80°, while in West-Central Pyrenees 35°. This difference is associated with a greater amount of subduction in the Central Pyrenees and the gravity effect associated, which increased the dip of the subducted plate.

The upper boundary and the electrical resistivity values of the area which resulted from partial melting by muscovite dehydration-melting are similar in both models. Conversely, the geoelectrical properties associated with partial melting by dehydration-melting of biotite and melt migration in the Central Pyrenees are screened due to the verticality of the IBSLC and cannot be compared.

6.2.2. Iberian plate

In the West-Central Pyrenees, the Iberian plate shows electrical resistivity values around 50 Ω m at upper and middle crustal depths. These values are lower than those observed for the lower crust which are around 200 Ω m. On the other hand, at the Central Pyrenees the electrical resistivity values for the Iberian upper, middle and lower crusts are similar and around 100 Ω m. In West-Central Pyrenees the electrical resistivity is increasing below the Moho, associated with the upper-mantle, but not in Central Pyrenees. Another important difference is the presence of the L1 structure below the Ebro basin in the West-Central Pyrenees profile and the absence of such structure in the Central Pyrenees profile. This difference and the lack of geoelectrical structures with electrical resistivity values as those from L1 in the Central Pyrenees suggest that the possible major Variscan tectonic boundary inferred in the West-Central Pyrenees profile would be located southwards from the southern edge of the Central Pyrenees MT profile, as suggested by structural interpretations (Martínez Catalán et al., 2007 and references therein).

6.2.3. European plate

The European plate displays high electrical resistivity values at crustal an upper mantle depths in both models, but a significant difference is observed. The region with low electrical resistivity values associated with L7 structure at the upper mantle depths in the West-Central Pyrenees, which has been interpreted as melt migration, is not observed in the Central Pyrenees where the vertical dip of the partial melting region in the IBSLC could be interpreted as the overlap between in situ partial melting and migrated melt.

6.2.4. Transition zone between plates at upper and middle crustal depths

In the Central Pyrenees, the transition zone between plates is dominated by low electrical resistivity structures containing fluids and Silurian sediments in the sub-vertical faults of the Axial Zone whereas in the West-Central Pyrenees. The transition zone between plates is dominated by high electrical resistivity values associated with the Guarga and Gavarnie basement-involved thrust sheets, at shallow depths, and by a very low electrical resistivity structure (L3), between 10 km and 20 km depth. The L3 structure is associated with the Gavarnie thrust and it is branching with the North Pyrenean sole thrust. The dip of the structures to the west, preserving higher structural levels in the West-Central Pyrenees than in the Central Pyrenees and the related westward termination of the Axial Zone antiformal stack of the Central Pyrenees would explain these differences. The sub-vertical low electrical resistivity structures in the northern limb of the Axial Zone antiformal stack in the Central Pyrenees are equivalent to the L3 structure in the West-Central Pyrenees.

6.2.5. Lithosphere–asthenosphere boundary (LAB)

The geoelectrical LAB observed in both models suggests an European plate thicker than the Iberian plate close to the collision zone. No major changes are observed in the depth of the LAB along the strike, which suggest similar form and depth of the LAB between these regions going from 90 km depth below the Iberian Plate to 130 km depth below the European plate. The similar electrical resistivity values obtained for the asthenosphere below the two profiles suggest no big differences on the asthenosphere properties below the Pyrenees.

7. Conclusions

The new geoelectrical characterisation of the West-Central Pyrenees constrains the electrical resistivity values at lithospheric scale. The main structure is the partial melting zone associated with the IBSLC which shows, for the first time in the Pyrenees, the geoelectrical responses associated with partial melting by dehydration of muscovite (L2 structure), dehydration-melting of muscovite and biotite (L6 structure) and melt migration (L7 structure). The coincidence of the bottom of structure L6 with the bottom of the negative V_s anomaly and the presence of seismic activity in this region suggest extending the IBSLC to the depth of 70 km. The coherence between the results gives new arguments in favour of the partial melting of the IBSLC.

The unexpected sub-vertical low electrical resistivity feature L1, constrained at upper-middle crustal depths and completely buried below the Ebro Basin, has been associated with graphite in a major Variscan tectonic boundary zone. In the transition zone between plates, at crustal depths, a low electrical resistivity structure associated with the presence of Silurian sediments and fluids suggests that there is an increase of the dip of the Gavarnie thrust at depth. The electrical resistivity values observed in the NPTS (L4) has been associated with the presence of Jurassic and Early Cretaceous sediments and we associate the anomalous phases observed in this region with the presence of current channelling in a 2D/3D region in the two-dimensional MT profile. The geoelectrical LAB constrained below the West-Central Pyrenees suggest an European plate thicker than the Iberian plate, close to the collision zone.

Comparison between the West-Central and Central Pyrenees MT profiles shows major differences related with the transition zone between plates and the Iberian plate. The steeper dip of the IBSLC indicates greater shortening in the Central Pyrenees. For the Iberian plate, the values of electrical resistivity in the Central Pyrenees are more homogeneous than those in the West-Central Pyrenees where geoelectrical differences between the upper-middle crust and lower crust depth and between crustal and upper mantle depths are observed. In the transition zone between plates, at crustal depths, differences in the location of the Silurian sediments preferentially located along major faults are explained by the west plunge of the basement-involved thrusts observed in the core of the Pyrenees. In the European plate, the low electrical resistivity values observed at upper mantle depths, which have been attributed to magma batches, are not observed in the Central Pyrenees due the vertical dip of the IBSLC. The geoelectrical LAB constrained below the two MT profiles suggest an European plate thicker than the Iberian plate, close to the collision zone, and an asthenosphere with electrical resistivity values between 10 Ω m and 70 Ω m.

Acknowledgements

We sincerely thank the anonymous reviewers and the Associate Editor for their useful comments on the original version of the manuscript. This research was funded by MAGBET (CGL2006-101660), PIERCO2 (CGL2009-07604), MODES4D (CGL2010-66431-CO2-02/BTE), INTECTOSAL (CGL2010-21968-CO2-01) projects, Grup de Recerca de Geodinàmica i Anàlisi de Conques (2009SRG1198) and the Departament d'Universitats, investigació i Societat de la informació de la Generalitat de Catalunya. We are grateful to Dr. Ivan Koulakov and to Dr. Maisha Amaru for providing tomographical profiles, to the land owners and the Parc national des Pyrénées, which allow us to install the sites in their fields, and to the fieldwork assistants, especially to Roger Llopart.

Appendix A. Supplementary material

Supplementary data associated with this article can be found in the online version at http://dx.doi.org/10.1016/j.epsl.2012.04.018.

References

Amaru, M., Spakman, W., Villaseñor, A., Sandoval, S., Kissling, E., 2008. A new absolute arrival time data set for Europe. Geophys. J. Int. 173, 465–472.
Arzi, A.A., 1978. Critical phenomena in the rheology of partially melted rocks. Tectonophysics 44, 173–184.
Beamish, D., Travassos, J.M., 1992. The use of the D+ solution in magnetotelluric interpretation. J. Appl. Geophys. 29, 1–19.
Beaumont, C., Muñoz, J.A., Hamilton, J., Fullsack, P., 2000. Factors controlling the Alpine evolution of the central Pyrenees inferred from a comparison of observations and geodynamical models. J. Geophys. Res. 105, 8121–8145.
Campanyà, J., Ledo, J., Queralt, P., Marcuello, A., Liesa, M., Muñoz, J.A., 2011. Lithospheric characterization of the Central Pyrenees based on new magnetotelluric data. Terra Nova 23, 213–219.
Casas, A., Kearey, P., Rivero, L., Adam, C.R., 1997. Gravity anomaly map of the Pyrenean region and a comparison of the deep geological structure of the western and eastern Pyrenees. Earth Planet. Sci. Lett. 150, 65–78.
Chave, A.D., Thompson, D.J., 2004. Bounded influence estimation of magnetotelluric response functions. Geophys. J. Int. 157, 988–1006.
Choukroune, Team, Ecors, 1989. The ECORS Pyrenean deep seismic profile: reflection data and the overall structure of the orogenic belt. Tectonics 8, 23–39.

Da Silva, N.V., Mateus, A., Santos, F.A.M., Almeida, E.P., Pous, J., 2007. 3-D electromagnetic imaging of a Palaeozoic plate-tectonic boundary segment in SW Iberian Variscides (S Alentejo, Portugal). Tectonophysics 445, 98–115.
Fernández Viejo, G., Gallart, J., Pulgar, J.A., Gallastegui, J., Dañobeitia, J.J., Córdoba, D., 2000. Seismic signature of Variscian and Alpine tectonics in NW Iberia: crustal structure of the Cantabrian Mountains and Duero basin. J. Geophys. Res. 105, 3001–3018.
Ferrer, O., Roca, E., Benjumea, B., Muñoz, J.A., Ellouz, N., 2008. the MARCONI Team, 2008. The deep seismic reflection MARCONI-3 profile: role of extensional Mesozoic structure during the Pyrenean contractional deformation at the eastern part of the Bay of Biscay. Mar. Pet. Geol. 25 (8), 714–730.
Fowler, C.M.R., 1994. The solid Earth: an introduction to global geophysics. Cambridge University Press, United Kingdom (second edition, 2005).
Friedrichs, B., 2003. Mapros, Magnetotelluric Processing Software (Metronix). User Manual.
Gabàs, A., Marcuello, A., 2003. The relative influence of different types of magnetotelluric data on joint inversions. Earth Planets Space 55, 243–248.
Glover, P.W.J., Pous, J., Queralt, P., Muñoz, A., Liesa, M., Hole, M.J., 2000. Integrated two-dimensional lithospheric conductivity modelling in the Pyrenees using field-scale and laboratory measurements. Earth Planet. Sci. Lett. 178, 59–72.
Groom, R.W., Bailey, R.C., 1989. Decomposition of magnetotelluric impedance tensor in the presence of local three-dimensional galvanic distortion. J. Geophys. Res. 94, 1913–1925.
Gunnell, Y., Zeyen, H., Calvet, M., 2008. Geophysical evidence of a missing lithospheric root beneath the Eastern Pyrenees: consequences for post-orogenic upflit and associated geomorphic signatures. Earth Planet. Sci. Lett. 276, 302–313.
Heinson, G., 1999. Electromagnetic Studies of the Lithosphere and Asthenosphere. Surv. Geophys. 20, 229–255.
Hogan, P.J., Burbank, D.,.W., 1996. Evolution of the Jaca piggyback basin and emergence of the External Sierras, southern Pyrenees. In: Friend, P., Dabrio, C. (Eds.), Tertiary Basins of Spain: The Stratigraphic Record of Crustal Kinematics 6. Cambridge University Press, Cambridge, pp. 153–160.
Jammes, S., Manatschal, G., Lavier, L., Masini, E., 2009. Tectonosedimentary evolution related to extreme crustal thinning ahead of a propagating ocean: the example of the western Pyrenees. Tectonics 28, TC4012.
Jammes, S., Lavier, L., Manatschal, G., 2010. Extreme crustal thinning in the Bay of Biscay and the Western Pyrenees: from observations to modeling. Geochem. Geophys. Geosyst. 11, Q10016.
Jegen, M.D., Hobbs, R.W., Tarits, P., Chave, A., 2009. Joint inversion of marine magnetotelluric and gravity data incorporating seismic constraints. Preliminary results of sub-basalt imaging off the Faroe Shelf. Earth Planet. Sci. Lett. 282, 47–55.
Jones, A.G., Plomerova, J., Korja, T., Sodoudi, F., Spakman, W., 2010. Europe from the bottom up: a statistical examination of the central and northern European lithosphere–asthenosphere boundary from comparing seismological and electromagnetic observations. Lithos 120, 14–29.
Korja, T., 2007. How is the European lithosphere imaged by magnetotellurics? Surv. Geophys. 28, 239–272, http://dx.doi.org/10.1007/s10712-007-9024-9.
Koulakov, I., Kaban, M.K., Tesauro, M., Cloetingh, S., 2009. P and S velocity anomalies in the upper mantle beneath Europe from tomographic inversion of ISC data. Geophys. J. Int. 179 (1), 345–366, http://dx.doi.org/10.1111/j.1365246X.2009.04279.x.
Lanaja, J.M., Querol, R. (Eds.), 1987. Instituto Geológico y Minero de España. 465 pp.
Ledo, J., 1996. Aplicación del método magnetotelúrico al estudio de la estructura litosférica de los Pirineos. Ph.D. Thesis. Universitat de Barcelona, Spain, 196 pp.
Ledo, J., Ayala, C., Pous, J., Queralt, P., Marcuello, A., Muñoz, A., 2000. New geophysical constrains on the deep structure of the Pyrenees. Geophys. Res. Lett. 27, 1037–1040.
Lezaeta, P., Haak, V., 2003. Beyond magnetotelluric decomposition: induction, current channelling, and magnetotelluric phases over 90°. J. Geophys. Res. 108 (B6), 2305, http://dx.doi.org/10.1029/2001JB000990.
Martí, A., Queralt, P., Ledo, J., 2009. WALDIM: a code for the dimensionality analysis of magnetotelluric data using the rotational invariants of the magnetotelluric tensor. Comput. Geosci. 35 (12), 2295–2303.
Martínez Catalán, J.R., Arenas, R., Díaz García, F., Gómez Barreiro, J., González Cuadra, P., Abati, J., Castiñeiras, P., Fernández-Suárez, J., Sánchez Martínez, S., Andonaegui, P., González Clavijo, E., Díez Montes, A., Rubio Pascual, F.J., Valle Aguado, B., 2007. Space and time in the tectonic evolution of the northwestern Iberian Massif. Implications for the comprehension of the Variscan belt. In: Hatcher Jr., R.D., Carlson, M.P., McBride, J.H., Martínez Catalán, J.R. (Eds.), 4-D Framework of Continental Crust, vol. 200. Geological Society of America Memoir, Boulder, Colorado, pp. 403–423.
Martínez Catalán, J.R., Arenas, R., Abati, J., Sánchez Martínez, S., Díaz García, F., Fernández-Suárez, J., González Cuadra, P., Castiñedas, P., Gómez Barreiro, J., Díez Montes, A., González Clavijo, E., Rubio Pascoal, F., Andonaegui, P., Jefferies, T.E., Alcock, J.E., Díez Fernández, R., López Carmona, A., 2009. A rootless suture and the loss of the roots of a mountain chain: the Variscan Belt of NW Iberia. C. R. Geoci. 341 (2–3), 114–126.
McNeice, G., Jones, A.G., 2001. Multisite, multifrequency tensor decomposition of magnetotelluric data. Geophys. J. Int. 163, 38–41.
Millán, H., 1996. Estructura del frente de cabalgamiento surpirenaico en las Sierras Exteriores Aragonesas. Unpublished Ph.D. Thesis. Univ. de Zaragoza.
Muller, M.R., Jones, A.G., Evans, R.L., Grutter, H.S., Hatton, C., Garcia, X., Hamilton, M.P., Miensopust, M.P., Hutchins, D., Fourie, C.J., Jelsma, H.A., Evans, S.F., Aravanis, T., Pettit, W., Webb, S.J., Wasborh, J., 2009. Lithospheric structure, evolution and diamond prospectivity of the Rehoboth Terrane and western Kaapvaal Craton, southern Africa: constraints from broadband magnetotellurics. Lithos 112, 93–105.
Muñoz, J.A., 1992. Evolution of a continental collision belt: ECORS-Pyrenees crustal balanced cross-section. In: McClay, K.R. (Ed.), Thrust Tectonics. Chapman and Hall, London, pp. 235–246.
Muñoz, J.A., 2002. The Pyrenees, in the geology of Spain. In: Gibbons, W., Moreno, T. (Eds.), Geological Society of London, London, pp. 370–385.
Muñoz, G., Mateus, A., Pous, J., Heise, W., Santos, F.M., Almeida, E., 2008. Unraveling middle-crust conductive layers in Paleozoic Orogens through 3D modeling of magnetotelluric data: the Ossa-Morena Zone case study (SW Iberian Variscides). J. Geophys. Res.—Solid 113, B6.
Olivet, J.L., 1996. La cinematique de la plaque Iberique. Bull. Centres Res. Explor. Prod. Elf Aquitaine 20, 131–195.
Patiño Douce, A.E., Harris, N., 1998. Experimental constraints on Himalayan Anatexis. J. Petrol. 39, 689–710.
Partzsch, G.M., Schilling, F.R., Arndt, J., 2000. The influence of partial melting on the electrical behavior of the crustal rocks: laboratory examinations, model calculations and the geological interpretations. Tectonophysics 317, 189–203.
Pedreira, D., Pulgar, J.A., Gallart, J., Díaz, J., 2003. Seismic evidence of Alpine crustal thickening and wedging from the western Pyrenees to the Cantabrian Mountains (north Iberia). J. Geophys. Res. 108 (B4), 2204, http://dx.doi.org/10.1029/2001JB001667.
Pedreira, D., Pulgar, J.A., Gallart, J., Torne, M., 2007. Three-dimensional gravity and magnetic modeling of crustal indentation and wedging in the western Pyrenees-Cantabrian Mountains. J. Geophys. Res.—Solid 112, B12.
Pinto, L.G.R., de Padua, M.B., Ussami, N., Vitorello, I., Padilha, A.L., Braitenberg, C., 2010. Magnetotelluric deep soundings, gravity and geoid in the south Sao Francisco craton: geophysical indicators of cratonic lithosphere rejuvenation and crustal underplating. Earth Planet. Sci. Lett. 297, 423–434.
Pous, J., Muñoz, J.A., Ledo, J., Liesa, M., 1995. Partial melting of subducted continental lower crust in the Pyrenees. J. Geol. Soc., London 152, 217–220.
Pous, J., Queralt, P., Marcuello, A., 2001. Magnetotelluric signature of the Western Cantabrian Mountains. Geophys. Res. Lett. 28, 1795–1798.
Pous, J., Muñoz, G., Heise, W., Melgarejo, J.C., Quesada, C., 2004. Electromagnetic imaging of Variscan cristal structures in SW Iberia: the role of interconnected graphite. Earth Planet. Sci. Lett 217, 435–450.
Pous, J., Poyatos, D.M., Heise, W., Santos, F.M., Galindo-Zaldivar, J., Ibarra, P., Pedrera, A., Ruiz-Constan, A., Anahnah, F., Goncalves, R., Mateus, A., 2011. Constrains on the crystal structure of the internal Variscan Belt in SW Europe: a magnetotelluric transect along the eastern part of Central Iberian Zone, Iberian Massif. J. Geophys. Res.—Solid Earth 116, B02103.
Pulgar, J.A., Gallart, J., Fernández Viejo, G., Pérez Estaún, A., Álvarez Marrón, J., 1996. the ESCI Group, 1996. Seismic image of Cantabrian Mountains in the western extension of the Pyrenean belt from integrated reflection and refraction data. Tectonophysics 264, 1–19.
Rigo, A., Souriau, A., Dubos, N., Sylvander, M., Ponsolles, C., 2005. Analysis of the seismicity in the central part of the Pyrenees (France), and tectonic implications. J. Seismol. 9, 211–222.
Roca, E., Muñoz, J.A., Ferrer, O., Ellouz, N., 2011. The role of the Bay of Biscay Mesozoic extensional structure in the configuration of the Pyrenean orogen: constraints from the MARCONI deep seismic reflection survey. Tectonics 30, TC2001.
Rodi, W., Mackie, R.L., 2001. Non linear conjugate gradients algorithm for 2D magnetotelluric inversion. Geophysics 66, 174–187.
Rosell, O., Martí, A., Marcuello, A., Ledo, J., Queralt, P., Roca, E., Campanyà, J., 2011. Deep electrical resistivity structure of the northern Gibraltar Arc (western Mediterranean): evidence of lithospheric slab break-off. Terra Nova 23, 179–186.
Rosenbaum, G., Lister, G.S., Duboz, C., 2002. Reconstruction of the tectonic evolution of the western Mediterranean since the Oligocene. In: Rosenbaum, G., Lister, G.S. (Eds.), Reconstruction of the Evolution of the Alpine-Himalayan Orogen. J. Virtual Explorer 8, 107–130.
Ruiz, M., Gallart, J., Díaz, J., Olivera, C., Pedreira, D., López, C., González-Cortina, J.M., Pulgar, J.A., 2006. Seismic activity at the western Pyrenean edge. Tectonophysics 412, 217–235.
Souriau, A., Chevrot, S., Olivera, C., 2008. A new tomographic image of the Pyrenean lithosphere from teleseismic data. Tectonophysics 460, 206–214.
Teixell, A., 1996. The Ansó transect of the southern Pyrenees: basement and cover thrust geometries. J. Geol. Soc. London 153, 301–310.
Teixell, A., 1998. Crustal structure and orogenic material budget in the west central Pyrenees. Tectonics 17, 395–406.
Tesauro, M., Kaban, M.K., Cloetingh, S.A.P.L., 2009. A new thermal and rheological model of the European lithosphere. Tectonophysics 476, 478–495.
Unsworth, M., 2009. Magnetotelluric studies of active continent–continent collisions. Surv. Geophys. 31, 137–161.
Vacher, P., Souriau, A., 2001. A three-dimensional model of the Pyrenean deep structure based on gravity modelling, seismic images and petrological constraints. Geophys. J. Int. 145, 460–470.
Vielzeuf, D., Holloway, J.R., 1988. Experimental determination of the fluid-absent melting relations in the pelitic system. Consequences for crustal differentiation. Contrib. Mineral. Petrol. 98 (1988), 257–276.
Weaver, J.T., Agarwall, A.K., Lilley, F.E.M., 2000. Characterisation of the magnetotelluric tensor in terms of its invariants. Geophys. J. Int. 141, 321–336.
Zeyen, H., Fernández, M., 1994. Integrated lithospheric modeling combining termal, gravity, and local isostasy analysis: application to the NE Spanish Geotransect. J. Geophys. Res. 99, 18089–18102.

Paper 3

Campanyà, J.; Ledo, J.; Queralt, P.; Marcuello, A., Jones, A.G., 2013. Processing of Magnetotelluric data using inter-station tensor relationships. *Geophysical Journal International*. (Under review)

Geophysical Journal International

Processing of Magnetotelluric data using inter-station tensor relationships

Journal:	*Geophysical Journal International*
Manuscript ID:	GJI-S-12-0764
Manuscript Type:	Research Paper
Date Submitted by the Author:	27-Nov-2012
Complete List of Authors:	Campanyà, Joan; Universitat de Barcelona, GEOMODELS Research Institute, Departament de Geodinàmica i Geofísica, Facultat de Geologia. Ledo, Juanjo; Universitat de Barcelona, GEOMODELS Research Institute, Departament de Geodinàmica i Geofísica, Facultat de Geologia. Queralt, Pilar; Universitat de Barcelona, Geodinàmica i Geofísica Marcuello, Alex; Universitat de Barcelona, GEOMODELS Research Institute, Departament de Geodinàmica i Geofísica, Facultat de Geologia. Jones, Alan; Dublin Institute for Advanced Studies, School of Cosmic Physics
Keywords:	Magnetotelluric < GEOMAGNETISM and ELECTROMAGNETISM, Electromagnetic theory < GEOMAGNETISM and ELECTROMAGNETISM, Magnetic and electrical properties < GEOMAGNETISM and ELECTROMAGNETISM

Processing of Magnetotelluric data using inter-station tensor relationships

Joan Campanyà[1], Juanjo Ledo[1], Pilar Queralt[1], Alex Marcuello[1] & Alan G. Jones[2]

[1]GEOMODELS Research Insitiute, Departament de Geodinàmica i Geofísica, Universitat de Barcelona, C/Martí Franqués s/n. Barcelona 08028.

[2] Dublin Institute for Advanced Studies, Dublin, Ireland

Submitted: 27th November of 2012

Short title: Processing of MT data

Corresponding author: Joan Campanyà i Llovet

Mail contact: jcampanya@ub.edu

Phone number: (+34) 93 4035913

Key words: Magnetotelluric, Tensor relationship, Horizontal magnetic fields, processing, impedance tensor, geomagnetic transfer function

SUMMARY

In the magnetotelluric method, the electric and magnetic fields have to be simultaneously recorded on the surface of the study area to constrain the geoelectrical structures of the subsurface. From this condition, if one of the components became unusable, the tensor relationship of the local site cannot be constrained. This problem could be solved if we are able to process the data of the local site using data recorded at a neighbouring site. In some cases, the horizontal magnetic fields of a neighbouring site have been already used to constrain the tensor relationships of the local site, using remote-referencing, but it can be only applied if there are no major differences between the horizontal magnetic fields of the two sites. We propose a method to process the magnetotelluric data at the local site using the horizontal magnetic fields of a neighbouring site, even if there are differences between the horizontal magnetic fields between the two sites. Following the proposed method, the tensor relationships of the local site are constrained combining the inter-station tensor relationships between the electric and magnetic fields of the local site and the horizontal magnetic fields recorded at a neighbouring site. We define the Ψ parameter to evaluate the applicability of the proposed method for each processing and for each period. If Ψ is close to the identity matrix, the proposed relationships are valid. Long period magnetotelluric data acquired in the Pyrenees and magnetic data provided by magnetic observatories are used to test the method, with positive results. The experiments carried out demonstrate that the results obtained following the proposed method fit with the magnetotelluric impedance tensor and the geomagnetic transfer function of the local site. The experiments also show that the results obtained do not depend of the adopted neighbour horizontal magnetic fields. Furthermore, given the nature of the method it opens new ways to acquire magnetotelluric data optimizing the available instruments.

INTRODUCTION

In the magnetotelluric (MT) method, the geoelectrical structures of the subsurface are basically characterized by the MT impedance tensor (Cantwell, 1960; Rokityanski, 1961) and the geomagnetic transfer function (Parkinson, 1962; Weise, 1962). To determine these tensor relationships, the electric and magnetic time-varying fields simultaneously recorded on the surface of the study area are related in the frequency domain. If one of the recorded components becomes unusable, the tensor relationships cannot be constrained. This problem can be solved if the MT data recorded at a neighbouring site can be used to determine the tensor relationships of the local site.

In audiomagnetotellurics (AMT), where the distance between sites is typically around 200 m (i.e. Asch & Sweetkind, 2011; Falgàs et al., 2011; La Terra & Mezenes, 2011), the horizontal magnetic fields recorded at a neighbouring site can be used to process the data of the local site. This technique is already used by Mount Isa Mines' MIMDAS (Sheard, 2001) and Quantec's TITAN-24 (White & Gordon, 2003), and can be applied to constrain the MT impedance tensor of the local site if there are no main differences between the horizontal magnetic fields of the two sites. McNeice and Jones (2001) showed that especially for sub-horizontal conductors, the total magnetic fields can vary significantly between sites, so care has to be taken when using these limited acquisition methodologies.

In case of broadband magnetotelluric (BBMT) and long period magnetotelluric (LMT) data, where the distance between sites is much larger than 200 m, the MT sites can be located above different geoelectrical structures having large differences between the horizontal magnetic fields recorded on the two sites (Egbert, 2002; Habibian et al., 2010). In this case, it is not recommended to use the horizontal magnetic field of a neighbouring site to obtain the

apparent resistivity and phase of the local site because the results obtained could suggest different geoelectrical structures than the ones we want to constrain.

Garcia & Jones (2005) also used the data recorded on a neighbouring site to process the data of a local site, helping to solve the problem of the AMT dead-band. They suggested a method for processing AMT data combining two tensor relationships constrained from time series recorded at a different times. The method consists in determine the quasi-magnetotelluric transfer function of a local site from the tensor multiplication of two tensor relationships: The transfer function between day time telluric channels between the local site and a base site and the night time conventional MT impedance tensor at the base site. The obtained transfer function represents the ratio of the local-telluric to base-magnetic fields obtaining the telluric-magnetotelluric (T-MT) (Hermance & Thayer, 1975) AMT transfer function of the local site. Garcia & Jones (2005) showed that it represent a reasonable approximation of the real AMT impedance tensor if there are no major differences between the horizontal magnetic fields recorded on the two sites.

In this paper we propose a method where the MT impedance tensor and the geomagnetic transfer function at a local site can be constrained using inter-station tensor relationships between the electric and magnetic fields of the local site and the horizontal magnetic fields of a neighbouring site. In this method, differences between the horizontal magnetic fields recorded at the two sites do not affect the results obtained, being able to use it when there are differences between the horizontal magnetic fields at the two sites. The inter-station tensor relationships used to constrain the MT impedance tensor of the local site represents the ratio of the local telluric to base magnetic fields and the ratio of the base magnetic to the local magnetic fields. To determine the geomagnetic transfer function the used inter-station tensor relationships represents the ratio of the local vertical magnetic to base magnetic fields

and the ratio of the base magnetic to the local magnetic fields. Note that the ratio of the base magnetic to local magnetic fields is the horizontal magnetic tensor (HMT) proposed by Berdichevsky (1968), Egbert & Booker (1989) and Schmucker (1970). Although it can be used to determine geoelectrical structures, it is also employed to improve the processing of MT data detecting and removing the effect of non-stationary events (Varentsov et al., 2003; Sokolova et al., 2007).

Following the proposed method, if some of the recoded fields became unusable, the other time series can be used to calculate the inter-station tensor relationships, helping to improve the results obtained in process the MT data of the local site. As show in an example below, working with LMT data, the HMT can be constrained only using a few days of data. However, we recommend testing it in each study area to ensure that this possibility is accomplished. In a positive case, this give the opportunity to modify the logistical of a field campaign recording only a few days of magnetic time series at each site while the electric fields will be recorded all the time.

To perform this study, LMT data acquired in the Pyrenees at three different sites (*a*, *b* and *c*) were used to calculate the MT impedance tensor and the geomagnetic transfer function at site *a* in combination with the magnetic data provided by the Chambon la Forêt magnetic observatory (CLF) and the Furstenfeldbruck magnetic observatory (FUR). Both observatories are part of INTERMAGNET (http://www.intermagnet.org) (Fig. 1).

THEORY

In the proposed method, three inter-station tensor relationships are calculated to constrain the MT impedance tensor and the geomagnetic transfer functions at the local site. These

tensor relationships relate the local telluric at site *a* with the neighbouring magnetic at site *b* (equation 1), the local vertical magnetic at site *a* with the neighbouring magnetic at site *b* (equation 2), and the neighbouring magnetic at site *b* with the local magnetic at site *a* (equation 3). In all cases dependence on frequency is assumed. The nomenclature of the tensor relationships is based on Berdichevsky & Dmitriev, (2008).

$$\boldsymbol{e}_a = \boldsymbol{Z}_{ab}\,\boldsymbol{h}_b \qquad (1)$$

$$h_z^a = \boldsymbol{S}_{ab}\,\boldsymbol{h}_b \qquad (2)$$

$$\boldsymbol{h}_b = \boldsymbol{M}_{ba}\,\boldsymbol{h}_a \qquad (3)$$

where $\boldsymbol{h}_a$ and $\boldsymbol{h}_b$ are vectors of length two comprising the two horizontal magnetic components of the sites *a* $[h_x^a, h_y^a]$ and *b* $[h_x^b, h_y^b]$, respectively. The $\boldsymbol{e}_a$ is a vector of length two comprising the horizontal electric components of the site *a* $[e_x^a, e_y^a]$ and h_z^a is the vertical component of the magnetic field recorded on *a*. $\boldsymbol{Z}_{ab}$ and $\boldsymbol{M}_{ba}$ are 2x2 complex matrix relating the two correspondent vectors and $\boldsymbol{S}_{ab}$ is a 1x2 complex vector relating h_z^a and $\boldsymbol{h}_b$.

With the aim to avoid the effect of local noise the remote reference method (Gamble et al., 1979 a,b) with a magnetic site *r* is applied when calculate $\boldsymbol{Z}_{ab}$, $\boldsymbol{S}_{ab}$ and $\boldsymbol{M}_{ba}$:

$$\boldsymbol{Z}_{ab}^{RR} = [\boldsymbol{e}_a \boldsymbol{h}_r][\boldsymbol{h}_b \boldsymbol{h}_r]^{-1} \qquad (4)$$

$$\boldsymbol{S}_{ab}^{RR} = [h_z^a \boldsymbol{h}_r][\boldsymbol{h}_b \boldsymbol{h}_r]^{-1} \qquad (5)$$

$$\boldsymbol{M}_{ba}^{RR} = [\boldsymbol{h}_b \boldsymbol{h}_r][\boldsymbol{h}_a \boldsymbol{h}_r]^{-1} \qquad (6)$$

where the value $[\boldsymbol{pq}]$ is the spectral density matrix for fields *p* and *q*, defined by Gamble et al. (1979b), viz.

$$[\boldsymbol{pq}] = \begin{bmatrix} \langle p_x q_x^* \rangle & \langle p_x q_y^* \rangle \\ \langle p_y q_x^* \rangle & \langle p_y q_y^* \rangle \end{bmatrix} \qquad (7)$$

The asterisk denotes the complex conjugate and $\langle \quad \rangle$ denotes ensemble averaging either by summation over neighbouring frequencies or by averaging different estimates at the same frequency, or both.

In case of $[h_z^a \boldsymbol{h}_r]$

$$[\boldsymbol{pq}] = [\langle p_x q_x^* \rangle \quad \langle p_x q_y^* \rangle] \quad (8)$$

Gamble et al. (1979b) also provide the inverse of the matrix $[\boldsymbol{pq}]$

$$[\boldsymbol{pq}]^{-1} = \frac{\begin{bmatrix} \langle p_y q_y^* \rangle & -\langle p_x q_y^* \rangle \\ -\langle p_y q_x^* \rangle & \langle p_x q_x^* \rangle \end{bmatrix}}{\langle p_x q_x^* \rangle \langle p_y q_y^* \rangle - \langle p_y q_x^* \rangle \langle p_x q_y^* \rangle} \qquad (9)$$

Combining equations (4), (5) and (6) we can obtain the MT impedance tensor and the geomagnetic transfer functions of the site *a*, $\boldsymbol{Z}_a$ and $\boldsymbol{W}_a$ respectively:

$$\boldsymbol{Z}_{ab}^{RR} \boldsymbol{M}_{ba}^{RR} = [\boldsymbol{e}_a \boldsymbol{h}_r][\boldsymbol{h}_b \boldsymbol{h}_r]^{-1}[\boldsymbol{h}_b \boldsymbol{h}_r][\boldsymbol{h}_a \boldsymbol{h}_r]^{-1} = [\boldsymbol{e}_a \boldsymbol{h}_r]\boldsymbol{I}[\boldsymbol{h}_a \boldsymbol{h}_r]^{-1} = \boldsymbol{Z}_a^{RR} \qquad (10)$$

$$\boldsymbol{S}_{ab}^{RR} \boldsymbol{M}_{ba}^{RR} = [h_z^a \boldsymbol{h}_r][\boldsymbol{h}_b \boldsymbol{h}_r]^{-1}[\boldsymbol{h}_b \boldsymbol{h}_r][\boldsymbol{h}_a \boldsymbol{h}_r]^{-1} = [h_z^a \boldsymbol{h}_r]\boldsymbol{I}[\boldsymbol{h}_a \boldsymbol{h}_r]^{-1} = \boldsymbol{W}_a^{RR} \qquad (11)$$

where $\boldsymbol{I}$ is the identity and $\boldsymbol{W}_a$ the geomagnetic transfer function of the site *a*.

Ensuring the applicability of the proposed method for each specific study, we define the Ψ parameter as:

$$\Psi = \boldsymbol{M}_{ba} \boldsymbol{M}_{ab} = [\boldsymbol{h}_b k][\boldsymbol{h}_a k]^{-1}[\boldsymbol{h}_a k][\boldsymbol{h}_b k]^{-1} = \boldsymbol{I} \quad (12)$$

Where k is the component used as a complex conjugate to constrain the tensor relationships. In the case of remote reference $k = h_r$. If the Ψ parameter differs from the identity matrix, the obtained $\boldsymbol{M}_{ba}$ is not properly relating the horizontal magnetic fields between sites *a* and *b*, and the proposed method should not be applied using this tensor relationship. The permitted differences between the Ψ parameter and the identity matrix are suggested below.

EXPERIMENTS AND RESULTS

The data used for the experiment consist of three LMT sites recorded in the Eastern Pyrenees and the magnetic time series provided by the INTERMAGNET observatories Chambon de la Forêt (CLF) and Furstenfeldbruck (FUR) (Fig. 1). The LMT data were recorded using the LEMI systems, designed by the Lviv Centre of the Institute of Space Research, at sites *a*, *b* and *c* between the 26th October and the 09th November of 2011 for site *b*, and between the 19th October and the 09th November of 2011 for sites *a* and *c*. In all the cases, sample rate is 1 Hz for the electric and magnetic fields. The distance between site *a* and sites *b* and *c* are 25 km and 50 km, respectively. The LMT data have been processed using the Birrp.5 program (Chave & Thompson, 2004) doing remote reference with the magnetic observatories. The same parameters have been imposed in the processing of the data, avoiding effects unrelated with the purpose of the study. When it has been necessary, error estimation has been carried out following the bootstrap method (Efron, 1979), computing a sample of 5000 bootstrapped standard deviation of 1000 samples from the analyzed parameter. The 1000 samples of the analyzed parameter have been calculated using 1000 random samples within the margin of error of each variable.

The first experiment has been developed to validate the applicability of the proposed method and consist in processing the MT data of the site *a* using different approaches. The LMT data at site *a* were processed using the magnetic data recorded at site *b*, doing remote reference with CLF, and using the magnetic data recorded on the site *c*, doing remote reference with FUR. Results obtained are compared using the *xy* and *yx* components of the MT impedance tensor and the geomagnetic transfer function. The *xx* and *yy* components of the MT impedance tensor (Figs S1, S2 and S3 in supplementary files) are not used due as they have lower quality and do not involve differences in the final conclusions.

The first two approaches consist in processing the LMT data at site *a* doing local processing without remote reference ($\boldsymbol{Z}_a$ and $\boldsymbol{W}_a$) and local processing with remote reference with a magnetic observatory ($\boldsymbol{Z}_a^{RR}$ and $\boldsymbol{W}_a^{RR}$) (Fig. 2). Results show the presence of local noise, which mainly affects the shorter periods of the *xy* component of the MT impedance tensor and the *Wy* component of the geomagnetic transfer function. These results suggest the necessity of undertaking remote referencing when processing the LMT data of the site *a*.

Focusing on the MT impedance tensor, the next approach consists in processing the LMT data of the site *a* using the horizontal magnetic fields of sites *b* or *c* instead of those recorded at site *a*:

$$\boldsymbol{e}_a = \boldsymbol{Z}_{ab}^{RR}\boldsymbol{h}_b \qquad (13)$$

$$\boldsymbol{e}_a = \boldsymbol{Z}_{ac}^{RR}\boldsymbol{h}_c \qquad (14)$$

Finally, we calculate the MT impedance tensor of the site *a* applying the proposed method in this paper:

$$\boldsymbol{Z}_a^{RR} = \boldsymbol{Z}_{ab}^{RR}\boldsymbol{M}_{ba}^{RR} \qquad (15)$$

$$\boldsymbol{Z}_a^{RR} = \boldsymbol{Z}_{ac}^{RR}\boldsymbol{M}_{ca}^{RR} \qquad (16)$$

Equivalent steps have been followed to calculate the geomagnetic transfer function of the site *a*. Apparent resistivity, phases and the geomagnetic transfer function obtained in processing the MT data of site *a* using the horizontal magnetic fields of sites *b* and *c*, are shown in Figs 3 and 4, respectively. In all the cases, results are compared with that obtained doing local processing with remote reference ($\boldsymbol{Z}_a^{RR}$ and $\boldsymbol{W}_a^{RR}$). The results obtained using the horizontal magnetic fields of the sites *b* or *c* ($\boldsymbol{Z}_{ab}^{RR}$, $\boldsymbol{Z}_{ac}^{RR}$, $\boldsymbol{W}_{ab}^{RR}$ and $\boldsymbol{W}_{ac}^{RR}$) do not fit with the MT results of the local site ($\boldsymbol{Z}_a^{RR}$ and $\boldsymbol{W}_a^{RR}$) (Figs 3a and 4a), except when applying the horizontal magnetic tensor, $\boldsymbol{M}_{ba}^{RR}$ or $\boldsymbol{M}_{ca}^{RR}$, following the proposed method (Figs 3b and 4b). The consistence of the results obtained applying the proposed method using different horizontal magnetic fields is shown in Fig. 5. The apparent resistivity, phase and geomagnetic transfer function values are practically the same, regardless of whether we use the horizontal magnetic fields at sites *b* or *c*.

Another experiment has been carried out to quantify the permissible differences between the parameter Ψ and the identity matrix. The experiment consisted in calculating the Ψ parameter with and without doing remote reference with a magnetic observatory. We used sites *a* and *b* doing remote reference with CLF and the sites *a* and *c* doing remote reference with FUR.

$$\Psi^{\mathrm{RR}} = \mathbf{M}_{\mathrm{ga}}^{\mathrm{RR}} \mathbf{M}_{\mathrm{ag}}^{\mathrm{RR}} \qquad (17)$$

$$\Psi = \mathbf{M}_{\mathrm{ga}} \mathbf{M}_{\mathrm{ag}} \qquad (18)$$

where *g* is *b* or *c* in each case. As shown in Fig. 6, in case of remote referencing, the Ψ parameter better fits with the identity matrix in both cases, with differences below ±0.06. In the case of not using remote referencing, differences are up to 0.25 at shorter periods.

PROPERTIES AND ADVANTAGES OF THE METHOD

From the results obtained we observe that the proposed method provides practically the same results, regardless of the horizontal magnetic fields used to process the MT data of the local site (Fig. 5). The results also corroborate the necessity to use the HMT when processing the MT data using the horizontal magnetic fields of a neighbouring site (Figs 3 and 4). The Ψ parameter, which should be the identity matrix, allows to determine the periods for which the HMT properly relates the horizontal magnetic fields between two sites, suggesting the periods for which the proposed method can be used.

Below we focus on the properties of the proposed method and the associated advantages. The main property of the proposed method is that the MT impedance tensor and the geomagnetic transfer function at the local site are obtained from a combination of inter-station tensor relationships that can be constrained separately using time series recorded at different times and with different lengths. Another property is that the electric and magnetic fields recorded at the local site are not directly related, obtaining the MT impedance tensor and geomagnetic transfer function from a signal that is coherent between local, neighbour and remote sites. Taking advantage of these properties, we developed an example where the proposed method allows improving the results in the processing of the LMT data at site *a* using the horizontal magnetic fields at sites *c* and FUR. For this example, we first determine the number of days necessary to constrain the HMT between the sites *c* and *a*. As shown in Fig. 7, two days of data is sufficient to obtain the $\boldsymbol{M}_{ca}^{RR}$.

The example consists of the hypothetical case where, having sites *c* and FUR constantly recording, after twenty days acquiring LMT data at site *a* the magnetic fields were truncated having a time series of only two days of data. With the aim of obtaining the apparent resistivity

and phases at site *a*, we process the LMT data doing local processing with remote referencing. In that case, due to the electric and magnetic fields having to be recorded simultaneously, we are only able to use the LMT data recorded during the first two days (Fig. 8a). However, using the proposed method we are able to calculate the inter-station tensor relationship between the electric fields recorded on *a* and magnetic fields recorded on *c*, $\boldsymbol{Z}_{ac}^{RR}$, using twenty days of data and then calculate the inter-station tensor relationship between the horizontal magnetic fields of *c* and *a*, $\boldsymbol{M}_{ca}^{RR}$, using two days of data (Fig. 8b). The apparent resistivity curves and the phases at site *a* are improved when the method is applied, as we are able to use the twenty days of the electric field data.

CONCLUSIONS

As demonstrated, the MT impedance tensor and the geomagnetic transfer function of a local site *a* [$\boldsymbol{Z}_a(\boldsymbol{e}_a, \boldsymbol{h}_a)$ and $\boldsymbol{W}_a(h_z^a, \boldsymbol{h}_a)$] can be calculated combining inter-station tensor relationships with another site *b* [$\boldsymbol{Z}_{ab}(\boldsymbol{e}_a, \boldsymbol{h}_b)$, $\boldsymbol{S}_{ab}(h_z^a, \boldsymbol{h}_b)$ and $\boldsymbol{M}_{ba}(\boldsymbol{h}_b, \boldsymbol{h}_a)$] following the proposed method [$\boldsymbol{Z}_a = \boldsymbol{Z}_{ab}\boldsymbol{M}_{ba}$ and $\boldsymbol{W}_a = \boldsymbol{S}_{ab}\boldsymbol{M}_{ba}$]. Remote referencing to calculate all tensor relationships is recommended to avoid the effects of local noise of the different MT sites. The experiments carried out corroborate the applicability of the method and the defined Ψ parameter constrains the periods where the proposed method can be used. As only inter-station tensor relationships are used the electric and magnetic fields of the local site do not need to be recorded simultaneously and during the same time. The applicability of the proposed method opens new ways to acquire MT data getting more out of the measuring instruments.

ACKNOWLEDGEMENTS

This research was funded by MAGBET (CGL2006-101660), PIERCO2 (CGL2009-07604), MODES4D (CGL2010-66431-CO2-02/BTE), INTECTOSAL (CGL2010-21968-CO2-01) projects, Grup de Recerca de Geodinàmica i Anàlisi de Conques (2009SRG1198) and the Departament d'Universitats, Investigació i Societat de la informació de la Generalitat de Catalunya. The results presented in this paper rely on the data collected at Chambon la Forêt (CLF) and Furstenfeldbruck (FUR) magnetic observatories. We thank the Institut de Physique du Globe de Paris and the Ludwig-Maximilians Universität München for supporting its operation and INTERMAGNET for promoting high standards of magnetic observatory practice (www.intermagnet.org). We are also grateful to the land owners and to l'Agence de l'Office National des Forêts (ONF), which allow install the LMT sites in their fields, and to the fieldwork assistants, especially to Lluís Guilà, Ivan Suñé and Roger Llopart.

REFERENCES

Asch, T.H. & Sweetkind, D.S., 2011. Audiomagnetotelluric characterisation of range-front faults, Snake Range, Nevada. *Geophys.*, 76 (1), B1-B7

Berdichevsky, M.N., 1968. Electrical prospecting by the method of Magnetotelluric Profiling, Nedra, Moscow.

Berdichevsky M.N. & Dmitriev V.I., 2008. *Models and Methods of Magnetotellurics*. Springer-Verlag Berlin Heidelberg.

Cantwell, T., 1960. *Detection and analysis of low frequency magnetotelluric signals*. Ph.D thesis. M.I.T.

Chave, A.D. & Thompson, D.J., 2004. Bounded influence estimation of magnetotelluric response functions. *Geophys. J. Int*., 157, 988–1006.

Efron, B., 1979. Bootstrap methods: Another look at the jackknife. *Annals of Statistics*, 7, 1-26

Egbert, G.D. & Booker, J.R.: 1989. Multivariate analysis of geomagnetic array data 1, The response space, *J. Geophys. Res*., 94, 14,227–14,248.

Egbert, G.D., 2002. Processing and interpretation of the electromagnetic induction array data. *Surv. in Geophys*., 23, 207-249.

Falgàs, E.; Ledo, J.; Benjumea, B. & Queralt, P., 2011. Integrating Hydrogeological and Geophysical Methods for the Characterization of a Deltaic Aquifer System, *Surv Geophys*. doi:10.1007/s10712-011-9126-2.

Gamble, T.D., Clarke, J. & Goubau, W.M., 1979a. Magnetotellurics with a remote magnetic reference, *Geophys*, 44, 1, 53-68.

Gamble, T.D., Clarke, J. & Goubau, W.M., 1979b. Error analysis for remote reference magnetotellurics: *Geophys*, 44, 959-968.

Garcia, X. & Jones, A.G., 2005. A new methodology for the acquisition and processing of audio-magnetotelluric (AMT) data in the AMT dead band. *Geophys.*, 70 (5), G119-G126. doi: 10.1190.2073889.

Habibian, B.D., Brasse, H., Oskooi, B., Ernst, T., Sokolova, E., Varentsov, Iv. & EMTESZ Working Group, 2010. The conductivity structures across the Trans-European Suture Zone from magnetotelluric and magnetovariational data modeling. *Physics of the Earth and Planetary Interiors*, 183,377-386.

Hermance, J. F. & Thayer, R.E.,, 1975. The telluric-magnetotelluric method. *Geophys.*, 40, 664-668.

La Terra, E.F. & Menezes, P.T.L., 2012. Audiomagnetotelluric 3D imaging of the Regis kimberlite pipe, Minas Gerais, Brazil, *Journ. of Appl. Geophys*., 77, 30-38.

McNeice and Jones 2001. Multi-site, multi-frequency tensor decomposition of magnetotelluric data. *Geophysics*, 66, 158-173.

Parkinson, W.D., 1962. The influence of the continents and oceans on geomagnetic variations. *Geophys. J.R. Astron. Soc*., 80, 177-194.

Rokityanski, I.I. 1961. On the application of the magnetotelluric method to anisotropic and inhomogeneous masses. *Izvestia,* 11, 1607-1613.

Schmucker, U.: 1970, *Anomalies of geomagnetic variations in the Southwestern United States*, Bull. Scripps Inst. Oceanogr. 13.

Sheard, N., 2001. The values of advanced geophysical technology in modern exploration. *Bulletin of the Australian Institute of Geoscientists*, 35, 53-56.

Sokolova, E.Yu., Varentsov, Iv.M. & BEAR Working Group, 2007. Deep array electromagnetic sounding on the Baltic Shield: External excitation model and implications for upper mantle conductivity studies, *Tectonophysics*, 445, 3-25.

Varentsov, Iv.M., Sokolova, E.Yu. & BEAR WG, 2003. Diagnostics and suppression of auroral distortions in the transfer operators of the EM field in the BEAR experiment, *Izv., Phys. Solid Earth,* 39, 4: 283–307.

Weise, H., 1962. Geomagnetische Tiefentellurik. *Geophys. Pure Appl*. 52, 83-103.

White, M. & Gordon, R., 2003. Deep imaging: New technology lowers cost discovery, *Canadian Mining Journal*, 27-28.

FIGURE CAPTIONS

Figure 1. Map with the location of the LMT sites. *a*, *b* and *c* are the LMT sites recorded in the Pyrenees and CLF and FUR are the Magnetic Observatories (INTERMAGNET).

Figure 2. Apparent resistivity, phase and geomagnetic transfer function of the site *a* processing the data of the local site doing local processing and local processing with remote reference with CLF (a) and with FUR (b). (a) data have been acquired between the 26th October and 09th November. (b) data have been acquired between 19th October and 09th November.

Figure 3. Apparent resistivity, phase and geomagnetic transfer function of the site *a* using the horizontal magnetic fields recorded on the site *b* and doing remote reference with CLF. (a) Using magnetic fields of the site *b* instead of the magnetic fields of the site *a*. (b) Following the proposed method. Results are compared with the local processing doing remote reference with CLF.

Figure 4. Apparent resistivity, phase and geomagnetic transfer function of the site *a* using the horizontal magnetic fields recorded on the site *c* and doing remote reference with FUR. (a) Using magnetic fields of the site *c* instead of the magnetic fields of the site *a*. (b) Following the proposed method. Results are compared with the local processing doing remote reference with FUR.

Figure 5. Apparent resistivity, phase and geomagnetic transfer function of the site *a* following the proposed method using the horizontal magnetic fields of the site *b* doing

remote reference with CLF and using the horizontal magnetic fields of the site *c* doing remote reference with FUR.

Figure 6. The Ψ parameter when calculate the HMT between *a* and *b* and between *a* and *c* with and without remote reference. Grey line includes the values with a difference lower than ±0.06 with the identity.

Figure 7. The HMT between sites *c* and *a* using time series with different length, between 1 day, the shortest, and 20 days, the longest. Remote reference has been done with FUR. Black are the real values and red are the imaginary values.

Figure 8. Apparent resistivity and phase of the site *a* when the magnetic fields are truncated after two days recording. (a) Doing local processing with remote reference with FUR. (b) Following the proposed method using the horizontal magnetic fields of the site *c* and doing remote reference with FUR.

SUPLEMENTARY MATERIAL (FIGURE CAPTIONS)

Figure S1. For the *xx* and *yy* components, apparent resistivity and phase values of the site *a* processing the data of the local site doing local processing and local processing with remote reference with CLF (a) and with FUR (b). In (a) data have been acquired between the 26th October and 09th November of 2011. In (b) data have been acquired between 19th October and 09th November of 2011.

Figure S2. For the *xx* and *yy* components, apparent resistivity and phase values of the site *a* using the horizontal magnetic fields recorded on the site *b* and doing remote reference with CLF. (a) Using magnetic fields of the site *b* instead of the magnetic fields of the site *a*. (b) Following the proposed method. Results are compared with the local processing doing remote reference with CLF.

Figure S3. For the *xx* and *yy* components, apparent resistivity and phase values of the site *a* using the horizontal magnetic fields recorded on the site *c* and doing remote reference with FUR. (a) Using magnetic fields of the site *c* instead of the magnetic fields of the site *a*. (b) Following the proposed method. Results are compared with the local processing doing remote reference with FUR.

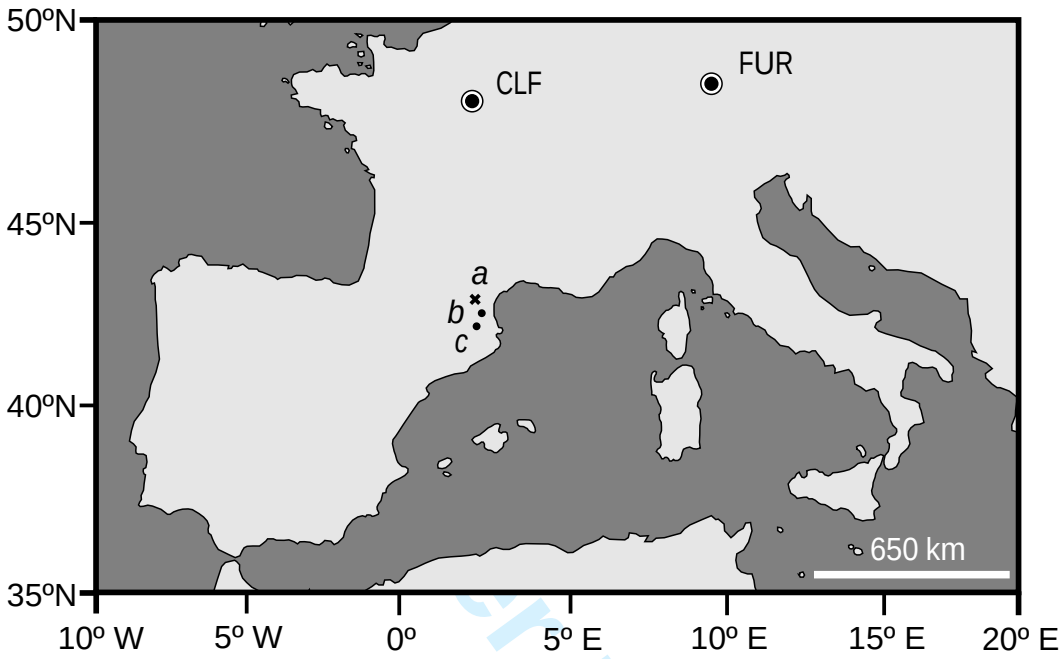

Figure 1 Campanyà et al. 2012

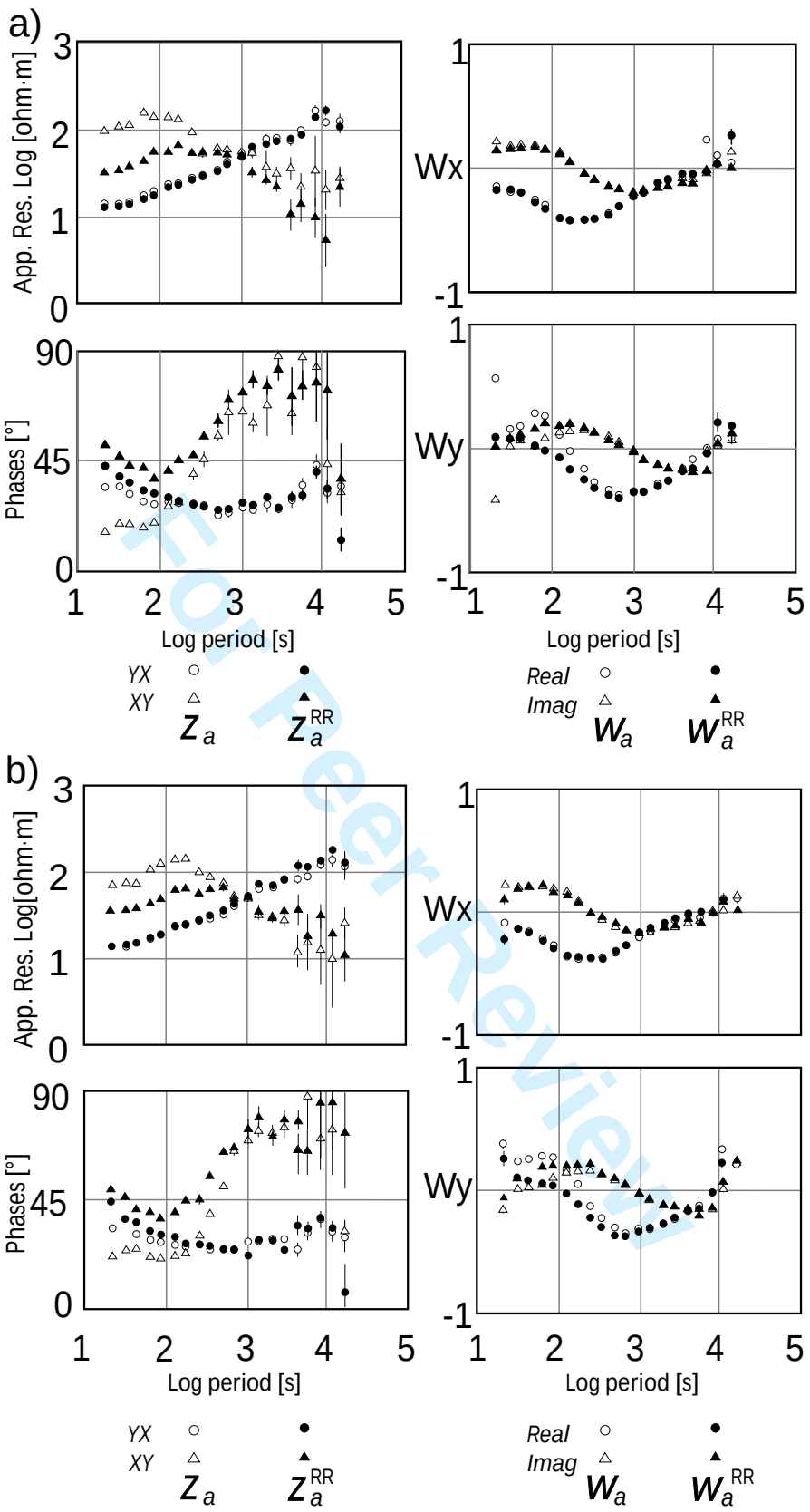

Figure 2 Campanyà et al. 2012

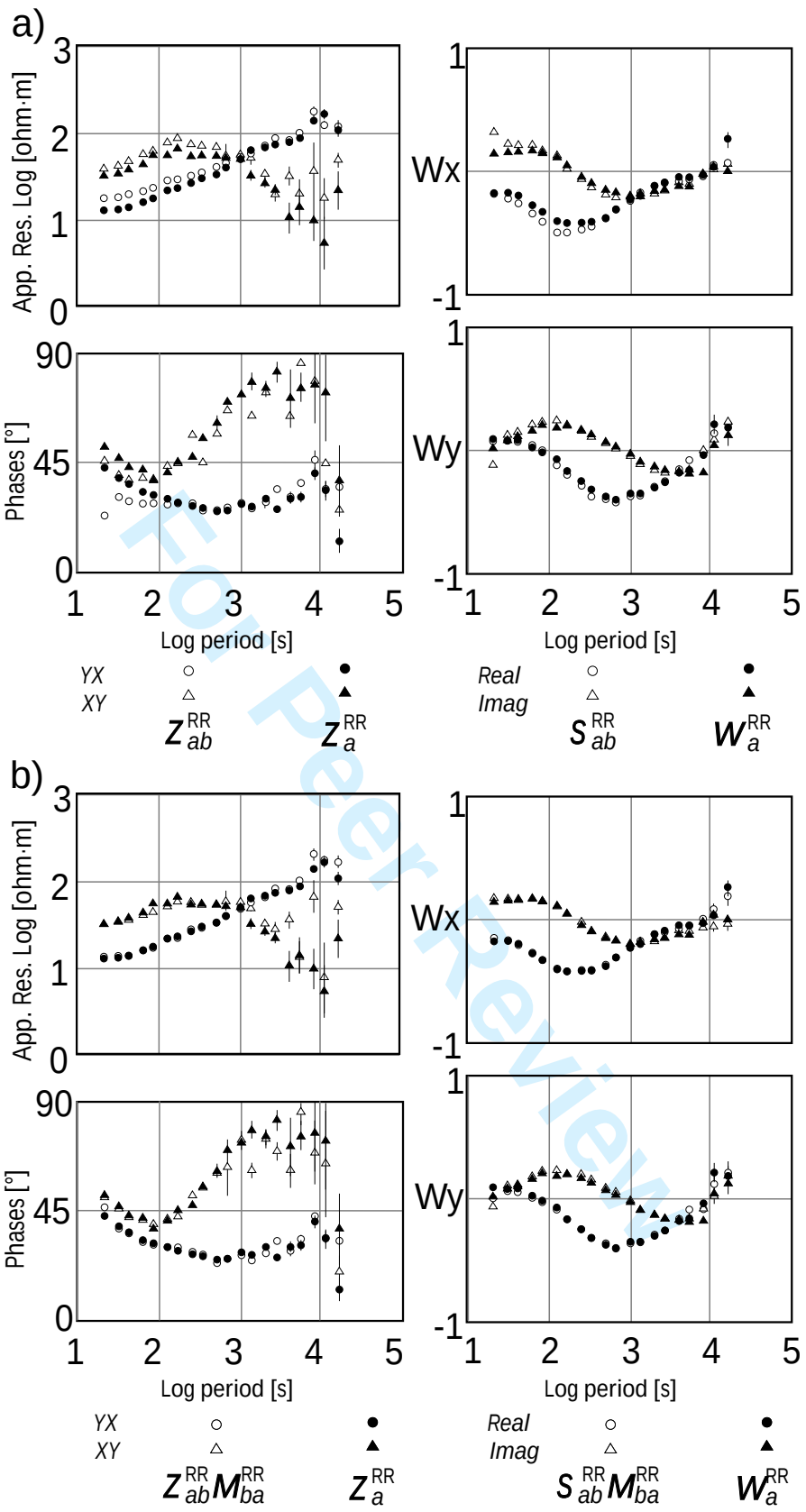

Figure 3 Campanyà et al. 2012

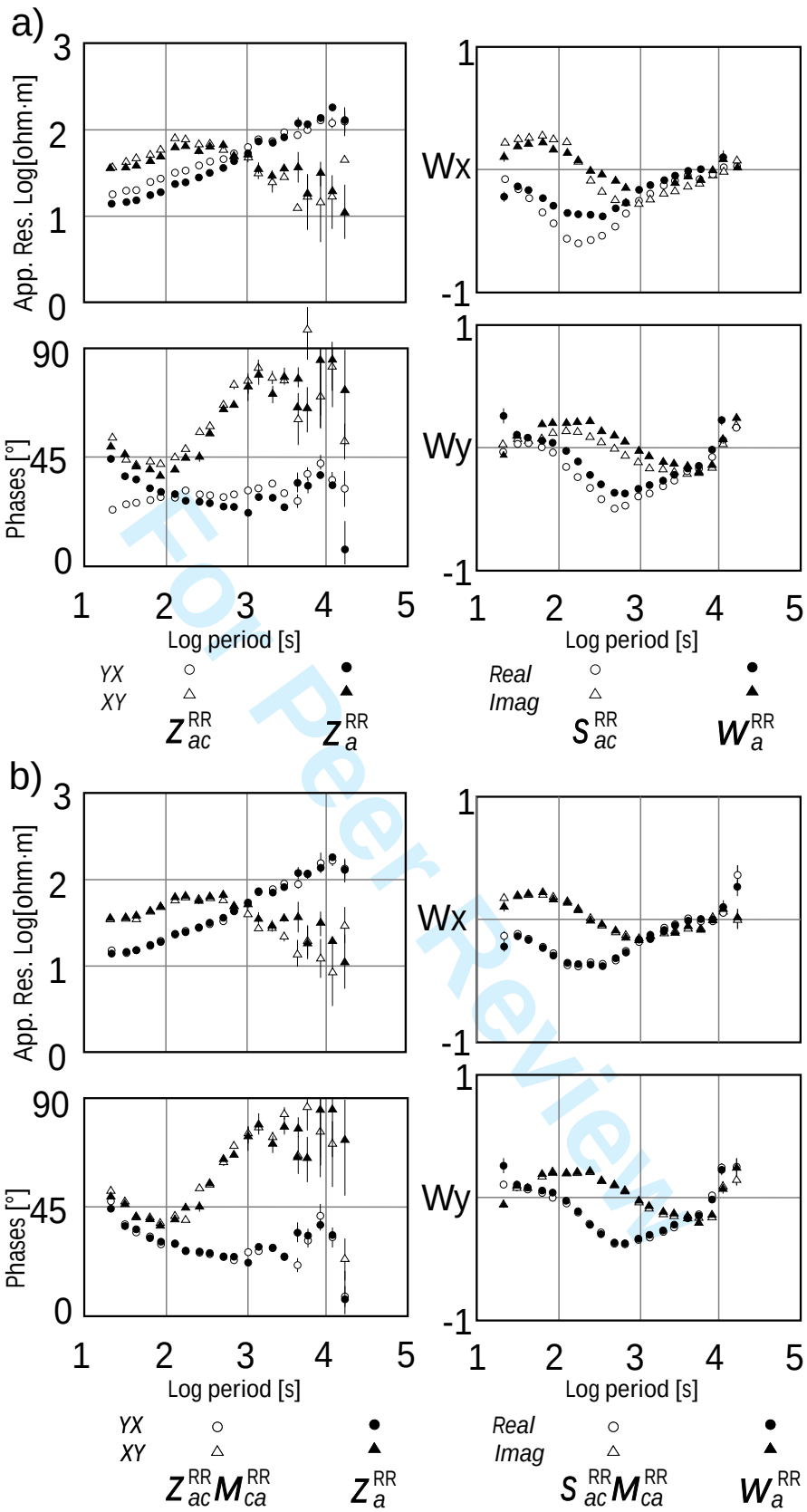

Figure 4 Campanyà et al. 2012

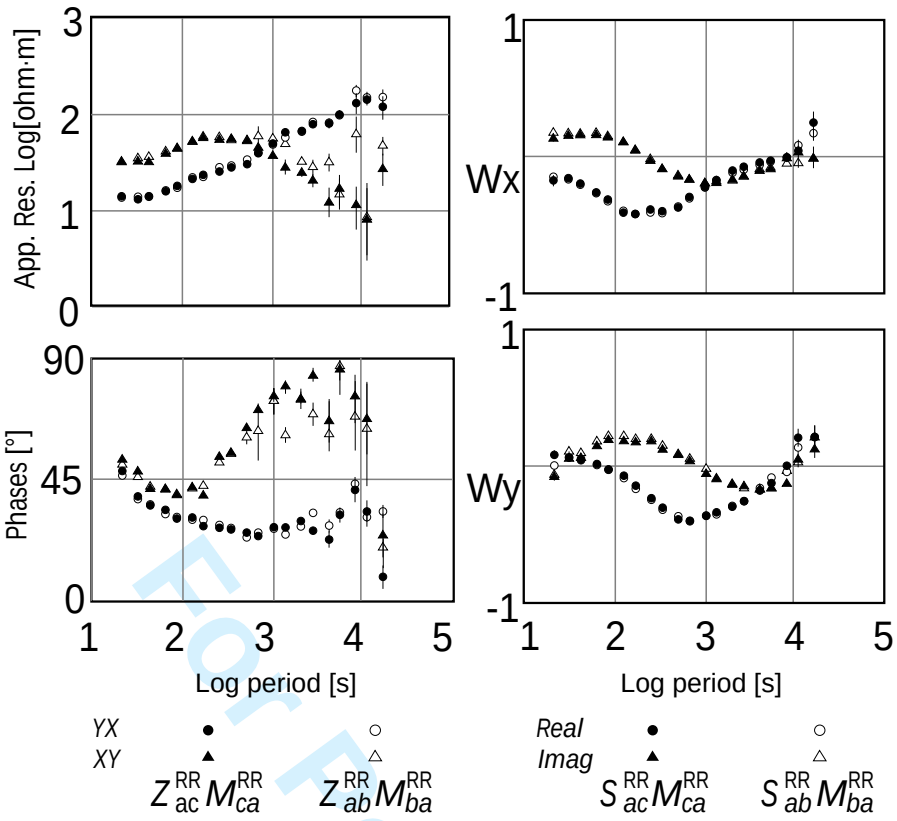

Figure 5 Campanyà et al. 2012

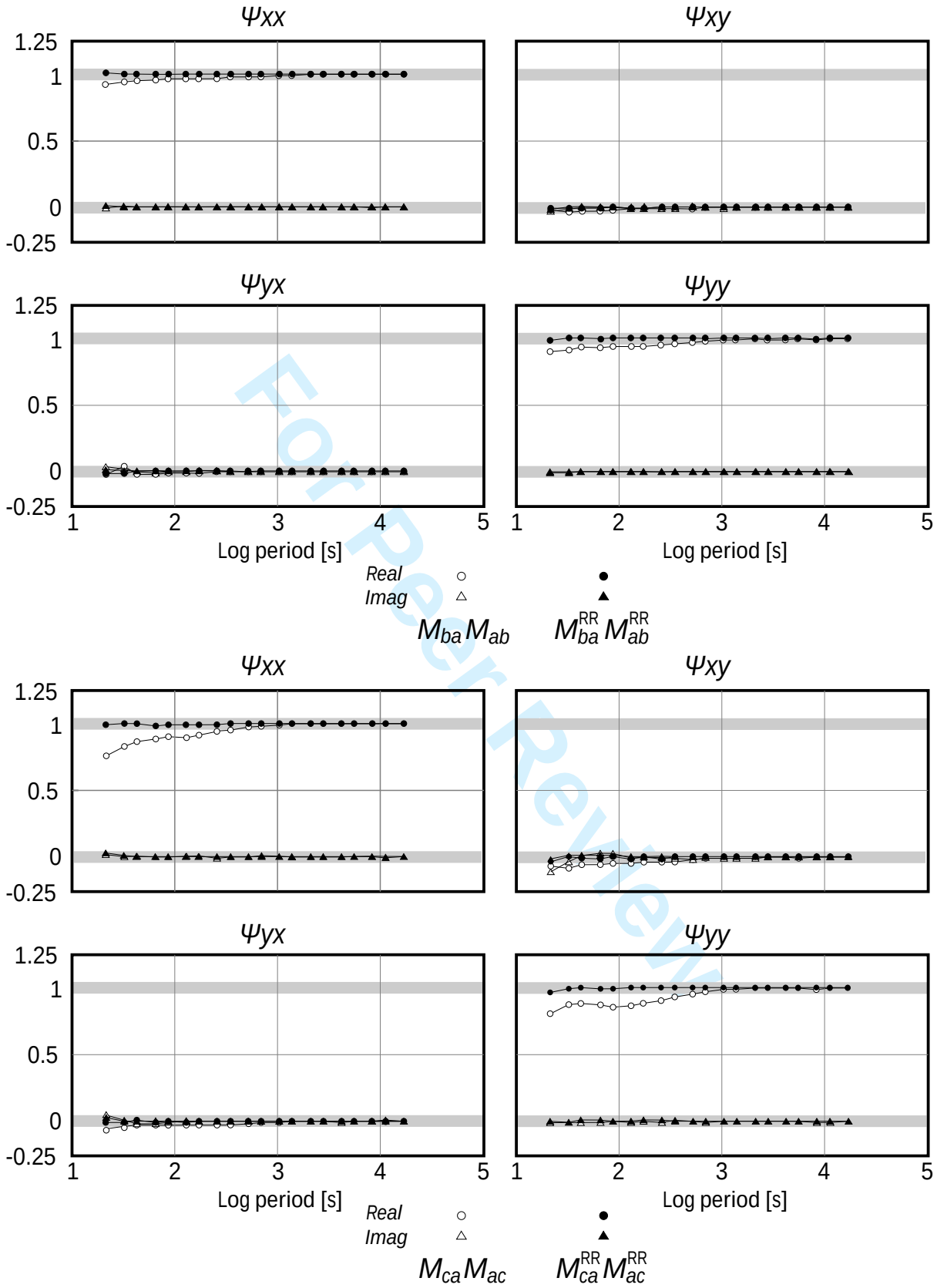

Figure 6 Campanyà et al. 2012

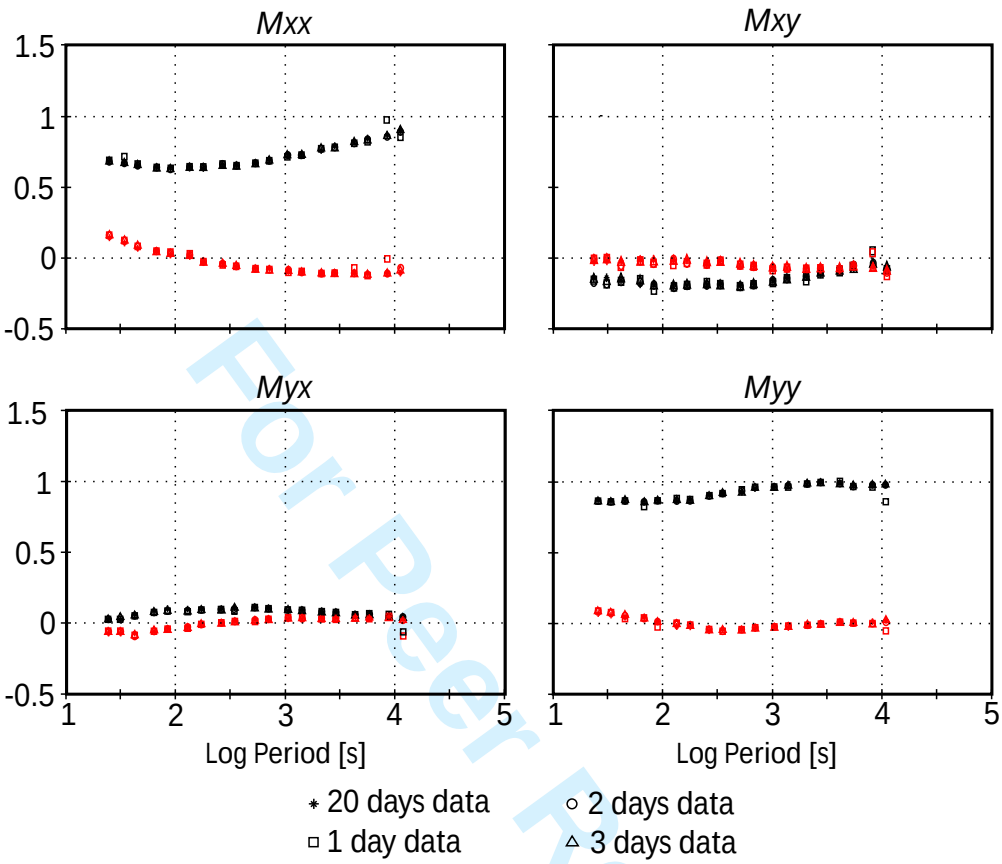

Figure 7 Campanyà et al. 2012

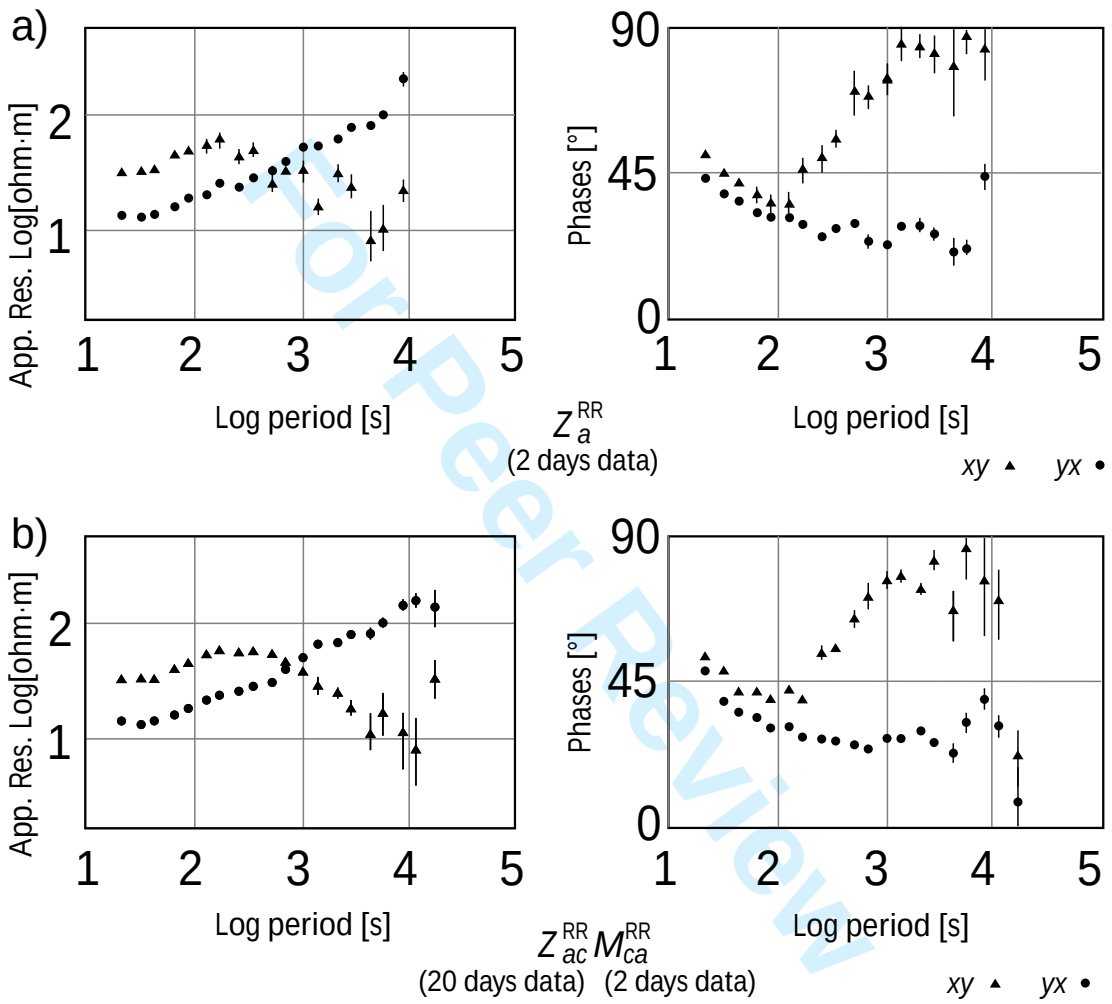

Figure 8 Campanyà et al. 2012

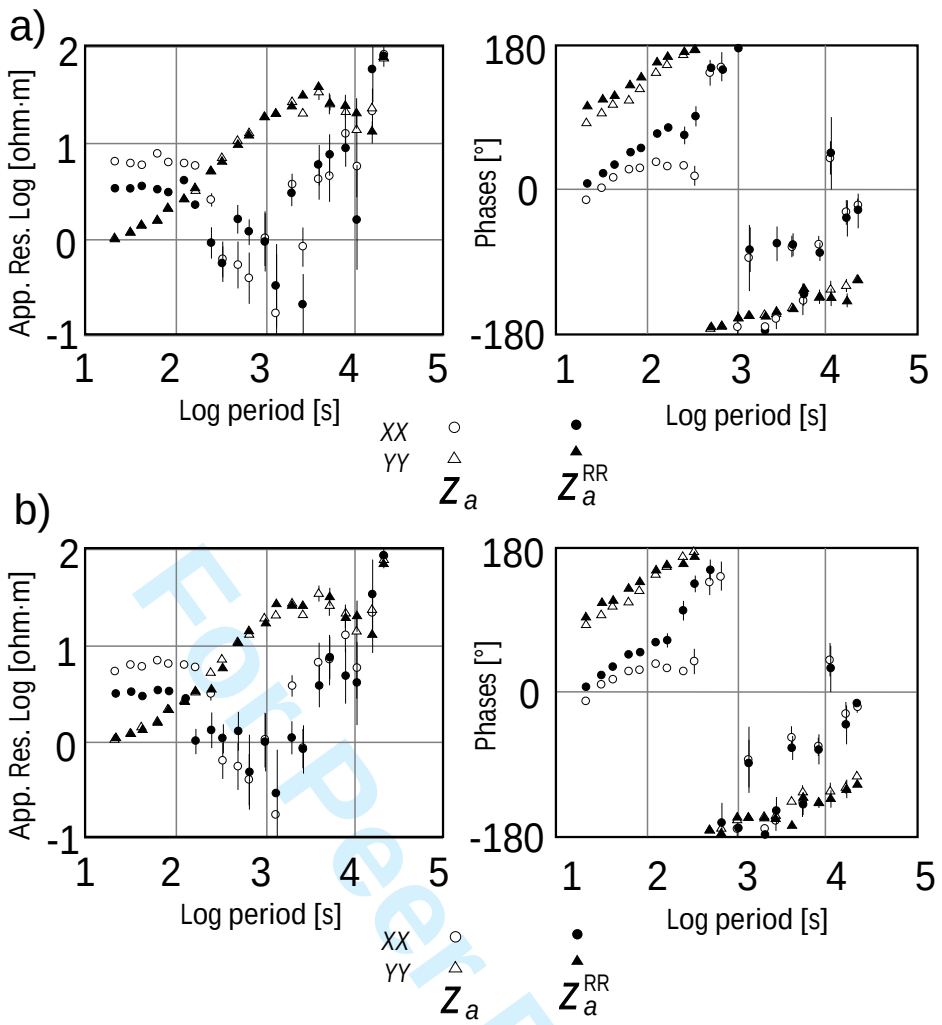

Figure S1 Campanyà et al. 2012

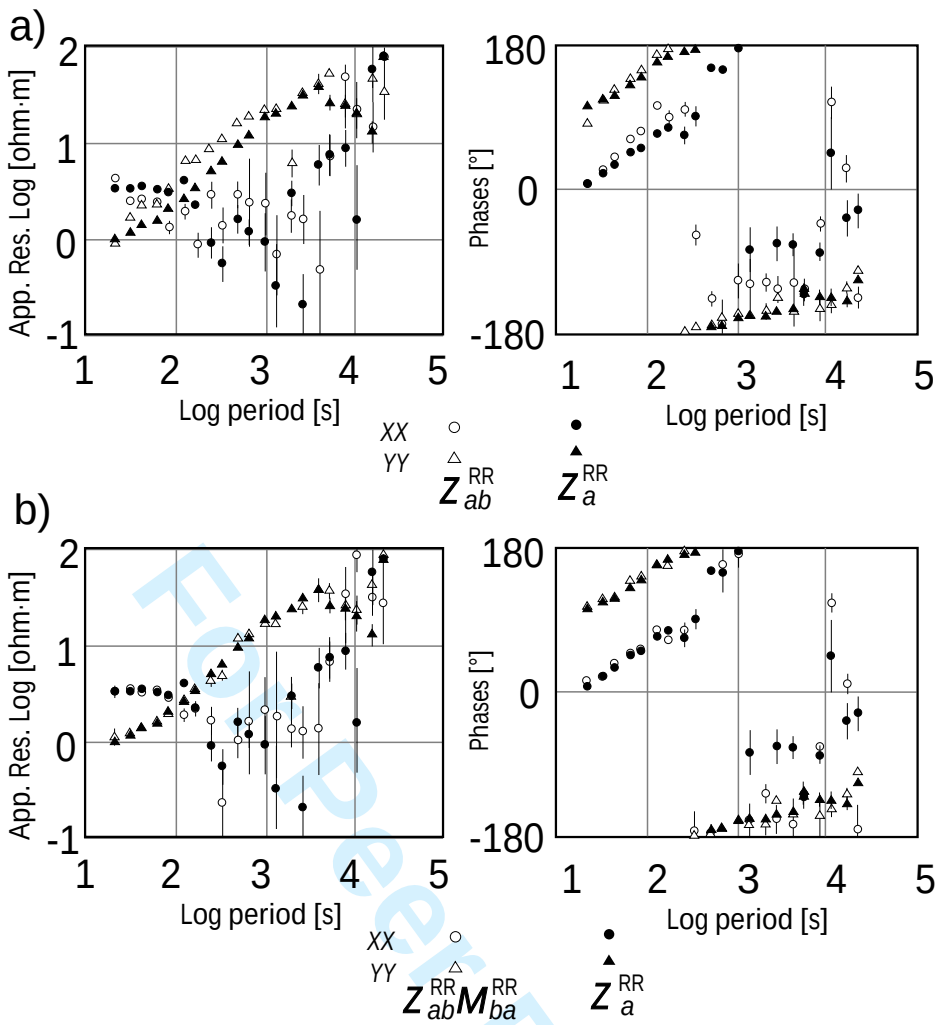

Figure S2 Campanyà et al. 2012

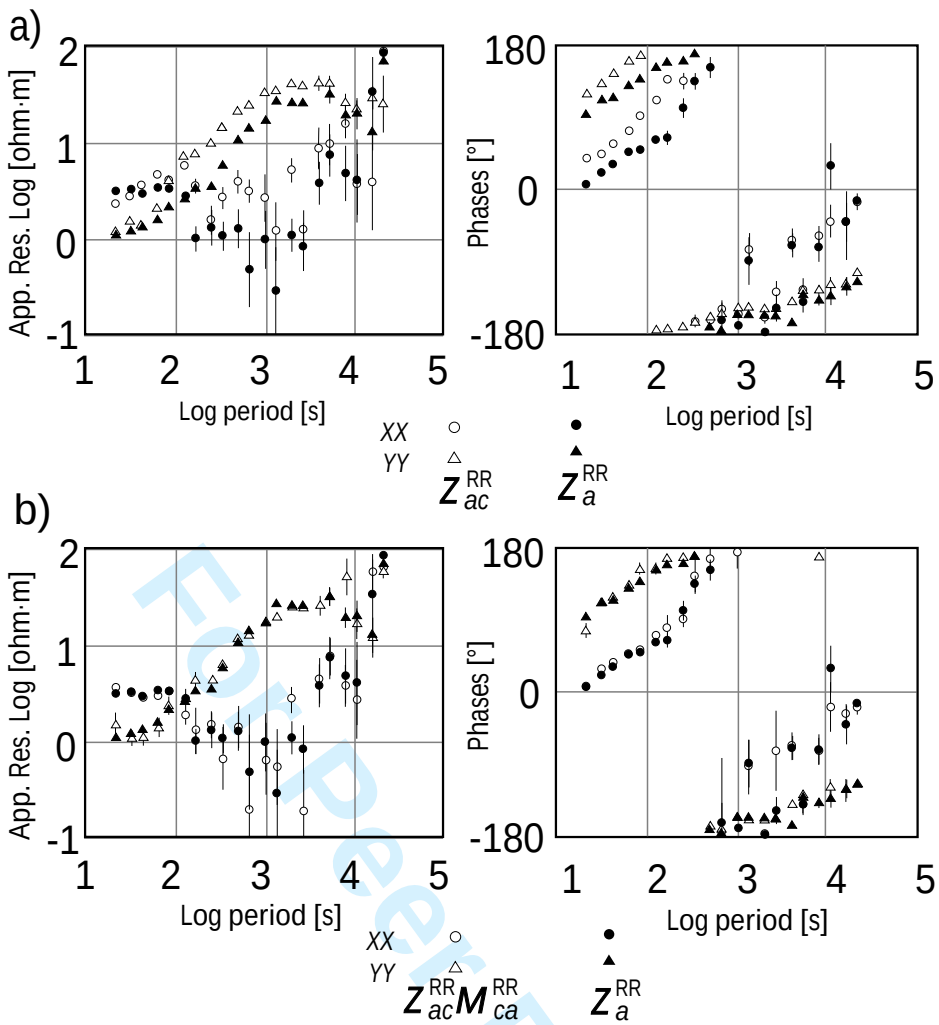

Figure S3 Campanyà et al. 2012